BRUWER, JULIANA SHANA

EXPERIMENTAL INVESTIGATION OF THE PHASE RELATIONS IN THE SYSTEM CU-NI-S IN THE TEMPERATURE RANGE 1200°C TO 700°C

MSc UP 1996

Experimental investigation of the phase relations in the system Cu-Ni-S in the temperature range 1200°C to 700°C

by Juliana Shana Bruwer
under the supervision of Dr. R. K. W. Merkle
and Prof. C.P. Snyman
Master of Science in Applied Mineralogy
Department of Geology

SUMMARY

Phase relations in the ternary system Cu-Ni-S were investigated using 275 samples in evacuated quartz-glass tubes. A comparative statistical evaluation was made between areas (0.12 mm^2) analysed using EDS (Energy Dispersive Spectrometry) with a Scanning Electron Microscope (SEM) and spot analyses on a grid pattern using WDS (Wavelength Dispersive Spectrometry) with the Electron Microprobe (EMP). EDS analyses of areas were found to give more reproducible and statistically more meaningful results. Averaged area analyses of phases in equilibrium phase assemblages were used for construction of the 1200°C, 1100°C, 1000°C, 900°C, 800°C and 700°C isothermal sections.

From the combined results of the isothermal sections, the liquidus phase diagram could be determined. This diagram, together with the liquid compositions of invariant phase equilibria from the isothermal sections, were used to determine the crystallisation paths of the Cu-Ni-S system.

Converter matte that is slow-cooled in the beneficiation process of Cu, Ni, and platinum group elements usually contains elements other than Cu, Ni, and S in small amounts. Of all of these elements Fe probably has the greatest effect on the phase diagram, especially when present in concentrations greater than the typical ~3wt% and the envisaged effects of Fe on the phase diagram is discussed. It is, however, reasonable to assume that the Cu-Ni-S system represents converter matte composition sufficiently well and the Cu-Ni-S phase

Experimental investigation of the phase relations in the system Cu-Ni-S in the temperature range 1200°C to 700°C

by

JULIANA SHANA BRUWER

Submitted in partial fulfilment of the requirements for the degree

Magister Scientia

in the Faculty of Science

University of Pretoria

Pretoria

July 1996

diagram can be used to describe the crystallisation path of slow-cooled matte. It can be concluded that the phase segregation observed in slow-cooled ingots (Sproule *et al.*, 1960) is due to the crystallisation of high-temperature Cu_2S early in the crystallisation history in the top portion of the ingot and the subsequent fractionation of the liquid towards relatively more Ni_3S_2 and alloy rich in the central and bottom portion of the ingot.

Furthermore, it can be concluded that the sulphur content of the matte is crucial for the phase formation sequence, phase formation temperatures, and the amount of alloy that will form. Slight changes of ~1wt% in the region from 18 to 22 wt % sulphur can lead to a variety of crystallisation sequences. There is a critical sulphur content at approximately 21 wt%, depending on the exact composition of the Cu_2S-type phase, the eutectic point and the overall Cu/Ni ratio of the sample. At the critical sulphur content both Ni_3S_2 and alloy will start to crystallise only at the eutectic point. If the sulphur content is higher, Cu_2S forms first followed by Ni_3S_2 and alloy is the last phase to crystallise at the eutectic point. With lower sulphur contents Cu_2S crystallises first followed by alloy, while Ni_3S_2 crystallises only at the eutectic point. With even lower sulphur contents alloy crystallises first followed by Cu_2S, while Ni_3S_2 crystallises only at the eutectic point.

The phase formation temperatures and the phase formation sequence can influence the partitioning behaviour of platinum group elements, and also the texture of slow-cooled matte.

Experimentele ondersoek van die fase verwantskappe in the sisteem Cu-Ni-S in die temperatuur interval 1200°C tot 700°C

deur Juliana Shana Bruwer
onder die toesig van Dr. R. K. W. Merkle
en Prof. C.P. Snyman
M. Sc. Toegepaste Mineralogie
Departement Geology

OPSOMMING

Die faseverwantskappe van die ternêre sisteem Cu-Ni-S is ondersoek met behulp van 275 monsters in geevakueerde kwartsglas-kapsules. Areas (0.12 mm^2) wat met 'n elektron-lading mikroskoop geanaliseer is met 'n energie dispersiewe spektrometrie (EDS), is statisties vergelyk met puntanalises in 'n roosterpatroon met 'n elektron microsonde met 'n golflengte dispersiewe spektrometrie (WDS). Daar is gevind dat EDS area analises meer herhaalbaar en statisties meer betekenisvol is. Die gemiddeld van area analises van fases in ewewig verwantskappe is gebruik vir die konstruksie van die 1200°C, 1100°C, 1000°C, 900°C, 800°C en 700°C isotermale snitte.

Die likwidus fasediagram is verkry vanaf 'n kombinasie van die resultate van die isotermale snitte. Hierdie fasediagram, tesame met die vloeistofsamestellings van unievariante fase-ewewigte, is gebruik om die kristalliseringspaaie van die Cu-Ni-S sisteem te bepaal.

Stadig afgekoelde mat in the ontginningsproses van Cu, Ni en platinum group elemente bevat gewoonlik ander elemente behalwe Cu, Ni en S in klein hoeveelhede. Van al die ander elemente het Fe waarskynlik die grootste effek op die fasediagram, veral wanneer dit voorkom in konsentrasies hoër as die tipiese ~3wt%. Die moontlike effek van Fe op die fasediagram word bespreek. Dit is egter redelik om te aanvaar dat die Cu-Ni-S sisteem die matsamestelling verteenwoordig. Die Cu-Ni-S fasediagram kon dus gebruik word om die kristalliseeringspaaie van stadig afgekoelde mat te beskryf. Daar is tot die gevolgtrekking gekom dat die fasesegregasie wat waargeneem is in stadig afgekoelde gietstukke (Sproule

et al., 1960) die gevolg is van die kristallisasie van vroegvormende, hoë temperatuur Cu_2S in die boonste gedeelte van die gietstuk, met die gevolg dat die vloeistof fraksioneer na meer Ni_3S_2- en alooi-ryk in die onderste gedeelte van die gietstuk.

Verder het dit geblyk dat die swawel-inhoud van die mat kritiek is vir die volgorde, en die vormingstemperatuur van kristalliserende fases, sowel as die hoeveelheid Cu-Ni allooi wat vorm. 'n Effense verhoging van ~1 gewigs % in die swawel-inhoud van die mat in die omgewing vanaf 18 tot 22 gewigs % kan 'n verskeidenheid van kristalliseringsvolgordes tot gevolg hê. Daar is 'n kritieke swawel-inhoud by ongeveer 21 gewigs % wat afhang van die presiese samestelling van die Cu_2S-tipe phase, die eutektiese punt en die aanvanklike Cu/Ni verhouding van die monster. By die kritieke swawel-inhoud word beide Ni_3S_2 en allooi eers by die eutektiese punt gekristalliseer. Indien die swawel-inhoud hoër is, vorm Cu_2S eerste gevolg deur Ni_3S_2, en allooi vorm eers by die eutektiese punt. Met laer swawel-inhoude kristalliseer Cu_2S eerste, gevolg deur allooi, terwyl Ni_3S_2 eers by die eutektiese punt kristalliseer. Met nog laer swawel-inhoude vorm alloy eerste, gevolg deur Cu_2S terwyl Ni_3S_2 eers by die eutektiese punt kristalliseer.

Hierdie verskillende kristalliseringsvolgordes en kristalliserings temperature kan 'n belangrike invloed hê op die diffusie van platinum groep elemente in die vormende fases, sowel as die tekstuur van 'n statig afgekoelde mat.

INDEX

LIST OF TABLES:

LIST OF FIGURES:

Please note that the ternary diagrams can become distorted during photocopying, especially when enlarging and reducing the diagrams.

LIST OF PHOTOMICROGRAPHS:

LIST OF ABBREVIATIONS

Liquid fields:

L_1 = Sulphur liquid containing approximately 1 wt% Cu and Ni.
L_2 = Immiscible copper sulphide-rich liquid.
L_3 = Immiscible metal-rich liquid.
$L_{(2,3)}$ = Homogeneous liquid field forming a eutectic at approximately 575°C (Sproule *et al.*, 1960) for $\mu+\theta+\alpha$.
L_4 = Liquid field that separates from the $L_{(2,3)}$ field and exists around 800°C.
L_5 = Liquid field that separates from the $L_{(2,3)}$ field and exists just above 700°C.

For the sake of consistency, the abbreviations for liquid fields found in the ternary system are used for all binary and pseudo-binary systems as well, even if determined by other investigators.

Mineral phases:

Mineral names, symbols, and chemical formulae for synthetic substances are used throughout the text.

δ = $Cu_{1.8}S$ digenite
μ = $Cu_{2-x}S$ (HT) digenite
β = Cu_2S (LT) chalcocite
γ = Cu_2S (MT) chalcocite
ν = $Cu_{1.96}S$ djurleite
ε = CuS covellite
π = Ni_3S_2 (LT) heazlewoodite
θ = $Ni_{3\pm x}S_2$ (HT) heazlewoodite. According to Lin *et al.* (1978) the high temperature $Ni_{3\pm x}S_2$ phase field does not consist of only one phase as was previously reported by Craig and Scott (1974), but it can instead be subdivided into two different phases fields. It was not possible to distinguish between the two phases in this investigation. For this reason, the symbol θ is used to represent both the high- and low-sulphur high temperature heazlewoodite phases in the encompassing $Ni_{3\pm x}S_2$ (θ) phase. Where it is possible to distinguish between the two phases, i.e. when encountered in the literature, the individual fields are labelled with the symbols θ_1 ($Ni_{3-x}S_2$) and θ_2 (Ni_4S_3).
ω = Ni_7S_6 (LT) godlevskite
φ = Ni_7S_6 (HT)
σ = NiS (LT) millerite
λ = $Ni_{1-x}S$ (HT)
κ = Ni_3S_4 polydymite
η = NiS_2 vaesite
T_1 = $CuNi_2S_6$ villamaninite
α = Cu-Ni alloy solid solution
An = $Cu_{1.75}S$ anilite
\+ = Phase assemblages are noted with a '+' between co-existing phases (e.g. liquid + alloy) refers to the field where these phases co-exist.

HT, MT, and LT refers to high, medium, and low temperature phase forms.

Most abbreviations of the mineral phases present in the system were taken from Chang *et al.* (1979).

General abbreviations:

μm = micrometer
SEM = Scanning Electron Microscope (EDS = Energy Dispersive Spectrometry)
EMP = Electron Microprobe (WDS = Wavelength Dispersive Spectrometry)
PGE = platinum group element
PGM = platinum group mineral
DTA = Differential Thermal Analysis
no = number

CHAPTER 1

INTRODUCTION

The applications for experimentally determined phase diagrams of the Cu-Ni-S system are discussed as motivation for the study. An overview of relevant literature is given.

---

1. INTRODUCTION

1.1 AIM OF THIS STUDY

The phase diagram of the system Cu-Ni-S can serve as a basis for quaternary diagrams such as the Cu-Fe-Ni-S system, where it has applications in the ore forming processes of Cu and Ni ores. It will probably be used most extensively for the beneficiation processes of Cu, Ni, and platinum group elements (PGEs). The Cu-Ni-S phase diagram will be useful as an approximation of converter matte composition, and especially for interpretation of the crystallisation paths that slow-cooled matte can follow.

The aim of the study was an experimental investigation of the Cu-Ni-S system from 1200°C to 700°C at 100°C intervals, in order to establish the phase relations, phase boundaries, and the relevant tie-lines between co-existing phases.

The binary (Cu-S, Ni-S and Cu-Ni) and the pseudo-binary (Cu_2S - Ni_3S_2) systems have been studied by various investigators. Because of its applications in Cu beneficiation, the immiscible liquid field in the system Cu-Ni-S at 1200°C has been investigated in detail. The existing isothermal sections of the system Cu-Ni-S at 1200°C, 780°C, 600°C, 500°C, and lower temperatures by Kullerud *et al.* (1969) are only schematic and some have been shown to be erroneous (Arnold and Malik, 1975).

There are, however, no published phase diagrams of the ternary system available in the temperature range between 1200°C to 780°C. Since the temperature range of importance for the crystallisation of slow-cooled matte is from 1200°C to 700°C, the determination of phase relations in this temperature interval is important.

1.2 APPLICATIONS

The most important application for the Cu-Ni-S phase diagram is in the converting of base-metal mattes. An understanding of the phase relations is of great importance for the beneficiation processes of Cu and Ni, and of platinum group elements (PGEs). The system Cu-Ni-S as such does not have many applications in natural geological settings, since all natural occurrences of Cu and Ni ores are accompanied by the ubiquitous, chalcophile element Fe. There are, however, exceptions like the Fe-depleted sulphides in chromites of the Bushveld Complex (Von Grunewald *et al.*, 1986; Merkle, 1992). In order to provide a better understanding of ore forming processes in a variety of geological settings (for example natural Cu-Ni deposits such as Sudbury and Nsizwa), knowledge of the quaternary Cu-Fe-Ni-S system is necessary. It is in this respect that the ternary Cu-Ni-S system will be very valuable, as it is indispensable as a basis for investigations of related quaternary systems.

1.2.1 BENEFICIATION OF PGEs FROM SULPHIDE ORE

The treatment of PGE-containing sulphide ores is very similar to that of Cu-Ni sulphide ores. Possible routes for PGE beneficiation are illustrated in Figure 1. Milled ore first goes through flotation to concentrate most PGEs, and to separate the silicate and sulphide fractions. The sulphide fraction is then melted in a furnace to produce two immiscible liquids, the lighter being slag (silicate melt) and the heavier being matte (sulphide melt). This furnace matte is converted, and in the process the Fe is oxidised, and reacts with the added SiO_2 to form fayalite (Fe_2SiO_4) slag. Some of the sulphur is lost during conversion and it is emitted as SO_2. Converter matte contains Cu, Ni, S, as well as small amounts of Fe and Co, and trace amounts of PGEs.

After conversion there are different possible routes that the matte can follow: the entire matte can either be leached chemically; or it can be cooled slowly before chemical treatment. Slow cooling concentrates the PGEs in a magnetic Cu-Ni alloy. The magnetic, alloy-rich, fraction containing most of the PGEs, is treated separately from the non-magnetic sulphide fraction. The

aim of slow cooling is to reduce the amount of material that must be chemically treated to unlock the PGEs, thus saving time and money.

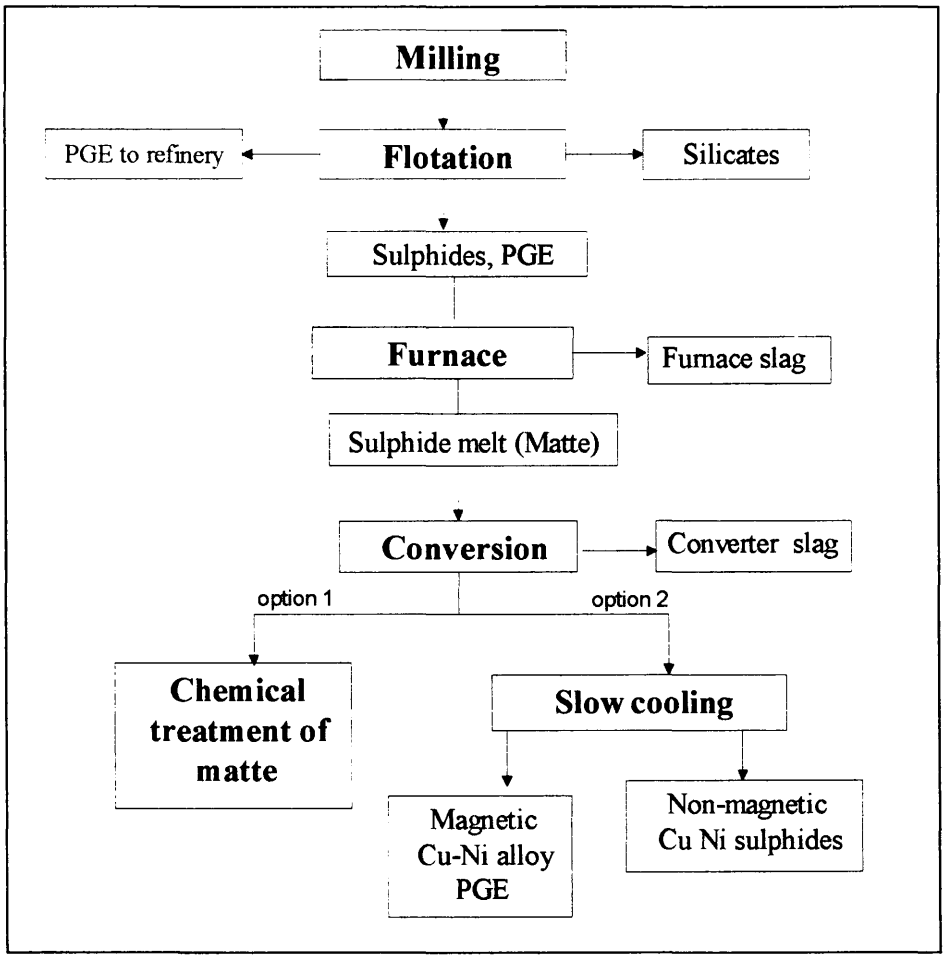

Figure 1. Simplified flow sheet showing two possible routes for PGE beneficiation from sulphide ores. Converter matte can either be directly treated chemically, or cooled slowly to collect PGEs in the magnetic alloy before chemical treatment.

1.2.2 BENEFICIATION OF Cu- AND Ni-SULPHIDE ORES

Conversion is a commonly used pyro-metallurgical process for the treatment of Cu and Ni matte. During this process, SO_2 gas can be recovered for the manufacture of sulphuric acid. There are, however, problems associated with the recovery of sulphur from the conversion step (Cooper, 1984). As an alternative to conversion, direct electro-refining of Cu and Ni has been studied for many years. The benefit of direct electro-refining is that elemental metals and sulphur are

produced directly. A commercial electro-refining plant for Ni exists, but there have been only unsuccessful attempts in the electro-refining of copper matte. McKay (1993) discusses the problems associated with the process, which are mainly due to the fact that copper sulphide ($Cu_{2-x}S$) does not decompose directly to form Cu and S. Instead it forms intermediate copper sulphide phases in the following sequence: Djurleite ($Cu_{1.96}S$), digenite ($Cu_{1.76-1.83}S$), blue-remaining covelite ($Cu_{1.1}S$), and covelite (CuS). Each of the intermediate phases has a different electrochemical behaviour, and this leads to complications during electro-refining. After many years of research, conversion is still the most widely used process for Cu- and Ni-beneficiation.

1.3 PREVIOUS INVESTIGATIONS OF THE SYSTEM Cu-Ni-S

Phase relations in the binary systems Ni-S, Cu-S, and Cu-Ni have been reported by numerous investigators. There have also been some studies in the pseudo-binary systems Cu_2S - Ni_3S_2. Some parts of the ternary system Cu-Ni-S have also been investigated. The available information from the literature is summarised briefly.

1.3.1 THE Ni-S SYSTEM

1.3.1.1 PHASE RELATIONS AND THERMODYNAMIC PROPERTIES

Phase relations of the Ni-S system were reported by, amongst others, Massalski (1986), and Kullerud and Yund (1962). Arnold and Malik (1975) concentrated on phase relations in the high sulphur region NiS-S. Most parts of the binary Ni-S phase diagram are known and the phase diagram has been investigated in detail. However, there are some differences between the phase diagrams determined by different researchers. For example, the formation temperature of $Ni_{1-x}S$ HT (λ) according to Lin *et al.* (1978) (Figure 2) differs slightly from that given by and Craig and Scott, (1974) (Figure 3). The diagram by Lin *et al.* (1978) (Figure 2) also indicates the two non-stoichiometric phases in the $Ni_{3\pm x}S_2$ (θ) phase field. Figure 2 is the more recent and it is used when referring to the binary Ni-S system.

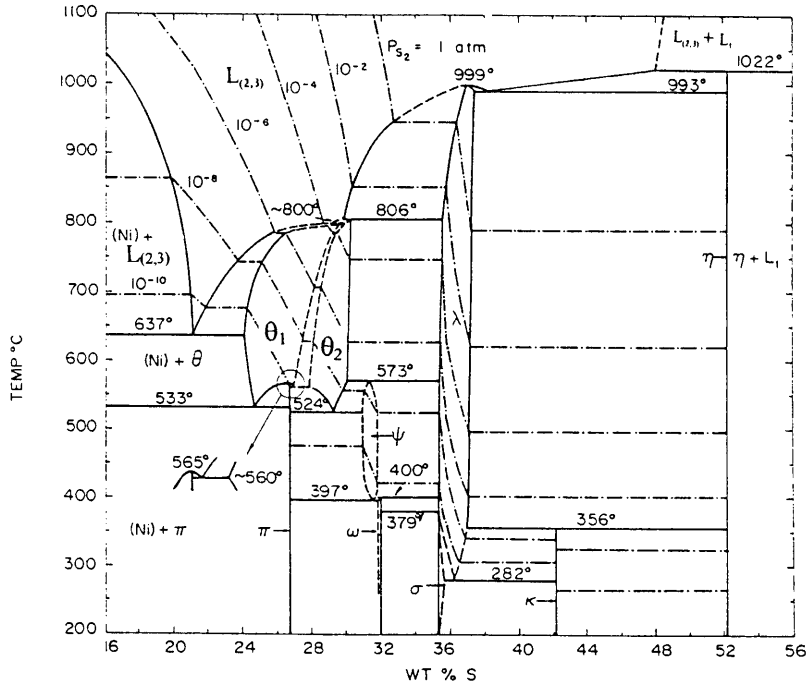

Figure 2. Ni-S phase diagram (Lin et al.*, 1978).*

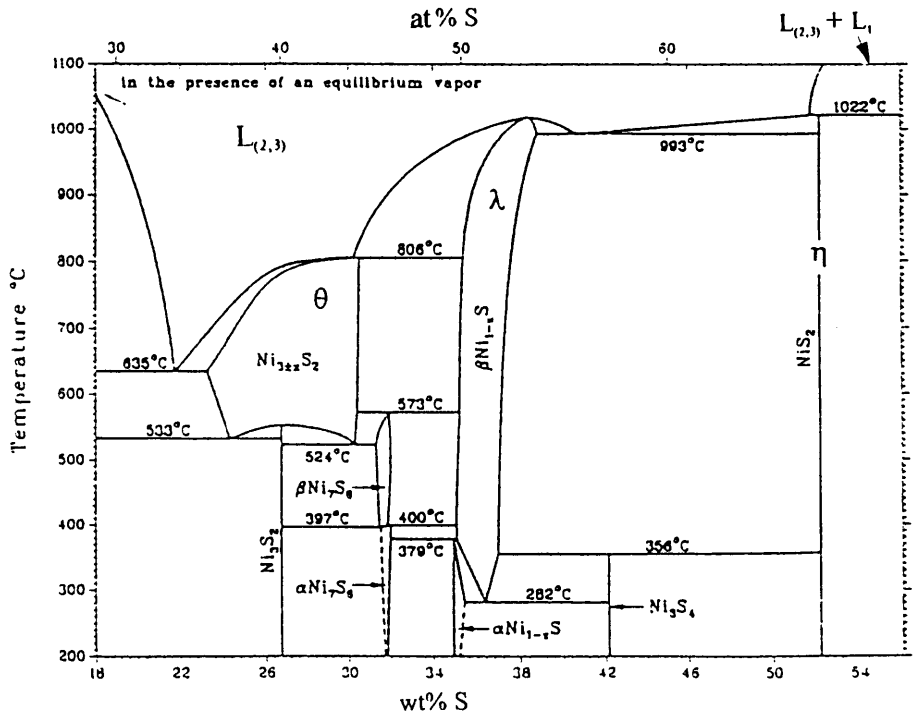

Figure 3. Ni-S phase diagram (Craig and Scott, 1974).

Problems encountered in the development of a converter process for the direct conversion of molten nickel-sulphide to metallic nickel led to studies of the thermodynamic properties of the Ni-S system: Lin *et al.* (1978) determined the activity of sulphur from 550°C to 750°C in a range of nickel sulphide minerals, and used their experimental results in combination with data obtained in the literature to calculate thermodynamic equations of state (Gibbs energy of formation) for all the intermediate nickel sulphide phases. Their extensive work in the high temperature heazlewoodite phase field led to the discovery that the field that was previously thought to contain only one phase ($Ni_{3-x}S_2$, shown as θ in Figure 3) consists of two non-stoichiometric phases, designated by Lin *et al.* (1978) as Ni_3S_2 and Ni_4S_3 (θ_1 and θ_2 respectively in Figure 2). The α function of sulphur [$\alpha_s = \ln \gamma_s/(1-x_S)^2$] is shown as a function of composition in the $Ni_{3\pm x}S_2$ field in Figure 4 (Lin *et al.*, 1978). The agreement between the results of Rau (1976) and Lin *et al.* (1978) is illustrated in Figure 4.

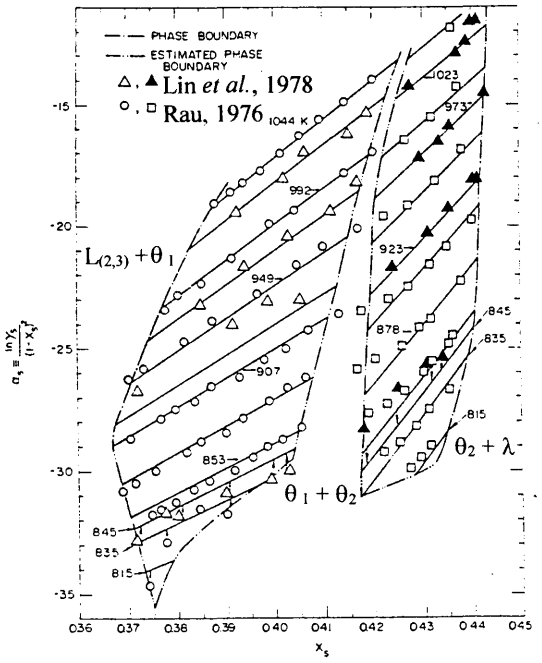

Figure 4. The subdivision of the high temperature $Ni_{3\pm x}S_2$ phase field into the phases Ni_3S_2 (θ_1) and Ni_4S_3 (θ_2). The α function of sulphur is shown as a function of composition for the two phases (Lin et al., *1978).*

Meyer *et al.* (1975) determined the partial pressure of sulphur vapour over Ni-S melts and used a mathematical model to correlate the obtained data with published p_{S2} data for lower temperatures. The calculated regression line for the phase boundary between liquid and liquid + Ni in the Ni-S system (Figure 5) was obtained from direct determinations of the melt composition combined with published phase boundary determinations by Bornemann (1908, 1910), Elliot (1965), and Nagmori and Ingraham (1970).

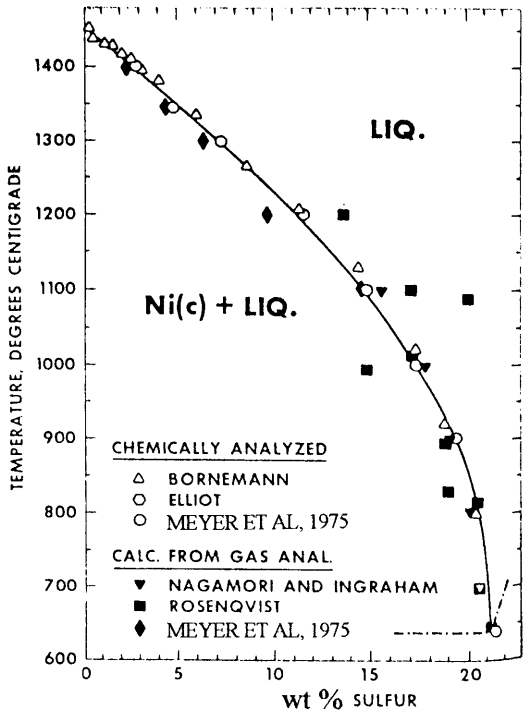

Figure 5. The boundary between liquid and Ni + liquid in the system Ni-S as determined by different investigators (summarised by Meyer et al., 1975).

Sharma and Chang (1980) described the thermodynamic properties of the liquid Ni-S phase with an associated solution model. Cemic and Kleppa (1986) determined the standard entalphies of formation of various intermediate nickel sulphides. They also investigated the thermodynamic properties of molten sulphides, and determined sulphur partial pressures (p_{S2}) from 1100°C to 1600°C over a compositional range from 0 to 27 wt% S. Nagamori and Ingraham (1970) determined the p_{S2} in the system Ni-S from 800°C to 1100°C, while Rosenqvist (1954) determined the p_{S2} in the temperature range from 800° to 1000°C.

1.3.1.2 PHASE STABILITY RANGES AND PHYSICAL PROPERTIES

The various intermediate nickel sulphide phases, with their symbols, and temperature ranges are listed in Table 1. Most of the symbols and mineral names are from Chang *et al.* (1979), and the stability ranges of the nickel sulphides are from the binary Ni-S phase diagram (Lin *et al.*, 1978) (Figure 2).

Table 1. Stability ranges of phases in the Ni-S system (Lin et al., *1978).*

Symbol	Formula	Name of natural mineral	Thermal stability range °C
π	Ni_3S_2 (LT)	heazlewoodite	<565
θ_1	$Ni_{3\pm x}S_2$ (HT)	-	533 to ~806
θ_2	Ni_4S_3 (HT)	-	524 to ~806
ω	βNi_7S_6(LT)	godlevskite	<400 ±2
φ	αNi_6S_5 (HT)	-	397 to 573
σ	NiS (LT)	millerite	<379
λ	$Ni_{1-x}S$(HT)	-	282 to 999
κ	Ni_3S_4	polydymite	<356
η	NiS_2	vaesite	<1022±3

From Figure 2 (Lin *et al.*, 1978) it can be seen that the stoichiometric, low temperature, Ni_3S_2 phase (π) is stable up to 565°C, above which it transforms to the high temperature, non-stoichiometric $Ni_{3\pm x}S_2$ phase (θ_1). The lower limits of stability of the heazlewoodite-type phases are composition dependent, with $Ni_{3\pm x}S_2$ (θ_1) being stable to 533°C, and Ni_4S_3 (θ_2) to 524°C, while the upper thermal stability limit is ~806°C (Lin *et al.*, 1978).

The physical properties of heazlewoodite were investigated by Liné and Huber (1963) using radiocrystallographic techniques. Metcalf *et al.* (1993) measured the electrical resistivity, magnetic susceptibility and the heat capacity of single crystals of heazlewoodite below room temperature, and found it to be a good metallic conductor.

1.3.2 THE Cu-S SYSTEM

1.3.2.1 PHASE RELATIONS

Phase relations of the system Cu-S have been reported by various investigators, such as Schlitt and Richards (1973), Kellogg (1969), Cook (1972), Flamini *et al.* (1973), Morimoto and Gyobu (1971), and Kullerud (1960). The phase relations in the Cu-S system were summarised by Massalski (1986) (Figure 6). Detail of the Cu_2S phase field is shown in Figure 7.

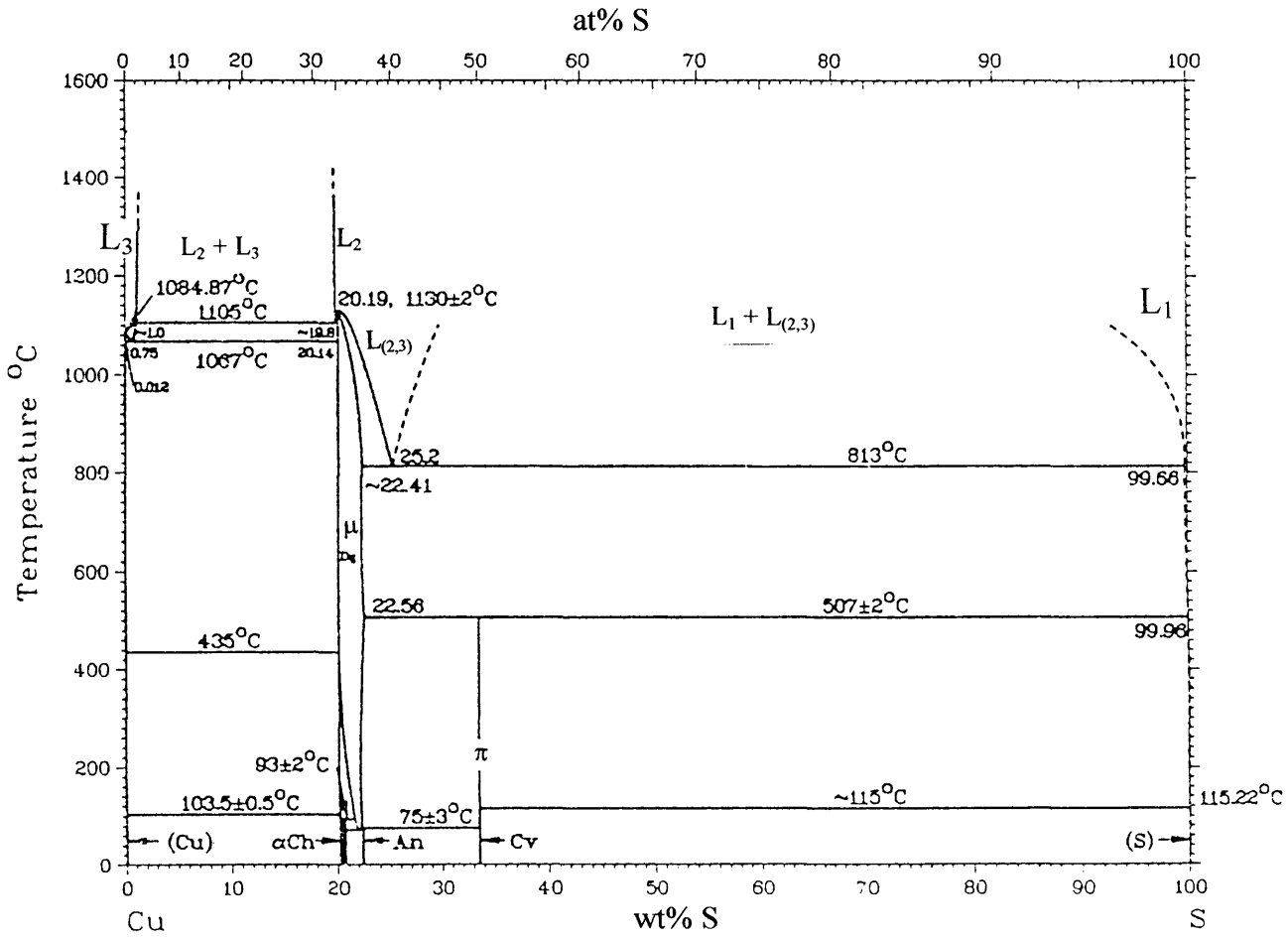

Figure 6. Cu-S phase diagram (Massalski, 1986). The liquid fields are labelled to be consisted with the ternary Cu-Ni-S phase diagram of this investigation.

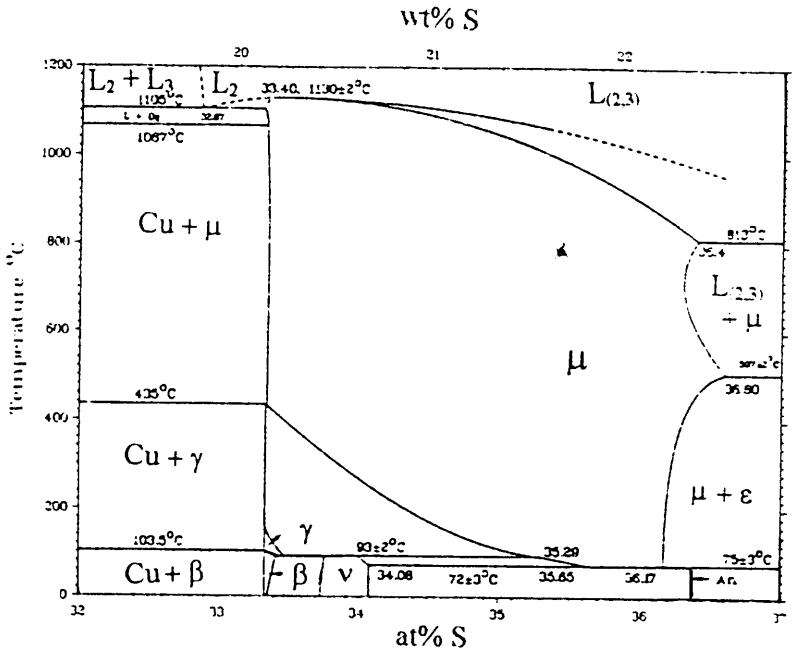

Figure 7. Enlarged portion of the Cu-S phase diagram showing the Cu_2S phase field (Massalski, 1986). The liquid fields are labelled to be consisted with the ternary Cu-Ni-S phase diagram of this investigation.

1.3.2.2 PHASE STABILITY RANGES

The stability ranges for intermediate sulphide phases in the Cu-S system (Massalski, 1986) are presented in Table 2.

Table 2. Stability ranges of phases in the Cu-S system (Massalski, 1986).

Symbol	Formula	Name of natural mineral	Thermal stability range °C
μ	$Cu_{2-x}S$ (HT)	digenite	75± 3 to 1130 ± 2
γ	β Cu_2S (MT)	chalcocite (high)	103.5 ± 0.5 to 435
β	α Cu_2S (LT)	chalcocite (low)	<103.5 ± 0.5
ν	$Cu_{1.96}S$	djurleite	< 93 ± 2
ε	CuS	covellite	<507 ± 2
An	$Cu_{1.75}S$	anilite	<75± 3

1.3.3 THE Cu-Ni SYSTEM

There is complete solid solution between Cu and Ni at high temperatures as shown in Figure 8 (Massalski, 1986).

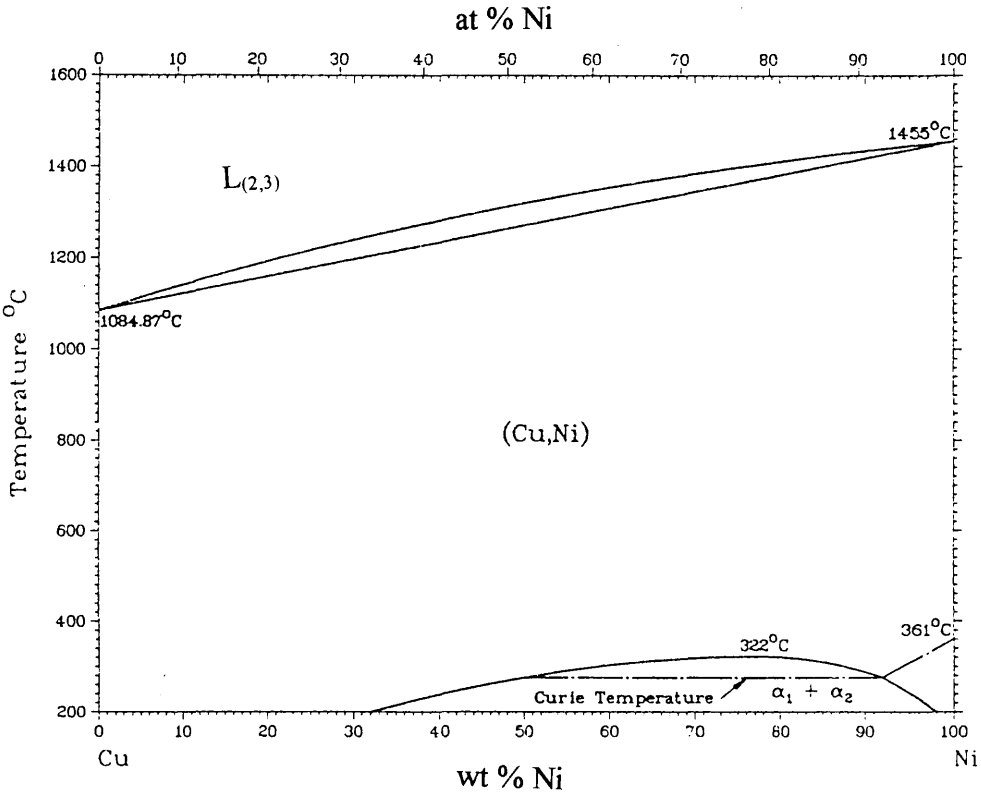

Figure 8. The Cu-Ni phase diagram (Massalski, 1986). The liquid fields are labelled to be consisted with the ternary Cu-Ni-S phase diagram of this investigation.

1.3.4 PSEUDO-BINARY SYSTEMS

1.3.4.1 THE Cu_2S-Ni_3S_2 SYSTEM

The Cu_2S-Ni_3S_2 pseudo-binary system was investigated by various researchers. For comparison of their findings, some of the phase diagrams are presented here. The diagram by Hayward (1915) is shown in Figure 9. The investigation by Köster and Mulfinger (1940) includes the phase diagram of the Cu_2S-Ni_3S_2 pseudo-binary system (Figure 10), as well as crystallisation curves for the sulphur deficient portion below the Cu_2S-Ni_3S_2 tie-line of the Cu-Ni-S system. The phase diagram by Chang *et al.* (1979; Figure 11) is based on the diagram by Köster and Mulfinger (1940). It is not clear where the pseudo-binary diagram in Sproule *et al.* (1960) (Figure 12) originates from, but it seems to be based on the diagram by Hayward (1915). Other investigations in the pseudo-binary system were by Chizhikov *et al.* (1975), Friedrich (1914), and Stansfield and Faith (1924).

The eutectic temperature determined by the different investigators varies considerably. Hayward (1915) and Sproule *et al.* (1960) reported the eutectic of the Cu_2S-Ni_3S_2 pseudo-binary system at 720°C, (Figures 9 and 12) while Köster and Mulfinger (1940) and Chang *et al.* (1979) depict it at 705°C (Figures 10, and 11).

1.3.4.2 THE Cu_2S - NiS SYSTEM

Using DTA, Craig and Kullerud (1969) found a thermal event at 730°C - 731°C in a single experiment in the pseudo-binary Cu_2S-NiS system. The composition of the sample was Cu_2S-NiS in a ratio of 1:1 and the effect was attributed to melting (Craig and Kullerud, 1969).

1.3.4.3 THE Cu_2S-NiS_2 SYSTEM

Craig and Kullerud (1969) also performed a single DTA experiment in the pseudo-binary Cu_2S-NiS_2 system and found a thermal event at 788 - 791°C. The composition of the sample was Cu_2S- NiS_2 in a ratio of 1:1 and the effect was attributed to melting (Craig and Kullerud, 1969). These DTA results from Craig and Kullerud (1969) are given in section 1.3.5.4.

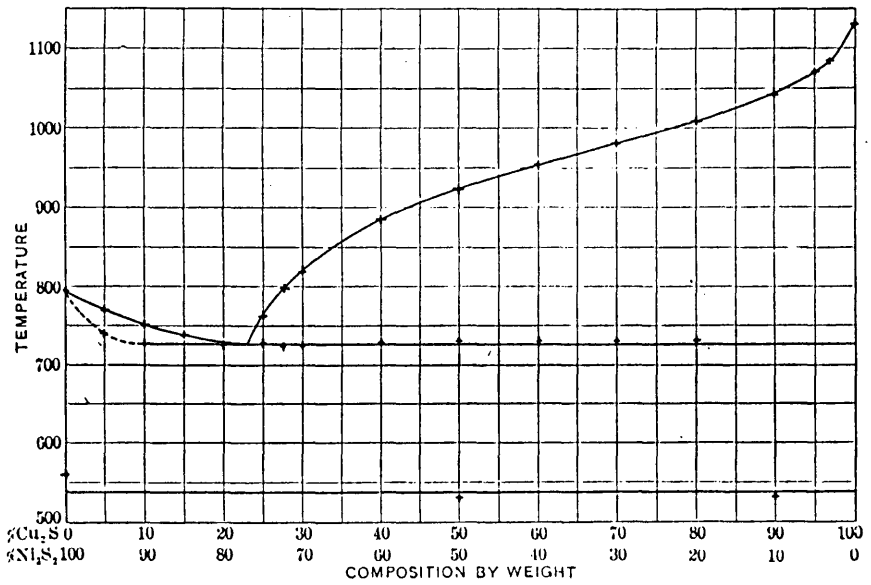

Figure 9. The pseudo-binary system Cu_2S-Ni_3S_2 (Hayward, 1915).

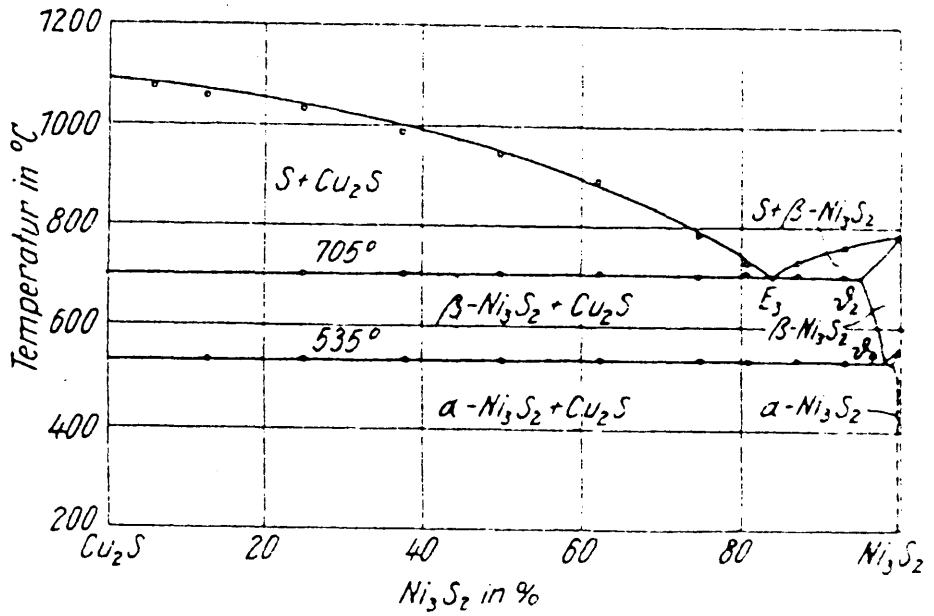

Figure 10. The pseudo-binary system Cu_2S-Ni_3S_2 (Köster and Mulfinger, 1940).

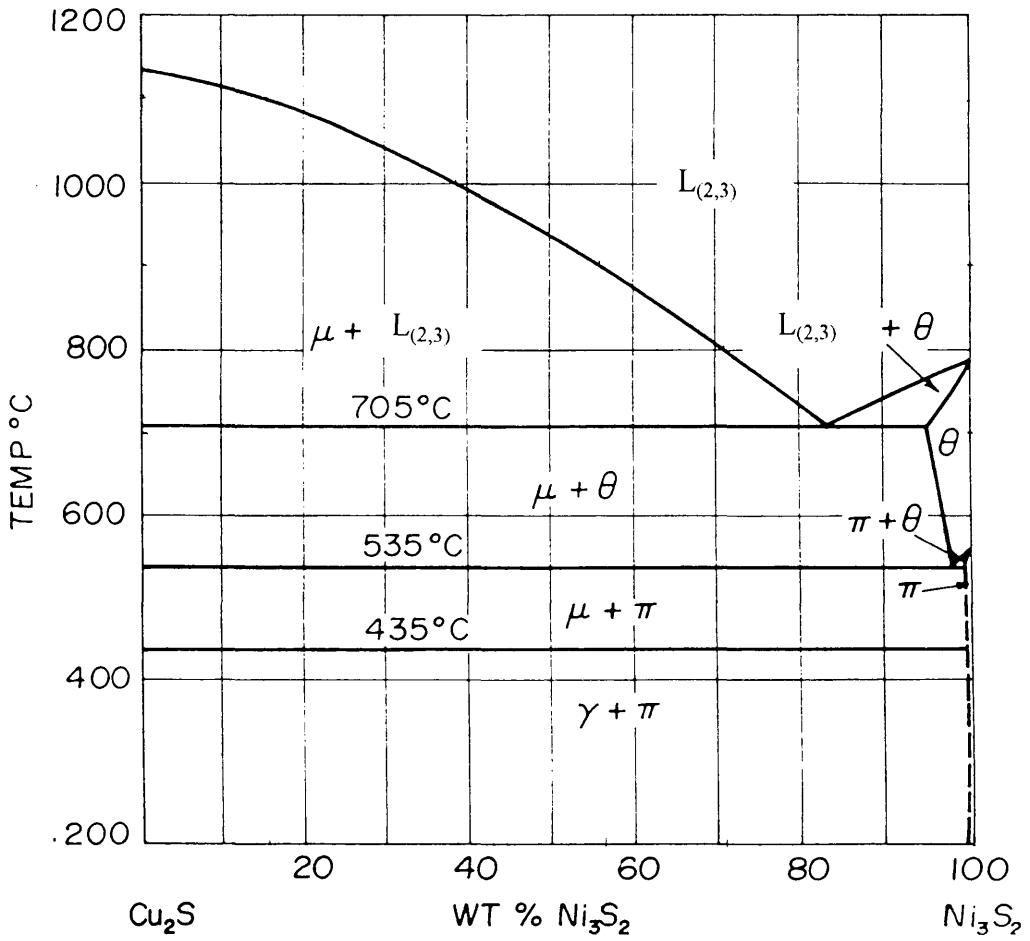

Figure 11. The pseudo-binary system Cu_2S - Ni_3S_2 (Chang et al., *1979, based on Köster and Mulfinger, 1940). The liquid fields are labelled to be consisted with the ternary Cu-Ni-S phase diagram of this investigation.*

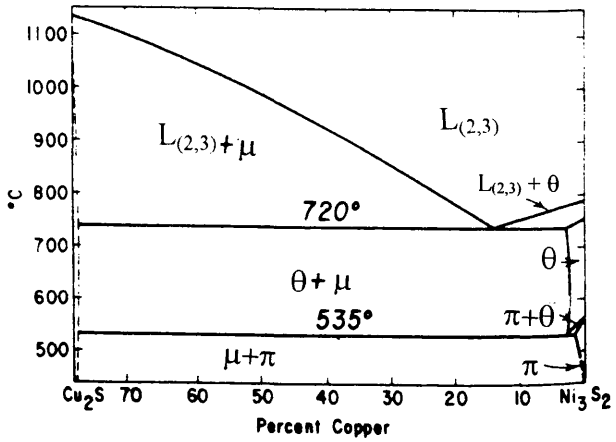

Figure 12. The pseudo-binary system Cu_2S-Ni_3S_2 (reported by Sproule et al., *1960). The liquid fields are labelled to be consisted with the ternary Cu-Ni-S phase diagram of this investigation.*

1.3.5 TERNARY SYSTEM Cu-Ni-S

Investigations in the ternary Cu-Ni-S system span several decades, from the DTA experiments on the Cu_2S-Ni_3S_2 system by Hayward in 1915 to the thermodynamic associated solution model by Chuang and Chang in 1982. Most investigations only focused on portions of the Cu-Ni-S phase diagram.

1.3.5.1 IMMISCIBLE LIQUID FIELD ($L_2 + L_3$)

Because of its importance for Cu beneficiation, many researchers determined the extent of, and the tie-lines in, the immiscible two-liquid field ($L_2 + L_3$) on the Cu-rich side of the Cu-Ni-S phase diagram:

i) Köster and Mulfinger (1940) used thermal analysis during cooling, and chemical analysis of the melts which solidified in two layers.
ii) Asano and Ichio (1962) determined the extent of the immiscible liquid field ($L_2 + L_3$) at 1200°C. They used evacuated quartz-glass tubes, with 5 g samples that were cooled in air. The samples were then separated for analysis.
iii) Schlitt *et al.* (1973) published their findings on the immiscible liquid field ($L_2 + L_3$) at 1200°C. The phases were equilibrated under nitrogen and the two liquid layers were sampled at the working temperature, and analysed *in toto*.
iv) Lee *et al.* (1980) investigated the immiscible liquid field ($L_2 + L_3$) at 1400°C and 1200°C.The technique employed by Lee *et al.* (1980) involved equilibration of alloy in an atmosphere of hydrogen sulphide and hydrogen. The two immiscible liquids were sampled at 1200°C, water-quenched and analysed. Sulphur was analysed with a direct combustion method, and Cu and Ni by electro-deposition.
v) Chuang and Chang (1982) investigated the extent of the immiscible liquid field ($L_2 + L_3$) at 1200°C and 1400°C by calculating a mathematical model.

The experimental and calculated tie-lines at 1200°C from various previous studies are presented in Figure 13 (Chuang and Chang, 1982) and Figure 14 (Schlitt *et al.*, 1973). The differences between the results from the various investigators probably stems from differences in the experimental procedures.

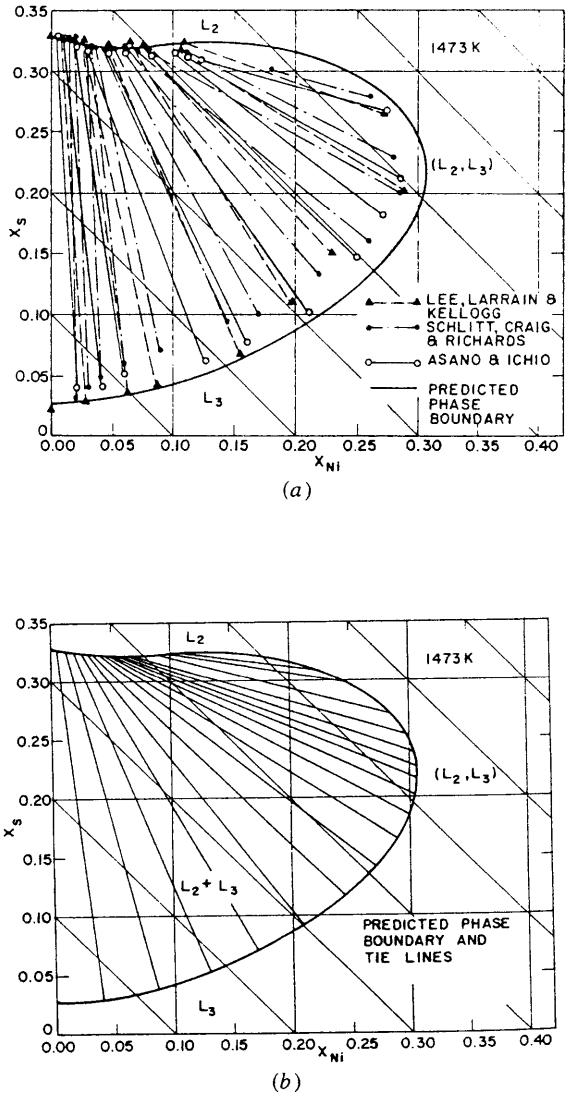

Figure 13. Portion of the 1200°C isothermal section of the system Cu-Ni-S with a) experimentally determined and b) calculated phase boundaries and tie-lines in the immiscible liquid field (Chuang and Chang, 1982).

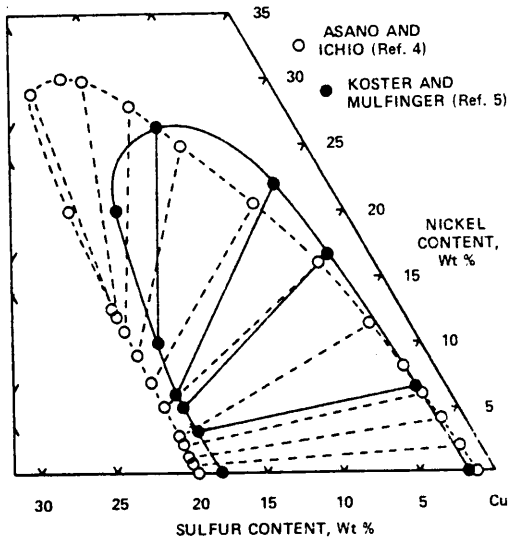

Figure 14. Portion of the 1200°C isothermal section of the system Cu-Ni-S comparing different investigations of the immiscible liquid field (Schlitt et al., *1973).*

1.3.5.2 THE Cu_2S-Ni_3S_2-ALLOY PORTION OF THE PHASE DIAGRAM

Köster and Mulfinger (1940), and Sproule *et al.* (1960) reported experimental findings in the sulphur-depleted portion of the Cu-Ni-S phase diagram. The crystallisation curves leading to the ternary eutectic point for the Cu_2S-Ni_3S_2-alloy part of the system of these two investigations are reproduced in Figures 15 and 16 respectively.

The eutectic temperature, the eutectic composition, and the composition of the eutectic alloy phase are given in Table 3 (please note that Sproule *et al.*, 1960, only specified the Cu content of the eutectic point).

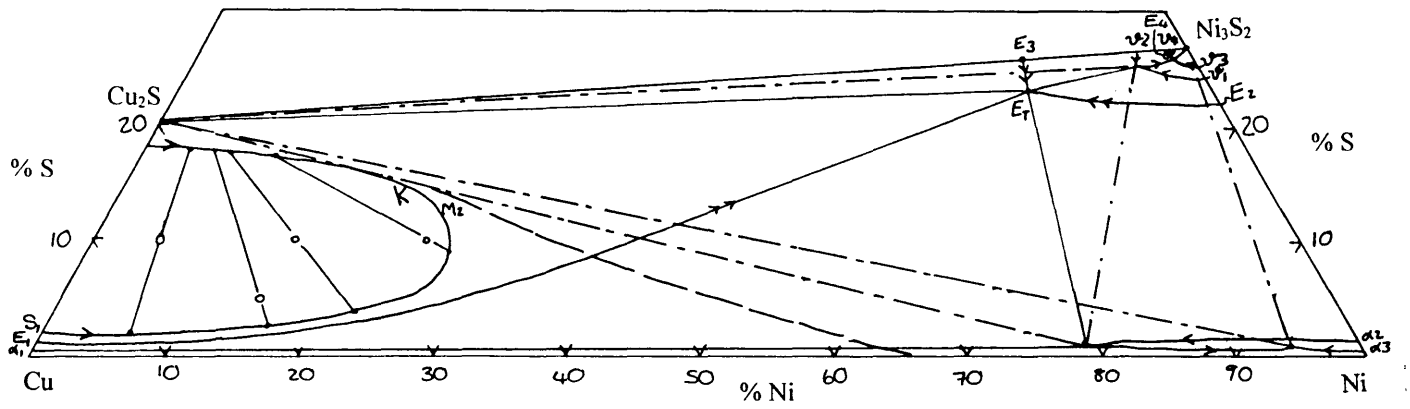

Figure 15. Portion of the ternary Cu-Ni-S phase diagram (from Köster and Mulfinger, 1940). Crystallisation paths leading to the ternary eutectic point E_T in the S-depleted portion of the diagram are shown. The point E_3 is the eutectic point for the pseudo-binary system Cu_2S-Ni_3S_2.

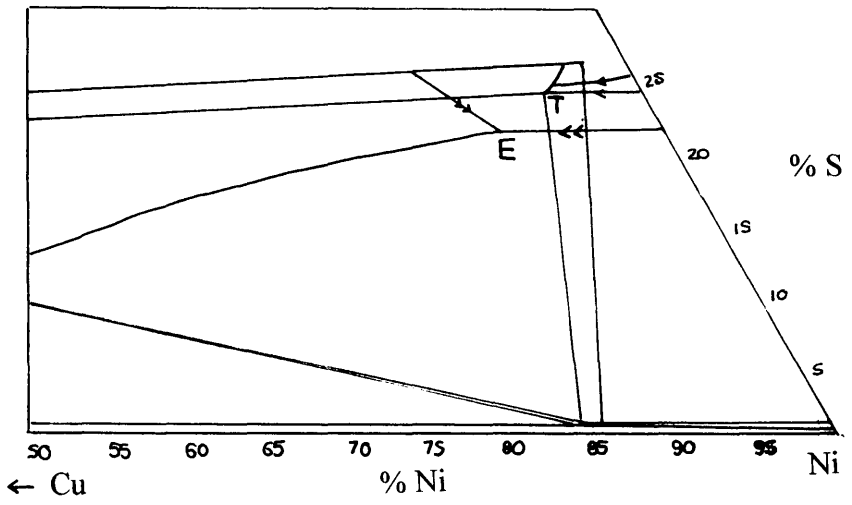

Figure 16. The sulphur-depleted portion of the ternary Cu-Ni-S phase diagram (from Sproule et al., *1960), showing the crystallisation paths which lead to the eutectoid (T) and eutectic (E) points.*

Table 3. Comparison of the composition (in wt%) of the $L_{(2,3)}$ ternary eutectic point in the $\mu + \theta + \alpha$ stability triangle, as well as the eutectic alloy composition, as given by various investigators.

		Eutectic			Alloy	
Investigator	***°C***	***Ni***	***S***	***Cu***	***Ni***	***Cu***
Köster and Mulfinger (1940)	580	63	23	14	79	21
Kullerud *et al.* (1969)	572±5	67	21	12		
Sproule *et al.* (1960)	575	-	-	10	80	20

1.3.5.3 ISOTHERMAL SECTIONS

Isothermal sections of the Cu-Ni-S system were investigated by one group of researchers:

i) Moh and Kullerud (1963) investigated the low temperature phase relations at 600°C, 500°C and 400°C,

ii) Moh and Kullerud (1964) reported preliminary data at 200°C and 100°C,

iii) Moh and Kullerud (1982) investigated the low temperature phase relations at 200°C and 100°C.

iv) The schematic 1200°C, 780°C, 600°C, and 500°C isothermal sections of the system Cu-Ni-S by Kullerud *et al.* (1969) were redrawn and are shown in Figures 17, 18, 19, and 20. This study was done before the general availability of micro-beam techniques such as the electron microprobe, and the investigators had to rely on microscopic examinations and X-ray techniques. The shape of the immiscible liquid field and the orientation of the tie-lines in the immiscible liquid field in the 1200°C isothermal section by Kullerud *et al.* (1969) (Figure 17) vary considerably from that of the other investigations and are purely schematic. Arnold and Malik (1975) also reported results that were contradictory to the findings of Kullerud and Yund (1962), on which the interpretations of Kullerud *et al.* (1969) were based: Kullerud and Yund (1962) reported the congruent melting of vaesite (NiS_2) at 1007°C, while Arnold and Malik (1975) found that vaesite melts incongruently to a sulphur-rich liquid (L_1) and a sulphide liquid ($L_{(2,3)}$) at 1022 ±3°C.

In Figure 20 the solidus phase diagram is shown at 500°C. Villamaninite ($CuNi_2S_6$), the only ternary component, and chalcocite (CuS) are present at this temperature (Kullerud *et al.*, 1969).

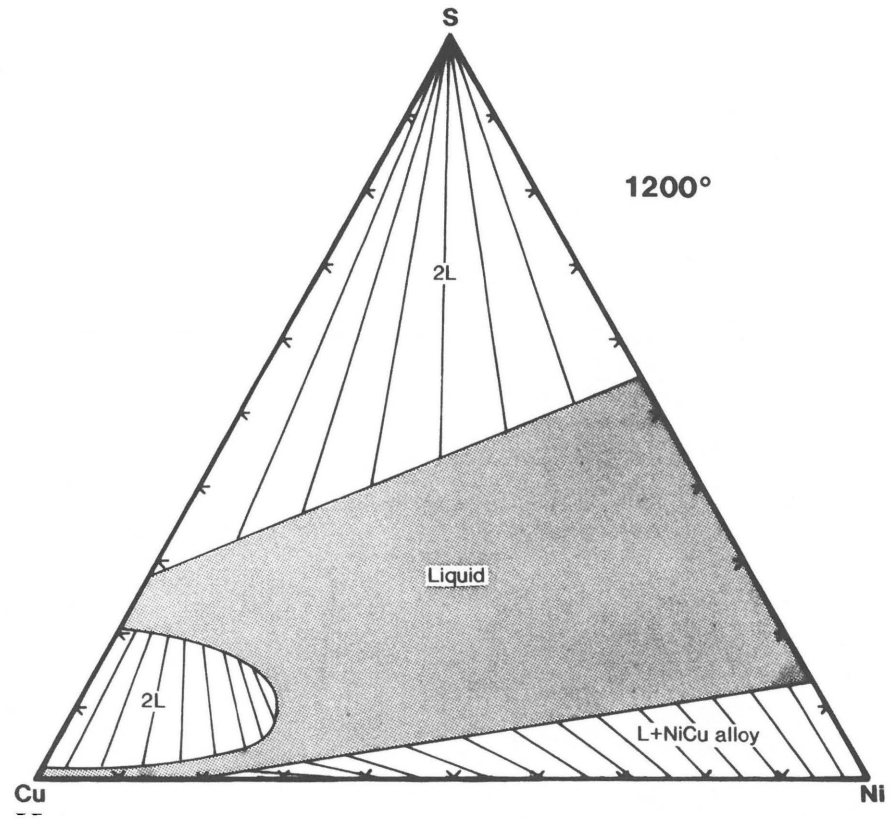

Figure 17. Phase relations in the Cu-Ni-S system at 1200°C (after Kullerud et al., *1969).*

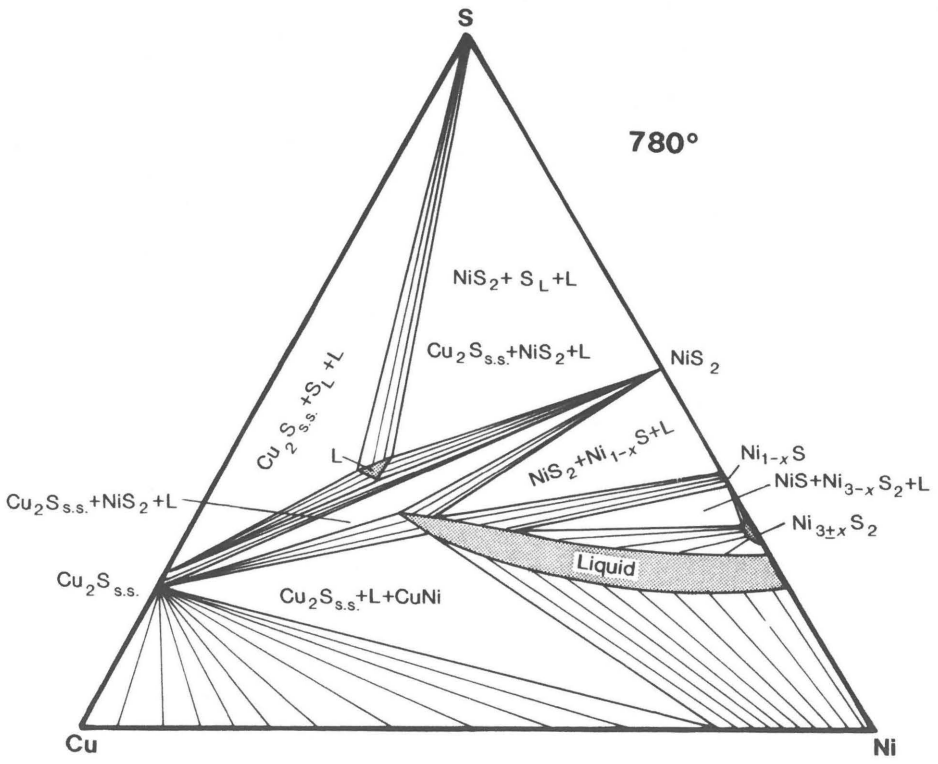

Figure 18. Phase relations in the Cu-Ni-S system at 780°C (after Kullerud et al., *1969).*

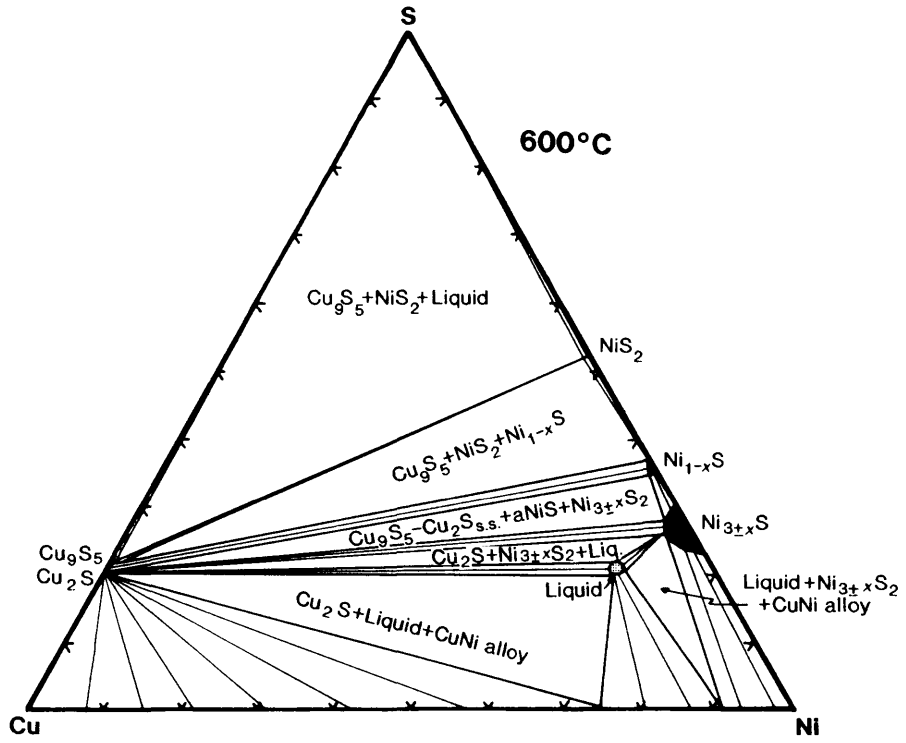

Figure 19. Phase relations in the system Cu-Ni-S at 600 °C (after Kullerud et al., *1969).*

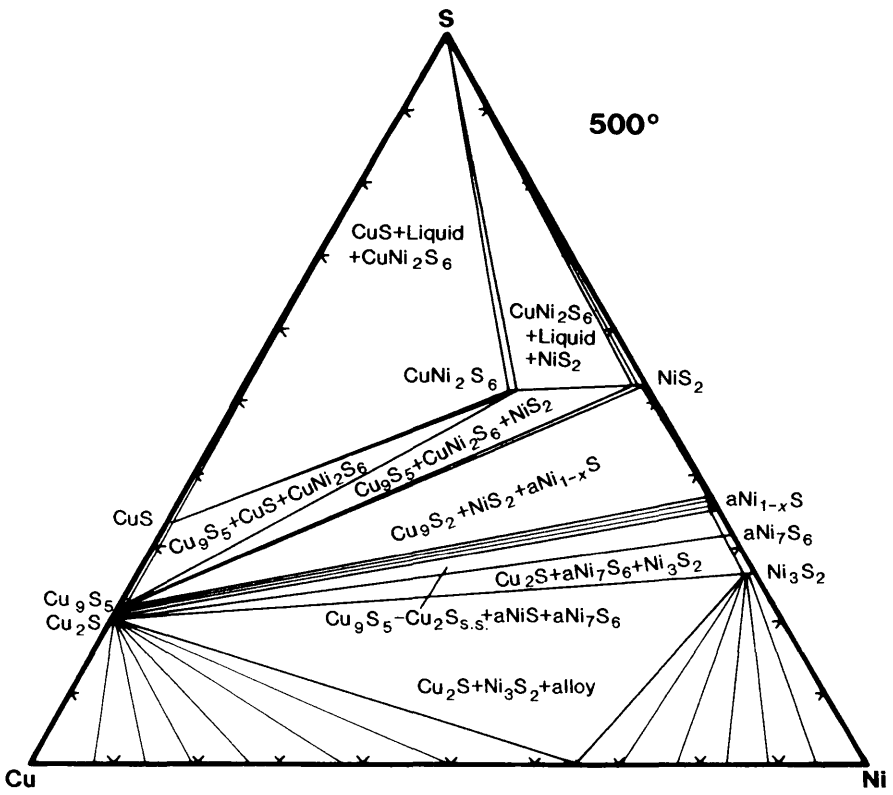

Figure 20. Phase relations in the Cu-Ni-S system at 500°C (after Kullerud et al., *1969).*

1.3.5.4 RELATED SYSTEMS

The majority of investigations in the quaternary Cu-Ni-Fe-S system focus on high iron contents, simulating ore compositions. The Cu-Ni-Fe-S system was studied by, amongst others, Hansen and Anderco (1958), Kullerud (1964), Elliot (1965), and Fleet and Pan (1994). Kushima and Asano (1953) studied the Cu_2S-FeS-Ni_3S_2 pseudo-ternary system. DTA experiments were carried out by Craig and Kullerud (1969), and Chizhikov *et al.* (1975), and their findings are shown in Tables 4 and 5 respectively.

Table 4. Differential Thermal Analyses of experiments by Craig and Kullerud (1969) in the Cu-Fe-Ni-S system.

Composition in wt%				**Temperature in °C**							
				1		**2**		**3**		**4**	
Cu	**Ni**	**S**	**Fe**	**heat**	**cool**	**heat**	**cool**	**heat**	**cool**	**heat**	**cool**
34	4	17	45	499	-					799-809	812
5	5	60	30	469	437	497	501			782	786
5	5	66	24	468	423	490	-			640	629
12	3	65	20			488	427	601	621		
34	4	17	45			499	-			799-809	812
5	5	60	30	469	437	497	501			782	786
5	5	66	24	468	423	490	-	640	629		
12	3	65	20	488	427			601	621		
Cu_5FeS_4=20; $(Fe,Ni)_9S_8$=80						576	576	594	588	837-858	853-840
$CuFeS_{1.8}$=20; $(Fe,Ni)_9S_8$=80						579	586	586	591	850	856
Cu_2S =50; NiS =50						384	-	555	521	730	731
Cu_2S =50; NiS_2 =50										791	788
$CuFeS_{1.92}$ =50; NiS =50				380	-					830	836

Table 5. Differential Thermal Analyses of experiments by Chizhikov et al. *(1975) in the Cu-S, Ni-S, Cu-Ni-S and Cu-Fe-Ni-S systems.*

Composition in wt%				Temperature in °C									
				1		2		3		4		5	
Cu	Ni	S	Fe	heat	cool	heat	cool	heat	cool	heat	cool	heat	cool
80.2	-	20.3	-	-	-	-	-	-	-			1145	1148
-	72.8	27.2	-	537	534	569	553	755	778			-	-
53.2	24.5	22.3	-	557	560	-	-	736	724			-	-
51.6	23.7	21.6	3	500	502	-	-	610	618	925	972	-	-
50.6	23.7	21.2	5	492	490	-	-	626	640	927	983	-	-
49.1	22.5	20.5	8	492	482	-	-	655	676	965	994	-	-
47.9	22.0	20.1	10	469	460	-	-	659	681	993	1043	-	-
46.8	21.5	19.6	12	447	433	-	-	664	694	976	1053	-	-
45.2	20.8	19.0	15	463	497	-	-	696	722	954	989	-	-
42.6	19.6	17.9	20	-	-	-	-	-	-	967	1009	-	-
39.9	36.7	23.4	-	560	564	-	-	738	753	-	-	-	-
38.7	35.6	22.7	3	478	451	-	-	685	700	875	895	-	-
37.9	34.8	22.3	5	494	493	-	-	631	685	950	938	-	-
36.7	33.0	21.1	8	475	470	-	-	659	670	910	948	-	-
35.9	33.0	21.1	10	467	462	-	-	661	659	938	946	-	-
35.1	32.3	20.6	12	470	478	-	-	705	712	947	948	-	-
33.9	31.2	19.9	15	471	460	-	-	702	729	947	948	-	-
31.9	29.3	18.7	20	-	-	-	-	-	-	917	956	-	-

CHAPTER 2

EXPERIMENTAL PROCEDURE

The planning of charges and the experimental procedure that was followed during the investigation are discussed in detail.

---

2. EXPERIMENTAL PROCEDURE

2.1 METHOD OF INVESTIGATION

The evacuated quartz-glass tube method for dry sulphide experiments as described by Kullerud (1971) was used for all the experiments. This method was chosen because it is a relatively cheap and simple technique, which does not require sophisticated equipment. The experiments can be carried out in any laboratory equipped with furnaces, a vacuum pump and an oxygen-liquid petroleum gas burner. This reduces the costs for a single charge to the cost of the starting materials and quartz-glass tubes and rods.

Instead of starting with one isothermal section and completing it, it was decided to overlap the experimental investigations of two or three temperatures. From the isothermal sections at 1200°C and 780°C (Kullerud *et al.*, 1969), and the binary Ni-S, Cu-S and Cu-Ni phase diagrams, the positions of the phase boundaries at intermediate temperatures were extrapolated. Based on this, the compositions of the charges were planned. A small set of charges was then tempered in order to obtain a crude indication of the positions of the phase boundaries. Only after analysing these samples and composing a crude diagram, the compositions of the rest of the samples were planned and prepared.

2.1.1 STARTING MATERIALS

Fine powders of the elements nickel (99.999%), copper (at least 99.98%), and sulphur (99.99%) were used for the experiments. Some difficulties were experienced in obtaining Cu powder of high purity. Clear quartz-glass rods and tubes were used throughout all the experiments. Most samples were contained in tubes with an inner diameter of 4 mm and a outer diameter of 6 mm. For samples with high S contents, tubes with 4 mm inner and 8 mm outer diameter, or with 4 mm inner and 7 mm outer diameter were used. The tubes were examined for hairline cracks, which could lead to sulphur loss or oxidation of the charge.

2.1.2 REDUCTION OF METALS

To avoid the introduction of oxygen into the charges due to surface oxidation from exposure to the atmosphere, the metals had to be reduced before use. Reduction took place in a quartz glass tube (~40 mm diameter) fitted into a horizontal tube furnace (Figure 21), with a mixture of hydrogen and argon gas flowing through. The furnace was flooded with argon gas and heated. Hydrogen gas was added to reduce the metal at high temperatures for ±6 hours before it was cooled to room temperature in an inert atmosphere. Copper was reduced at approximately 650°C and nickel at approximately 750°C. The stream of gas flowing through the reduction furnace also served to remove any water vapour that might have formed from the reaction between hydrogen and oxygen. The continuous flow of gas through the furnace was monitored by bubbling the outlet from the furnace through a beaker of water.

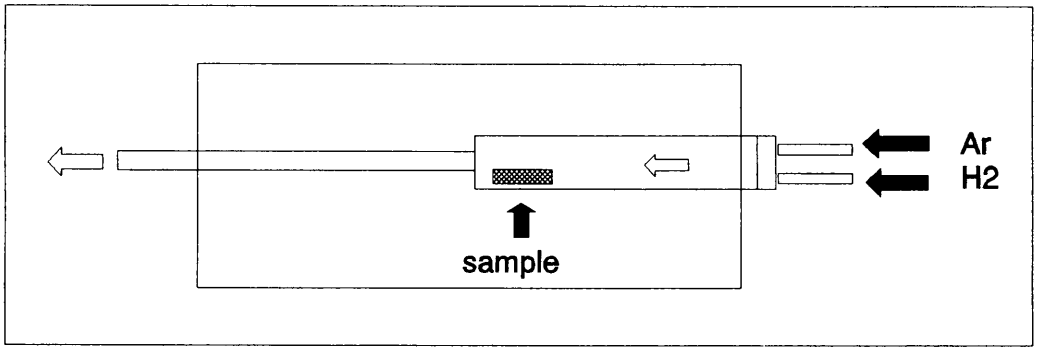

Figure 21. Tube furnace used for the reduction of Cu and Ni with hydrogen and argon gas.

At an early stage of the project, it was found that water condensated in the cooler parts of the quartz glass tube, were it blocked the tube and caused pressure to build up. This led to the separation of the fittings, and the starting materials were exposed to air and consequently oxidised. These large quantities of water must have been due to an external source of oxygen, since the volume of water that formed was much larger than that of the metal that was being reduced. It was soon discovered that oxygen could diffuse through the tubes feeding the two gases, and it was replaced with gas-tight tubing. The metals were reduced immediately before use. Sulphur was dehydrated at approximately 90°C and stored in a desiccator.

2.1.3 EVACUATED QUARTZ-GLASS TUBE TECHNIQUE

All quartz-glass material was thoroughly cleaned and rinsed with acetone before being used. This was done in order to remove any impurities that might have been present from handling the glass. Salts react with quartz glass at elevated temperatures, causing a lower melting point and weakening of the glass. Acetone also reduces the build-up of static electricity, which can cause the fine powder of the starting materials to stick to the sides of the tubes. In later experiments glassware was first washed in a soapy solution of Extran, and thoroughly rinsed with water and then acetone. This was found to reduce the build-up of static electricity even further.

One end of a ±70 mm long piece of quartz glass tube was fused shut (Figure 22 b) by means of a welding torch burning on a manually adjustable mixture of oxygen and liquid petroleum gas. With this flame, temperatures higher than the melting temperature of quartz glass (1730°C) could be reached.

The weight of each element was calculated to make up a total sample of between 0,25 and 0,30 g. The weight of the tube was noted and pre-weighed amounts of S, Cu, and Ni were added into the tube with a small funnel made of weighing paper. Each time one of the elements was added, the weight was noted, so that there were no unaccountable losses during transportation into the tube.

The elements were weighed into the tube and mixed by shaking. After mixing a ~20 mm piece of tight-fitting rod was placed into the tube (Figure 22c). The rod prevented the reagents from being disturbed by the vacuum pump, and reduced the open volume in the tube. This reduced the amount of sulphur vapour needed to sustain the sulphur partial pressure (p_{S2}) in the tube. The charges were evacuated to reduce the amount of atmospheric gas present in the tube, and to ensure a small starting pressure in the system. The tubes were sealed after pressures between 10 and 60 milliTorr (1.3 to 8 Pa) had been reached (Figure 22d). While under vacuum, the tube was inserted into the flame and turned steadily so that the walls of the tube collapsed evenly onto the rod. The tube is still open to the vacuum pump while it is being fused shut. With sulphur starting to volatilise at temperatures as low as 100°C, certain measures had to be taken to prevent the loss of starting materials due to volatilisation. It was found that the end of the tube containing the starting materials could be kept sufficiently cool by wrapping it with wet paper towel. Care was

taken not to pull the molten tube when attempting to fuse it shut, as it caused thinning of the walls, which could lead to possible failure of the tube at high temperatures and internal pressures.

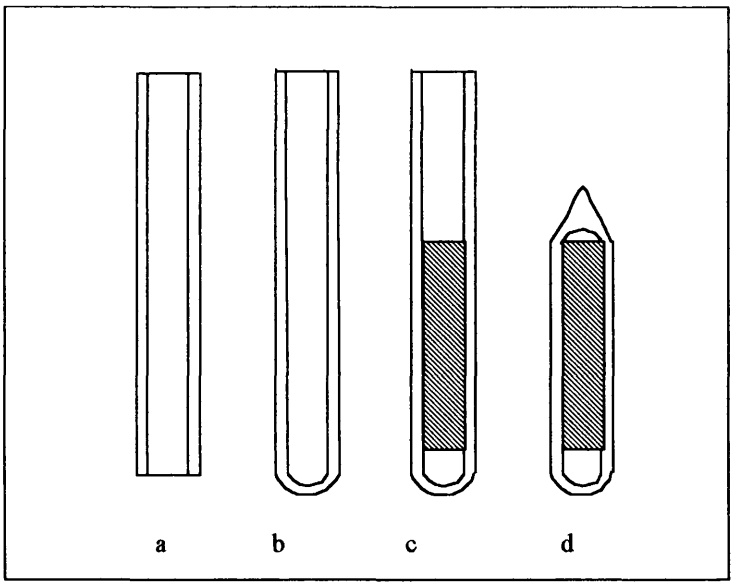

Figure 22. The evacuated quartz-glass tube technique. Tube (a) with one side fused shut (b). A piece of tight-fitting rod was inserted into the tube once the starting materials had been weighed in (c). The tube was evacuated and fused shut (d).

2.1.4 PRE-REACTION

The charges were pre-reacted in a small box furnace at approximately 750°C for variable time periods (from one day to several weeks, Appendix A) to give the sulphur ample time to react with the metals. This procedure was followed because free sulphur has a very high partial pressure at high temperatures, which can lead to explosion of the tubes (Appendix B). After pre-reaction, the tubes were left to cool and the charges were inspected through the walls of the glass tubes using a binocular microscope, to see whether any visible sulphur remained. When it was certain that the reaction between the metals and the sulphur was completed, the charges were placed into the furnace at the temperature of investigation and left to equilibrate.

2.1.5 TEMPERING OF CHARGES

Tempering took place in two large chamber furnaces which had been modified to multiple tube furnaces with horizontal tubes (Figure 23). The temperature variation throughout these tubes was measured with a calibrated thermocouple at various set points of the furnace. The temperature profile of each tube was very similar, with differences being due to the distance of the tube from the heating elements (Appendix C). The furnaces had tube lengths of 40 cm, which ensured a large ~10cm hot zone with constant temperature. Tubes 4 and 6 were used for tempering of the charges. The exact temperature in the hot zone of each tube was routinely monitored with a calibrated thermocouple.

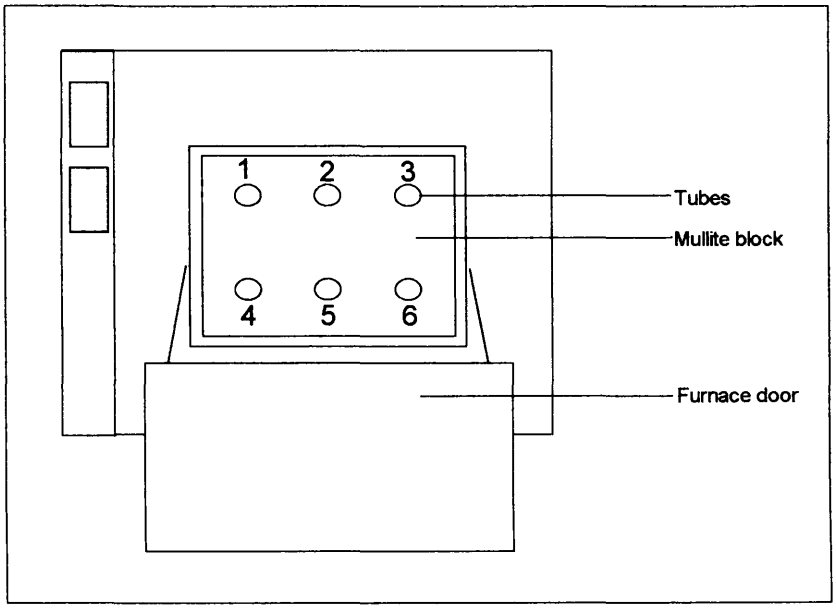

Figure 23. Modified chamber furnace containing six horizontal tubes.

Some charges were tempered at MINTEK in a vertical tube furnace to determine the reproducibility of the experiments. After pre-reaction, various heating procedures up to the required temperature were compared in order to verify equilibrium:

i) The charge was placed into the furnace directly at the required temperature.

ii) The charge was heated up to a higher temperature than required, molten, quenched and put into the furnace at the required temperature.

iii) The third method was a variation of the second, with the only difference that the charge was slowly cooled down from the higher temperature to the required temperature.

There were no discrepancies between samples tempered using different procedures.

Quartz glass cannot be tempered for an unlimited period of time, since it starts to re-crystallise at high temperatures. This led to the expansion of some tubes, which caused the charges to oxidise or lose sulphur. A specific sample (no 58), which was undersaturated in sulphur with regard to the NiS_2-Cu_2S tie-line, was melted at 1200°C for 8 days and tempered at 1000°C for 28 days. This tube had expanded while other samples, containing higher sulphur proportions and heated in the same way, showed either no signs of re-crystallisation of the glass or it only became a milky white colour, but did not expand. Some quartz glass tubes exploded at high temperatures, and possible reasons for this are discussed in Appendix B.

2.1.6 QUENCHING

After tempering, the charges were quenched by dropping them into a quench medium. Unfortunately, sulphide liquid crystallises on quenching into a fine intergrowth of crystals of lower temperature phases. In an attempt to obtain the best quench, researchers usually prefer a certain quenching procedure. Some, for example, exclusively use samples dropped from a vertical tube furnace into liquid nitrogen, whereas others quench in air. There is, however, no published comparison proving that any one of the methods is superior to the others.

Quenching in a liquid medium has the inherent problem that a thin film of vapour can form around the hot glass tube. Since vapour has a much lower heat transfer coefficient than liquid, the formation of this vapour film will slow down the heat transfer from the glass tube to the quenching medium. A possible solution for preventing the formation of the vapour film is to stir the medium vigorously before or while the sample is dropped into it, with the result that the gas film is broken down by turbulence. There are, however, practical and safety problems associated with stirring the medium where charges with temperatures of up to 1200°C are dropped into. It was decided that the use of electrical devices such as magnetic stirrers, water pumps, and propellers was not practical in terms of space available and possible damage that could be done

to the quartz glass tubes. A simpler solution with the same effect of stirring was to drop the charges into a long cylinder filled with the quenching medium.

Various quenching media were tested:

i) Most charges were quenched in water.

ii) A mixture of water and ice was also used as a quench medium. However, since the tubes were not very heavy, they tended to float on the ice, and gradually melted their way through the ice. This medium was found not to be very successful and the charges took several seconds longer to quench, which caused some samples with coarser textures.

iii) NaCl was dissolved in the water and ice mixture to form a supercooled brine. This lowered the freezing point of water which prevented ice floating on top, due to the depression of the freezing point of water by addition of NaCl.

iv) A number of charges were quenched in liquid nitrogen. In most cases there was no noticeable effect of the quenching medium on the coarseness of the quenched phases. In some cases, however, the charges quenched in liquid nitrogen showed very coarse exsolutions, probably due to the fact that liquid nitrogen vaporises easily and the charge falling through the cylinder is likely to have a thin insulating film of gas around it.

There are many factors besides the quenching medium that can influence the size of the exsolved phases, such as the rate of formation of seed crystals versus growth rate, the extent of supercooling, as well as crystal and dendrite growth which are all extremely complex processes (Godréche, 1992). One of the most important factors that has an influence on the quenching speed of the charges is the thermal conductivity of quartz glass. The low thermal conductivity of quartz glass, rather than the quenching medium, is probably the most significant limiting factor on the quench speed of the charges.

2.1.7 POLISHED SECTIONS

Once pre-reacted, tempered, and quenched, the glass capsule was broken and the sample split in half. One half of the sample was mounted in epoxy and polished for microscopic investigation, and the other half was kept as a reference.

The phases in the system Cu-Ni-S have a large spectrum of polishing hardnesses. Digenite for instance is a very brittle mineral, quenched liquid is normally hard, and Cu-Ni alloy is malleable and tends to smear. These differences in the physical properties of the phases often lead to polishing problems. All the samples were impregnated with epoxy under light vacuum to fill possible voids in the samples, and this was found to improve the polish considerably.

The sectioning of samples for mounting in polished sections presented a problem, since it is possible that there may be a small droplet or crystal of a phase present somewhere in the mounted sample, but it is not necessarily visible at the surface of the polished section. This problem was first encountered when a sample exhibiting only a quenched liquid in the polished section was re-polished in order to improve the existing polish. After re-polishing, both a liquid phase and a Cu-Ni alloy was observed.

This is an inherent problem associated sectioning, and it becomes increasingly problematic as the sample composition approaches phase boundaries, i.e. where only very small amounts of a phase is present. The only possible way to detect if there were any other phases present in the sample that were not exposed to the surface was to analyse the phase(s) present and if the phase compositions were different from the weighed-in composition of the sample, it was obvious that there was another phase present somewhere in the sample. Where possible, such samples were re-polished.

2.1.8 SEPARATION OF CHARGES

Tempering of charges in both horizontal and vertical positions caused some samples to separate into isolated drops that often differed in composition. This phenomenon was observed in various charges:

Charge no. 111, plotting in the liquid ($L_{(2,3)}$) + alloy field at 1000°C, contained a droplet consisting of Ni + Ni-S liquid (80 wt% Ni and 20 wt% S). The other droplet contained only Cu_2S. Charge no. 56 also separated into a droplet containing NiS_2 + $Ni_{1-x}S$ and another droplet containing a liquid (with composition Cu=1.8 Ni=59.8 and S=35.3 wt%). In charge no. 94, separate droplets formed, but this seemed to be induced by quenching, since the compositions of the droplets were identical.

One possible reason for separation of the charges could be that the starting materials were inserted into the tubes in layers. The starting materials were, however, thoroughly mixed after insertion into the tubes, and in some cases (charges nos. 183, 185, 186, 187), the separated phases were clearly (visible with the naked eye) euhedral crystals. Long tempering times also seemed to increase the likelihood of charges to separate into different drops or crystals. It is therefore possible that the phases separated during tempering, and the formation of different drops is possibly due to differences in surface tension (J. Nell, pers. comm., 1994).

In order to reduce the open space in the tube, thereby reducing the possibility of phases separating that are not due to surface tension effects, it was attempted to press the starting materials into a pellet. A fitting for a hydraulic press was made to produce pellets which would fit into the quartz glass tubes. The pressure exerted on the small area was unfortunately too large and the fitting for the press was damaged beyond repair the first time it was used. It was also attempted to grind the content of separated charges with an agate mortar and pestle under acetone and in this way homogenise it. However, if a charge is opened and ground, there is always a possibility that some of the content is spilled while grinding, especially with such hard materials. The most suitable treatment for separated charges was found to be melting at a higher temperature, followed by tempering at the desired temperature. This was a quick and effective solution for charges which did not contain too much sulphur.

2.1.9 DEGASSING

According to E. Makovicky (pers. comm. to R. Merkle, 1995), sulphur can be lost from melts in the sulphur-rich parts of phase diagrams on quenching. In this investigation, the phenomenon can best be explained by the presence of the immiscible liquid field $L_1 + L_{(2,3)}$. Charge no. 15, falls into the immiscible $L_1 + L_{(2,3)}$ field at 1100°C. This charge contained visible sulphur after quenching, which probably corresponds to the sulphur-rich liquid L_1. Liquid L_1 could, however, not be detected in the polished section. The polished section contained only $L_{(2,3)}$, and the analysed composition of the $L_{(2,3)}$ liquid differed by approximately 5 wt% sulphur from the weighed-in composition of the charge.

CHAPTER 3

ANALYTICAL PROCEDURE

The analytical methods used are described and a statistical evaluation of the different methods is presented.

---

3. ANALYTICAL PROCEDURE

Sulphide liquids exsolve into a mixture of lower temperature phases on quenching, which poses a problem when analysing the phases with micro-beam techniques. In cases where the different phases in a sample can be completely separated, the compositions of the phases can be determined accurately using wet chemical analysis. It is, however, difficult to determine whether complete separation was obtained, because the sample has to be studied microscopically in order to see small inclusions of one phase in the other. With bulk chemical analysis, there is also no possibility of determining whether the phases have reached equilibrium or not: In experiments carried out in the Cu-Ni-S system at 1000°C it was found that some samples contained digenite and alloy. It would have been possible to separate the digenite and the alloy, since digenite is very brittle. However, the alloy had a gradual change in composition throughout the sample. With bulk chemical analysis this compositional change would not have been noticed, and the results would have depended on where the sample was taken from the charge. This indicates that micro-beam techniques are more suitable than bulk chemical analysis for analysing quenched phases, and it offers additional information not obtainable by bulk chemical analysis.

Some difficulties were experienced in analysing Cu-Ni alloys with the electron microprobe (EMP), possibly due to the correction procedure (ZAF) that was in use at the time. Similar problems as experienced with EMP analyses on Cu-Ni alloys were observed by Reid *et al.* (1988) for alloys of Ag-Au, and by Merkle and Verryn (1991) for alloys of Pt-Pd. Because of the high absorption of X-rays from one component of the alloy by the other component, the corrected value for one component of the alloy phase is considerably different from the uncorrected value. This means that any errors in the correction procedure would be amplified and can lead to a significant error in the analysis. In order to quantify the error in the correction procedure, Cu-Ni alloys of known composition had to be analysed by EMP. Cu-Ni alloys with four different compositions were prepared at 20, 40, 60, and 80 atomic % Cu. The samples were melted in an inert atmosphere (Ar) in an arc furnace, and were homogenised for 24 hours before quenching. These samples showed inhomogeneity in the backscattered mode of the electron microprobe and there were large differences in composition, making the quantification of the error in the correction procedure impossible.

Dendritic intergrowths could also be observed under the microscope in one of the alloy samples. Depletion of the low-melting component in the alloy leads to supercooling (Doherty *et al.*, 1973, and Feest and Doherty, 1973). The dendrites can be broken by mechanical rolling of the samples, but this did not solve the problem. Alloy dendrites could not be observed in backscattered mode with the EMP, or under the microscope in any of the experimental evacuated quartz-glass samples, but it was nonetheless decided to analyse all phases as areas instead of spots.

3.1 TECHNIQUES

The bulk composition of quenched sulphide phases can be analysed with micro-beam techniques, using analyses of areas, defocused beam spots, or a large number of spot analyses on a grid pattern. These different techniques were employed in analysing inhomogeneous phases.

3.1.1 ELECTRON MICROPROBE

3.1.1.1 SPOT ANALYSES

One method tested for the determination of the composition of quenched liquids with a Wavelength Dispersive Spectrometry (WDS) using an electron microprobe (EMP) was to analyse a large number of spots and taking the average of all the spots. The Jeol electron microprobe was operated at 20 kV excitation voltage, a current of 30 nA, and with counting times of 30 seconds. Analysing approximately 100 spots on a grid pattern with a electron microprobe took 10-12 hours. During such a long time interval machine drift or technical problems can occur and the runs often had to be interrupted and repeated. To obtain suitable sets of results for two samples required more than a week. This method was statistically evaluated in order to determine how many spots would be needed for a reliable estimate of the average.

3.1.1.2 DEFOCUSED BEAM

Fleet and Pan (1994) used 9 to 12 spot analyses with a defocused beam of 10 μm for monosulphide solid solution (mss) phases in the Fe-Ni-Cu-S system. For analyses of quenched sulphide liquid they used 12 to 16 defocused beam spots of up to 80 μm. They report standard deviations of less than 5% for Cu, the most heterogeneously distributed element. The averaged analyses reported by Fleet and Pan (1994) are normalised to 100% and one can therefore not evaluate the variation of the totals.

The defocused beam technique was also employed in this investigation and beams of 20 to 50 μm were used to determine the average composition of quenched liquid phases. The Jeol electron microprobe was operated at 20 kV excitation voltage, a current of 30 nA, and with counting times of 100 seconds. Analyses of solidified liquids varied considerably, and totals were generally far too low. The low totals were probably due to the scattering of X-rays which results from defocusing the beam. In cases where the totals were acceptable, averages of the analyses compared well with area analyses obtained by SEM, although defocused beam analyses with the EMP have higher standard deviations. In Table 6 a comparison is made of analyses of the liquid phase in sample no. 6 with defocused beam spots by EMP and area analyses (0.12 mm^2) with the SEM. The standard deviation of Ni analysed with the EMP is relatively high.

Table 6. Comparison of 32 defocused electron microprobe (EMP) spot analyses (with totals within 1,5 wt% of 100 wt%) and 7 scanning electron microscope (SEM) analyses in the liquid field of sample no 6.

Microbeam Technique	Ni	S	Cu	Total	No of analyses
EMP (defocused)	62.41	8.86	28.74	100.02	32
Standard deviation (1σ)	4.26	2.98	1.99	-	
SEM (areas)	63.54	10.13	26.91	100.58	7
Standard deviation (1σ)	2.74	2.40	2.87	-	

3.1.2 SCANNING ELECTRON MICROSCOPE

3.1.2.1 AREA ANALYSES

Analyses on the Scanning Electron Microscope (SEM) at MINTEK using an Energy Dispersive Spectrometry (EDS) covered areas of approximately 0.12 mm^2. The Jeol 840 SEM was operated at 20 kV excitation voltage, a current of 30 nA, with counting times of 100 seconds, and using $\phi(\rho z)$ correction procedures. As many areas as possible on each sample were analysed. Comparison of the compositions of scanned areas is probably the only method that can reveal compositional anomalies in heterogeneous quenched sulphide melts. The anomalies can be due to an additional phase under the surface, non-equilibrium (gradual change), or due to variations in grain sizes of the phases. In the first two situations the analyses were not used for construction of the phase diagrams.

3.2 STATISTICAL EVALUATION

3.2.1 AREA ANALYSES VERSUS SPOT ANALYSES

Comparison of area analyses (SEM/WDS) versus spot analyses on a grid (EMP/EDS) was made. The area analyses and the grid covered large parts of the liquid phase. Two samples (nos. 84 and 86) containing only liquid of known composition were analysed. One hundred points were analysed in a grid pattern, and it was assumed to be a sufficient number for the average to be within 1σ standard deviation of the actual composition.

i) Sample no. 86

Figures 24 and 25 show the frequency diagrams of the elements for the EMP spot and SEM area analyses. In Table 7 it can be seen that the results of the two methods differ considerably. In contrast with the six area analyses with the SEM, the averaged spot analyses with the EMP do not agree with the actual weighed-in composition, and it shows too high Ni and S values and low Cu values. The 1σ standard deviations of the EMP analyses are very high.

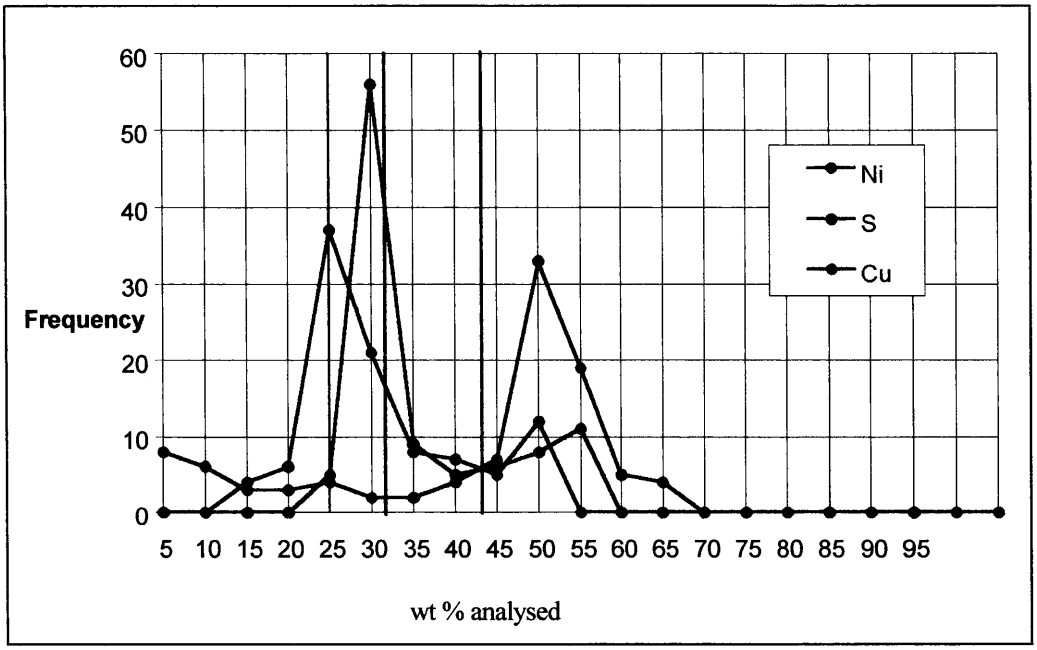

Figure 24. Frequency diagrams of Cu, Ni and S of 100 spot analyses with the EMP (sample 86), with the actual composition shown as vertical lines.

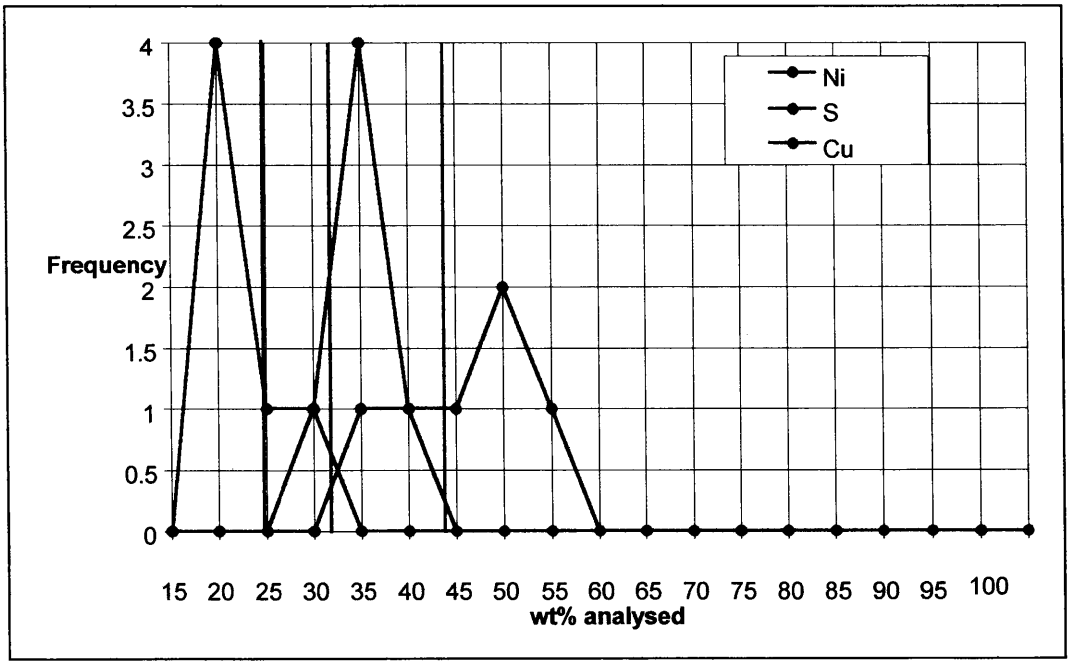

Figure 25. Frequency diagrams of Cu, Ni and S of SEM analyses of 6 areas (sample no. 86), with actual compositions shown as vertical lines.

Table 7. Comparison of the actual, weighed-in liquid composition in sample no. 86 with 100 averaged EMP spot analyses and 6 areas analysed with the SEM. The standard deviations (1σ) of the average analyses are also given.

Method	wt % Ni	wt% S	wt% Cu	Total	No of analyses
EMP	28.8 (± 9.0)	33.6 (± 9.07)	39.4 (± 17.8)	101.7	100
SEM	25.2 (± 3.7)	31.8 (± 3.38)	42.7 (± 7.0)	99.6	6
Actual composition	**25.0**	**31.3**	**43.8**	**100.0**	-

ii) Sample no. 84

Sample no. 84 was tempered at 900°C, and contained only quenched liquid. On this sample, six areas were analysed with the SEM and 100 spots on a grid pattern were analysed with the EMP. Three of the 100 analyses had very low totals and were excluded, leaving 97 analyses (Table 8). The SEM analyses compare very well with the actual values. The average spot analyses are close to the actual value, but the standard deviations (1σ) for the probe analyses are very high. This difference is probably due to the small scale heterogeneity of the quenched liquid phase. From individual spot analyses with such large variations it is not possible to detect compositional gradients in a sample.

The frequency diagrams for the elements of the two sets of analyses are presented in Figures 26 and 27. The probe analysis data of Cu and Ni are not normally distributed (Figure 26). The probe beam either hits one of the different exsolved phases or the phase boundaries. If, by chance, the beam hits a Cu sulphide, the Ni value will be very low, and vice versa. If a larger number of spots were analysed, the effect of individual analysis would be averaged out. This indicates that the sample population is too small and that more than one hundred spot analysis are required to give a good indication of the average.

Table 8. Comparison of the actual liquid composition in sample no. 84 with 97 averaged EMP spot analyses and 6 areas analysed with the SEM. The standard deviations (1σ) of the averages are given.

Method	wt % Ni	wt% S	wt% Cu	Total	No. of analyses
EMP	14.3 (± 11.7)	26.1 (± 5.7)	61.1 (± 17.2)	101.5	97
SEM areas	11.8 (± 1.7)	25.1 (± 0.5)	62.3 (± 2.7)	99.2	6
Actual composition	**12.3**	**26.0**	**61.7**	**100.0**	-

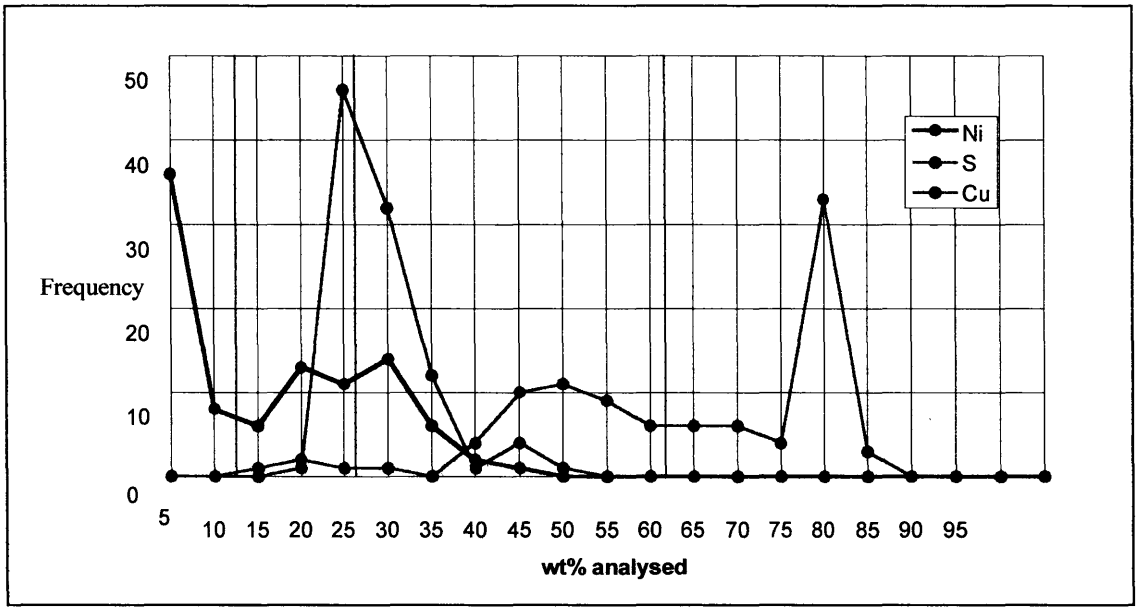

Figure 26. Frequency diagrams of Cu, Ni and S of 97 spot analyses with the EMP (sample no. 84), with the actual compositions shown as vertical lines.

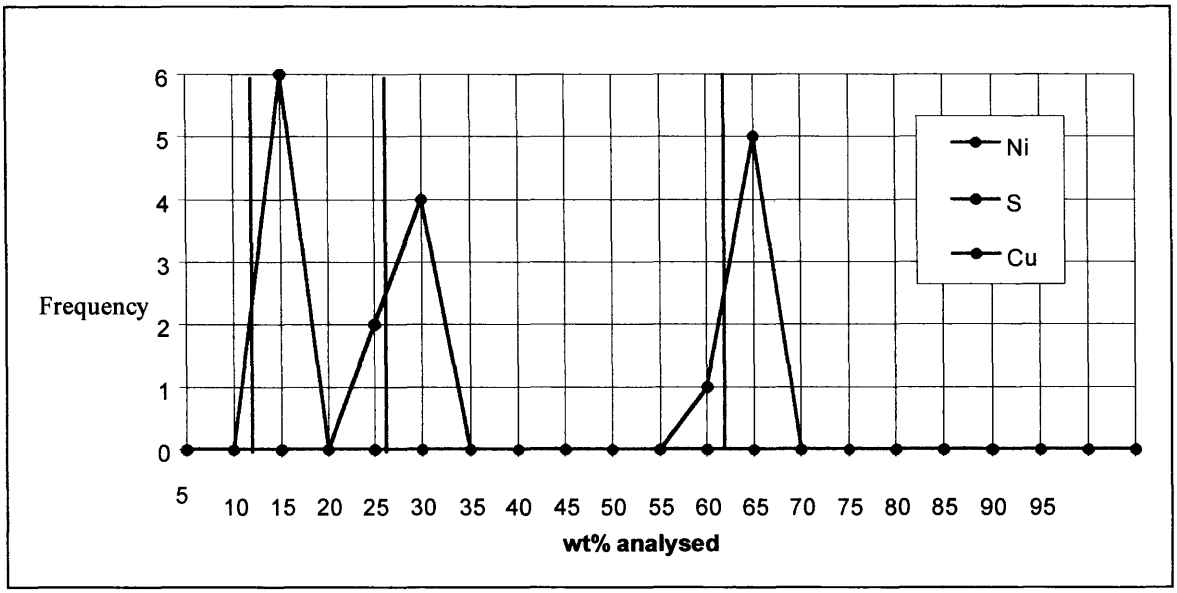

Figure 27. Frequency diagrams of Cu, Ni and S of SEM analyses of 6 areas (sample no. 84), with the actual compositions shown as vertical lines.

3.2.2 STATISTICAL DISTRIBUTION

Since some of the frequency diagrams are not normally distributed, it was decided to compare the arithmetic mean (average), geometric mean, and the actual weighed-in composition for the two samples (nos. 86 and 84). This was done to determine if the average of the set of analyses is the best indication of the true phase composition, or if some other statistical calculation was required. From Tables 9 and 10, it can be seen that the arithmetic mean (average) and the geometric mean for the SEM analyses are virtually identical to the actual composition (for sample nos. 86, and 84 respectively). The EMP analyses, however show large differences when the statistical functions are calculated. The bimodal distribution of Ni for the EMP analyses in sample no. 84 (Figure 26) probably causes the low geometric mean value of Ni in Table 10.

Table 9. Comparison of the Arithmetic mean and Geometric mean applied to the analytical results of 100 EMP spot analyses and 6 SEM area analyses with the actual liquid composition of sample no. 86.

Statistical function	**6 areas SEM**				**100 spots EMP**			
	Ni	**S**	**Cu**	**Total**	**Ni**	**S**	**Cu**	**Total**
Arithmetic	25.2	31.8	42.7	99.6	28.8	33.6	39.4	101.7
Geometric	24.9	31.6	42.2	98.7	27.5	32.5	31.6	91.6
Actual	**24.99**	**31.25**	**43.77**	**100**	**24.99**	**31.25**	**43.77**	**100**

Table 10. Comparison of the Arithmetic mean and Geometric mean applied to the analytical results of 97 spot EMP analyses and 6 SEM analyses with the actual liquid composition of sample no. 84.

Statistical function	**6 areas SEM**				**97 spots EMP**			
	Ni	**S**	**Cu**	**Total**	**Ni**	**S**	**Cu**	**Total**
Arithmetic	11.8	25.1	62.3	99.2	14.3	26.1	61.1	101.5
Geometric	11.7	25.1	62.3	99.0	8.3	25.5	58.0	91.8
Actual	**12.27**	**26.01**	**61.72**	**100**	**12.27**	**26.01**	**61.72**	**100**

3.2.3 REPRODUCIBILITY

Sample no. 94 had two separated grains after quenching. In this sample the liquid composition was not known since there were two phases present in the sample. Both grains contained digenite co-existing with liquid, which was analysed with the SEM. The first objective was to determine whether the separated grains were in equilibrium (i.e. had the same composition). Should this be the case, a comparison could be made between two similar areas analysed with the same method in order to determine the reproducibility of the method.

The larger grain had 9 areas analysed in the liquid, and the smaller only 5. The compositions of the two quenched liquids were found to be identical (Table 11). Since there are no differences in composition or texture of these two grains, the liquids must have separated just before quenching, probably caused by the movement during the quenching process. The frequency distribution diagrams of the two different grains are show in Figures 28 and 29. A comparison of their statistical characteristics was made and it is listed in Table 11. Despite the fact that all the elements are not normally distributed, the arithmetic mean (average) and geometric mean of the individual grains are virtually identical. Furthermore, a comparison of the two analysed grains of liquid also give similar results, which means that one can get reproducible results with only a small number of areas on a solidified liquid phase analysed by SEM.

Table 11. Comparison of the average (arithmetic mean), standard deviation (1σ), and geometric mean of 5 and 9 SEM analyses respectively of the liquid phase of two grains of sample no. 94.

Statistical function	Small grain with 5 area analyses				Large grain with 9 area analyses			
	Ni	S	Cu	Total	Ni	S	Cu	Total
Arithmetic	37.9	24.3	36.4	98.7	37.7	24.5	36.2	98.4
Deviation 1σ	5.8	0.9	6.8	-	4.6	0.8	6.1	-
Geometric	37.4	24.3	35.9	97.7	37.5	24.5	35.8	97.7

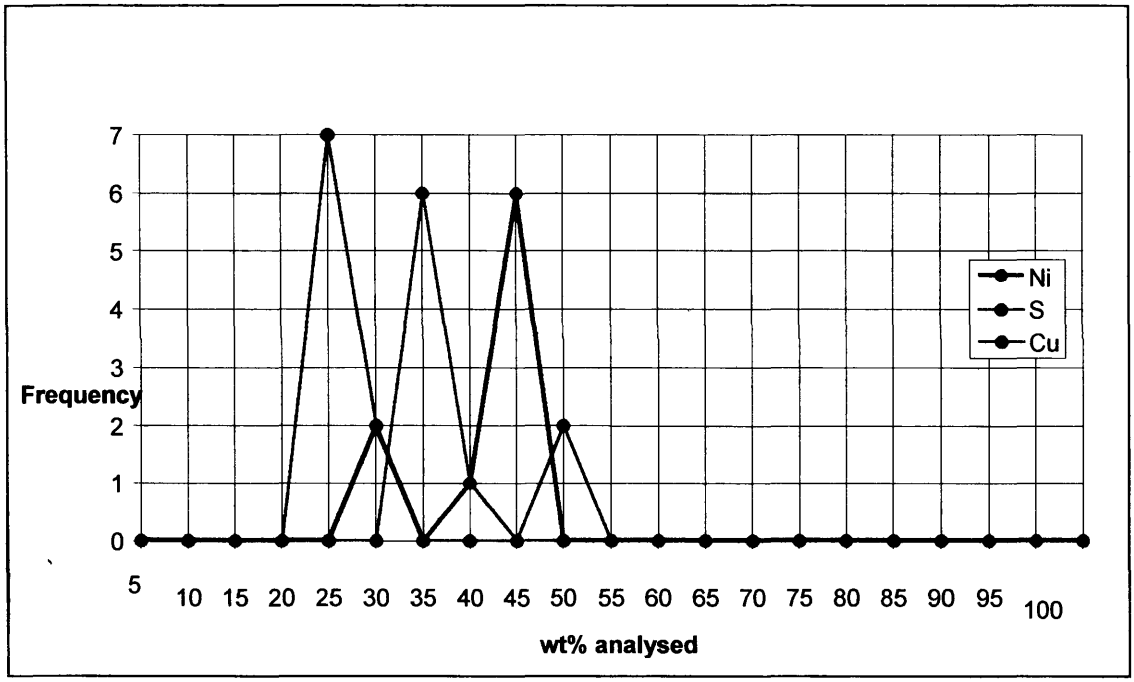

Figure 28. Frequency diagrams of Cu, Ni and S of SEM analyses (9 areas) in the liquid phase of the large grain (sample no. 94).

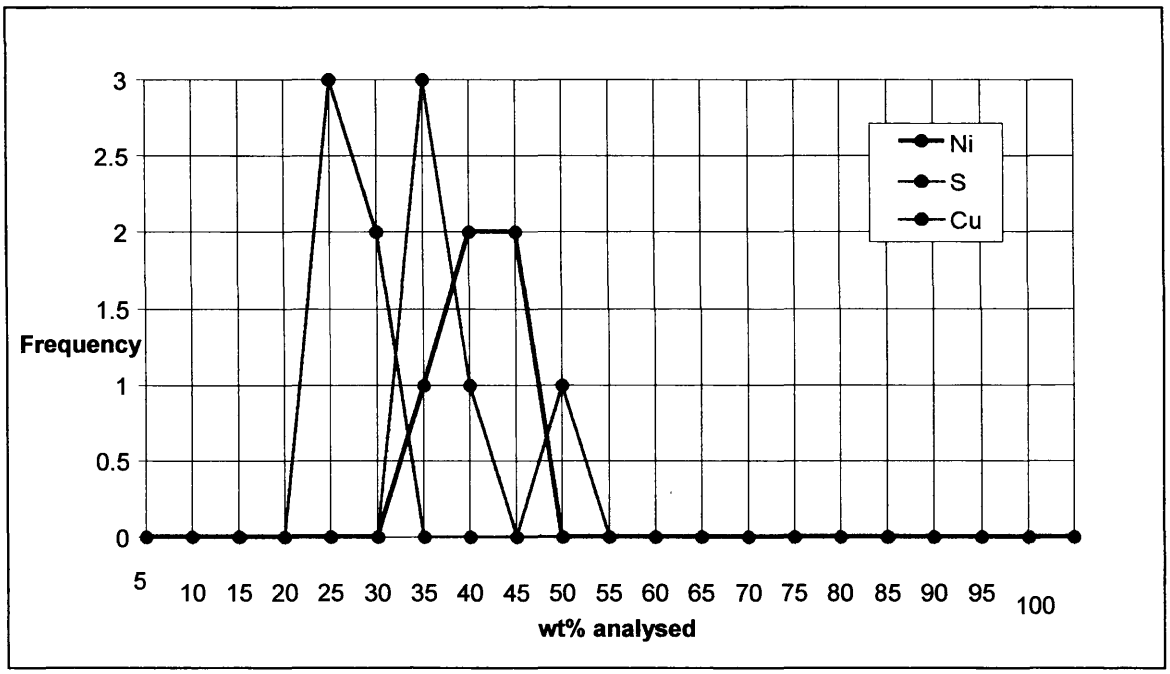

Figure 29. Frequency diagrams of Cu, Ni and S of SEM analyses (5 areas) in the liquid phase of the small grain (sample no. 94).

3.3 CONCLUSIONS

Due to the nature of the quenched samples, the physical separation of the individual phases for bulk chemical analysis could be problematic, and the technique would also not give an indication of non-equilibrium in the samples. Microbeam techniques are considered to be more suitable for analysis of these types of phases. Sulphide liquid inevitably exsolves into a heterogeneous mixture of low temperature phases on quenching, and certain adjustments have to be made to the normal *in situ* analytical techniques. Different techniques were evaluated, by using quenched liquid phases of known composition. Areas of the phases were analysed using the SEM and the averages were found to be very close to the actual weighed-in liquid compositions. Averages of ~100 spot analyses with the EMP have very high standard deviations, and in some cases neither the average (arithmetic mean) or geometric mean is close to the actual liquid composition.

Analysing areas with the SEM was found to be far superior to analysing spots in a grid pattern, especially if one considers that approximately six areas with the SEM were compared with ~100 spot analyses. In contrast to spot analysis, each area analyses with the SEM is already an average, with the additional advantage that compositional trends in the results can be seen and non-equilibrium samples can be identified.

There is a large difference in the total area analysed with the two techniques:

With the diameter of an EMP beam spot being ~5 μm, each spot represents the analysis of an area of ~$2x10^{-5}$ mm^2. With one hundred spot analyses, this means that a total area of ~$2x10^{-3}$ mm^2 was analysed. In contrast to this, six area analyses (each covering 0.12 mm^2) with the SEM cover a total area of 0.72 mm^2. In order to cover the same area as the six area analyses by SEM, approximately 36 000 EMP spot analyses are required. This means that the initial assumption, that the average of 100 spot analysis would give a reasonable estimate of the actual composition, is incorrect.

CHAPTER 4

ISOTHERMAL SECTIONS

Phase associations and textures that were observed in the Cu-Ni-S system are discussed, and photomicrographs of some phase assemblages are presented. The experimental results are presented in tables, containing the compositions of co-existing phases, and as the 1200°C, 1100°C, 1000°C, 900°C, 800°C and 700°C isothermal sections, with phase boundaries and tie-lines between co-existing phases.

---

4. ISOTHERMAL SECTIONS

4.1 MINERAL PHASES

All the charges made for the investigation of the system were studied microscopically in reflected light. The optical properties of the minerals observed in the study are listed in Table 12 (Uytenbogaart and Burke, 1971). Phase associations are vital for ascertaining equilibrium in a charge, as all the phases present have to be in contact with each other. The textures were used, where possible, to distinguish between quenched liquid and exsolution due to the low temperature phase transformations of a solid phase. Quenched sulphide liquid mostly showed dendritic, small round, or fine fingerprint-like intergrowths of three phases. Exsolution from the solid state was of a single other phase that was present in very small proportions (with the exception of exsolutions from $Ni_{3\pm x}S_2$). The phase that exsolved from the solid phase was evenly distributed, and it consisted of small, round grains.

Table 12. Optical properties of minerals in the Cu-Ni-S system (Uytenbogaart and Burke, 1971).

Phase	**Colour**	**Bireflectance**	**Anisotropism**
Cu_2S (digenite)	greyish blue	none	Isotropic, weak anisotropism
Ni_3S_2 (heazlewoodite)	yellow-cream	very weak	strong, lilac - greyish green
NiS (millerite)	yellow	in oil: distinct, bright yellow to greyish yellow	lemon-yellow to blue and violet, no complete extinction, basal section appears isotropic
NiS_2 (vaesite)	grey	none	isotropic, can be anisotropic
Cu-Ni alloy	pink to cream	none	Isotropic

4.2 THE 1200°C ISOTHERMAL SECTION

The samples prepared for the investigation of the 1200°C isothermal section are listed in Appendix A-1. The average SEM analyses of the various phases as they occur at 1200°C are presented in Table 13 and plotted in Figure 30.

Table 13. The averaged SEM analyses (wt%) of co-existing phases at 1200°C, with the number of areas that were analysed, and the calculated standard deviations (1σ).

	L(2,3)				
No	**Ni**	**S**	**Cu**	**Total**	**Analyses**
No 4	39.3	5.7	54.4	99.3	7
stdev.	1.5	1.0	0.9		
No 5	63.1	13.3	23.7	100.0	5
stdev.	0.8	2.3	3.0		
No 2	16.6	2.1	81.5	100.1	2
stdev.	0.1	0.0	1.2		

	L(2,3)					α				
No	**Ni**	**S**	**Cu**	**Total**	**Analyses**	**Ni**	**S**	**Cu**	**Total**	**Analyses**
No 6	63.5	10.1	26.9	100.6	7	75.9	0.1	23.7	99.7	3
stdev.	2.7	2.4	2.9							
No 69	80.1	11.7	7.9	99.7	3	93.4	0.1	5.4	98.8	4
stdev.	1.5	1.4	0.9							
No 70	75.0	11.6	15.8	102.4	4	85.6	0.0	13.2	98.8	5
stdev.	1.4	2.6	2.6							
No 72	53.9	7.2	38.2	99.2	8	66.1	0.1	33.2	99.4	3
stdev.	2.2	2.3	2.8							
No 73	45.4	5.0	49.3	99.7	6	58.2	0.0	41.4	99.5	5
stdev.	3.6	1.6	2.2							
No 101	54.6	6.8	38.2	99.6	7	65.7	0.1	33.1	98.8	3
stdev.	2.2	1.8	2.9							
No 102	53.0	7.2	39.6	99.7	7	65.6	0.0	34.1	99.7	6
stdev.	4.4	1.4	3.8							
No 103	31.1	2.6	65.9	99.6	9	42.8	0.1	56.0	98.8	4
stdev.	2.5	1.3	1.3							

At 1200°C a large part of the Cu-Ni-S phase diagram is liquid ($L_{(2,3)}$) as shown in Figure 30. The liquidus boundary on the metal-rich side of the diagram could be determined from the liquid composition of the $L_{(2,3)} + \alpha$ phase association (Table 13). The immiscible liquid field $L_1 + L_{(2,3)}$ on the sulphur-rich part of the diagram is drawn by extrapolation from the binary phase diagrams of Cu-S (Massalski, 1986) and Ni-S (Lin *et al.*, 1978), and is shown schematically.

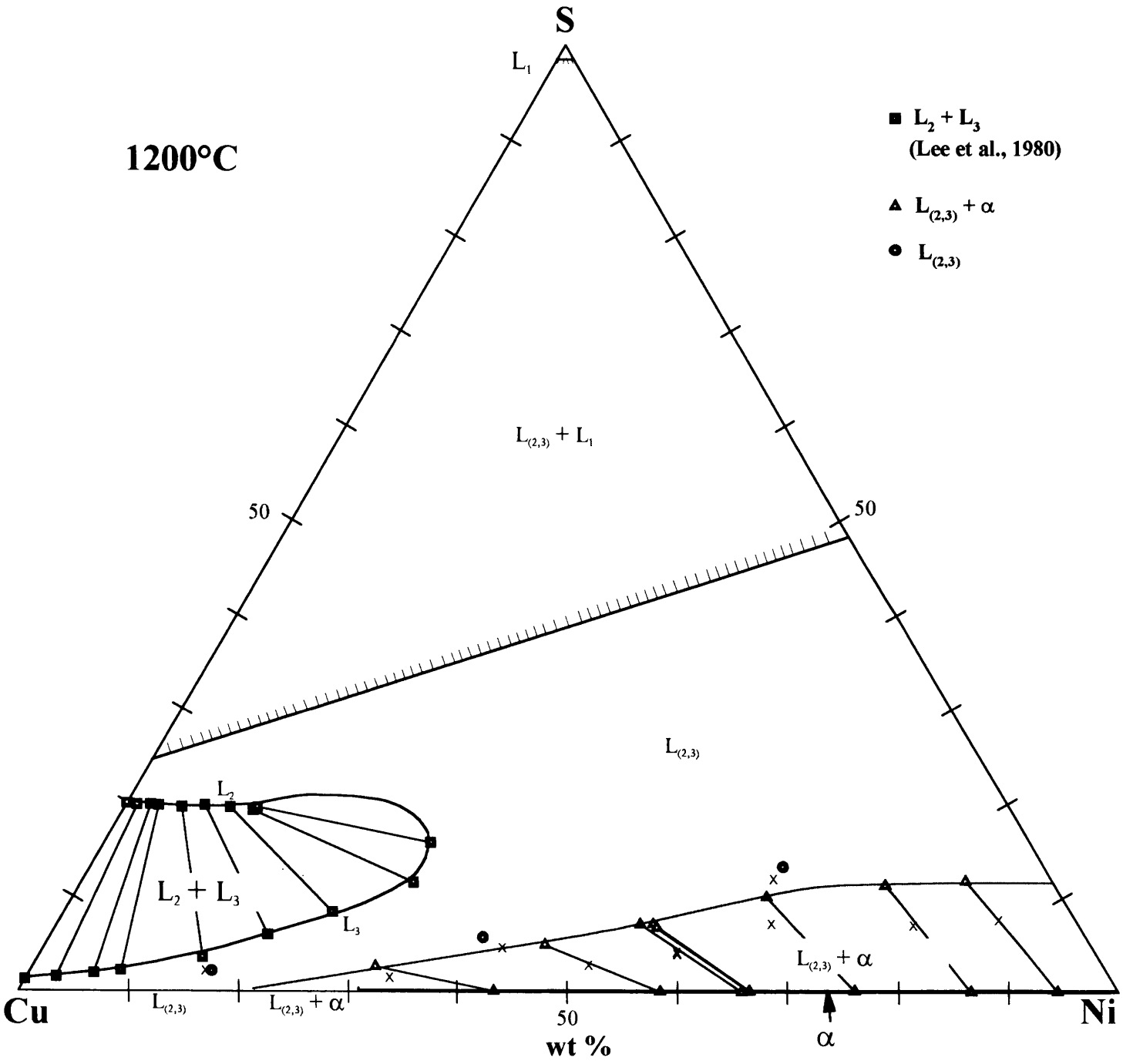

Figure 30. The 1200°C isothermal section of the system Cu-Ni-S, with tie-lines between the analysed compositions of co-existing phases. The bulk compositions of the experimental samples are shown as x's. The immiscible liquid field ($L_2 + L_3$) is drawn from Lee et al. *(1980). The immiscible $L_1 + L_{(2,3)}$ field is drawn by extrapolation from the binary Cu-S (Massalski, 1986) and Ni-S (Lin* et al., *1978) phase diagrams and is shown schematically.*

Quenched sulphide melts crystallise into a fine intergrowth of different phases. The quenched sulphide melt has a characteristic texture, showing dendritic intergrowths of minerals. A typical example of this texture is shown in Photomicrograph 1 which was taken from a sample that was equilibrated at 900°C. Processes causing dendritic growth make out a very complex field of study. The thermodynamic aspects are identified and discussed by Godréche (1992).

The immiscible liquids at 1200°C show complex textures (Photomicrograph 2). The solidified liquids are made up of Cu-Ni alloy (α, yellow) and Cu_2S (μ, grey). The only difference between the two solidified liquids is the different proportions of these two phases. L_2, which is close in composition to Cu_2S, contains large quantities of Cu_2S while L_3 contains more alloy.

Two experimental samples containing immiscible liquids were produced and the analyses are shown in Table 14.

Table 14. Averaged SEM analyses (in wt%) for two samples containing immiscible liquids at 1200°C.

	L_2					L_3				
No	**Ni**	**S**	**Cu**	**Total**	**Analyses**	**Ni**	**S**	**Cu**	**Total**	**Analyses**
No 1	3.4	19.6	75.0	98.0	6	16.1	5.0	79.1	100.3	4
stdev.	2.0	0.4	2.3			1.0	0.6	0.4		
No 46	6.0	19.0	74.0	98.9	2	23.5	7.7	69.6	100.8	3
	0.0	0.4	0.5			3.8	0.5	1.7		

In the two samples containing $L_2 + L_3$, large drops of one liquid could be seen in the other liquid, which is probably due to mechanical mixing of the molten liquids during removal from the furnace before quenching. Consequently, only selected areas of the immiscible liquids were analysed with the SEM, avoiding areas where mixing might have taken place, i.e., close to the contacts (small scale mixing) and where inclusions of one phase in the other were observed (large scale mixing). Even though these precautions were taken, the results obtained in this way deviated from previous investigations where the liquids were sampled separately at 1200°C. For comparison, the immiscible liquid tie-lines at 1200°C as determined by various investigators are shown in Figure 31.

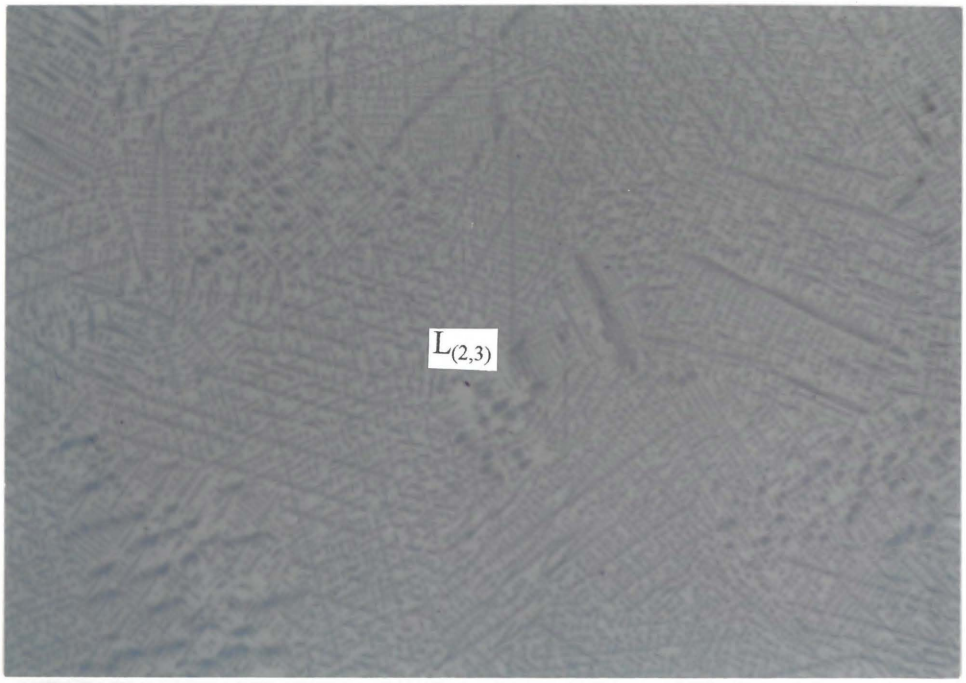

Photomicrograph 1. Dendritic intergrowth of phases in a quenched liquid ($L_{(2,3)}$). Charge no. 99 at 900°C (long side of the photomicrograph is 1.25mm).

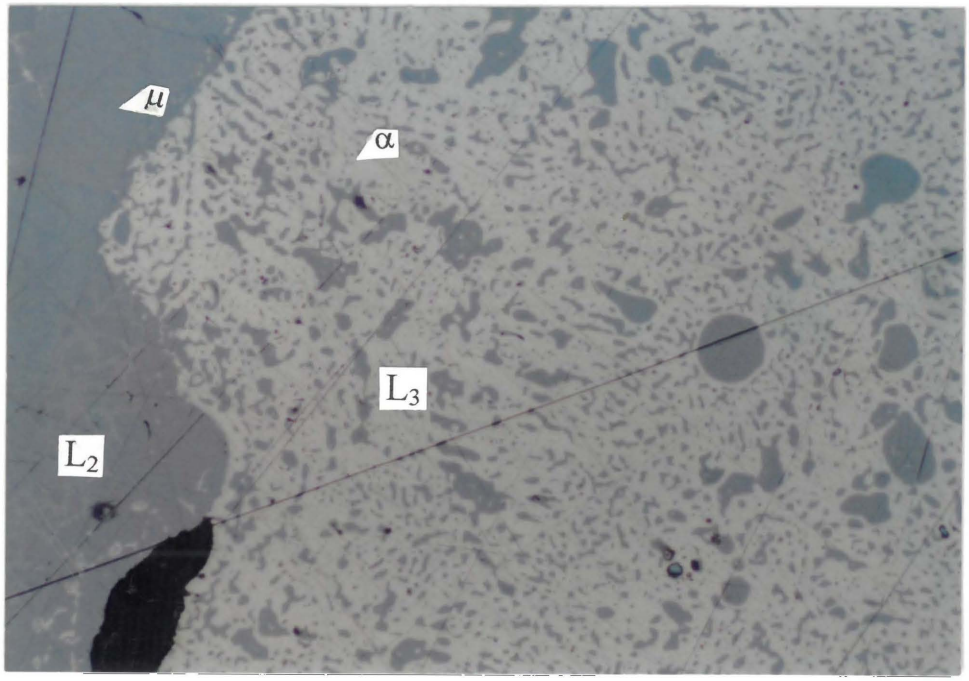

Photomicrograph 2. Charge no. 46 at 1200°C in the immiscible liquid field, showing intergrowths of alloy (α, yellow) and Cu_2S (μ, grey). The two immiscible liquids (L_2 + L_3) can be distinguished by the relative amounts of digenite and alloy. The sulphide-rich liquid (L_2) contains mostly digenite and the alloy-rich liquid (L_3) contains mostly alloy (long side of the photomicrograph is 1.25mm).

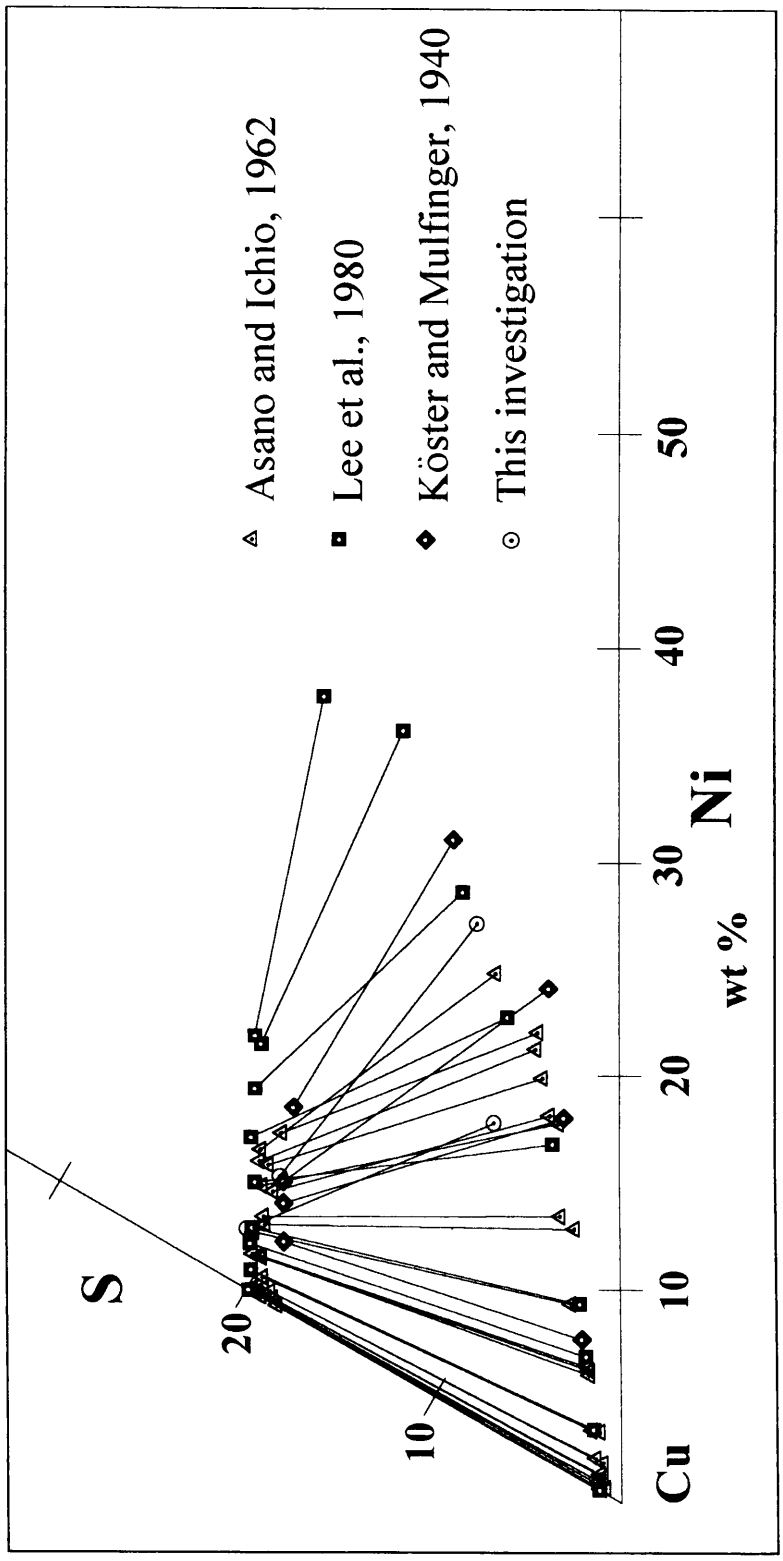

Figure 31. Portion of the isothermal section of Cu-Ni-S diagram at 1200°C. Results form different investigations (as listed) are shown for comparison.

Two samples from this investigation fall in the immiscible liquid field (Table 14, and Figure 31). The composition of L_2 and L_3 in sample no 46 is reasonably consistent with the results from Köster and Mulfinger (1940), while the liquid compositions in sample no 1 deviate considerably from the results of any of the investigations. The tie-lines determined by Köster and Mulfinger (1940) are inconsistent with those determined by Lee *et al.* (1980). These differences are probably due to the different investigation techniques employed by the researchers. Methods involving the quenching of the two liquid phases while still in contact can, and probably do, lead to mechanical mixing because of the movement of the charge during quenching. These problems usually go undetected if the solidified phases are separated and chemically analysed. Techniques where the immiscible liquid layers were sampled at 1200°C and subsequently quenched (Schlitt *et al.*, 1973; Lee *et al.*, 1980) are probably more accurate, provided that no mixing occurred during sampling.

The seemingly thick tie-line in the $L_{(2,3)} + \alpha$ field (Figure 30) represents a triplicate set of samples (nos. 72, 101 and 102) all with the same bulk composition in order to verify the reproducibility of results.

The concentration of the alloy phase towards one side of liquid was frequently observed. A typical example of this is from a sample that was equilibrated at 800°C (Photomicrograph 3). This could be due to gravity settling, as the liquid phase has a very low viscosity. Alloy usually formed large round grains, except for some samples at 700°C, where euhedral (cubic) crystals were observed (Photomicrograph 4).

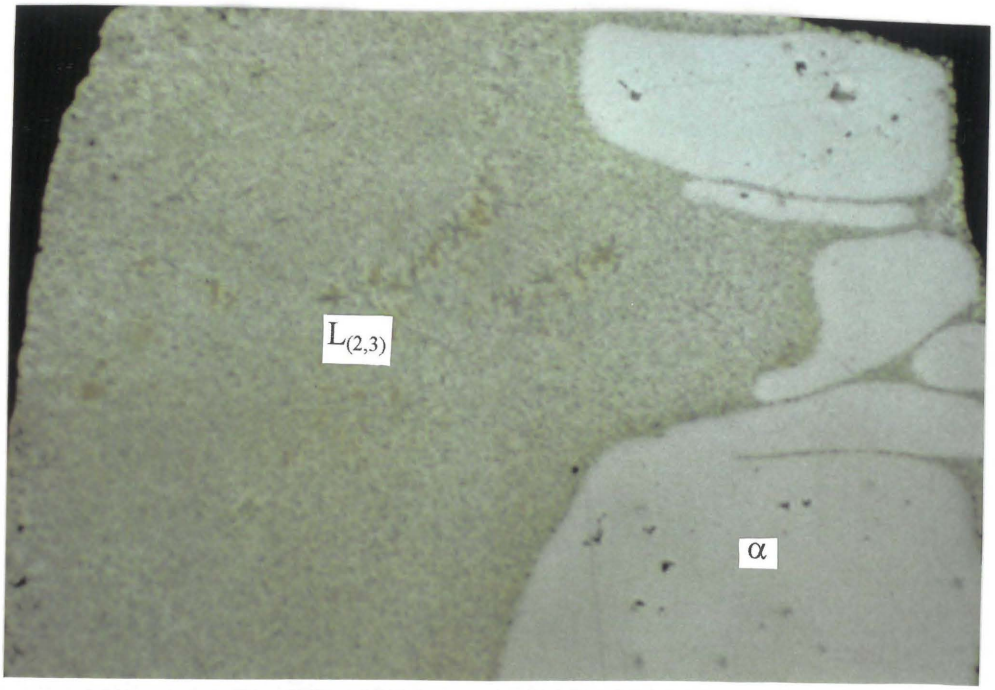

Photomicrograph 3. Typical texture found in charges containing liquid ($L_{(2,3)}$, exsolutions) + alloy (α, cream). Settling of alloy in liquid was frequently observed. Charge no. 176, at 800°C (long side of the photomicrograph is 4mm).

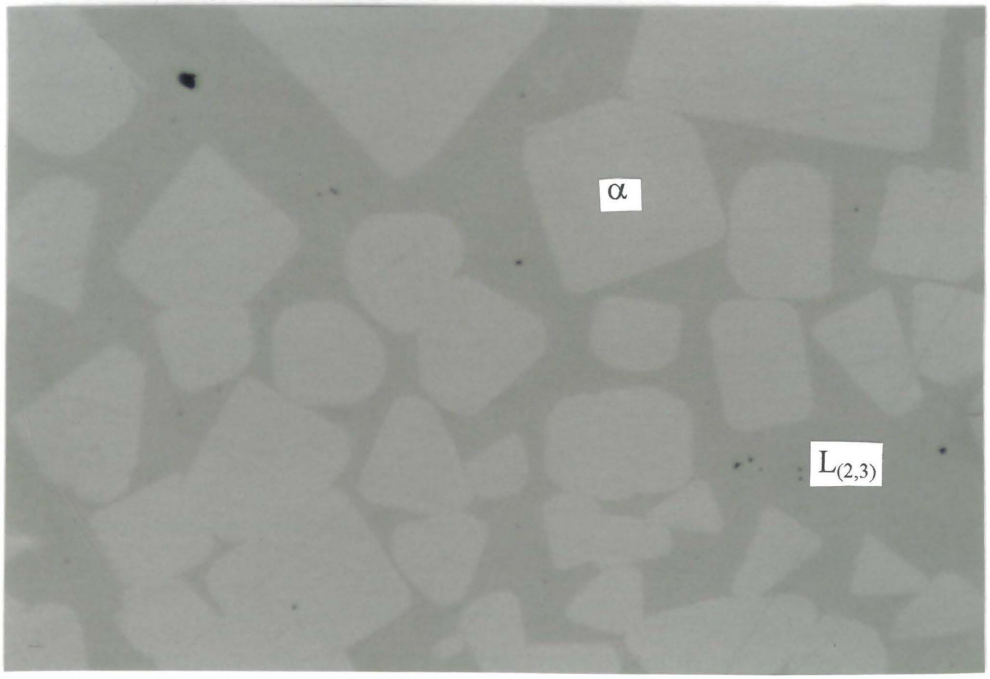

Photomicrograph 4. Cubic crystal of alloy (α) in charge no. 259 containing liquid + alloy ($L_{(2,3)}$ + α). Charge no. 259 at 700°C (long side of the photomicrograph is 4mm).

4.3 THE 1100°C ISOTHERMAL SECTION

The samples prepared for the determination of the 1100°C isothermal section are listed in Appendix A-2. Table 15 shows the averaged SEM analyses of the phases present at 1100°C, and Figure 32 represents the results of the investigation of the 1100°C isothermal section.

Table 15. The averaged SEM analyses (wt%) of co-existing phases at 1100°C, with the number of areas that were analysed, and the calculated standard deviations (1σ).

	L(2,3)				
No	**Ni**	**S**	**Cu**	**Total**	**Analyses**
No 15	4.2	24.7	68.5	97.4	3
stdev.	1.1	2.1	1.6		
No 17	35.3	29.7	32.2	97.2	2
stdev.	0.6	0.4	0.8		
No 242	2.7	1.5	95.9	100.1	2
stdev.	0.0	0.0	0.5		
No 241	27.0	19.2	54.7	100.8	1
No 274	27.6	17.3	56.1	101.0	1
No 21	16.4	5.5	80.1	101.9	2
stdev.	0.2	1.2	0.7		

	L(2,3)					α				
No	**Ni**	**S**	**Cu**	**Total**	**Analyses**	**Ni**	**S**	**Cu**	**Total**	**Analyses**
No 9	65.4	14.6	19.7	99.7	6	81.1	0.1	18.7	99.9	3
stdev.	3.2	2.8	3.0							
No22	19.0	5.4	76.0	100.3	9	21.4	0.0	78.9	100.3	2
stdev.	1.4	1.5	0.8							
No23	33.7	9.0	57.7	100.3	10	39.0	0.1	61.0	100.1	2
stdev.	2.6	1.8	2.6							
No129	79.4	16.7	2.2	98.3	5	97.4	0.1	1.1	98.6	6
stdev.	2.7	2.6	0.4							
No130	73.9	17.0	8.6	99.5	15	92.0	0.1	7.2	99.3	2
stdev.	1.0	1.7	1.5							
No131	67.6	16.2	15.3	99.1	21	84.7	0.0	14.1	98.8	3
stdev.	4.4	2.0	4.5							
No132	58.1	13.8	27.8	99.7	9	72.0	0.1	28.1	100.1	3
stdev.	3.6	1.9	3.3							
No133	47.8	13.6	37.9	99.4	7	62.1	0.1	37.4	99.6	3
stdev.	4.2	1.1	3.9							
No135	38.0	11.4	51.2	100.6	11	45.6	0.1	54.6	100.2	2
stdev.	2.6	2.2	2.6							
No136	29.8	9.1	60.5	99.4	11	35.5	0.0	64.6	100.0	3
stdev.	3.6	2.7	3.0							
No137	25.2	6.8	68.4	100.4	20	27.3	0.1	72.3	99.7	1
stdev.	3.3	1.7	2.2							
No 139b	11.3	2.2	86.3	99.8	6	13.3	0.2	86.1	99.6	1
stdev.	0.4	0.2	0.7							
No 226	43.2	12.0	44.5	99.7	12	54.8	0.0	45.6	100.4	2
stdev.	5.2	1.8	4.4			0.8	0.0	0.4		
No 227	39.2	11.6	49.1	99.8	2	47.8	0.1	53.5	101.3	10
	3.8	1.3	4.5			0.2	0.1	0.2		

	L3					L2				
No	Ni	S	Cu	Total	Analyses	Ni	S	Cu	Total	Analyses
No 12	-	-	-	-	-	2.6	19.2	75.8	97.6	3
stdev.						0.4	0.0	0.5		
No 13	14.3	3.9	80.7	98.9	3	3.5	19.1	72.8	95.4	4
stdev.	0.8	0.1	1.5			1.4	0.1	1.4		
No 20	-	-	-	-	-	7.0	20.3	71.2	98.4	2
stdev.						0.4	0.2	0.4		
No 47	16.1	5.0	79.8	100.8	4	3.5	19.6	76.1	99.1	6
stdev.	1.6	1.7	0.5			0.2	0.2	0.2		
No 142	6.9	2.9	89.2	99.0	7	2.3	19.6	77.7	99.6	4
stdev.	0.6	1.4	1.0			1.5	0.2	1.2		
No 144	15.1	4.7	80.5	100.2	8	3.4	19.3	76.2	98.9	4
stdev.	1.2	1.1	1.6			0.7	0.8	2.0		
No 146	-	-	-	-	-	7.8	19.1	72.0	98.9	3
stdev.						1.5	0.4	0.9		
No 222	22.1	9.0	68.7	99.8	12	7.0	19.2	72.1	98.3	5
stdev.	2.8	1.8	1.4			1.6	0.6	2.3		
No 223	-	-	-	-	-	12.3	19.2	67.1	98.6	5
stdev.						2.8	0.2	2.6		
No 224	-	-	-	-	-	10.9	19.2	68.5	98.6	4
stdev.						0.7	0.3	0.6		
No 225	19.1	6.1	75.0	100.2	14	5.5	19.6	73.0	98.0	4
stdev.	2.1	1.7	1.2			0.6	0.1	1.0		
No 239	27.7	12.4	59.6	99.6	5	8.4	19.5	70.9	98.8	2
stdev.	2.8	1.9	1.7			0.1	0.1	1.2		
No 240	30.4	13.9	56.0	100.2	8	12.6	18.9	68.0	99.4	5
stdev.	5.4	1.5	3.5			5.2	1.6	6.2		
No 273	30.4	14.1	57.0	101.5	2	10.0	19.9	70.1	100.0	2
stdev.	0.3	0.3	0.7			1.8	0.3	1.2		
No 277	3.5	1.6	96.4	101.5	1	1.0	19.5	79.5	100.1	1

As shown in Figure 32, the 1100°C isotherm consists largely of liquid $L_{(2,3)}$. Cu is still a liquid at 1100°C (melting temperature of Cu is 1084,9°C, Massalski, 1986), and there is a thin strip of liquid connecting the main liquid field ($L_{(2,3)}$) with molten Cu. The presence of the liquid field in the Cu-corner of the ternary diagram at 1100°C is consistent with phase relations in the binary Cu-S diagram (Figure 6, Massalski, 1986) and Cu-Ni diagram (Figure 8, Massalski, 1986).

As at 1200°C, a field of coexisting liquid + alloy ($L_{(2,3)} + \alpha$) exists at 1100°C (Figure 32). Liquid co-existing with α becomes more S-rich with decreasing temperature.

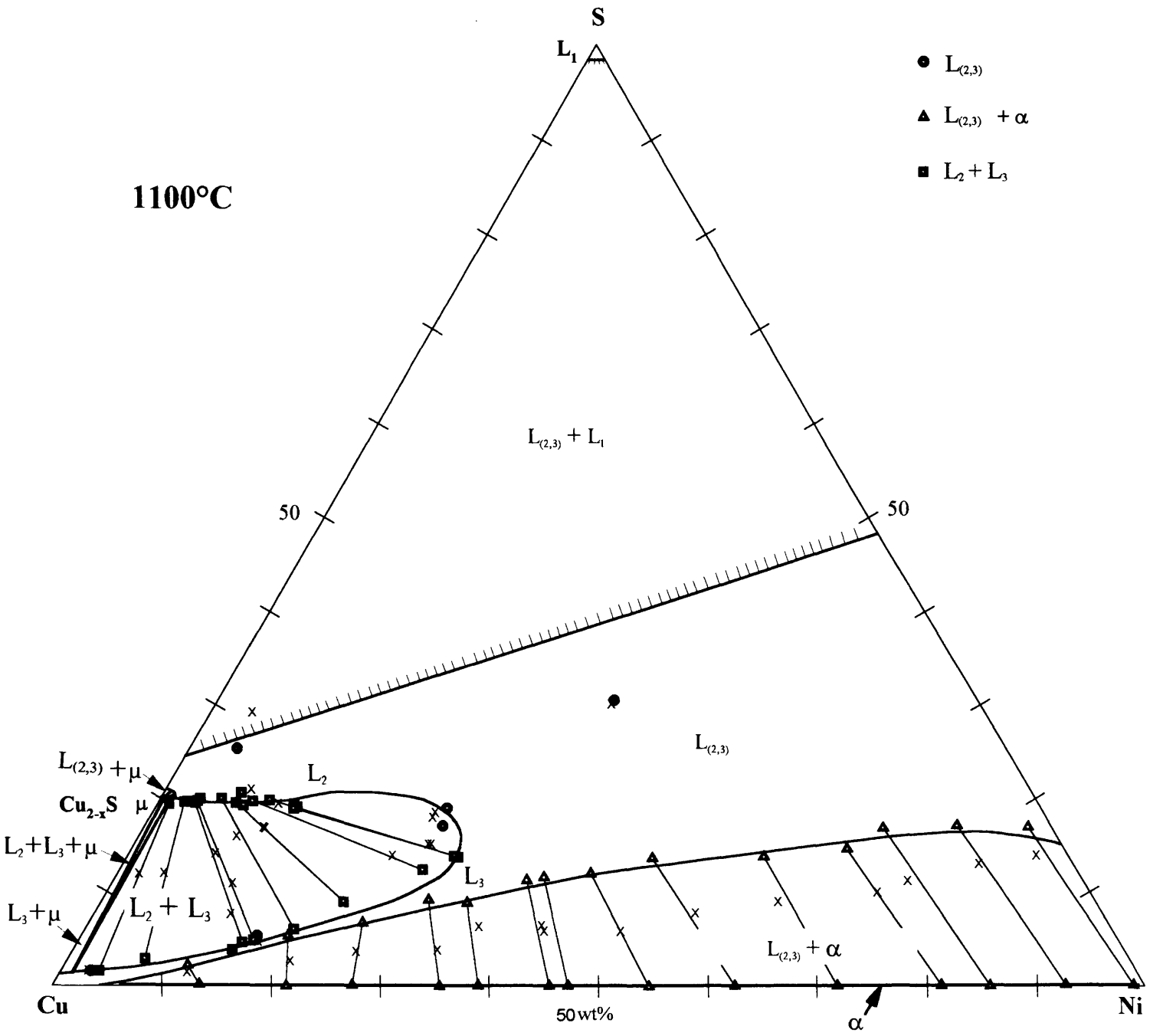

Figure 32. The 1100°C isothermal section showing the analysed compositions of co-existing phases. The bulk compositions of the experimental samples are shown as x's. The immiscible L_1 + $L_{(2,3)}$ field is drawn by extrapolation from the binary Cu-S (Massalski, 1986) and Ni-S (Lin et al., *1978) phase diagrams and is shown schematically.*

With high temperature digenite (μ) being solid below 1130°C (Figures 6 and 7, Massalski, 1986), it can be seen that instead of the immiscible liquid field (L_2+L_3), fields of co-existing liquid and digenite (L_2+μ, L_3+μ and $L_{(2,3)}$+μ) should be present on the Cu-S binary between 1130°C and 1067°C. The monotectic reaction temperature in the binary Cu-S is at 1105°C, below which L_2 disappears leaving L_3 + μ according to the reaction: $L_3 + L_2 = L_3 + \mu$. The L_3 + μ phase assemblage co-exists on the Cu-S binary until L_3 disappears at 1067°C, leaving Cu + μ (Figure 6, Massalski, 1986). L_2 co-exists with μ between 1130°C and 1105°C on the binary Cu-S (Figure 7, Massalski, 1986), and the composition of L_2 is less sulphur-rich than that of high temperature digenite (μ). Liquid and digenite also co-exists on the sulphur-rich side of μ between 1130°C and 813°C. This field is labelled $L_{(2,3)}$+μ to be consistent with the nomenclature of the ternary Cu-Ni-S system.

According to Kullerud *et al.* (1969), the two-liquid immiscible field (L_2+L_3) in the ternary Cu-Ni-S system retracts on cooling towards the Cu-S join. However, the thermal analysis results by Schlitt *et al.* (1973) show that the monotectic reaction temperature (at which the first solid $Cu_{2-x}S$ appears) decreases away from the Cu-S binary (Figure 33). In this investigation it was not possible to distinguish between solid high temperature digenite (μ) and L_2 or $L_{(2,3)}$ at 1100°C because of the similarities in composition. There was also no indication of the presence of the L_2+L_3+μ field at 1100°C.

In the ternary Cu-Ni-S system, the L_2+L_3+μ field at 1100°C field could be delineated using the results from Schlitt *et al.* (1973) as an approximation. It can be seen in Figure 33 that the reaction line at 1100°C should be close to the Cu-S binary and the approximate position of the L_2+L_3+μ field is shown in Figure 34. In Figure 35 the position of this field is shown for comparison on an enlarged portion of the 1100°C isothermal section.

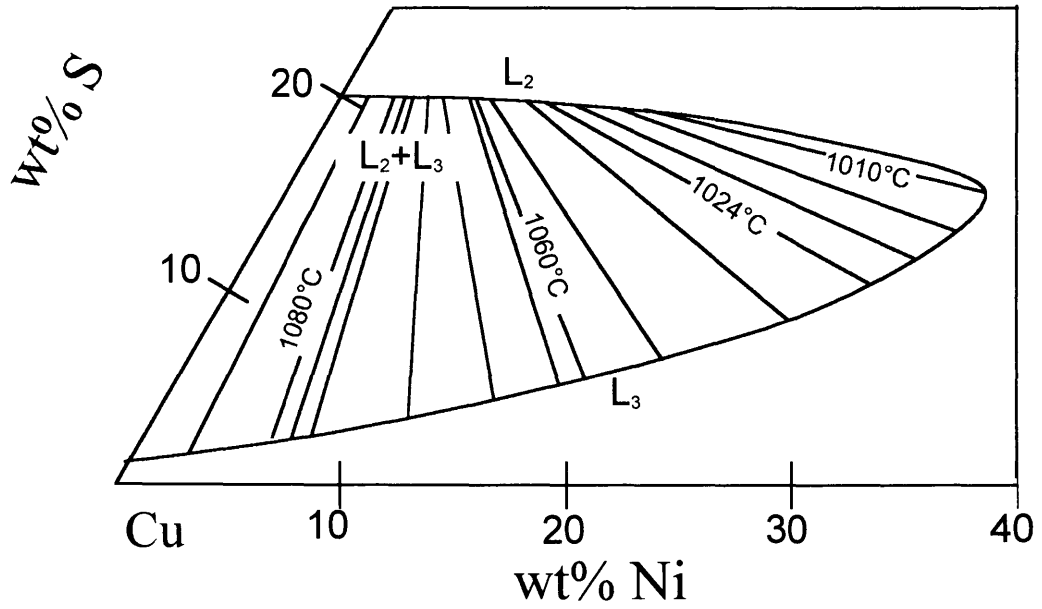

Figure 33. Portion of the Cu-Ni-S phase diagram showing the immiscible liquid region at 1200°C as well as the monotectic reaction temperatures (from Schlitt et al., *1973).*

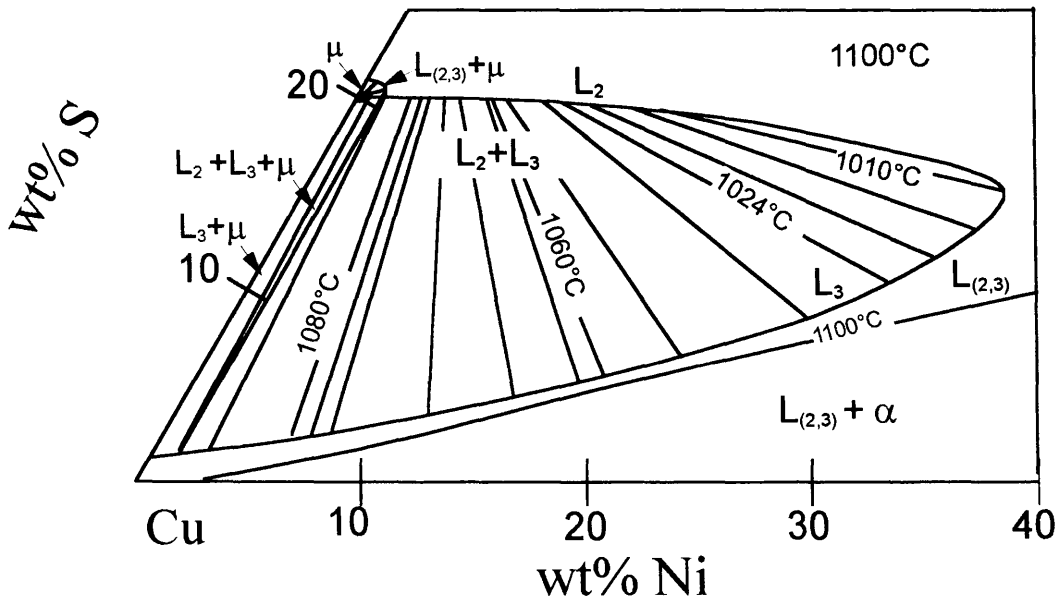

Figure 34. Portion of the Cu-Ni-S phase diagram showing the approximate position of the $L_2+L_3+\mu$ field at 1100°C using the monotectic reaction temperatures of Schlitt et al., *1973.*

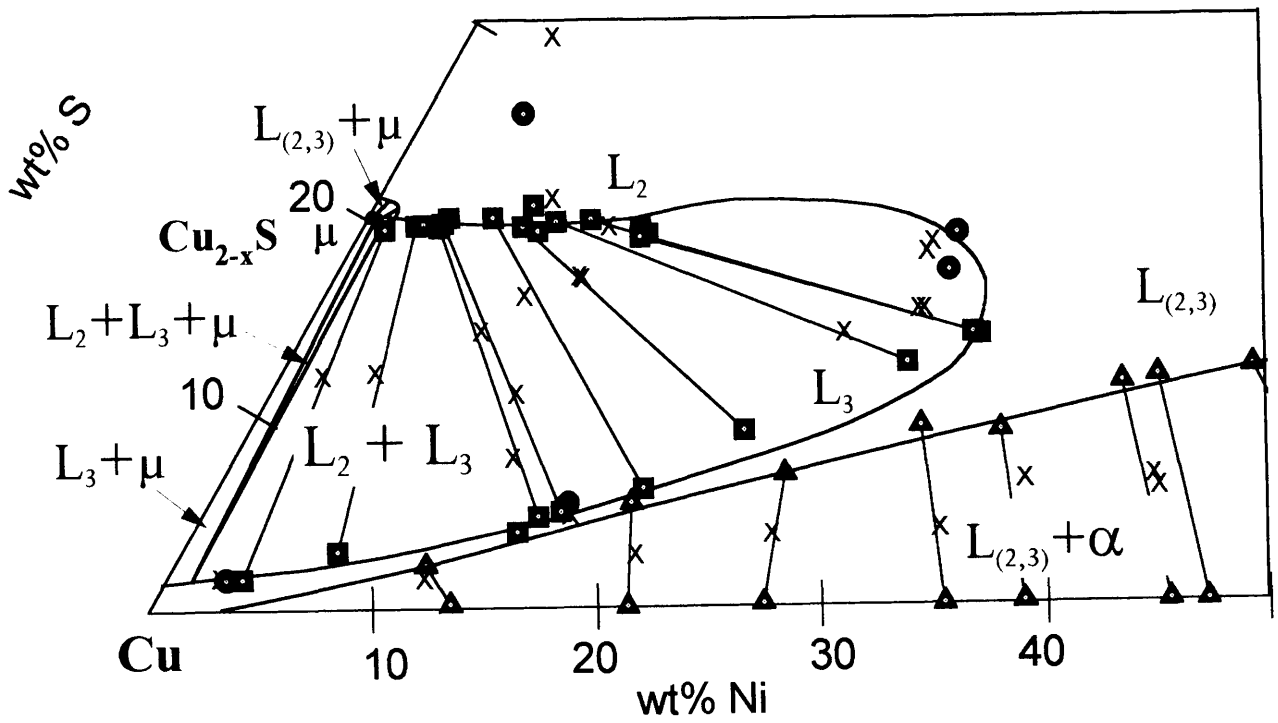

Figure 35. Portion of the 1100°C isothermal section. The bulk compositions of the experimental samples are shown as x's. The $L_3+\mu$, $L_{(2,3)}+\mu$, and the $L_2+L_3+\mu$ fields are shown schematically. The fields are consistent with the Cu-S binary phase diagram (Massalski, 1986) and the approximate position of the monotectic reaction line at 1100°C (Schlitt et al., *1973).*

The development of the phase diagram with decreasing temperature can be presented schematically, using Figure 33 and the binary Cu-S diagram in Figures 6 and 7 (Massalski, 1986). The sequence of events is presented schematically in Figures 36 and 37. At 1080°C, the position of the three phase field $L_2+L_3+\mu$ can be expected to be as shown in Figure 36. Copper is solid at 1080°C (melting point at 1084,9°C, Massalski, 1986) and the liquid + alloy ($L_{(2,3)}+\alpha$) phase field extents from the Ni-S binary to the Cu-S binary.

From 1067°C (Massalski, 1986) the liquid field retracts from just above the Cu apex on the Cu-S binary and it follows the crystallisation path that is delineated by the liquidus at 1100°C (Figure 32), with the arrow indicating the direction of retraction in Figure 37. The retraction of the liquid field enables the establishment of $Cu_{2-x}S$ + alloy ($\mu+\alpha$) tie-lines, and of the three phase liquid + $Cu_{2-x}S$ + alloy ($L_3+\mu+\alpha$) field. The positions of these fields are shown schematically on the 1024°C isotherm in Figure 37. As cooling progresses further, the immiscible liquid field of L_2+L_3 is expected to disappear so that only fields of $Cu_{2-x}S$ + alloy ($\mu+\alpha$), liquid + $Cu_{2-x}S$ ($L_{(2,3)}+\mu$) and liquid + $Cu_{2-x}S$ + alloy ($L_{(2,3)}+\mu+\alpha$) exist at temperatures below ~1000°C.

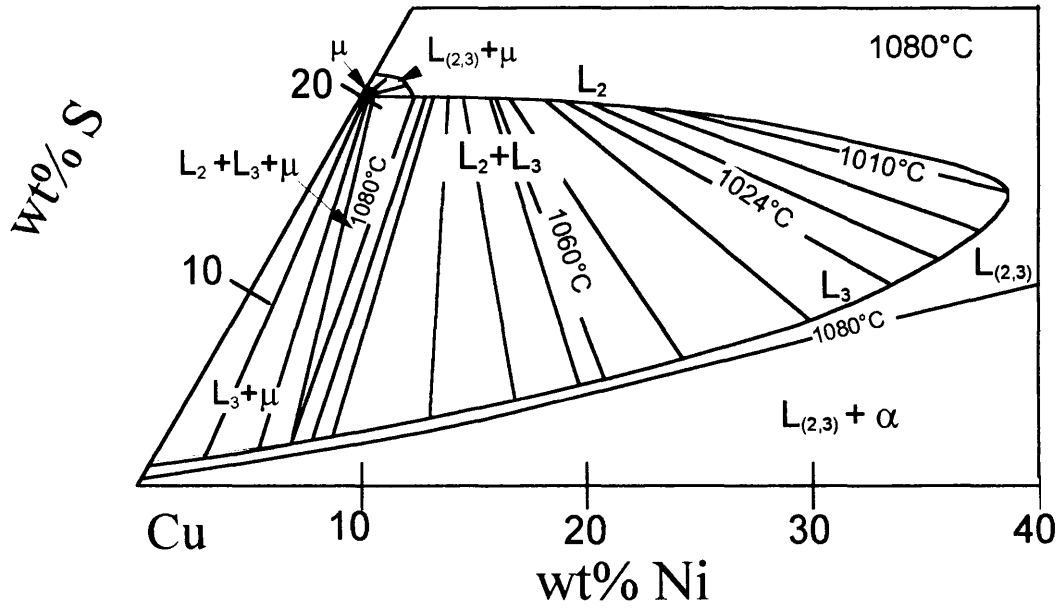

Figure 36. Portion of the schematic 1080°C isothermal section using the monotectic lines of Schlitt et al. (1973) (J.R. Taylor, pers. comm., 1996).

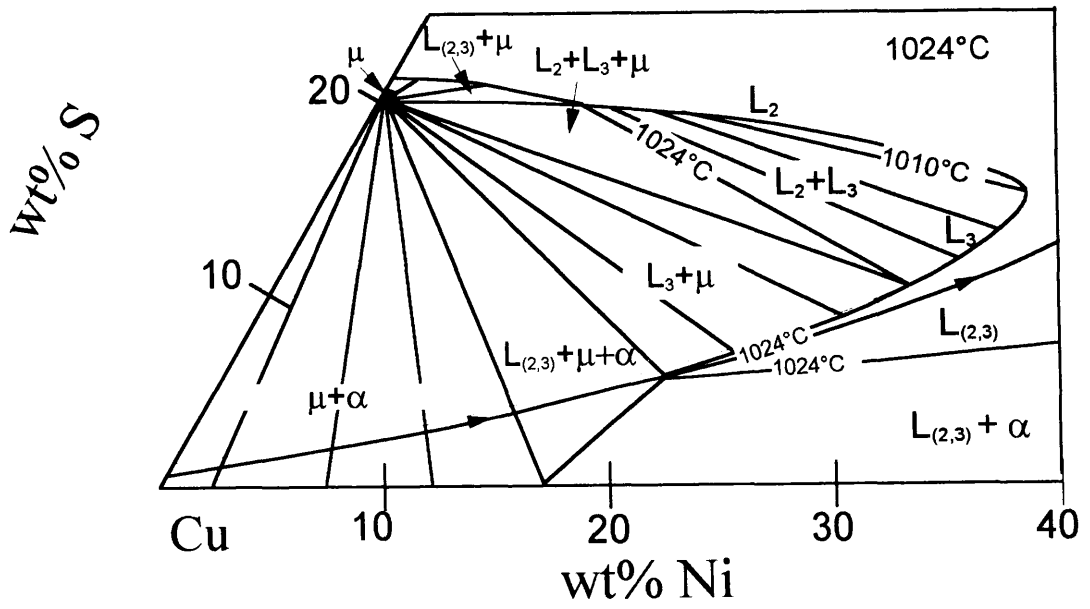

Figure 37. Portion of the schematic 1024°C isothermal section using the monotectic lines of Schlitt et al. (1973) (J.R. Taylor, pers. comm., 1996). The crystallisation path is in accordance with the binary Cu-S diagram (Massalski, 1986) and the liquidus at 1100°C (this investigation). The direction of retraction of the liquid field is indicated by the arrows.

4.4 THE 1000°C ISOTHERMAL SECTION

The samples made for investigation of the 1000°C isothermal section are listed in Appendix A-3.

The averaged SEM analyses are listed in Table 16 and presented in Figure 38.

Table 16. The averaged SEM analyses (wt%) of co-existing phases at 1000°C, with the number of areas that were analysed, and the calculated standard deviations (1σ).

		L(2,3)			
No	Ni	S	Cu	Total	Analyses
No 34	34.4	29.3	35.4	99.0	2
stdev.	0.2	0.1	0.3		
No 35	16.6	31.6	50.9	99.2	1
No 37	70.8	23.1	3.9	97.8	2
stdev.	1.0	0.1	0.0		
No 38	53.6	22.9	22.4	98.9	3
stdev.	1.7	0.3	1.9		
No 55	60.2	34.1	3.6	97.9	1
No 57	59.5	35.7	2.9	98.1	1
No 59	63.7	32.0	2.4	98.1	3
stdev.	0.0	0.5	0.3		
No 62	62.5	22.1	14.1	98.6	7
stdev.	2.0	0.3	2.1		
No 61	67.1	25.5	5.7	98.2	3
stdev.	0.4	0.3	0.5		
No 60	62.7	33.4	1.8	98.0	3
stdev.	0.8	0.4	0.4		
No 67	9.3	23.8	65.1	98.2	6
stdev.	3.3	1.4	4.8		
No 106	67.4	25.4	6.2	99.1	1
No 107	65.7	25.5	6.6	97.8	2
stdev.	1.9	0.1	1.3		

		L(2,3)					α			
No	Ni	S	Cu	Total	Analyses	Ni	S	Cu	Total	Analyses
No40	36.8	15.1	46.6	98.6	3	36.0	0.0	64.8	100.8	3
stdev.	1.8	2.5	4.4							
No 66	60.3	16.5	22.5	99.3	6	72.3	0.0	26.6	98.9	4
stdev.	3.7	2.6	4.2							
No 160	42.2	15.0	41.2	98.4	14	45.1	0.2	53.9	99.2	1
stdev.	5.4	2.0	5.2							
No 162	52.1	15.6	31.3	98.9	13	56.8	0.0	42.3	99.1	1
stdev.	1.5	2.1	2.7							
No 166	66.5	17.0	16.0	99.4	8	83.5	0.0	15.9	99.4	1
stdev.	3.6	2.4	3.7							

		L(2,3)					μ			
No	Ni	S	Cu	Total	Analyses	Ni	S	Cu	Total	Analyses
No 68	27.7	19.8	50.3	97.7	2	2.8	19.5	75.8	98.0	6
stdev.	0.9	0.3	1.6							
No.169	23.8	20.6	53.1	97.5	2	3.5	20.4	78.6	102.4	1
stdev.	2.1	2.4	4.9							
No 174	40.7	19.2	38.9	98.9	9	2.4	19.6	76.1	98.1	1
stdev.	3.1	0.3	3.4							
No 48	-	-	-	-	-	3.3	22.4	73.6	99.3	9
stdev.						2.7	0.9	3.8		
No 168	-	-	-	-	-	2.5	20.7	77.2	100.4	1

		μ					α			
No	Ni	S	Cu	Total	Analyses	Ni	S	Cu	Total	Analyses
No 45	0.2	18.9	73.6	92.7	1	9.0	0.0	91.1	100.1	7
No 153	0.5	19.6	78.8	99.0	1	7.7	0.0	91.8	99.5	2
No 154	0.3	19.2	78.2	97.7	1	13.9	0.0	87.0	100.9	2
No 155	0.3	19.5	78.0	97.8	1	20.0	0.1	80.6	100.7	2
No 156	0.0	19.3	78.6	97.9	1	27.2	0.0	72.5	99.7	2

		L(2,3)					μ					α			
No	Ni	S	Cu	Total	Analyses	Ni	S	Cu	Total	Analyses	Ni	S	Cu	Total	Analyses
No 41	36.1	15.7	47.6	99.3	9	2.3	19.8	76.9	99.0	4	34.8	0.0	65.3	100.2	4
stdev.	7.1	2.0	6.8			0.3	0.1	0.3			0.2	0.1	0.9		
No 171	37.5	17.1	47.3	101.8	29	1.0	19.5	77.5	97.9	1	-	-	-	-	-
stdev.	6.3	2.0	6.2												

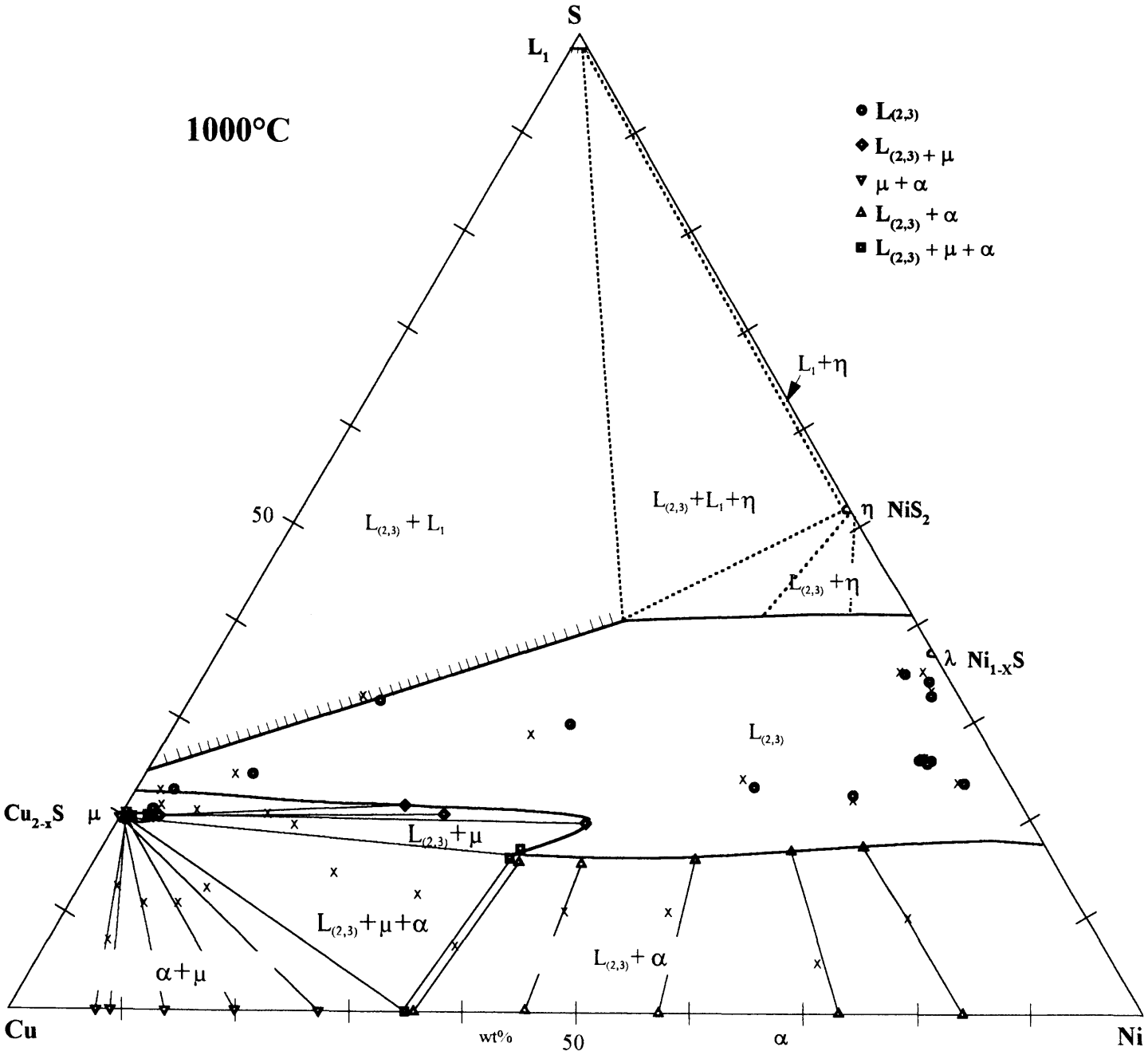

Figure 38. Phase boundaries and tie-lines between the analysed compositions of co-existing phases present at 1000°C. The bulk compositions of the experimental samples are shown as x's. The immiscible L_1 + $L_{(2,3)}$ field is drawn by extrapolation from the binary Cu-S (Massalski, 1986) and Ni-S (Lin et al., *1978) phase diagrams, and the sulphur-rich part of the diagram is shown schematically.*

The 1000°C isothermal section shows radical differences from the isothermal sections at higher temperatures. The immiscible liquid field L_2+L_3 is not present at 1000°C and instead fields of co-existing $L_{(2,3)}+\mu$, $L_{(2,3)}+\mu+\alpha$, and $\mu+\alpha$ occur (Figure 38).

There is limited solid solution of Ni in high temperature $Cu_{2-x}S$ (μ) (up to 3.5 wt% Ni, Table 16), as shown by the extent of the μ field in the liquid + $Cu_{2-x}S$ ($L_{(2,3)}+\mu$) phase assemblage at 1000°C (Figure 38). The Ni exsolves, presumably as nickel sulphide, on cooling. The $L_{(2,3)}+\mu$ phase assemblage is shown in Photomicrograph 5.

It was often found that samples in the liquid + $Cu_{2-x}S$ ($L_{(2,3)}+\mu$) field contained a sphere of $L_{(2,3)}$ surrounded by μ. This is probably due to differences in the intersurface tension between the two phases. Experiments by Ip and Toguri (1993) in the Ni-Fe-S and Ni-Cu-S systems showed that the surface tension of a Cu-Ni-S matte increases with decreasing Cu_2S content. The increase in surface tension can be interpreted as the tendency for the liquid to occupy the smallest possible surface area per unit volume, i.e. a sphere. The increase in surface tension of the liquid might possibly aid the expulsion of Cu_2S from the liquid, and it may be an explanation for the observation that Cu_2S was found surrounding the liquid $L_{(2,3)}$ phase.

A three phase field was observed at 1000°C (Figure 38) with coexisting liquid + $Cu_{2-x}S$ + alloy ($L_{(2,3)}+\mu+\alpha$). No gravity segregation of the different phases was observed, and the typical phase assemblage is shown in Photomicrograph 6.

The S-rich phase boundary of the liquid field and the predicted phase associations of $L_{(2,3)}+L_1$, $L_{(2,3)}+\eta$, $L_1+\eta$ are consistent with the binary Cu-S and Ni-S systems and is shown schematically in Figure 38. The position of the $L_{(2,3)}+L_1$ and $L_{(2,3)}+L_1+\eta$ boundary is estimated.

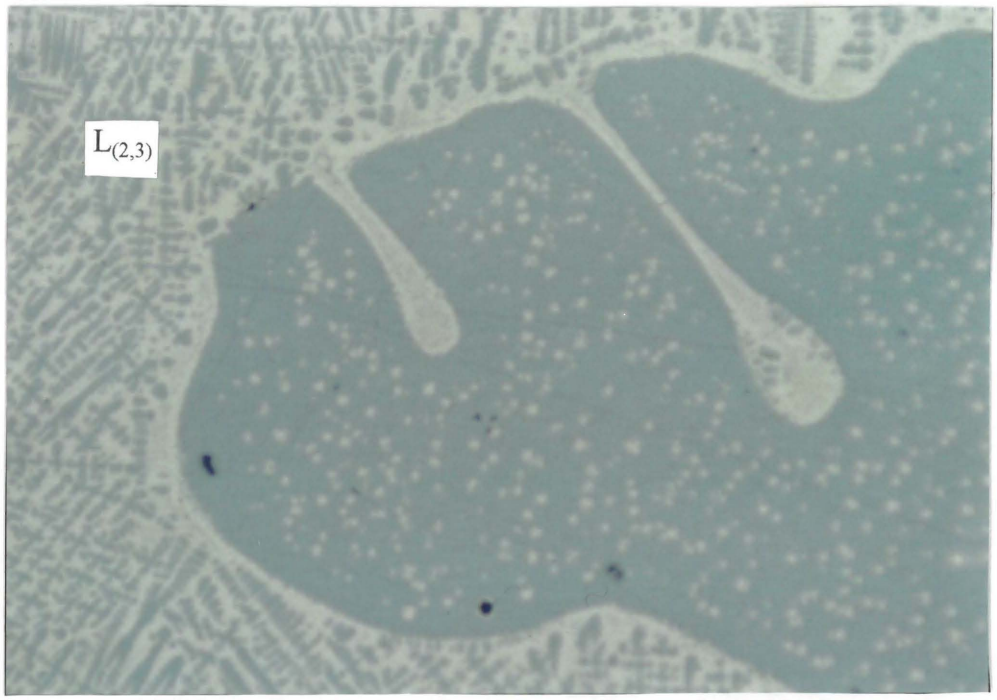

Photomicrograph 5. Typical texture found in charges containing liquid ($L_{(2,3)}$) + high temperature $Cu_{2-x}S$ (μ, grey with small round exsolutions). $Cu_{2-x}S$ can contain other elements at high temperatures, which are exsolved when quenched. Charge 94, at 900°C (long side of the photomicrograph is 1.25mm).

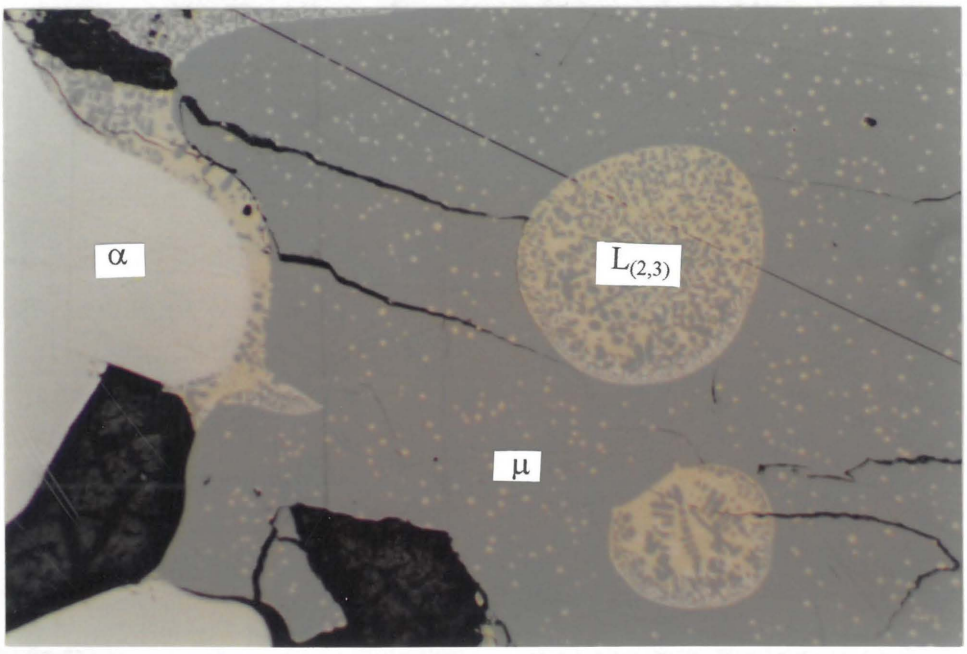

Photomicrograph 6. Typical texture found in charges containing liquid ($L_{(2,3)}$) + alloy (α, yellow) + $Cu_{2-x}S$ (μ, grey). Charge 41, at 1000°C (long side of the photomicrograph is 1.25mm).

The association of $Cu_{2-x}S$ + alloy ($\mu+\alpha$) could be observed at 1000°C (Figure 38). This all-solid assemblage (shown in Photomicrograph 7) required long tempering times to reach equilibrium. In solid phase assemblages diffusion rates are slower than in liquid phases. Diffusion rates are also slow at low temperatures. Incomplete reaction was found in two charges, nos. 42 and 43, containing $Cu_{2-x}S$ + alloy ($\mu+\alpha$) where the phases did not reach equilibrium in 18 and 45 days respectively. This was obvious from a gradual colour change through the alloy phase, which was caused by a difference in the composition of the alloy by up to 13 wt % Cu from one side of the sample to the other. The microscopic investigation of charges for signs of non-equilibrium was therefore very important, and non-equilibrium charges were not included in the construction of phase diagrams.

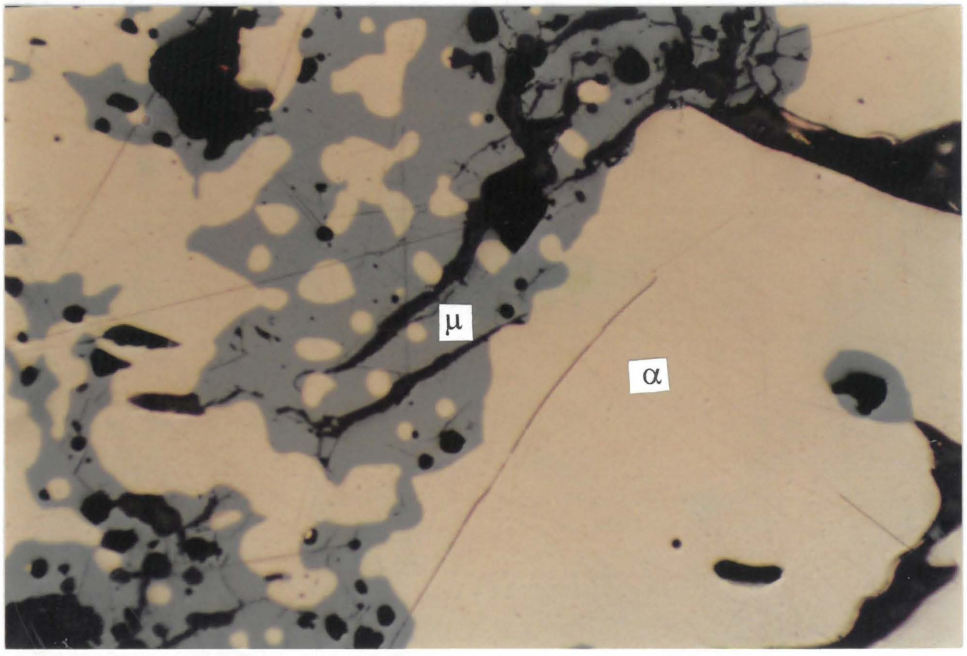

Photomicrograph 7. High temperature $Cu_{2-x}S$ (μ, grey) co-existing with Cu-rich alloy (α, pinkish). Charge 45 at 1000°C (long side of the photomicrograph is 500 μm).

4.5 THE 900°C ISOTHERMAL SECTION:

The compositions of the charges made for the investigation of the 900°C isothermal section, and the experimental details are listed in Appendix A-4. The averaged SEM analyses of co-existing phases are listed in Table 17 and are presented in Figure 39.

Table 17. The averaged SEM analyses (wt%) of co-existing phases at 900°C, with the number of areas that were analysed, and the calculated standard deviations (1σ).

	L(2,3)				
No	Ni	S	Cu	Total	Analyses
No85	12.8	28.9	58.1	99.8	8
stdev.	1.0	0.7	1.9		
No 86	25.2	31.8	42.7	99.6	6
stdev.	3.7	3.4	7.0		
No 87	28.1	26.5	45.0	99.7	18
stdev.	5.2	1.3	6.7		
No 92	60.6	29.3	8.4	98.3	1
No 235	26.2	28.1	45.7	99.9	1
No 248	27.0	26.5	46.7	100.1	1
No 84	11.8	25.1	62.3	99.2	6
stdev.	1.7	0.5	2.7		

	L(2,3)					α				
No	Ni	S	Cu	Total	Analyses	Ni	S	Cu	Total	Analyses
No 74	71.4	18.8	8.3	98.5	8	90.3	0.1	9.1	99.5	3
stdev.	2.1	3.0	1.6							
No 75	65.0	19.3	14.1	98.3	9	80.4	0.1	18.1	98.6	3
stdev.	1.2	2.5	2.3							
No 76	56.1	17.3	25.1	98.5	15	67.5	0.0	31.4	99.0	3
stdev.	4.3	2.1	4.4							
No 77	45.5	17.5	35.9	98.9	23	50.2	0.1	50.0	100.3	1
stdev.	4.9	1.3	4.8							

	L3					u				
No	Ni	S	Cu	Total	Analyses	Ni	S	Cu	Total	Analyses
No 82	5.0	24.8	69.1	98.9	11	1.9	21.9	74.8	98.7	4
stdev.	0.6	0.6	0.9							
No 94	37.8	24.4	36.3	98.6	14	4.06	19.8	74.7	98.66	3
stdev.	5.2	0.8	6.3							
No 98	16.4	25.1	56.3	97.8	9	3.8	21.1	72.6	97.5	2
stdev.	2.3	0.8	3.2							
No 99	25.6	24.9	47.7	98.2	12	5.5	20.5	72.0	98.0	2
stdev.	4.2	1.0	5.1							
No 237	51.2	20.9	25.7	97.8	5	2.7	19.5	75.5	97.7	2
stdev.	0.4	1.1	1.2							

	u					α				
No	Ni	S	Cu	Total	Analyses	Ni	S	Cu	Total	Analyses
No 81	1.0	19.5	76.9	97.3	4	21.2	0.1	78.2	99.5	6
No 80	0.3	19.4	78.8	98.48	2	37.5	0.1	62.3	99.9	8

	L(2,3)					λ				
No	Ni	S	Cu	Total	Analyses	Ni	S	Cu	Total	Analyses
No 90	61.6	31.2	5.1	97.9	11	62.6	34.8	0.8	98.2	3
stdev.	3.3	0.7	4.3							
No 93	50.3	32.3	15.9	98.5	13	60.5	35.1	2.2	97.8	3
stdev.	4.3	1.0	5.8							

	L(2,3)					μ					α				
No	Ni	S	Cu	Total	Analyses	Ni	S	Cu	Total	Analyses	Ni	S	Cu	Total	Analyses
No 78	44.0	17.6	37.6	99.2	14	1.8	19.5	76.2	97.5	3	48.0	0.0	51.4	99.4	6
stdev.	6.9	1.8	7.2												
No 79	-	-		-		1.4	19.3	77.6	98.3	3	47.9	0.1	51.8	99.8	6
No22	45.1	17.0	38.8	100.8	2	1.9	19.8	77.4	99.2	1	46.7	0.0	54.2	100.9	1
stdev.	3.6	0.1	4.3												

	L(2,3)					η					λ				
No	Ni	S	Cu	Total	Analyses	Ni	S	Cu	Total	Analyses	Ni	S	Cu	Total	Analyses
No 89	45.8	34.6	18.4	98.8	9	46.7	50.4	0.8	97.9	3	60.0	35.8	2.5	98.3	2
stdev.	6.3	1.2	5.7												

According to the binary phase diagrams of the Cu-S and Ni-S systems there is immiscibility between sulphur liquid (L_1) and sulphide liquid ($L_{2,3}$) from about 1200°C to 813°C on the Cu-S binary (Massalski, 1986, Figure 6), and immiscibility from about 1200°C to 1022°C on the Ni-S binary (Lin *et al.*, 1978, Figure 2). This means that the miscibility gap between L_1 and $L_{(2,3)}$ does not occur on the Ni-S side of the ternary diagram at temperatures below 1022°C, although it does occur on the Cu-S side down to 813°C. On the S-rich side of the diagram one would thus expect a phase boundary separating the Cu and Ni sides on the 1000°C and 900°C isothermal sections. This is schematically shown in Figures 38 and 39.

NiS_2 is solid below 1022°C and high temperature $Ni_{1-x}S$ (λ) solidifies at 999°C (Lin et al., 1978). These nickel sulphides can be found in the liquid + $Ni_{1-x}S$ ($L_{2,3}$)+λ) and liquid + NiS_2 + $Ni_{1-x}S$ ($L_{2,3}$)+η+λ) phase associations at 900°C, as shown in Photomicrographs 8 and 9 respectively.

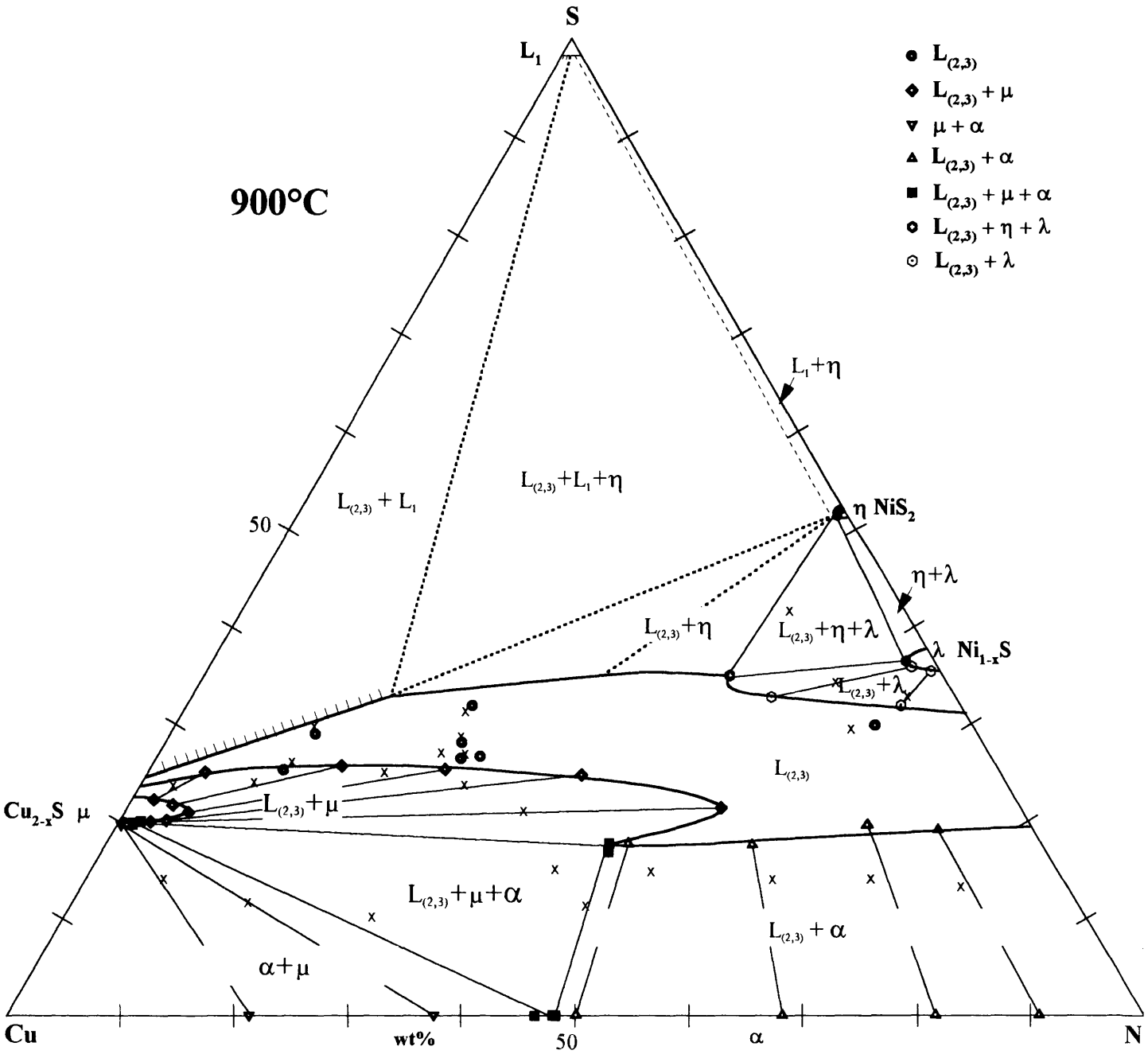

Figure 39. The 900°C isothermal section, with phase boundaries and tie-lines between analysed compositions of co-existing phases. The bulk compositions of the experimental samples are shown as x's. The phase associations on the sulphur-rich side of the diagram is shown schematically.

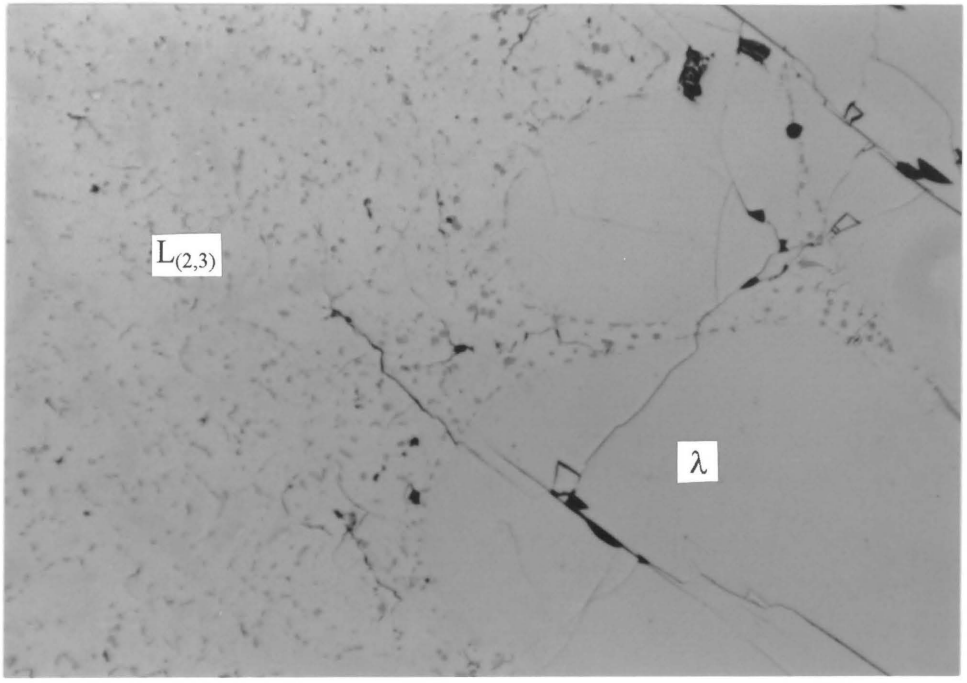

Photomicrograph 8. Typical texture found in charges containing liquid ($L_{2,3}$) + $Ni_{1-x}S$ (λ, yellow). Charge 90, at 900°C (long side of the photograph is 1.25 mm).

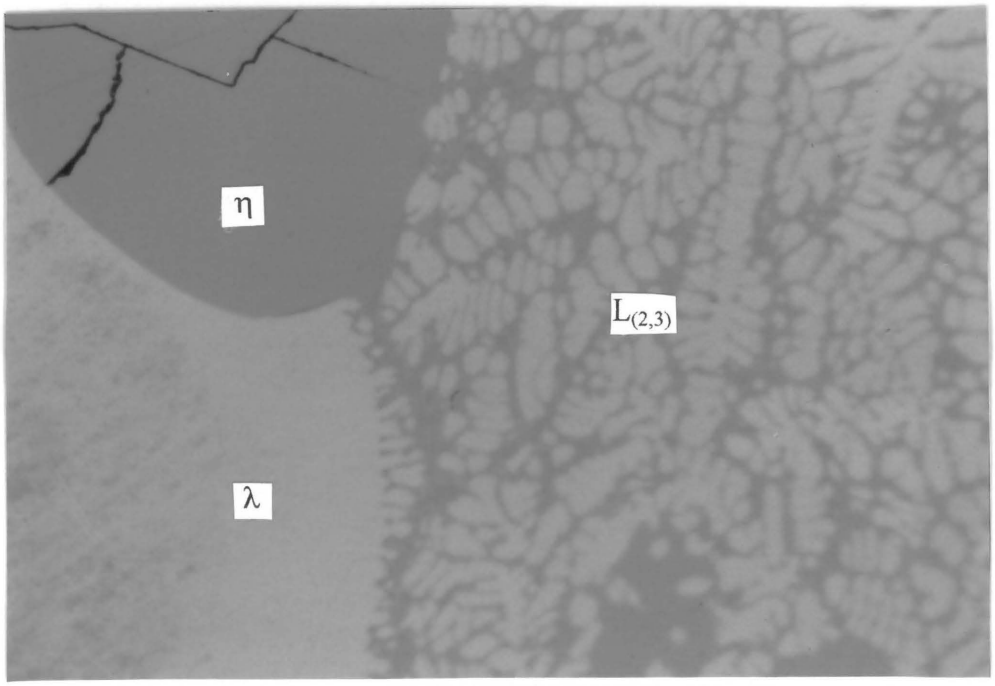

Photomicrograph 9. Charge 89 containing liquid ($L_{2,3}$) + NiS_2 (η, grey) + $Ni_{1-x}S$ (λ, yellow), at 900°C (long side of photograph is 500μm).

4.6 THE 800°C ISOTHERMAL SECTION

The compositions of charges made for investigation of the 800°C isothermal section, with their pre-reaction and tempering histories are listed in Appendix A-5. The averaged SEM analyses of co-existing phases are presented in Table 18 and in Figure 40.

Table 18. The averaged SEM analyses (wt%) of co-existing phases at 800°C, with the number of areas that were analysed, and the calculated standard deviations (1σ).

	L(2,3)				
No	Ni	S	Cu	Total	Analyses
No 182	65.9	28.4	2.1	96.4	4
stdev.	0.8	0.2	0.5		

	L(2,3)					α				
No	Ni	S	Cu	Total	Analyses	Ni	S	Cu	Total	Analyses
No 176	58.4	19.6	20.6	98.6	14	62.2	0.1	38.6	100.8	2
stdev.	4.3	1.5	4.6							
No 177	60.2	19.9	18.1	98.1	8	69.8	0.1	29.3	99.2	2
stdev.	4.2	2.0	5.1							
No 178	63.8	20.6	13.9	98.2	5	76.6	0.0	22.2	98.7	2
stdev.	1.5	0.3	1.2							
No 180	68.9	19.9	9.3	98.1	7	88.4	0.2	10.0	98.6	1
stdev.	0.9	1.9	1.5							
No 181	73.2	19.8	4.8	97.9	10	92.6	0.0	5.3	97.9	2
stdev.	22.1	6.3	1.6							
No 199	67.5	20.7	12.4	100.6	3	84.8	0.1	16.3	101.2	1
stdev.	0.3	0.3	0.5							

	α					μ				
No	Ni	S	Cu	Total	Analyses	Ni	S	Cu	Total	Analyses
No 121	6.2	0.0	93.8	100.0	2	0.2	19.5	79.2	98.9	2
No 122	13.5	0.0	87.3	100.8	2	0.6	19.7	78.8	99.2	2
No 123	19.7	0.0	80.8	100.5	2	0.5	19.7	78.7	98.8	2
No 124	28.3	0.0	71.8	100.1	2	1.0	19.4	77.8	98.2	2

	L(2,3)					μ				
No	Ni	S	Cu	Total	Analyses	Ni	S	Cu	Total	Analyses
No 191	57.7	24.4	16.3	98.5	16	3.1	19.8	76.2	99.0	1
stdev.	1.3	0.2	1.4							
No 192	48.7	26.5	23.9	99.1	16	4.7	20.3	72.8	97.8	1
stdev.	2.8	0.5	3.3							

	L(2,3)					λ				
No	Ni	S	Cu	Total	Analyses	Ni	S	Cu	Total	Analyses
No 183	66.9	29.5	1.4	97.8	6	63.0	34.3	0.6	97.8	5
stdev.	1.6	0.5	1.5							
No 184	64.2	28.6	4.1	97.0	7	62.8	34.5	0.3	97.6	1
stdev.	0.7	1.0	0.6							
No 231	46.3	28.6	24.2	99.2	8	60.8	34.5	2.5	97.7	2
stdev.	2.8	0.7	3.4							
No 245	62.3	29.8	8.9	101.0	3	63.9	35.1	1.2	100.2	1
stdev.	0.8	0.5	0.3							

		L(2,3)					μ					α			
No	Ni	S	Cu	Total	Analyses	Ni	S	Cu	Total	Analyses	Ni	S	Cu	Total	Analyses
No 125	59.0	19.2	20.9	99.1	10	1.8	20.1	77.7	99.6	1	58.3	0.1	41.2	99.5	2
stdev.	1.1	1.6	2.0												
No 126	59.0	19.9	20.1	99.0	6	3.1	19.5	76.7	99.3	2	58.7	0.0	42.1	100.8	2
stdev.	0.7	0.9	1.5												
No 127	58.3	18.8	21.8	98.9	5	1.7	19.6	78.2	99.6	2	58.7	0.0	41.1	99.8	2
stdev.	4.4	1.8	5.4												

		L(2,3)					μ					λ			
No	Ni	S	Cu	Total	Analyses	Ni	S	Cu	Total	Analyses	Ni	S	Cu	Total	Analyses
No 193	36.5	28.9	33.0	98.4	20	5.3	20.9	71.8	98.1	5	61.6	34.3	2.0	97.9	1
stdev.	3.6	0.7	4.7												
No 198	36.5	29.6	31.9	98.0	5	5.4	21.1	72.5	99.0	3	61.3	34.6	2.0	97.8	2
stdev.	1.4	0.4	1.5												

		L4					μ					η			
No	Ni	S	Cu	Total	Analyses	Ni	S	Cu	Total	Analyses	Ni	S	Cu	Total	Analyses
No 190	5.4	25.0	68.4	98.8	6	1.2	21.6	75.5	98.3	6	41.9	49.9	5.6	97.4	5
stdev.	0.9	0.4	1.4												
No 196	8.7	26.5	64.2	99.4	6	2.8	21.4	75.2	99.3	3	44.6	49.6	2.9	97.1	2
stdev.	0.9	0.7	1.2												

		L4					μ					λ			
No	Ni	S	Cu	Total	Analyses	Ni	S	Cu	Total	Analyses	Ni	S	Cu	Total	Analyses
No 194	19.9	28.0	49.7	97.6	6	4.1	21.2	72.4	97.7	2	57.7	35.3	3.9	96.8	2
stdev.	0.7	1.0	1.8												

		L4					η					λ			
No	Ni	S	Cu	Total	Analyses	Ni	S	Cu	Total	Analyses	Ni	S	Cu	Total	Analyses
No 233	21.5	28.0	49.5	98.9	6	59.0	35.2	3.7	97.9	3	46.2	50.0	1.3	97.5	2
stdev.	0.9	0.8	1.8												

Samples containing either one of the two liquids $L_{(2,3)}$ or L_4 in association with μ and λ indicates that the liquid field splits into two separate fields at a temperature below 900°C. The boundary of L_4 towards the Cu-side was determined from analyses of the liquid phase of samples 190 and 196 containing $L_4+\eta+\mu$ (Photomicrograph 10). The liquid + $Cu_{2-x}S$ + $Ni_{1-x}S$ ($L_4+\mu+\lambda$) phase assemblage in sample no 194 is shown in Photomicrograph 11. The composition of the liquid phase in the liquid+NiS_2+$Ni_{1-x}S$ ($L_4+\eta+\lambda$) phase assemblage in sample no 233 was used to construct the boundary of L_4 towards the Ni side (Photomicrograph 12). A separate liquid field similar to the L_4 field at 800°C was also observed by Kullerud *et al.* (1969) at 780°C (Figure 18).

The Cu-rich boundary of $L_{(2,3)}$ was determined from the composition of the liquid phase in samples 193 and 198 containing liquid + $Cu_{2-x}S$ + $Ni_{1-x}S$ ($L_{(2,3)}+\mu+\lambda$).

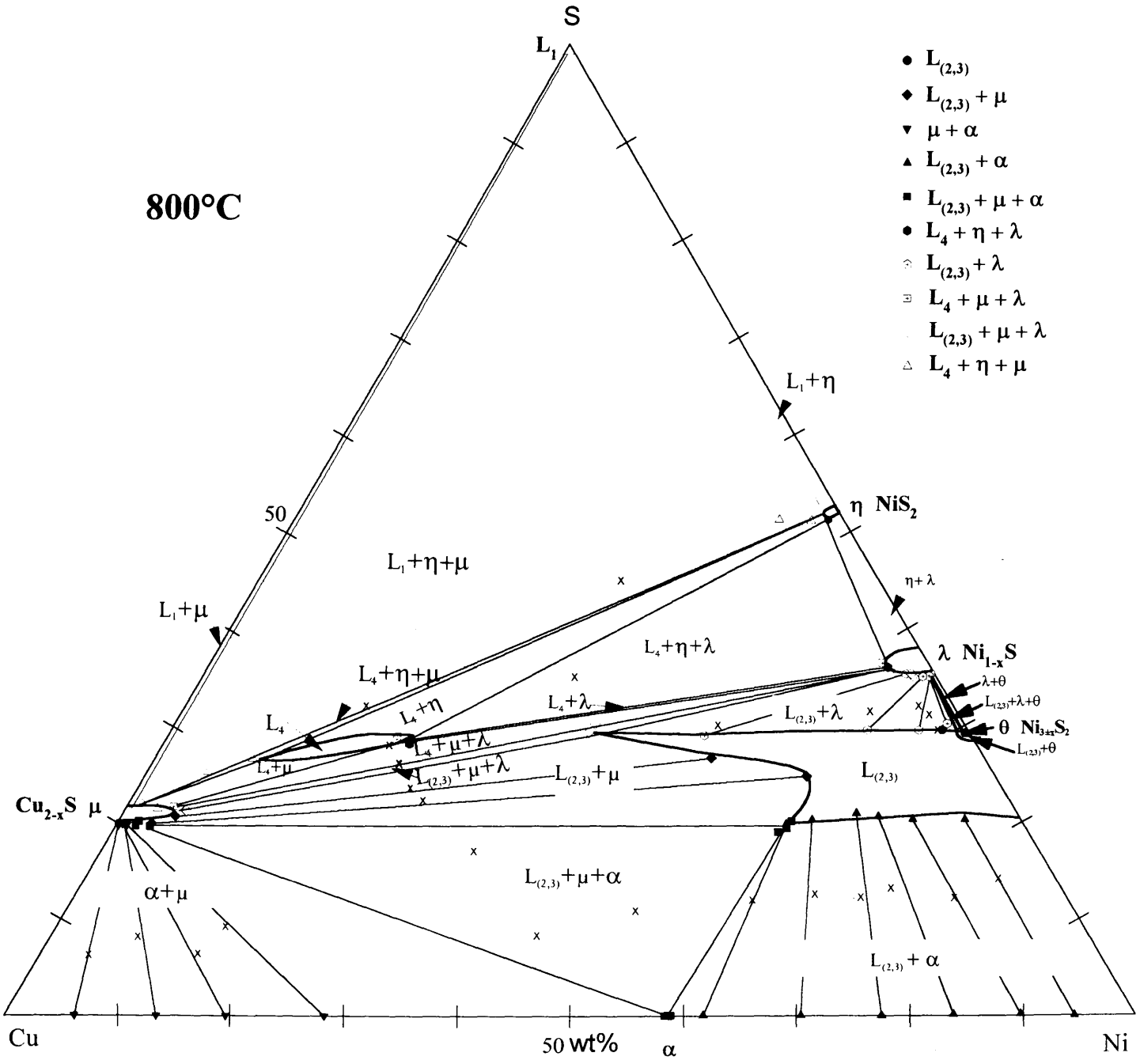

Figure 40. The 800°C isothermal section with phase boundaries and tie-lines between co-existing phases. The bulk compositions of the experimental samples are shown as x's.

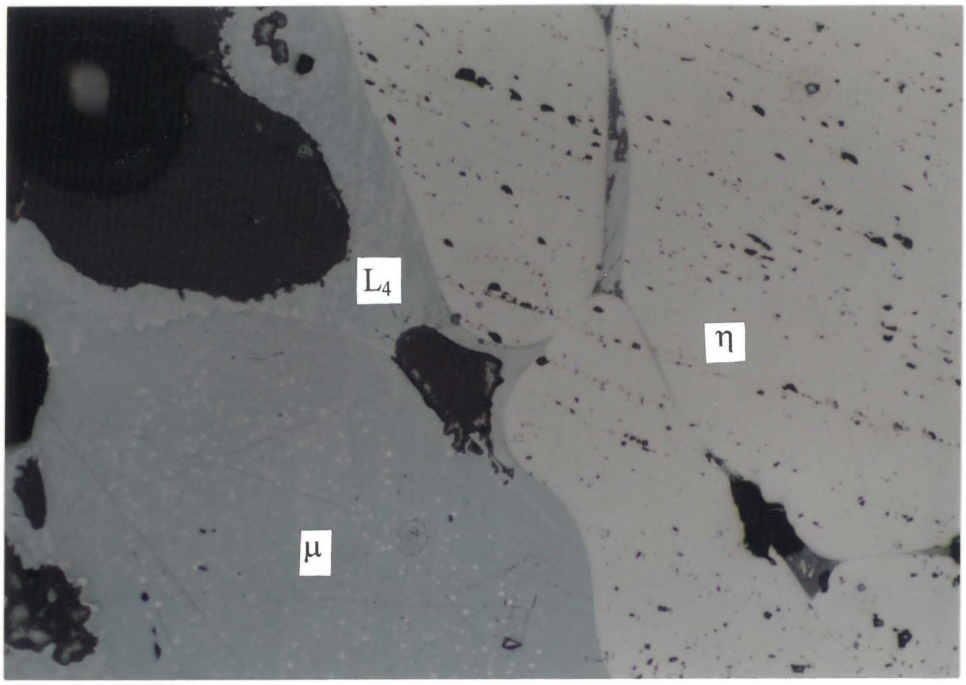

Photomicrograph 10. Typical texture found in charges containing liquid (L_4) + vaesite (η, grey)+ $Cu_{2-x}S$ (μ, bluish grey). Charge 190, at 800°C, (long side of the photomicrograph is 250 μm).

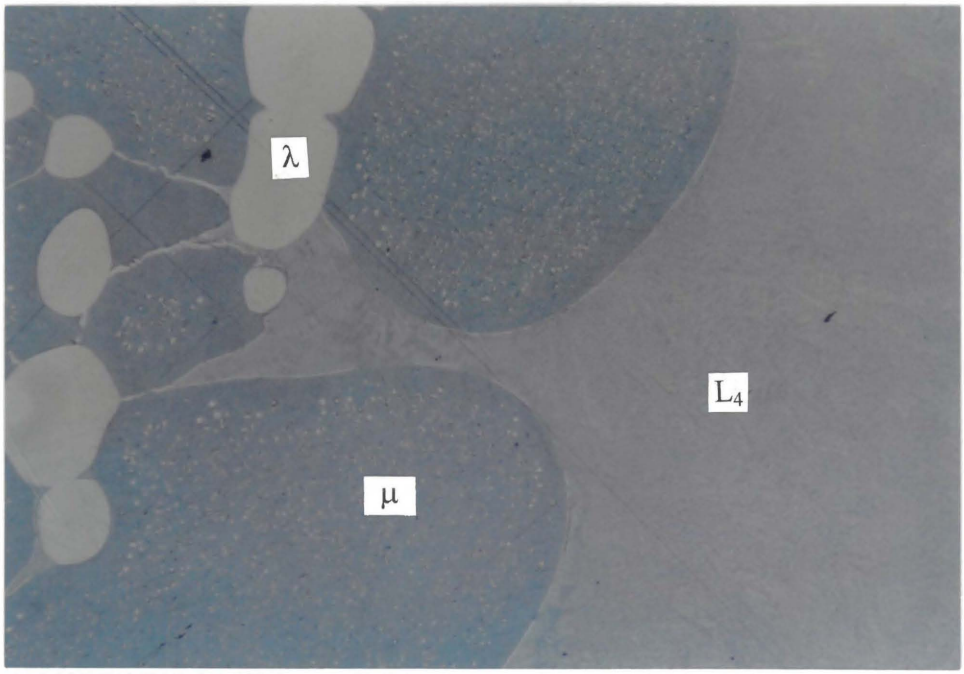

Photomicrograph 11. Liquid (L_4) with exsolutions, co-existing with $Cu_{2-x}S$ (μ, blue) and $Ni_{1-x}S$ (λ, yellow). Charge 194, at 800°C, (long side of the photomicrograph is 1.25mm).

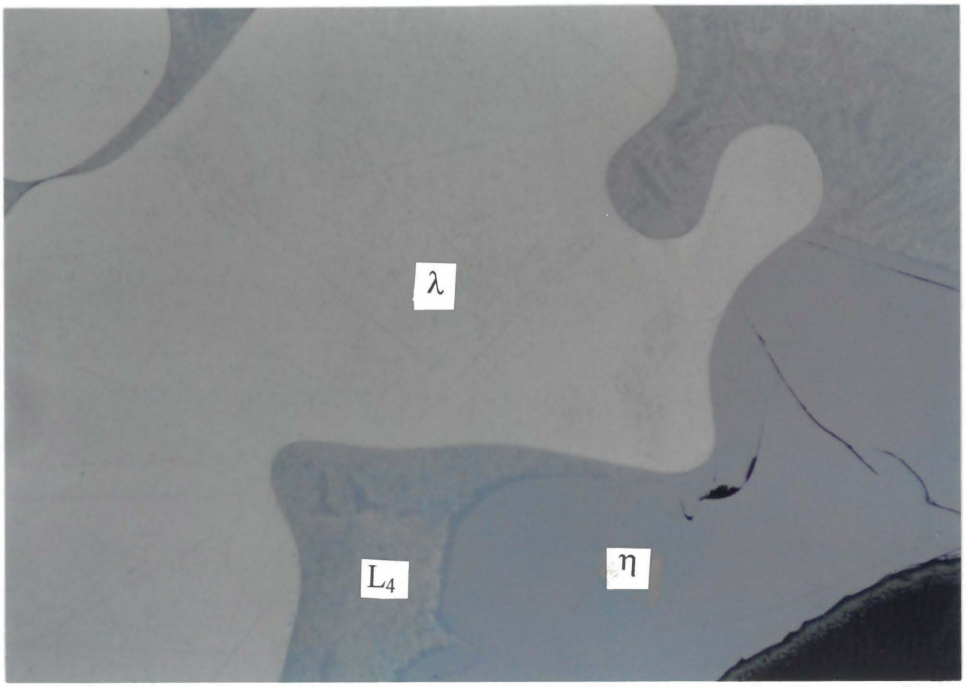

Photomicrograph 12. Liquid (L_4) + vaesite (η, grey) + $Ni_{1-x}S$ (λ, yellow) in charge no. 233 at 800°C, (long side of the photomicrograph is 1.25mm).

According to the Ni-S binary phase diagram (Figure 2, Lin *et al.*, 1978) $Ni_{3\pm x}S_2$ (θ) starts to crystallise at ~806°C. From Figure 2 it can be seen that the initial $Ni_{3\pm x}S_2$ composition that would crystallise at ~806°C is more sulphur-rich than stoichiometric low-temperature Ni_3S_2. On the Ni-S binary of the 800°C isothermal section of the Cu-Ni-S system one would therefore expect a field of solid $Ni_{3\pm x}S_2$. The presence of this high sulphur θ phase is shown in Figure 41.

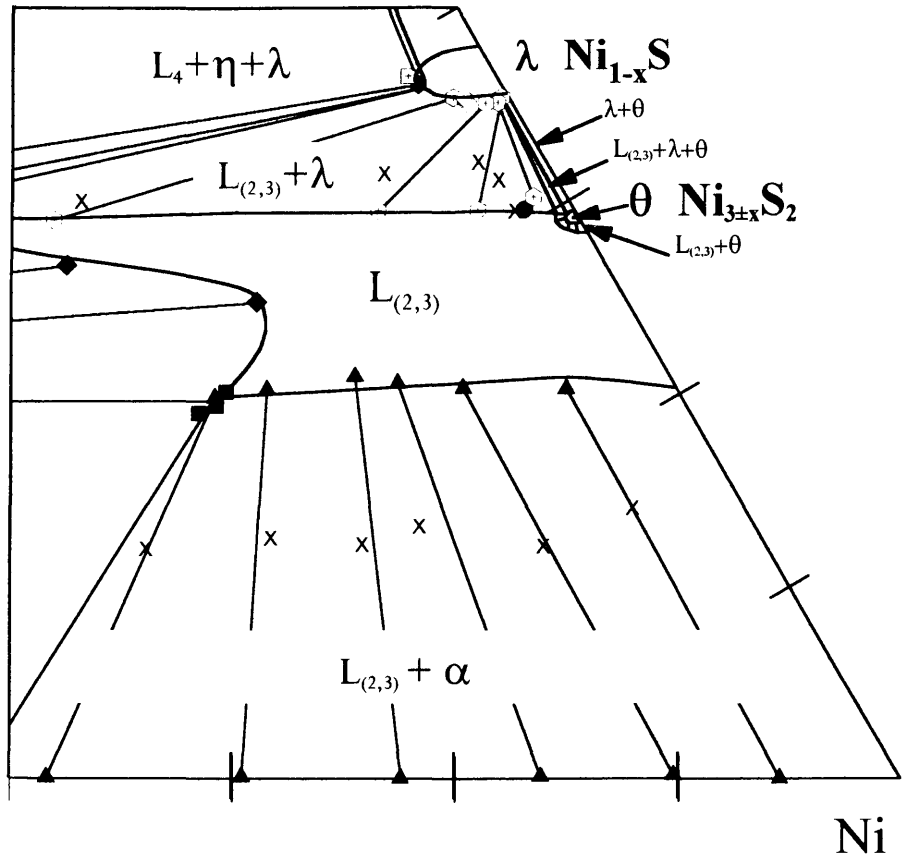

Figure 41. Portion of the 800°C isothermal section of the Cu-Ni-S system. The positions of the $Ni_{3\pm x}S_2$ (θ), liquid + $Ni_{3\pm x}S_2$ ($L_{(2,3)}$+θ), and $Ni_{1-x}S$ + $Ni_{3\pm x}S_2$ (λ+θ) fields are in accordance with the Ni-S binary diagram (Lin et al., *1978). The liquid + $Ni_{1-x}S$ + $Ni_{3\pm x}S_2$ ($L_{(2,3)}$+λ+θ) phase field is shown schematically.*

According to Cemic and Kleppa (1986), NiS_2 can be synthesised from NiS and sulphur as starting materials within 48 hours at 600°C. The result was said to consist entirely of crystalline cubic NiS_2. However, this does not seem to be the case in the system Cu-Ni-S at 800°C using the pure elements as starting materials. Two samples (no. 213 with Cu=32.3, Ni=31.9, and S=35.8; and no. 189 with Cu=16.9, Ni=39.1, and S=44.0) were not in equilibrium after being pre-reacted at <800°C for 22 days and tempered at 800°C for 26 days. Both contained NiS_2, $Ni_{1-x}S$, $Cu_{2-x}S$ and liquids. Although the NiS_2 grains, the $Cu_{2-x}S$, and the liquid were in contact with each other, $Ni_{1-x}S$ only occurred as cores in the NiS_2 grains and was not in contact with the other phases, and hence not in equilibrium. The non-equilibrium phase assemblage is shown in Photomicrograph 13.

The reaction between Ni and S_2 to form a bisulphide consists of two steps: First the monosulphide is formed and then the disulphide forms according to the reactions:

$$2Ni + S_2 = 2NiS \text{ (millerite)}$$
$$2NiS + S_2 = 2NiS_2 \text{ (vaesite)}$$

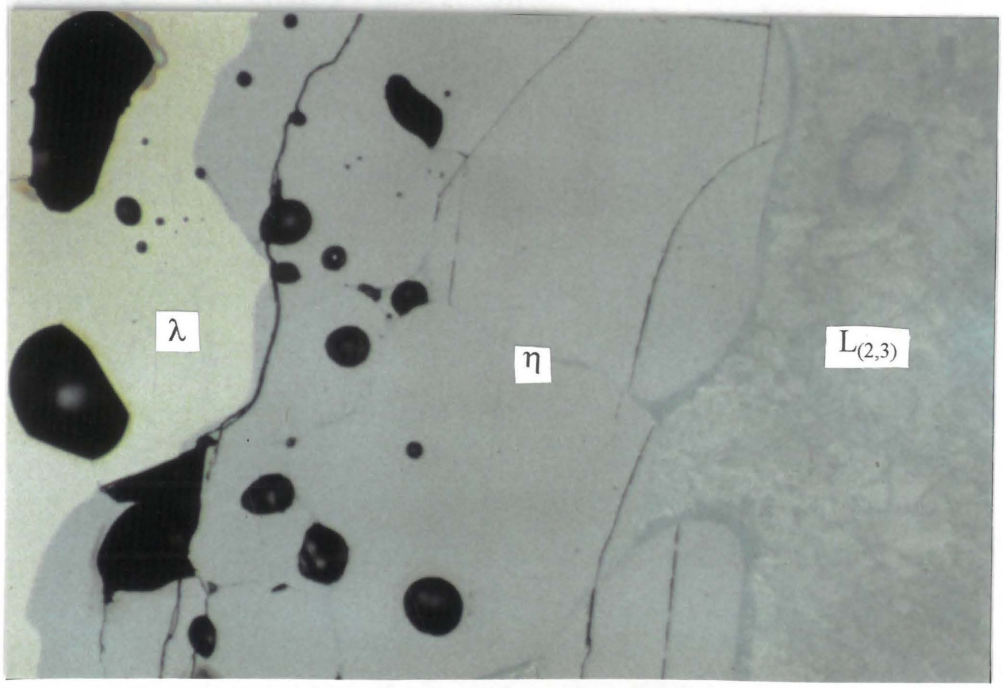

Photomicrograph 13. Charge (no. 189) at 800 °C did not have sufficient time to reach equilibrium. NiS_2 (η, grey) contains $Ni_{1-x}S$ cores (λ, yellow) together with liquid (intergrowths) and $Cu_{2-x}S$ (μ, not visible in this photograph) (long side of the photomicrograph is 1.25 mm).

A possible solution to the problem might be to melt the charges before tempering. Charges containing large quantities of sulphur, however, can not always be molten at higher temperatures as high sulphur partial pressures can lead to the failure of the glass tubes.

4.7 THE 700°C ISOTHERMAL SECTION

The charges made for investigation of the 700°C isothermal section and their compositions, and pre-reaction and tempering histories are listed in Appendix A-6. The averaged SEM analyses are listed in Table 19 and are presented in Figure 42.

Table 19. The averaged SEM analyses (wt%) of co-existing phases at 700°C, with the number of areas that were analysed, and the calculated standard deviations (1σ).

		L(2,3)			
No	Ni	S	Cu	Total	Analyses
No 261	69.0	23.1	5.8	97.9	1
No 262	69.0	23.1	5.8	97.9	3
Stdev.	1.9	0.2	1.0		

		L(2,3)					α			
No	Ni	S	Cu	Total	Analyses	Ni	S	Cu	Total	Analyses
No 257	66.3	20.7	11.6	98.6	6	78.7	0.1	21.5	100.2	2
Stdev.	1.1	0.7	1.1							
No 258	71.0	20.5	8.2	99.7	10	90.6	0.0	10.5	101.1	1
Stdev.	1.2	1.4	2.4							
No 259	74.6	21.9	3.0	99.5	4	96.5	0.1	5.2	101.8	1
Stdev.	0.0	0.6	0.5							

		μ					α			
No	Ni	S	Cu	Total	Analyses	Ni	S	Cu	Total	Analyses
No 250	0.5	19.6	78.8	98.8	1	15.7	0.0	85.2	100.8	2
No 251	0.0	19.3	78.7	98.1	1	31.3	0.0	69.2	100.6	2
No 252	1.1	20.0	78.5	98.5	1	45.4	0.0	56.2	101.6	3
No 253	1.2	19.3	78.9	98.1	1	56.2	0.0	45.1	101.3	2

		L(2,3)					μ			
No	Ni	S	Cu	Total	Analyses	Ni	S	Cu	Total	Analyses
No 260	64.9	22.8	12.1	99.8	3	1.8	19.7	78.0	99.4	1
Stdev.	0.4	0.1	0.6							
No 265	64.1	22.1	14.0	100.2	9	1.1	19.4	79.0	99.5	2
Stdev.	1.7	0.6	1.7							
No 266	61.4	26.5	11.6	99.4	3	1.2	19.9	77.6	98.8	2
Stdev.	1.8	0.7	1.7							
No 270	65.2	23.5	11.0	99.8	2	1.8	19.7	78.6	100.1	1
Stdev.	0.3	0.0	1.0							

		λ					θ			
No	Ni	S	Cu	Total	Analyses	Ni	S	Cu	Total	Analyses
No 219	64.0	34.7	0.3	99.0	3	66.9	29.3	4.0	100.1	3

		μ					λ			
No	Ni	S	Cu	Total	Analyses	Ni	S	Cu	Total	Analyses
No 268	0.9	20.2	77.3	98.4	1	60.4	35.1	2.2	97.7	2

		L(2,3)					μ					α			
No	Ni	S	Cu	Total	Analyses	Ni	S	Cu	Total	Analyses	Ni	S	Cu	Total	Analyses
No 256	64.5	19.9	15.0	99.5	6	-	-	-	-		69.0	0.0	31.7	100.7	1
Stdev.	1.3	2.1	1.7												
No 255	64.8	20.2	14.4	99.4	5	0.9	19.4	78.0	98.4	1	68.2	0.0	32.4	100.6	1
Stdev.	1.4	1.1	1.3												

		μ					λ					η			
No	Ni	S	Cu	Total	Analyses	Ni	S	Cu	Total	Analyses	Ni	S	Cu	Total	Analyses
No 195	1.1	21.0	74.4	96.5	2	45.1	50.7	2.1	97.8	1	56.6	34.4	2.6	93.6	1
No 232	0.7	20.7	78.0	99.4	1	60.7	36.6	2.6	99.9	1	46.8	50.9	1.4	99.1	1

		μ					λ					θ			
No	Ni	S	Cu	Total	Analyses	Ni	S	Cu	Total	Analyses	Ni	S	Cu	Total	Analyses
No 267	0.9	19.6	78.8	99.3	1	62.4	34.1	2.3	98.9	1	66.6	29.4	1.9	97.9	2
Stdev.											3.0	1.4	0.2		

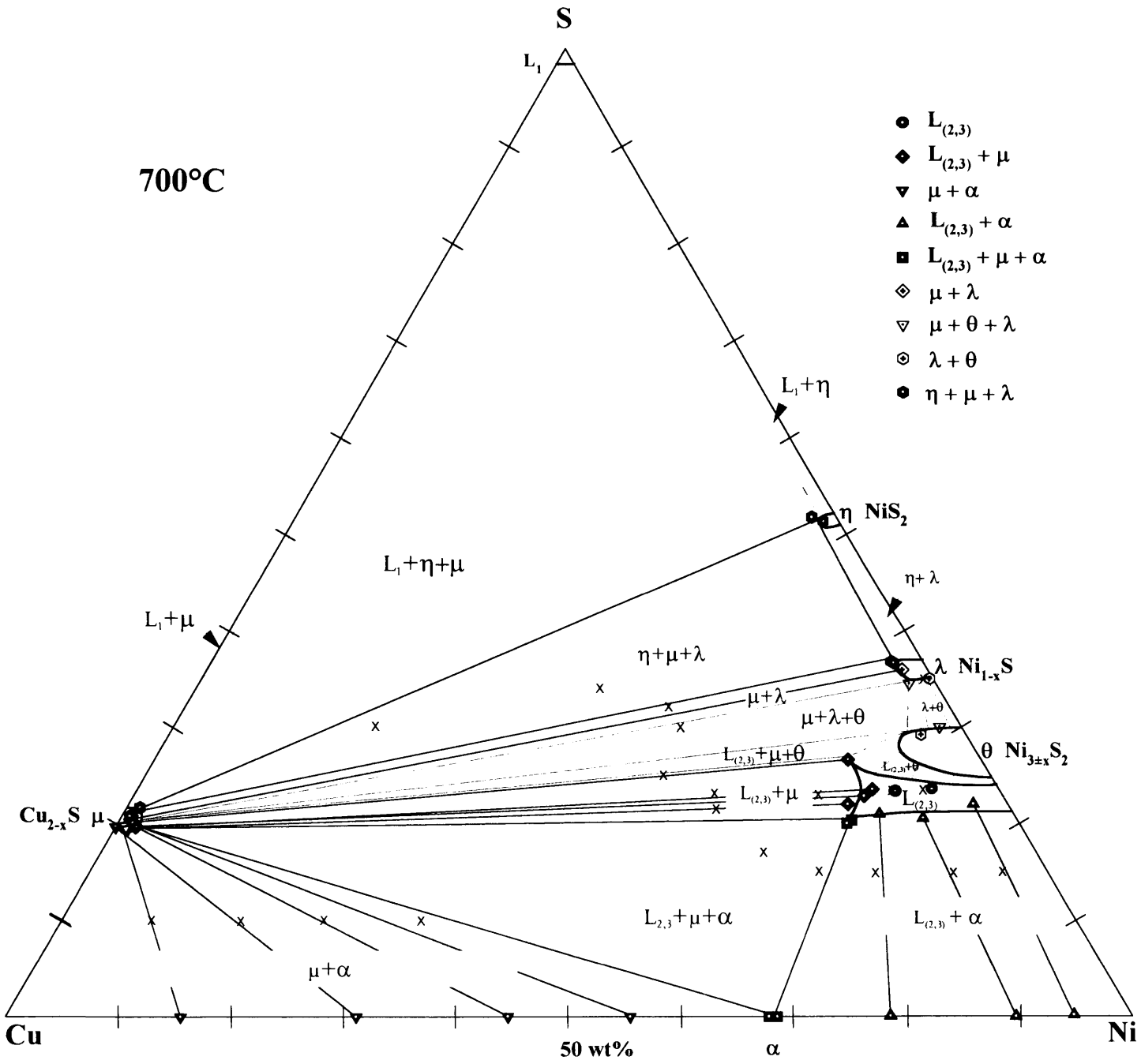

Figure 42. The 700°C isothermal section of the Cu-Ni-S system with tie-lines between co-existing phases. The bulk compositions of the experimental samples are shown as x's.

The liquid L_4 field disappears at a temperature between 800°C and 700°C, and only a small portion of liquid $L_{(2,3)}$ is present just below the $Ni_{3\pm x}S_2$ phase field. As a result, the 700°C isothermal section (Figure 42) contains mostly solid phase assemblages, such as $Cu_{2-x}S + Ni_{1-x}S$ ($\mu+\lambda$) (Photomicrograph 14), $NiS_2 + Cu_{2-x}S + Ni_{1-x}S$ ($\eta+\mu+\lambda$) (Photomicrograph 15), and $Cu_{2-x}S + Ni_{1-x}S + Ni_{3\pm x}S_2$ ($\mu+\lambda+\theta$) (Photomicrograph 16). These observed phase associations at 700°C (Figure 42) are in accordance with the 600°C isothermal section (Moh and Kullerud, 1963, redrawn by Chang *et al.*, 1979) as shown in Figure 43.

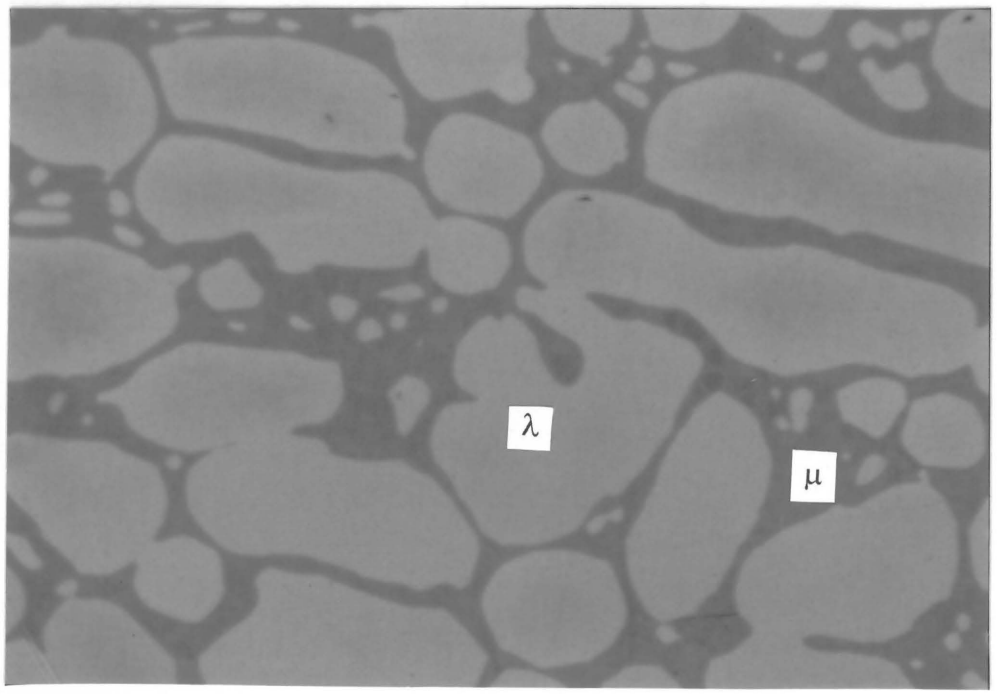

Photomicrograph 14. $Cu_{2-x}S$ (μ, grey) + $Ni_{1-x}S$ (λ, yellow) in charge no. 268 at 700°C, (long side of the photomicrograph is 250 μm).

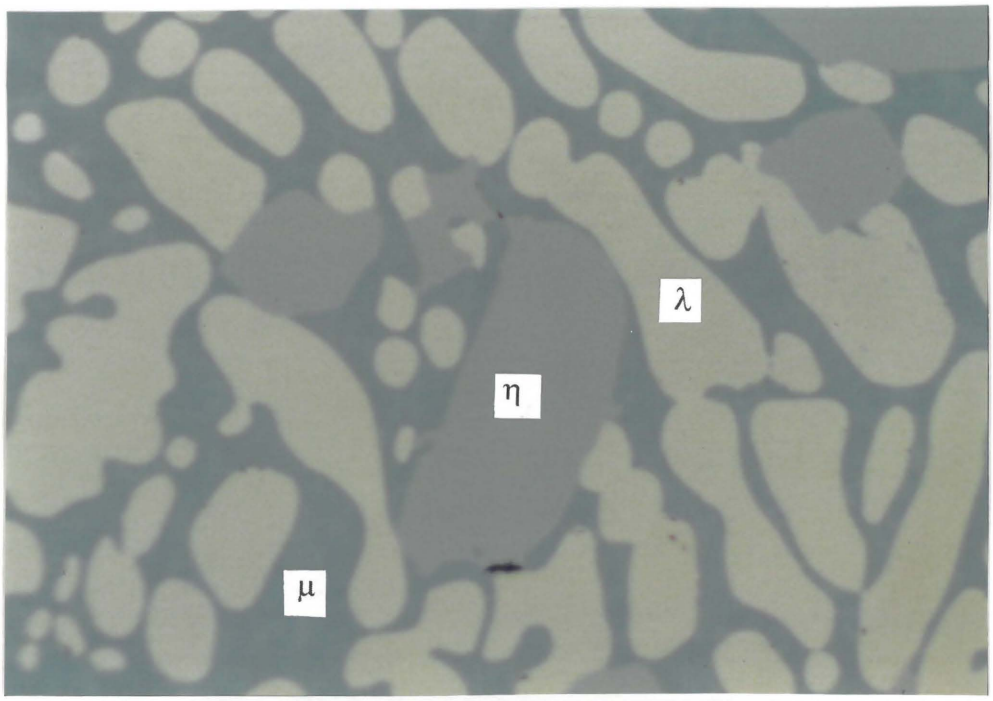

Photomicrograph 15. This assemblage of solid phases in the absence of a liquid phase was observed in charge 232, at 700°C. The phases are NiS_2 (η, grey) + $Cu_{2-x}S$ (μ, bluish grey in comparison) + $Ni_{1-x}S$ (λ, yellow), (long side of the photomicrograph is 250 μm).

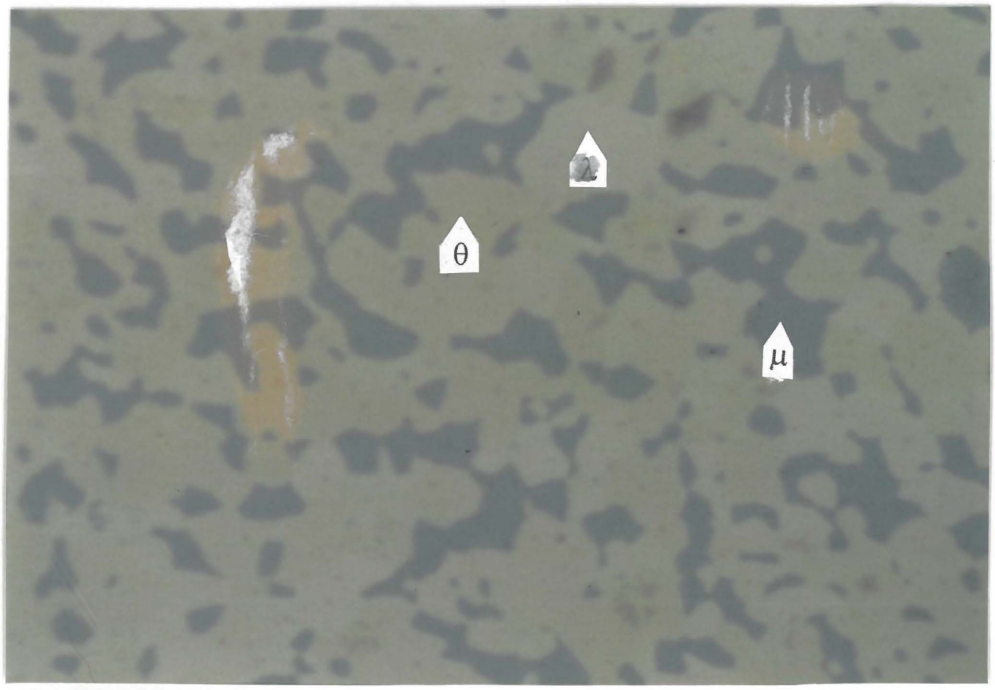

Photomicrograph 16. Intergrowth of $Cu_{2-x}S$ (μ, grey) + $Ni_{1-x}S$ (λ, light yellow) + $Ni_{3\pm x}S_2$ (θ, darker and lighter yellow). It is not possible to distinguish between $Ni_{1-x}S$ and $Ni_{3\pm x}S_2$ on the photograph, due to their similar colours. Charge 267, at 700°C, (long side of the photomicrograph is 250 μm).

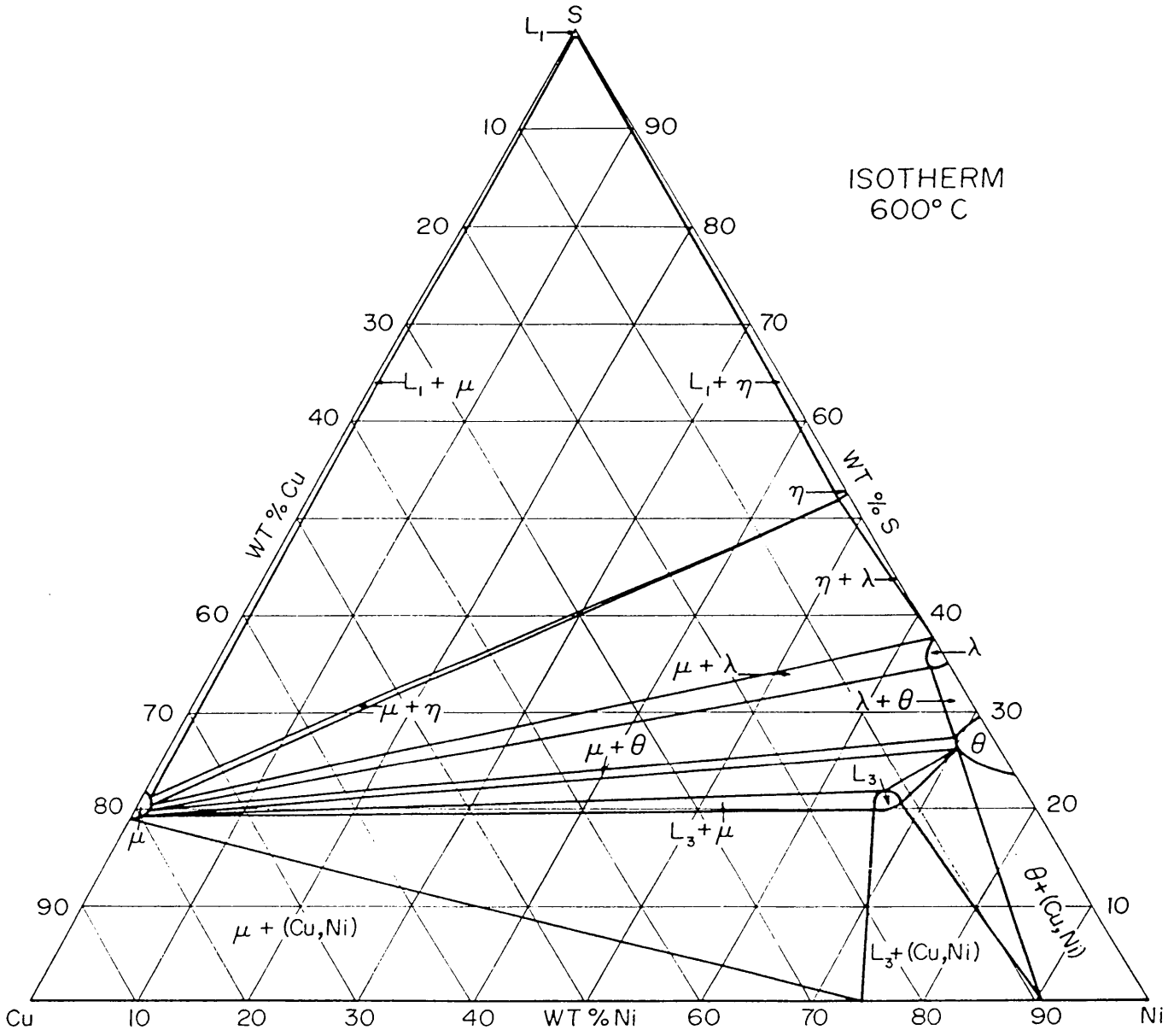

Figure 43. The 600°C isothermal section of the Cu-Ni-S system (Moh and Kullerud, 1963, redrawn by Chang et al., *1979).*

CHAPTER 5

DISCUSSION

The isothermal sections are combined to produce the liquidus phase diagram. The crystallisation paths are deduced from the liquidus diagram and from the phase relations of the individual isothermal sections.

---

5. DISCUSSION

5.1 LIQUIDUS ISOTHERMS

The liquidus isotherms from the individual isothermal sections from 1200°C to 700°C were combined to produce the liquidus phase diagram (Figure 44). The immiscible liquid field of L_1 + $L_{(2,3)}$ on the sulphur-rich side of the phase diagram corresponds with the binary Cu-S (Massalski, 1986) and Ni-S (Lin *et al.*, 1978) phase diagrams and the 1000°C and 900°C isotherms in this field is shown schematically. There is a miscibility gap on the Cu-rich side of the diagram with co-existing L_2 + L_3 above ~1000°C (Schlitt *et al.*, 1973). The extent of this miscibility gap at is from Lee *et al.*, (1980).

From Figure 44 it can be seen that the liquid field shrinks on cooling. Figure 44 can be used to determine the liquidus temperature of the first phase that will crystallise from a Cu-Ni-S melt by plotting the sample composition on the diagram and interpolating between the isotherms if necessary. In order to determine which mineral phase will be the first to crystallise, the stability fields of the minerals and the crystallisation paths of the system must be known.

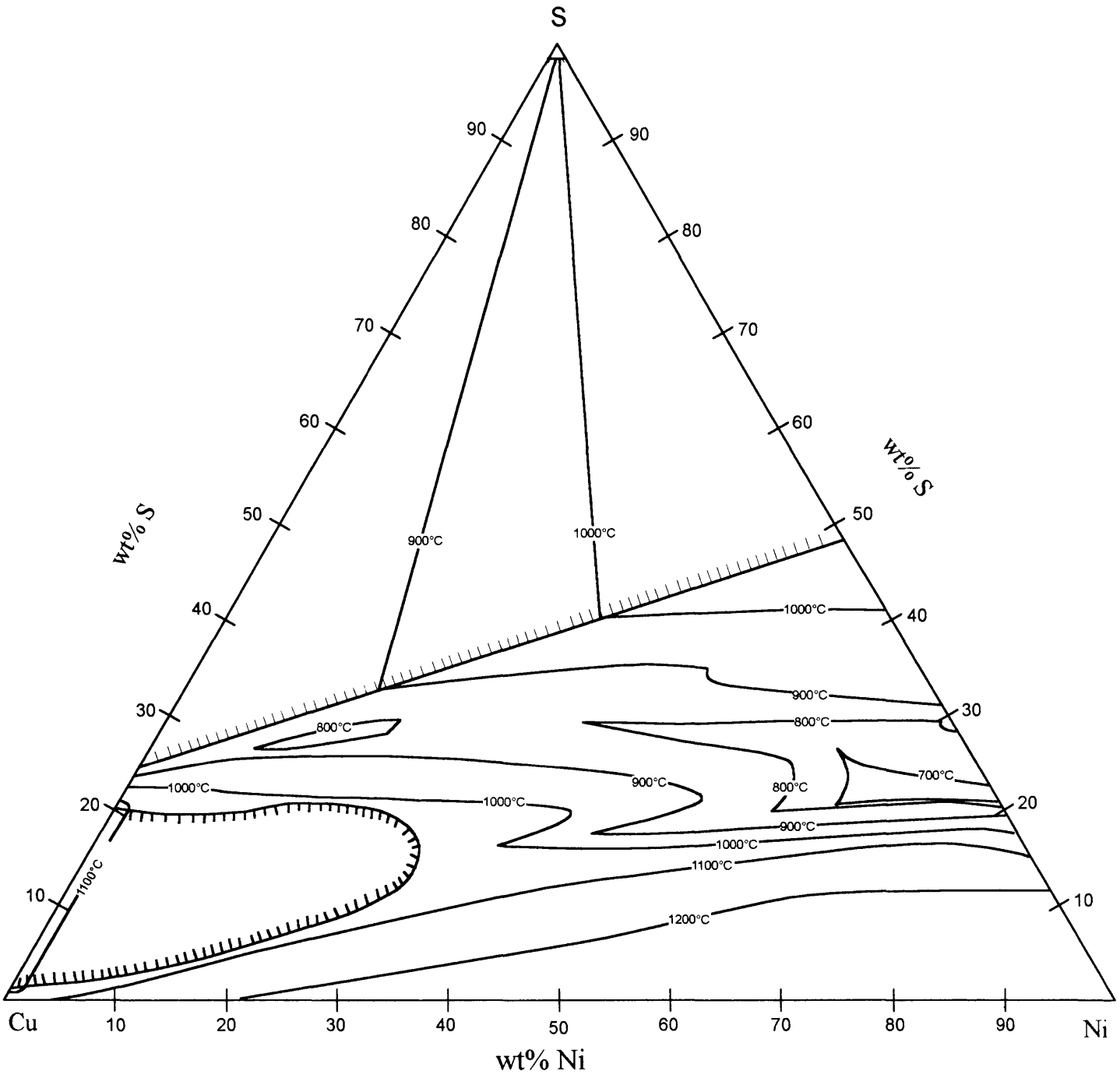

Figure 44. Liquidus isotherms of the system Cu-Ni-S from 1200°C to 700°C. The extent of the immiscible liquid field on the Cu-side of the diagram is from Lee et al. *(1978) and the approximate position of the 1100°C monotectic line is by extrapolation from Schlitt* et al., *(1973). The immiscible liquid field on the sulphur-rich side of the diagram, and the 1000°C, and 900°C isotherms in this field are shown schematically.*

5.2 CRYSTALLISATION PATHS

At 1000°C and lower temperatures three-phase fields containing one liquid and two solid phases, i.e. the liquid + $Cu_{2-x}S$ + alloy ($L_{(2,3)}+\mu+\alpha$) field, were observed. Such fields of invariant equilibria in the isothermal sections were used for construction of the crystallisation paths of the Cu-Ni-S system (Figure 45). In effect, the change in the liquid composition with temperature for these phase associations simulates the fractionation of the sulphide melt on cooling.

In Figure 45 the analysed liquid compositions for invariant equilibria, as determined at each individual isothermal section, are depicted. Several reference points from the binary phase diagrams of Ni-S (Lin *et al.*, 1978, Figure 46; Meyer *et al.*, 1975, Figure 47), Cu-S (Massalski, 1986, Figure 48), and Cu-Ni (Massalski, 1986, Figure 49) are shown on the axes of Figure 45. These are points are listed alphabetically and correspond to binary liquidus compositions and eutectic points in Figures 46, 47, 48, and 49.

It can be seen in Figure 45 that the crystallisation paths of the ternary phase diagram is consistent with the binary phase diagrams and ternary liquid isotherms. The determination of the exact positions of the eutectic points E2, E3, and E4 was beyond the scope of this investigation, but the approximate positions could be deduced from the information summarised in Figure 45. The crystallisation paths on the sulphur apex of the diagram is shown schematically (J. Nell, pers. comm., 1997).

Because of the complexity and relatively small scale of Figure 45, enlargements of different portions of the diagram will presented and discussed separately.

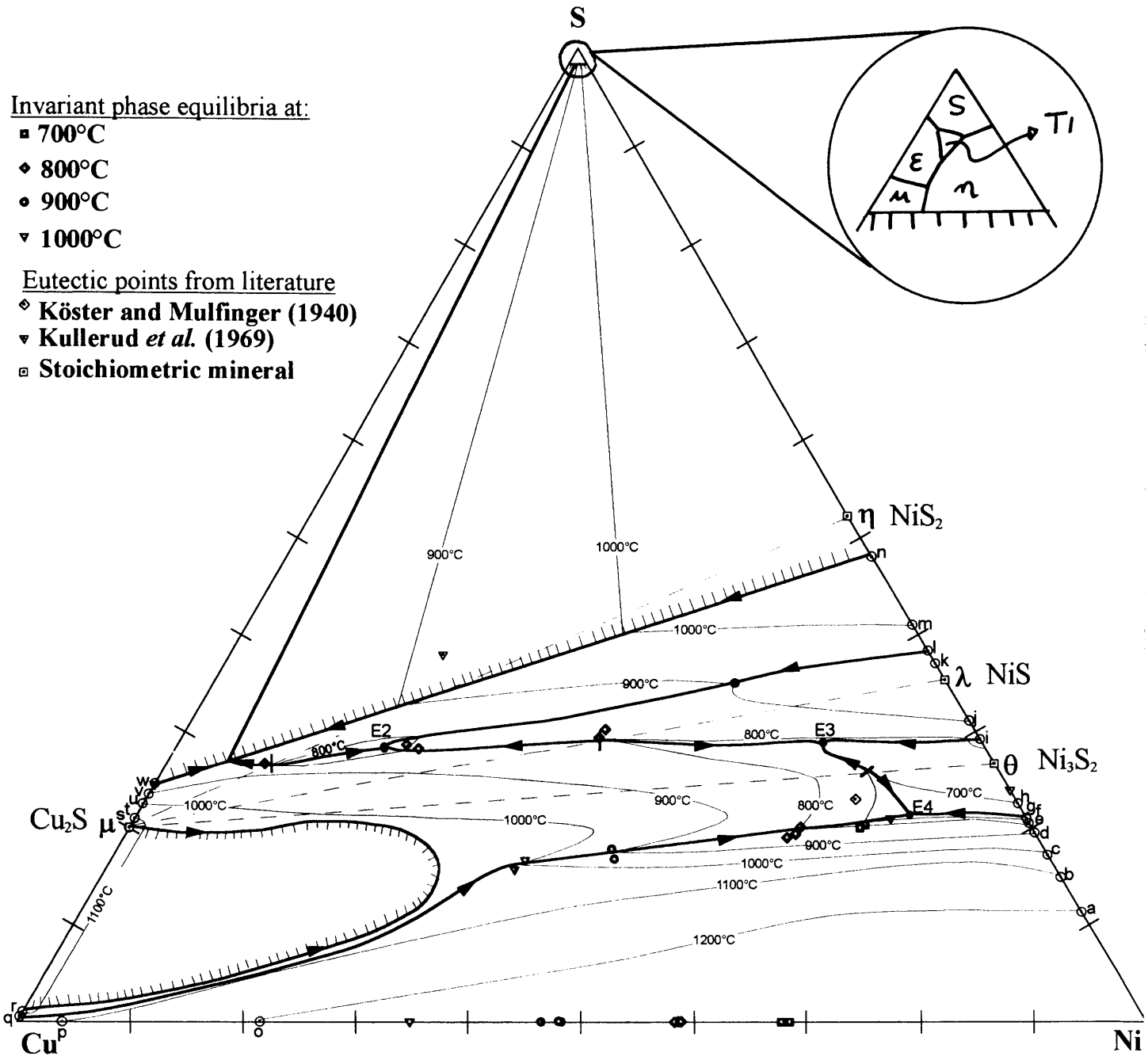

Figure 45. Liquid compositions of invariant equilibria, as determined in the isothermal sections, were used for the construction of crystallisation paths of the Cu-Ni-S system. Several reference points from the binary phase diagrams of Ni-S (Lin et al., *1978, and Meyer* et al., *1975) Cu-Ni (Massalski, 1986), and Cu-S (Massalski, 1986) are shown (circles, alphabetically). The compositions of the eutectic points are inferred from the isothermal liquid fields. Eutectic points from the literature are shown, as listed. The sulphur-rich part of the diagram is shown schematically (J. Nell, pers. comm., 1997).*

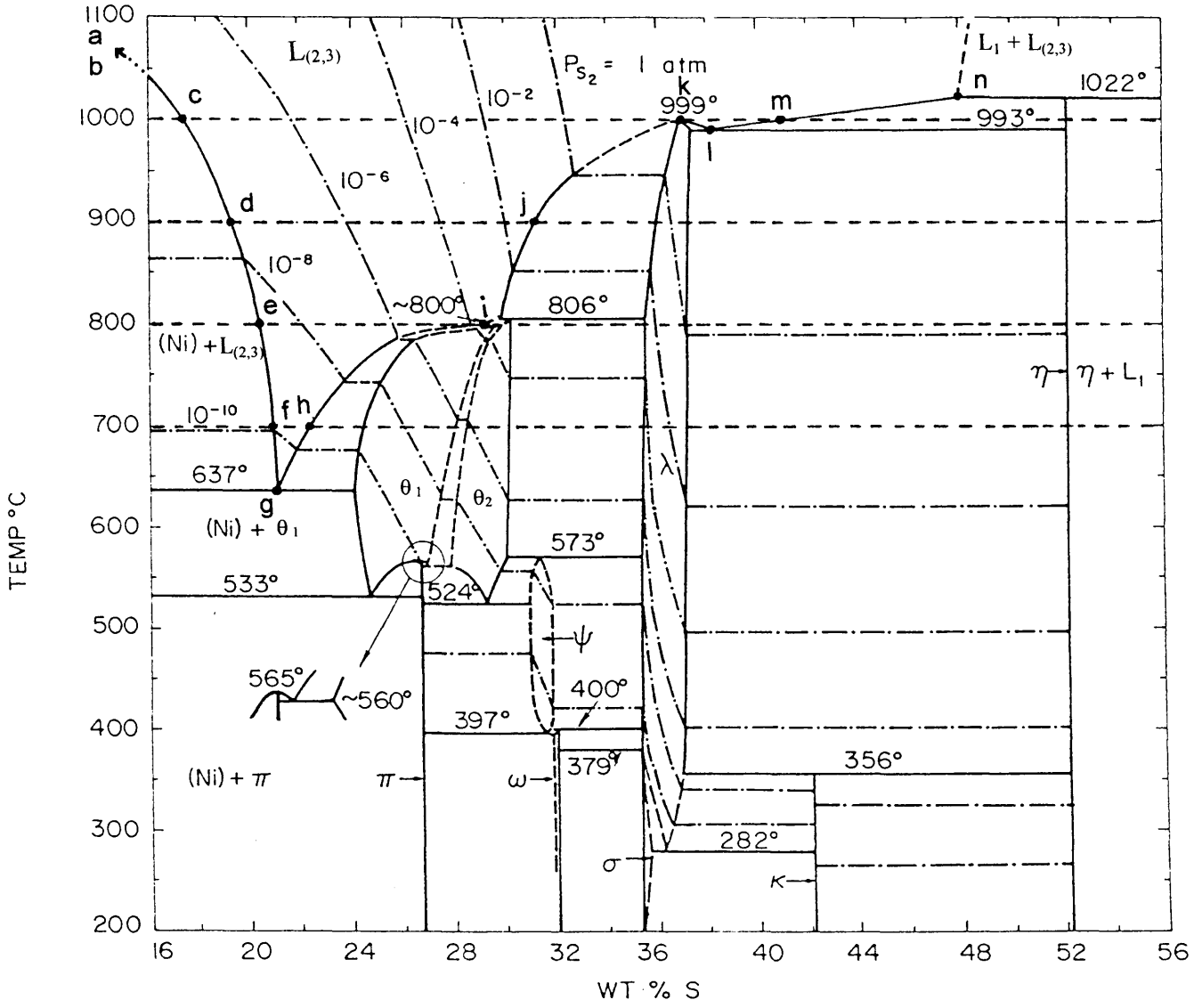

Figure 46. Ni-S phase diagram (Lin et al.*, 1978). Alphabetical reference points are shown for comparison with the ternary Cu-Ni-S phase diagram.*

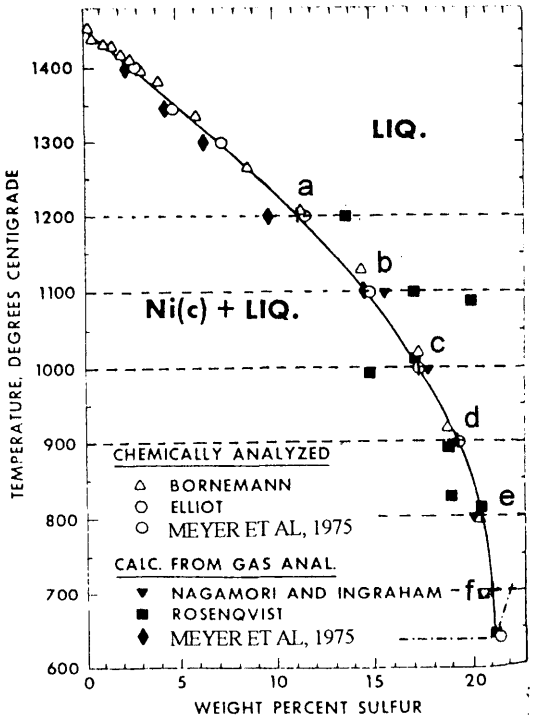

Figure 47. The liquidus for the Ni-S system was determined by various investigators (summarised by Meyer et al., *1975). Alphabetical reference points are shown for comparison with the ternary Cu-Ni-S phase diagram.*

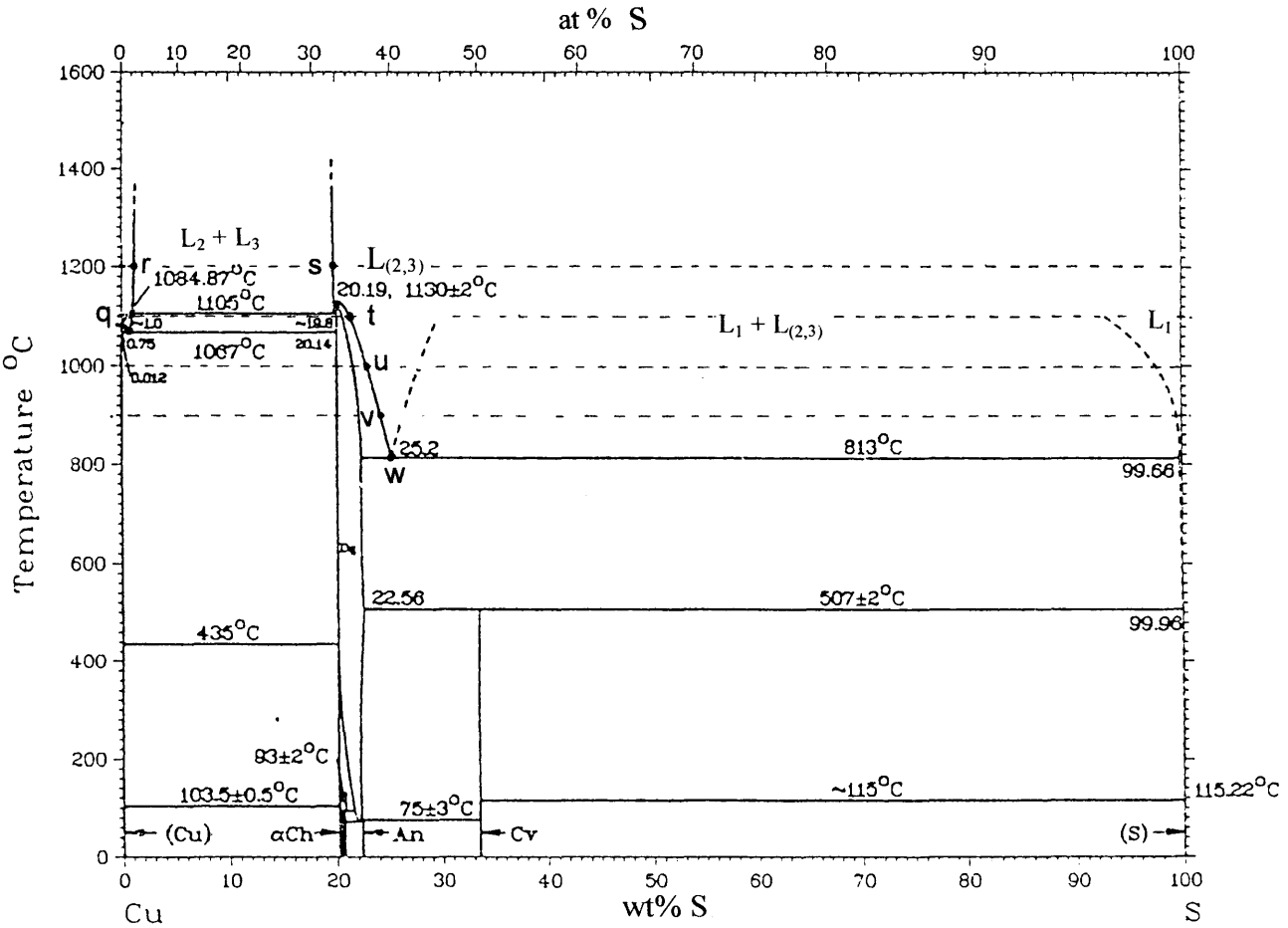

Figure 48. Cu-S phase diagram (Massalski, 1986). Alphabetical reference points are shown for comparison with the ternary Cu-Ni-S phase diagram.

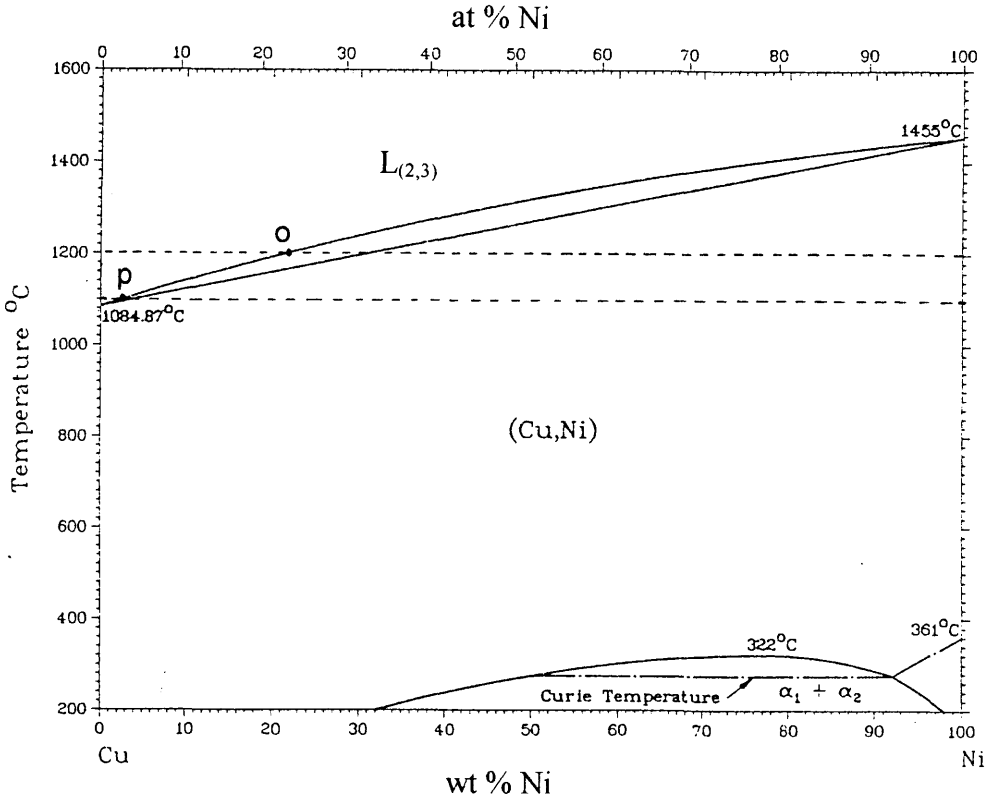

Figure 49. The Cu-Ni phase diagram (Massalski, 1986). Alphabetical reference points are shown for comparison with the ternary Cu-Ni-S phase diagram.

i) Sulphur-rich portion

The retraction of the liquid field $L_{(2,3)}$ from the Cu-S binary is evident from the eutectic in the Cu-S system at 813°C (Massalski, 1986; point w in Figures 48, 45 and 50) and from the Ni-S binary at 1022°C (Lin et al., 1978; point n in Figures 45, 46 and 50). The crystallisation paths leading to eutectic points on the sulphur-rich side of the diagram is shown schematically in Figures 45 and 50. For clarity on the incongruent melting of NiS_2 (η), the liquidus stability fields are highlighted in Figure 50.

The intersection of the Cu_2S-NiS_2 tie-line with the crystallisation path indicates a thermal maximum (point M1, Figure 50). Point U1 represents the liquid composition of the invariant equilibrium of $L_4+\mu+\eta$ at 800°C (Figure 50, see also Table 15).

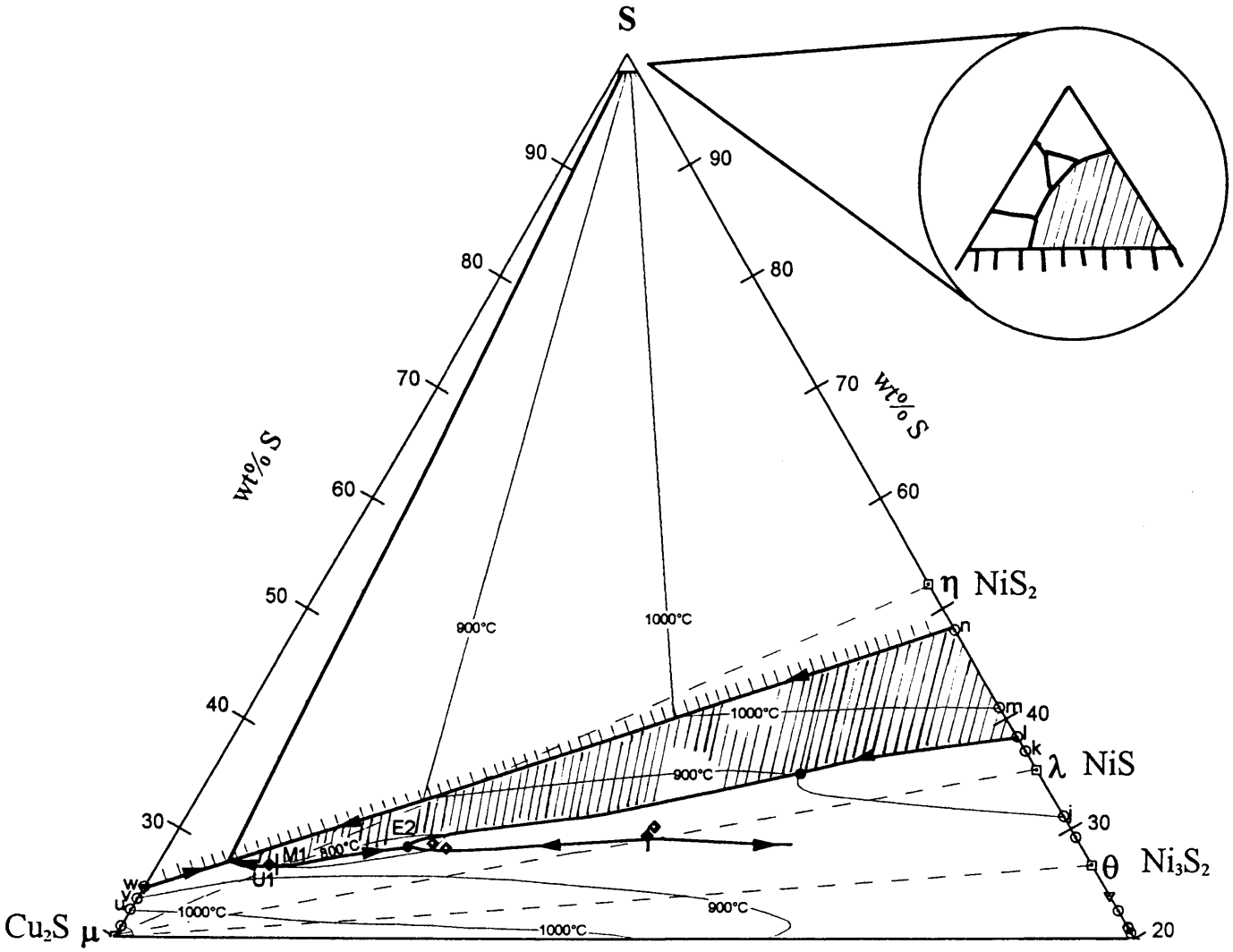

Figure 50. Crystallisation paths in the sulphur rich portion of the Cu-Ni-S phase diagram is shown schematically. The liquidus stability fields for NiS_2 (η) are highlighted.

ii) Eutectic point E2

The crystallisation path leads from the intersection with the Cu_2S-NiS_2 tie-line (point M1, Figure 51) through the 800°C liquid field (L_4) to point E2.

The liquid field retracts from Ni-S binary with an eutectic occurring between NiS and NiS_2 at 993°C (Lin *et al.*, 1978). This binary eutectic is indicated by point l in Figures 46 and 51. The crystallisation path follows through the liquid composition of the invariant $L_{(2,3)}+\eta+\lambda$ phase equilibrium at 900°C (point U4, Figure 51, see also Table 14) and the $L_4+\eta+\lambda$ equilibrium at 800°C[‡] (point U2, Figure 51, see also Table 15) to point E2.

[‡] The nomenclature for L_4 and $L_{(2,3)}$ is only to distinguish the two liquid fields from one another at 800°C.

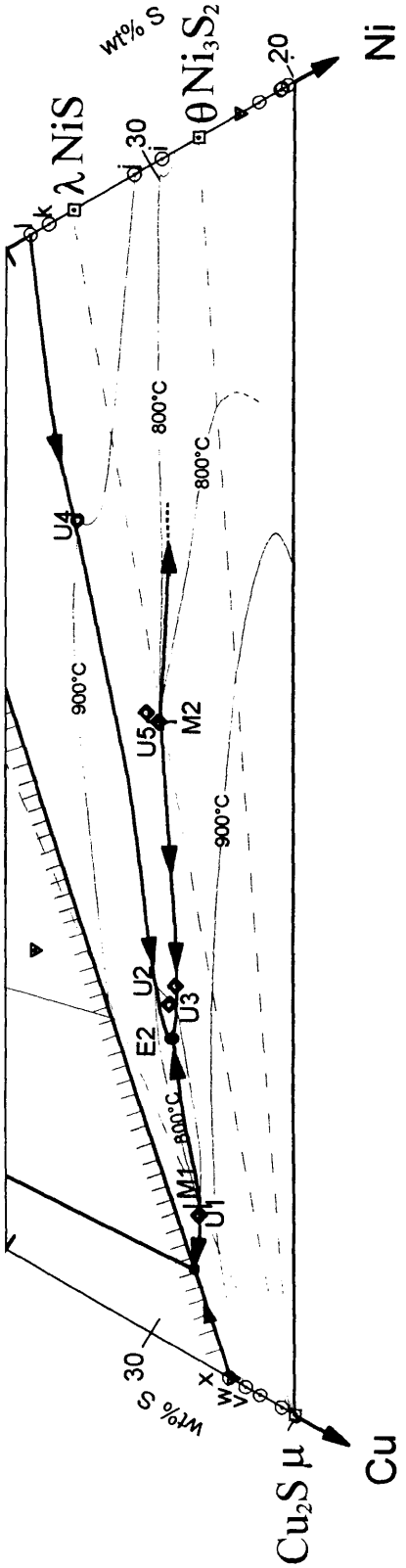

Figure 51. Portion of the Cu-Ni-S phase diagram, showing the crystallisation paths leading to the eutectic point E2, with the position of point E2 shown schematically. The liquid field retracts from point l on the Ni-S binary at 993°C (Lin et al., *1978).*

The invariant equilibrium in the liquid + $Cu_{2-x}S$ + $Ni_{1-x}S$ ($L_{(2,3)}+\mu+\lambda$) phase assemblage at 800°C (point U5 in Figure 51, see also Table 15) is indicated by the analysed compositions of $L_{(2,3)}$ from two samples. Point U5 is in close proximity to the thermal maximum (M2) at the intersection of the Cu_2S-NiS tie-line with the crystallisation path. The crystallisation path follows through these points and through the invariant equilibrium in the $L_4+\mu+\lambda$ phase assemblage at 800°C (point U3 in Figure 51, see also Table 15) to the eutectic point E2. Point E2 is shown schematically in Figure 51.

According to Kullerud *et al.* (1969), the liquid field retracts from the Cu-S binary and the separate liquid field (L_4) disappears at 770°C at the ternary eutectic point with: Ni = 19 wt%; S = 38 wt%; Cu = 43 wt% (down triangle in Figure 51). The position of this eutectic point described by Kullerud *et al.* (1969) is not in accordance with the retraction trend of the liquid from the Cu-S binary, or the position of the liquid field L_4 at 800°C (Figure 51).

iii) Eutectic point E3

The binary eutectic between Ni_3S_2 and NiS in the Ni-S system at 800°C is indicated by point i in Figure 46 (Lin *et al.*, 1978) and in Figure 52. The crystallisation path leads from point i on the Ni-S binary to an eutectic point with the approximate position indicated by point E3 (Figure 52). The other crystallisation paths that lead to point E3 in Figure 52 are from the thermal maxima at M2 and M3.

According to the Ni-S binary phase diagram (Figure 53, Lin *et al.*, 1978), high temperature $Ni_{3\pm x}S_2$ (θ) can crystallise from ~806°C. The first $Ni_{3\pm x}S_2$ (θ) to crystallise (indicated by point a, Figure 53) will have a composition more sulphur-rich than stoichiometric low temperature Ni_3S_2 (point b, Figure 53). It can also be seen in Figure 53 that with decreasing temperature the $Ni_{3\pm x}S_2$ phase field spans a considerable range of compositions. The large variation in the eutectic point determinations of the Cu_2S-$Ni_{3\pm x}S_2$ system (as discussed in Chapter 1) can thus be explained. Since the sulphur content of $Ni_{3\pm x}S_2$ can vary considerably, the sulphur content in $Ni_{3\pm x}S_2$ will depend on the experimental set-up used by the investigators, i.e. whether the sulphide minerals used as starting materials were prepared with over-, or under-saturation of sulphur. The starting materials produced by, for example, Hayward (1915) contained impurities, and the sulphur content of the prepared sulphides was determined by calculating the difference between the metal

content and 100%. It is not clear from the experimental method employed by Köster and Mulfinger (1940) and in Sproule *et al.* (1960) what the actual sulphur content of the $Ni_{3\pm x}S_2$ used for the experiments was.

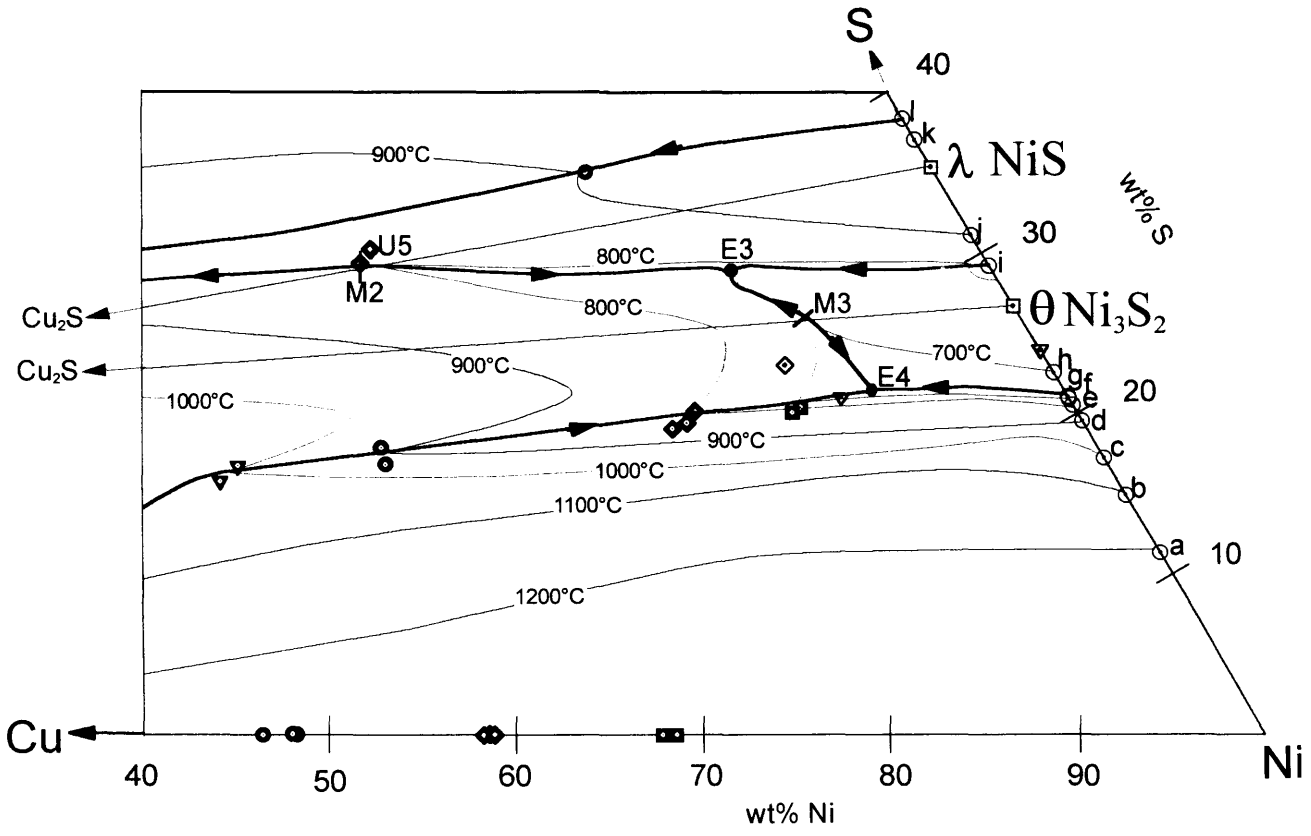

Figure 52. Portion of the Cu-Ni-S phase diagram, showing the crystallisation paths leading to point E3 with the position of point E3 shown schematically. The liquid field retracts from point i on the Ni-S binary at ~800°C (Lin et al., *1978).*

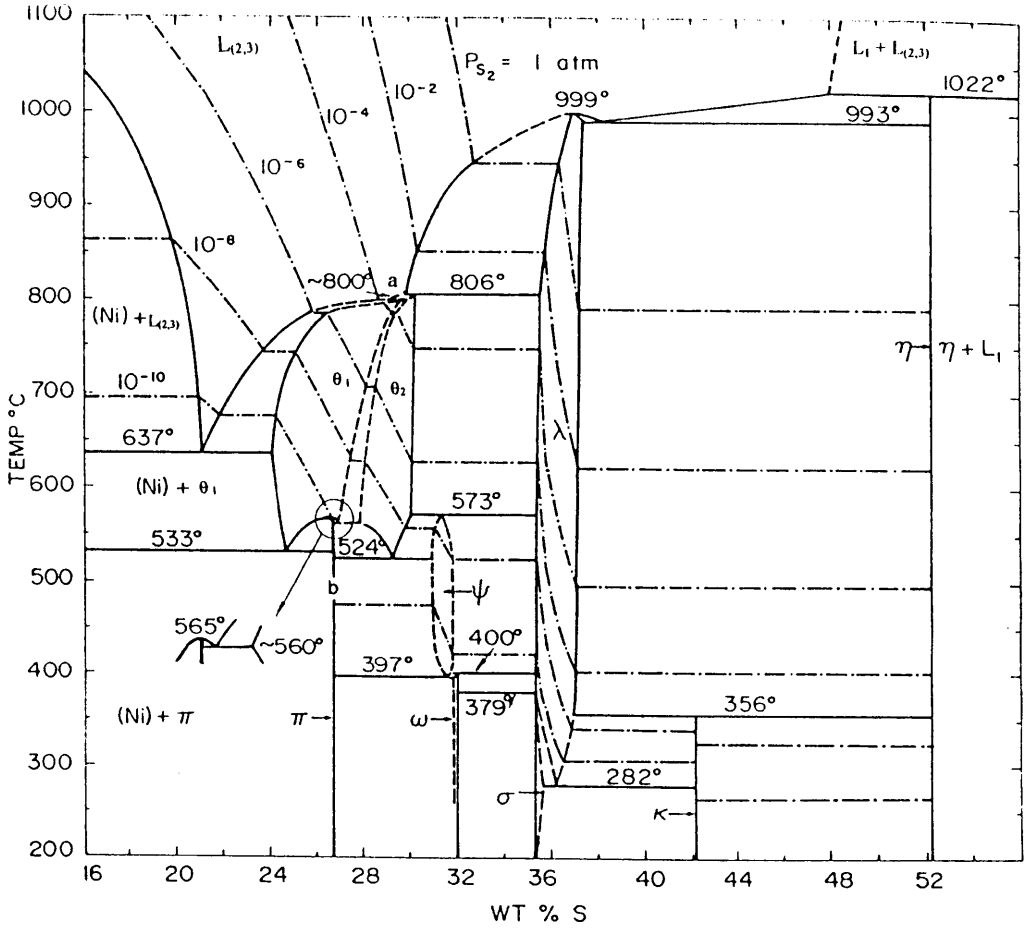

Figure 53. The Ni-S binary phase diagram (Lin et al., 1978). The $Ni_{3\pm x}S_2$ (θ) phase will initially (at ~806°C) contain a higher sulphur content (point a) than stoichiometric Ni_3S_2 (point b).

Deviation from the stoichiometric Ni_3S_2 phase composition introduces an additional degree of freedom in the Cu_2S-Ni_3S_2 system, and it will cause the Cu_2S-Ni_3S_2 tie-line in the ternary Cu-Ni-S system to be variable. This tie-line will only be fixed when the low temperature, stoichiometric Ni_3S_2 phase becomes stable. In Figure 54 the extent of the liquid $L_{(2,3)}$ field at a temperature between 700°C and 800°C is shown schematically. The crystallisation paths are also shown to explain the development of the phase fields on cooling. Two Cu_2S-Ni_3S_2 tie-lines are shown in Figure 54 (dashed lines; Cu_2S - a, and Cu_2S - b). Point a and b corresponds,

respectively, to a binary thermal maximum and the stoichiometric Ni_3S_2 phase composition in the Ni-S system (Figure 53).

With cooling below 800°C the liquid $L_{(2,3)}$ field in the Cu-Ni-S system is expected to split into two different fields $L_{(2,3)}$ and L_5. If the Cu_2S-Ni_3S_2 system was a pseudo-binary system, the intersection of line Cu_2S - b with the crystallisation curve would have been a temperature maximum (Figure 54). However, with the Cu_2S-Ni_3S_2 system not being a pseudo-binary, the temperature maximum is unlikely to be on the Cu_2S - b tie-line. The two liquid fields $L_{(2,3)}$ and L_5 are shown in Figure 55. The most likely position for the ternary thermal maximum (point c) is indicated on the dashed line Cu_2S - a.

The disappearance of the L_5 field with further cooling to 700°C and the consequent formation of the $Cu_{2-x}S$ + $Ni_{1-x}S$ + $Ni_{3\pm x}S_2$ ($\mu+\lambda+\theta$) phase field (Figure 56) is in accordance with the 600°C isothermal section from Moh and Kullerud (1963) (redrawn by Chang *et al.*, 1979) as shown in Figure 43.

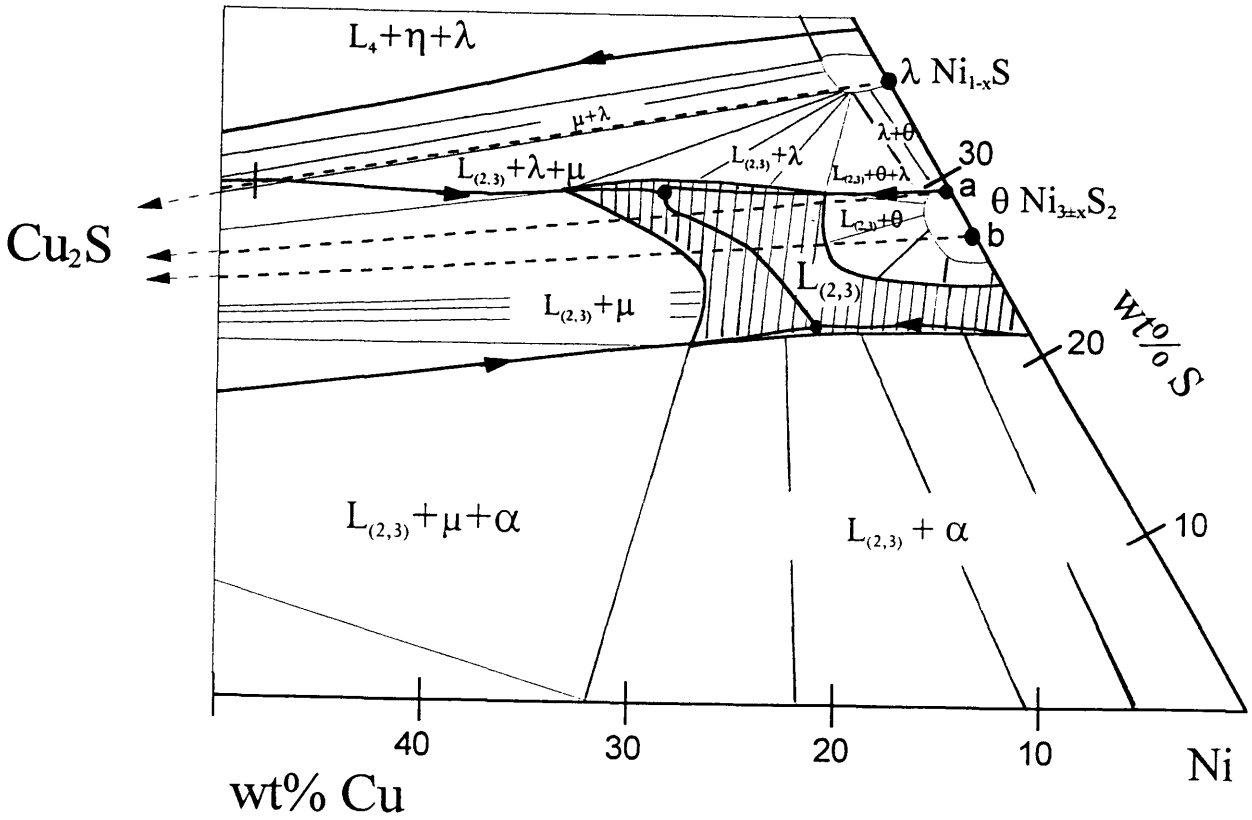

Figure 54. Portion of the Cu-Ni-S phase diagram at a temperature below 800°C. The extent of the liquid field $L_{(2,3)}$ is in accordance with the 800°C and 700°C isothermal sections and the crystallisation paths.

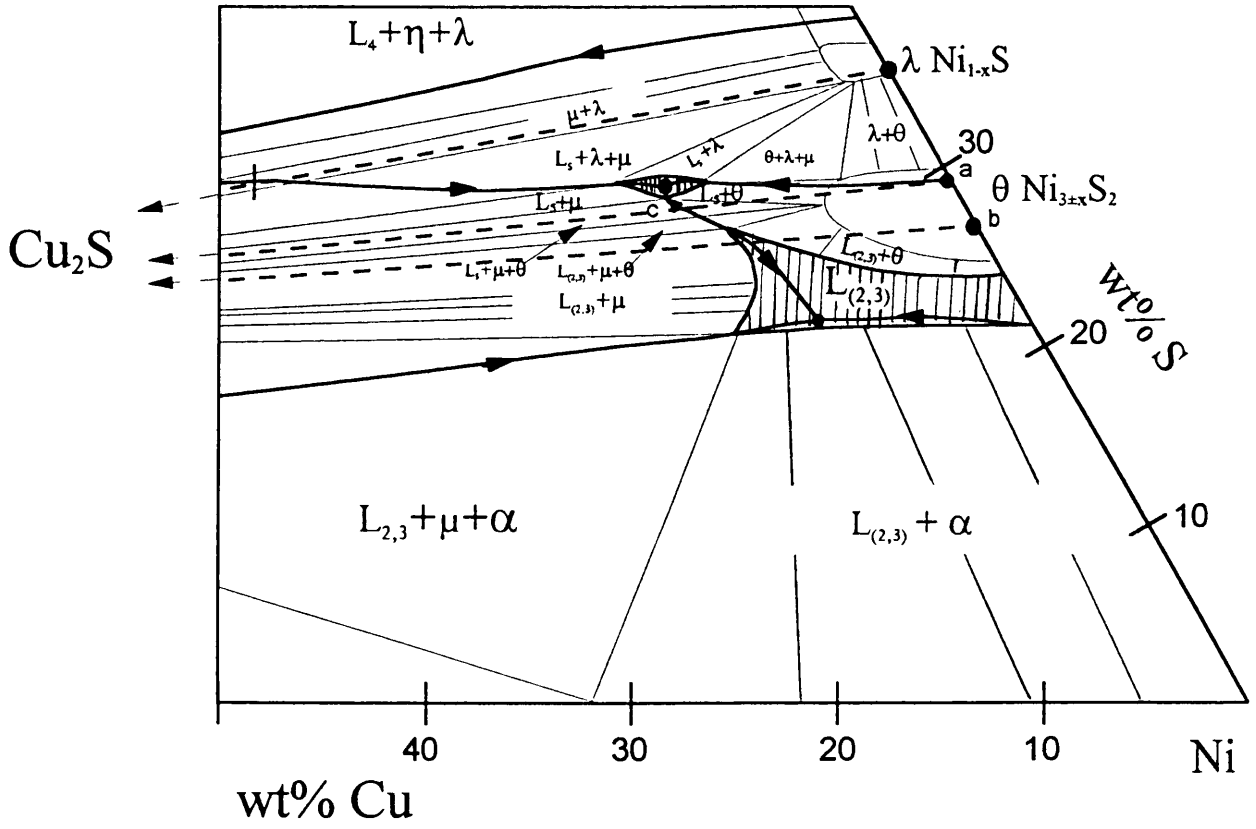

Figure 55. Portion of the Cu-Ni-S phase diagram above 700°C. The liquid field $L_{(2,3)}$ splits into two fields, and the $L_{(2,3)}$ and L_5 fields are shown schematically.

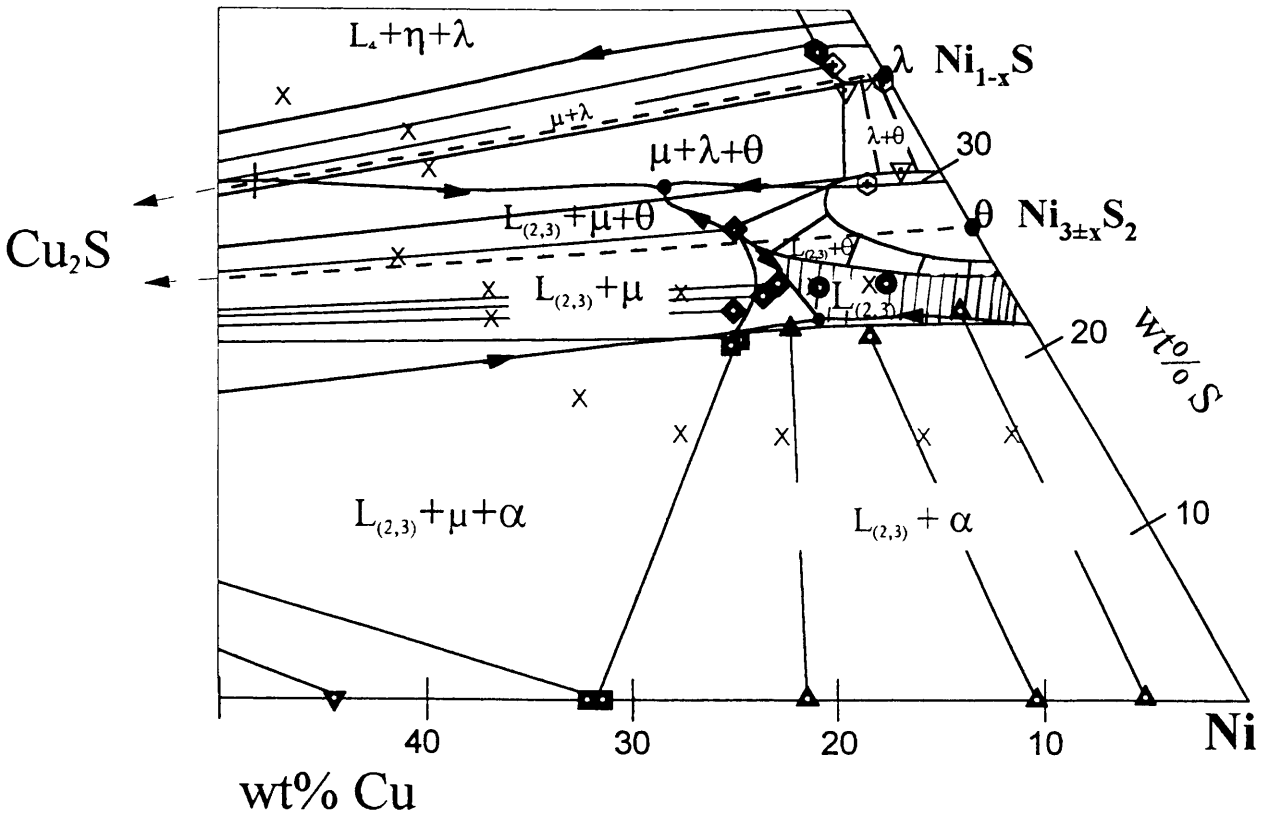

Figure 56. Portion of the Cu-Ni-S phase diagram at 700°C together with the crystallisation paths.

iv) Eutectic point E4

There is a binary eutectic point at 1085°C in the Cu-S phase diagram, indicated by point q in Figure 48 (Massalski, 1986). The liquid field retracts from point q on the Cu-S binary in Figure 57, and the liquid composition follows the crystallisation path described by the liquid + $Cu_{2-x}S$ + alloy ($L_{(2,3)}+\mu+\alpha$) phase assemblage at 1000°C, 900°C, 800°C, and 700°C. This path leads to the eutectic point E4 at 575°C (Sproule *et al.*, 1960)

The binary eutectic between Ni and Ni_3S_2 at 637°C is indicated by point g in Figure 46 (Lin *et al.*, 1978) and Figure 57. The liquid field retracts from point g to point E4. The third crystallisation path that leads to point E4 indicates the retraction of the liquid field from the thermal maximum at the intersection of the Cu_2S-Ni_3S_2 tie-line (point M3) as discussed earlier.

There is some discrepancy between the temperature of the binary eutectic in the Ni-S system determined by Lin *et al.* (1978) with the data of Kullerud *et al.* (1969) and Köster and Mulfinger (1940). Lin *et al.* (1978) reported the binary eutectic at 637°C, while Kullerud *et al.* (1969) reported the retraction of the liquid field from the Ni-S binary at 24.2 wt% S at 553°C, and Köster and Mulfinger (1940) found that the liquid field retracts from the Ni-S boundary (and Ni_3S_2 + Ni becomes stable) at 645°C. The composition of the eutectic point E4 by Köster and Mulfinger (1940) differs from the other previous investigations, and it is not consistent with the crystallisation paths and liquidus isotherms of this investigation (Figure 57).

To summarise the discussion of the crystallisation paths, the phase diagram of the Cu-Ni-S system is presented in Figure 58. The solidus diagram below the E4 eutectic point at ~575°C is shown in Figure 59. The solidus diagram that includes the ternary component $CuNi_2S_6$ at 500°C is shown in Figure 20 (after Kullerud *et al.*, 1969).

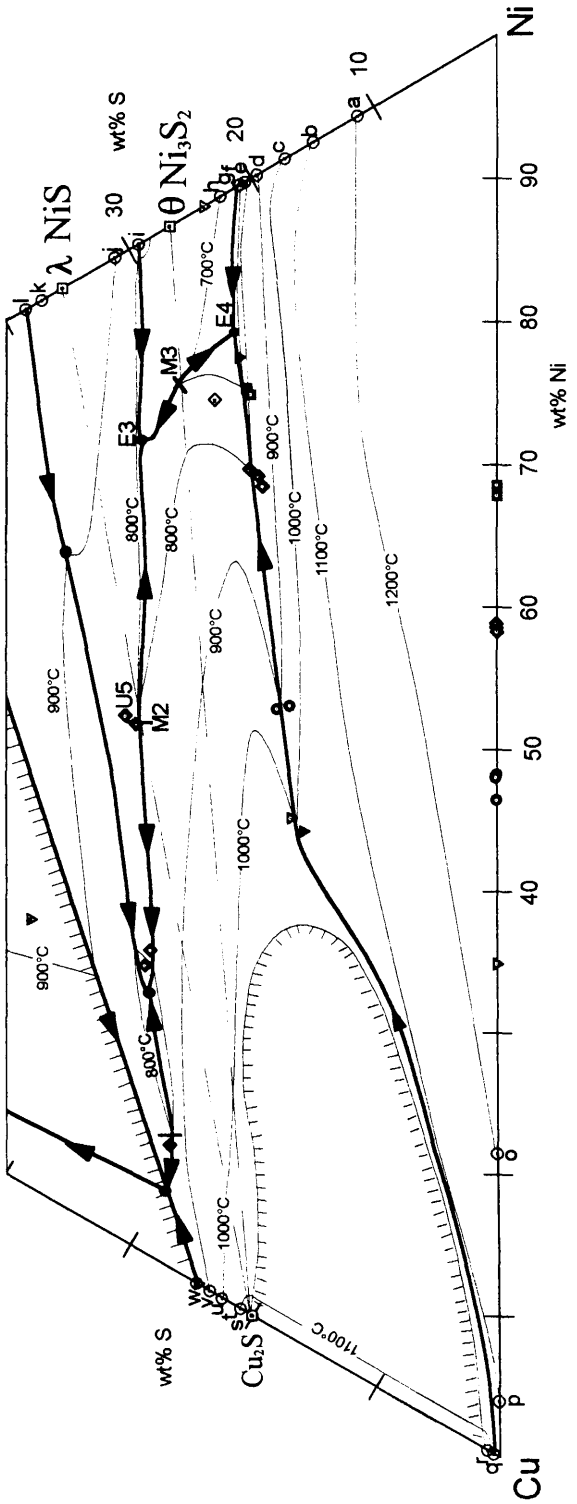

Figure 57. Portion of the Cu-Ni-S phase diagram, showing the crystallisation paths leading to the eutectic point E4.

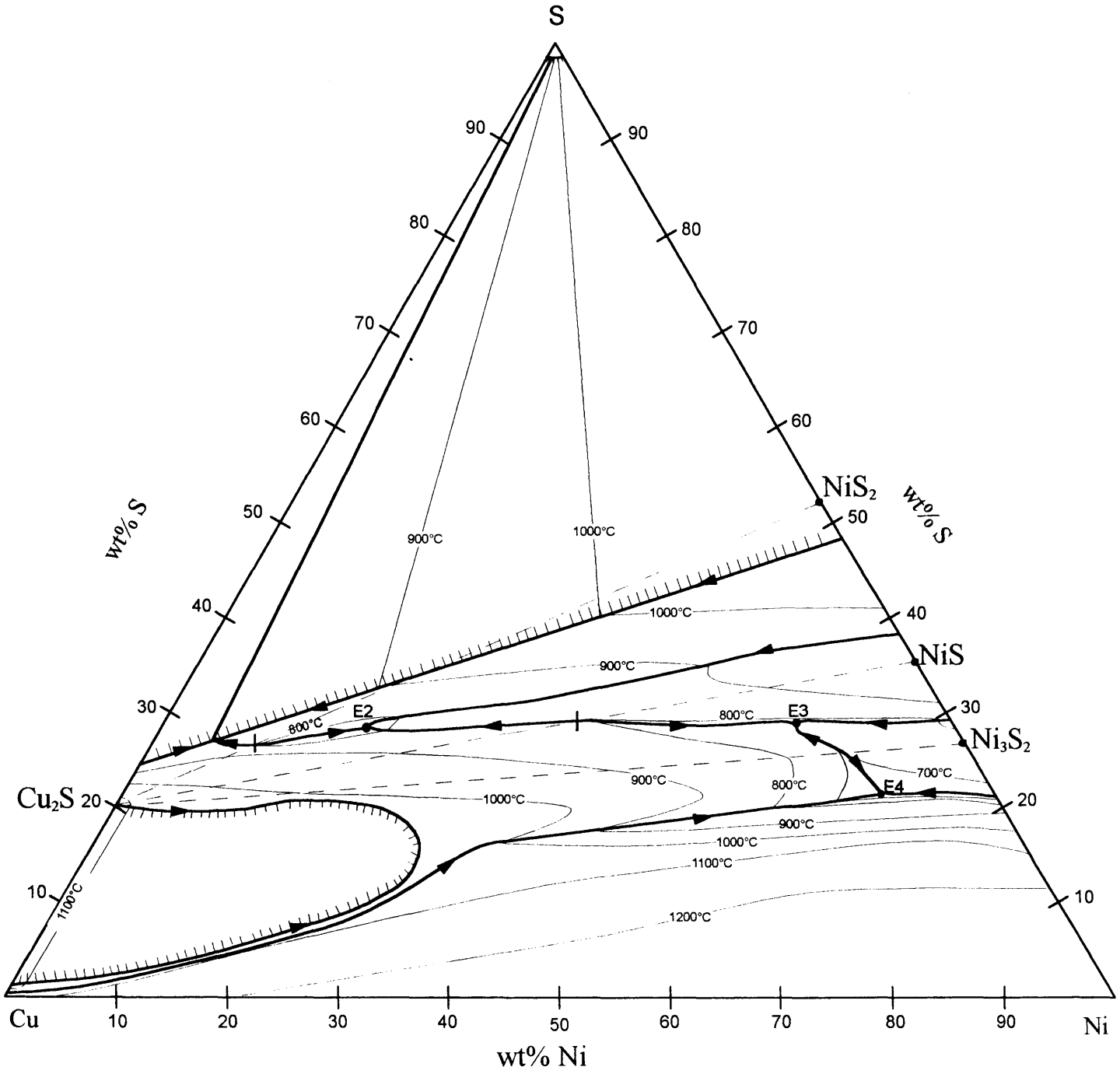

Figure 58. Liquidus isotherms and crystallisation paths of the system Cu-Ni-S, showing the approximate positions of the eutectic points. The sulphur-rich portion of the diagram could not be determined due to experimental difficulties and is shown schematically.

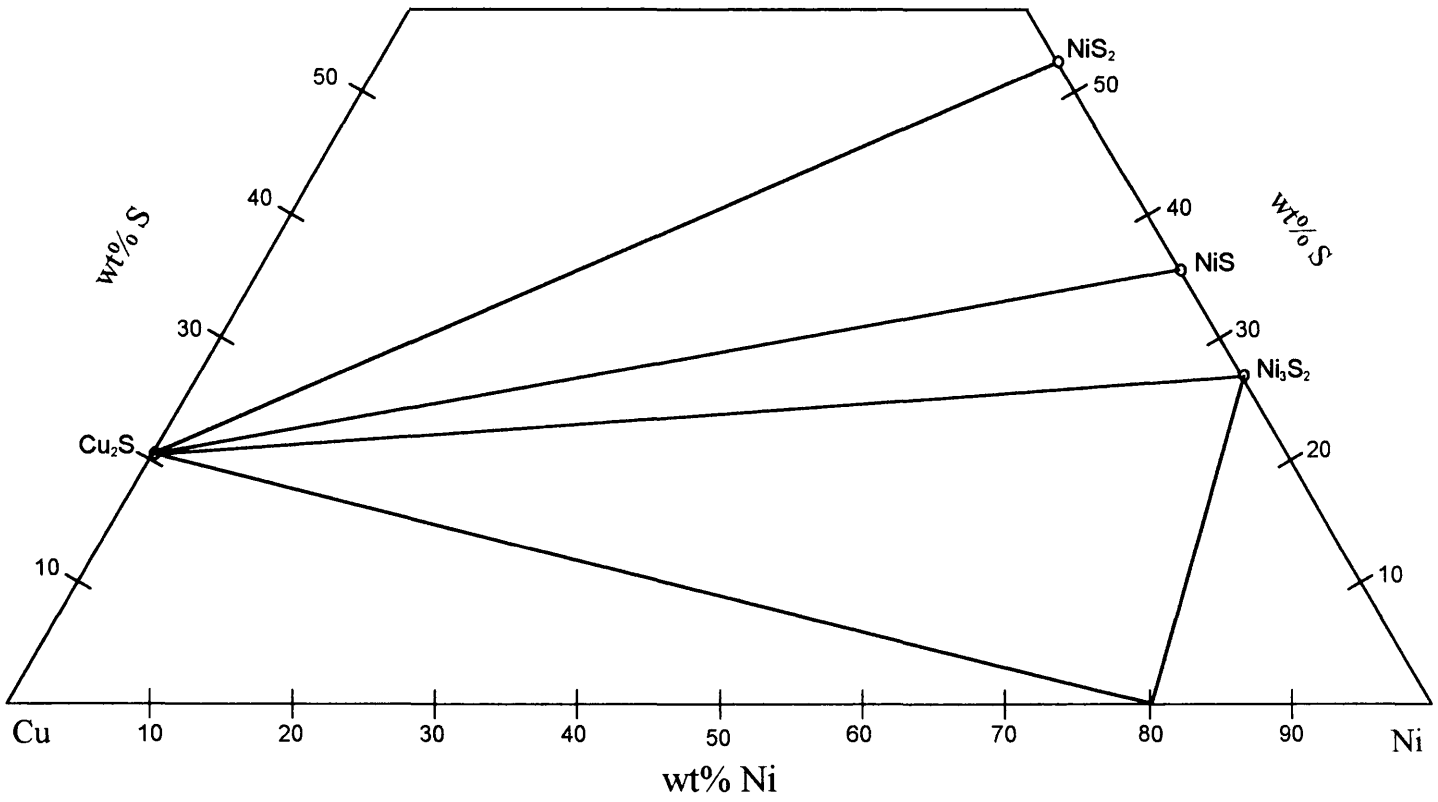

Figure 59. Portion of the Cu-Ni-S solidus phase diagram below the eutectic point E4 at ~575°C.

CHAPTER 6

IMPLICATIONS

Applications of the experimentally determined phase diagrams are discussed, with implications for the slow cooling process of PGE beneficiation. The effect of Fe on the phase relations and formation temperatures of phases in the Cu-Ni-S system is evaluated.

---

6. IMPLICATIONS

6.1 CRYSTALISATION SEQUENCE OF SLOW-COOLED MATTE

The liquidus temperatures and the phase formation sequences of slow-cooled matte can be determined using the Cu-Ni-S phase diagram as an approximation. Examples of possible converter matte compositions (Cu/Ni ratios of 0.8 and 0.4, and S contents of 18 to 22 wt% S) are plotted on the Cu-Ni-S phase diagram (Figure 60). The converter matte compositions with Cu/Ni ratios of 0.8 and 0.4 plotting in the primary Cu_2S field will start crystallising Cu_2S at temperatures between ~950°C and ~850°C respectively. Samples with Cu/Ni ratios of 0.4 plotting in the primary alloy field will crystallise alloy as the first phase, with liquidus temperatures of ~900°C (18 wt% S) or ~850°C (19 wt% S). Samples with these compositions will contain alloy ($Cu_{20}Ni_{80}$, Sproule *et al.*, 1960), Cu_2S and Ni_3S_2 after solidification, as shown in Figures 61 to 64.

On evaluation of the possible phase formation sequence of slow-cooled matte, it was found that the sulphur content is very critical and that only a 1 wt% change in the sulphur content of the matte in the range from 18 to 22 wt% will lead to different crystallisation sequences. There is a certain critical sulphur content that will cause the composition of the liquid to fractionate directly to the eutectic point E4: higher sulphur contents will cause crystallisation of the alloy phase only at the eutectic point, and lower sulphur contents will lead to the formation of alloy before the eutectic point. The critical sulphur content is shown in Figure 60 as a straight line between Cu_2S and E4 (with point E4 from Sproule *et al.*, 1960). The critical sulphur content of the sample depends on the Cu/Ni ratio of the bulk sample composition. The exact composition of the first phase that will crystallise (usually a Cu_2S-type phase) will influence the critical sulphur content, as the phase composition will determine the composition of the liquid during fractionation. The exact position of the eutectic point E4 is also important, but previous investigations showed disagreement (Table 3).

Using the stoichiometric Cu_2S phase as the composition of primary Cu_2S and the eutectic point from Sproule *et al.* (1960) as point E4, the theoretical crystallisation paths that can be expected for mattes with different sulphur contents are illustrated in Figures 61 to 64.

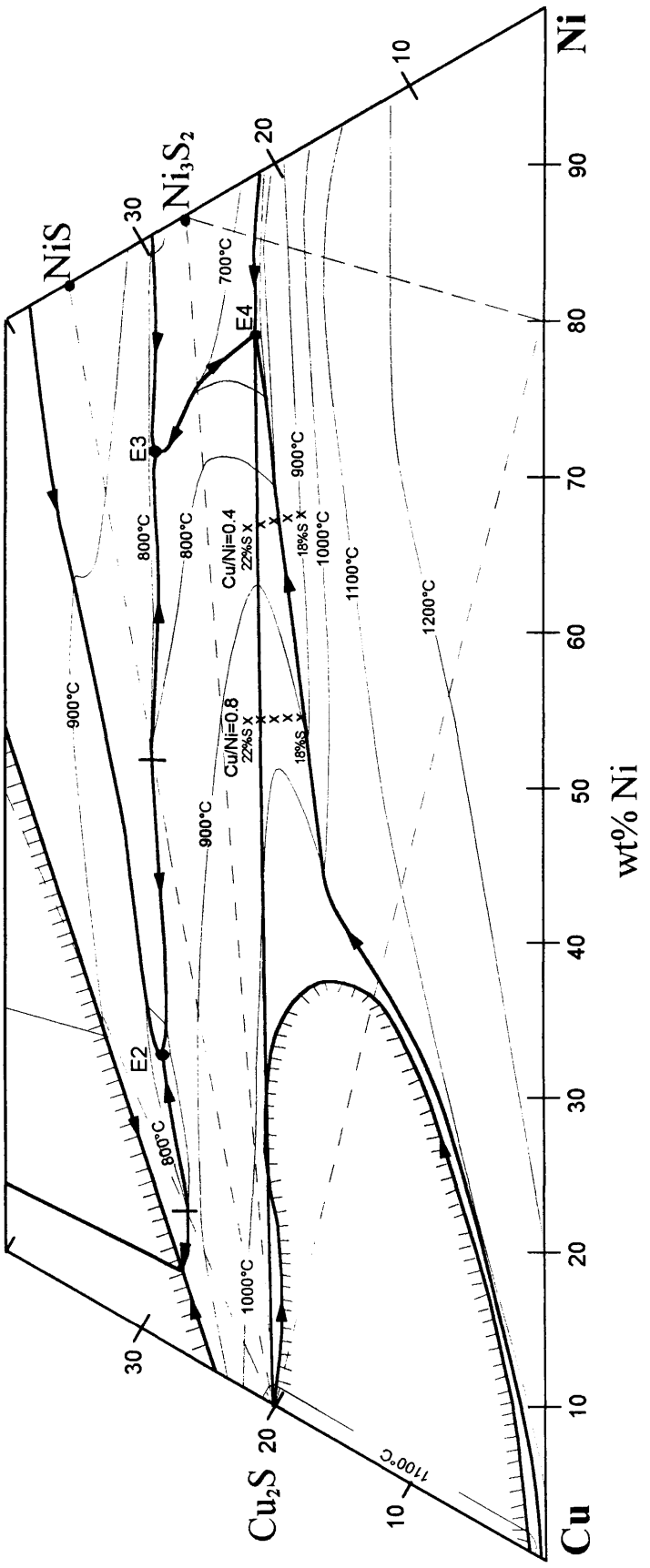

Figure 60. Examples of possible converter matte compositions (shown as x's) with Cu/Ni ratios of 0.8 and 0.4 and S contents ranging from 18 to 22 wt% S are projected on the Cu-Ni-S phase diagram. The eutectic point E4 is from Sproule et al. *(1960).*

i) Path A

Matte containing < 18 wt % S (with Cu/Ni ratio =0.8) or < 19.5 wt% S (Cu/Ni ratio of 0.4), plots in the primary alloy field, and alloy will be the first phase to crystallise. The crystallisation path of such mattes is shown in Figure 61, using as an example a sulphur content of 18 wt% and a Cu/Ni ratio of 0.6. The liquid composition will change with cooling, following a straight line through the alloy and the matte composition (x, Figure 61), until the Cu_2S - alloy eutectic line is reached (d, Figure 61). From point d onwards, Cu_2S will start to crystallise and liquid + Cu_2S + alloy will co-exist until the liquid composition reaches the eutectic point E4. At point E4, Ni_3S_2 will start crystallising and Ni_3S_2 + Cu_2S + alloy will crystallise simultaneously until the matte is solidified, before the temperature can drop below the eutectic temperature (575°C, Sproule *et al.*, 1960).

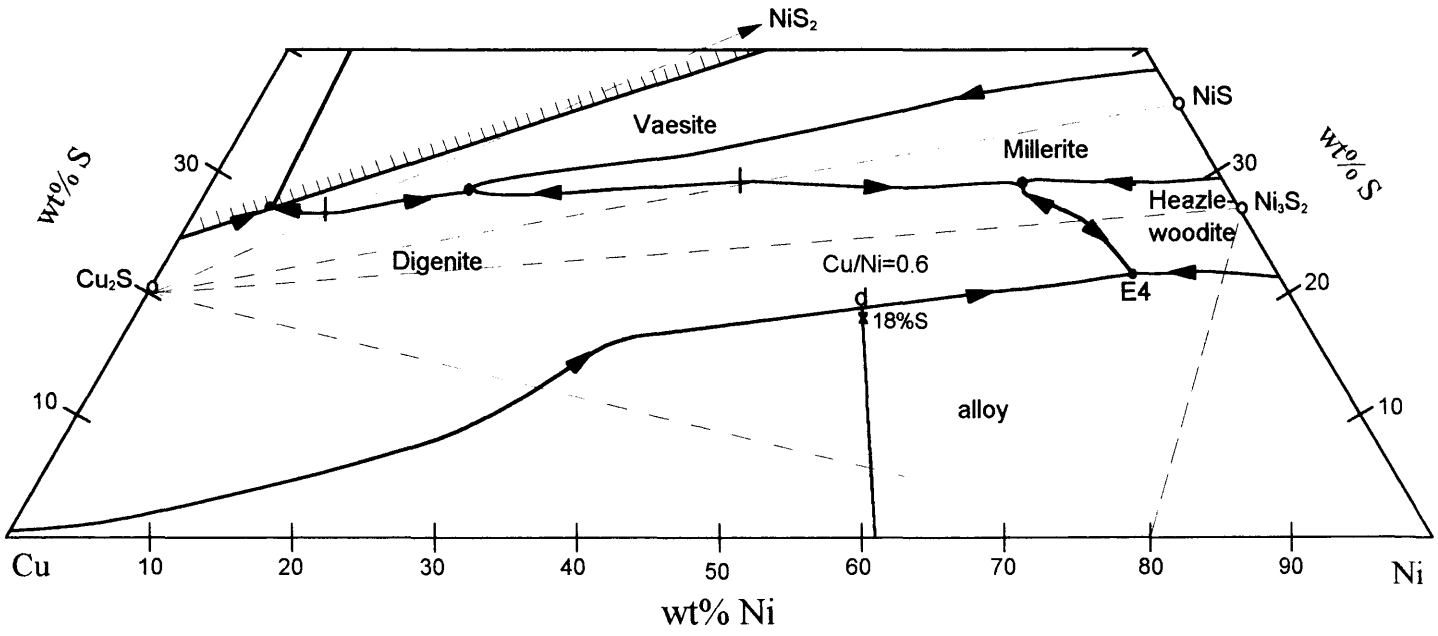

Figure 61. The crystallisation path of a sample with 18 wt% S and a Cu/Ni ratio of 0.6 (marked with x). Alloy crystallises first, causing the liquid to fractionate from point x to d, where Cu_2S and alloy crystallise simultaneously (d-E4), until the eutectic point E4 is reached, where Cu_2S, alloy, and Ni_3S_2 crystallise until the sample is solidified. Point E4 is from Sproule et al. *(1960).*

ii) Path B

Mattes plotting in the primary Cu_2S field (Figure 60) with S contents between 18 and 21 wt % S (Cu/Ni ratio of 0.8) or between 19.5 and 21.3 wt% S (Cu/Ni ratios of 0.4) will form Cu_2S first. An example of the crystallisation path that such mattes will follow is shown in Figure 62, using a matte composition of 20 wt%S and a Cu/Ni ratio of 0.6. The liquid composition will follow the path determined by a straight line from the Cu_2S composition through the point representing the matte composition (x, Figure 62), until the Cu_2S - alloy crystallisation path is reached at point a. From point a on alloy will start crystallising and liquid + Cu_2S + alloy will co-exist until the liquid reaches the eutectic point E4. At the eutectic point Ni_3S_2 will also start to crystallise, and the temperature will stay at the eutectic temperature while Cu_2S + alloy + Ni_3S_2 crystallise until the matte is solidified, before the matte can cool below the eutectic temperature.

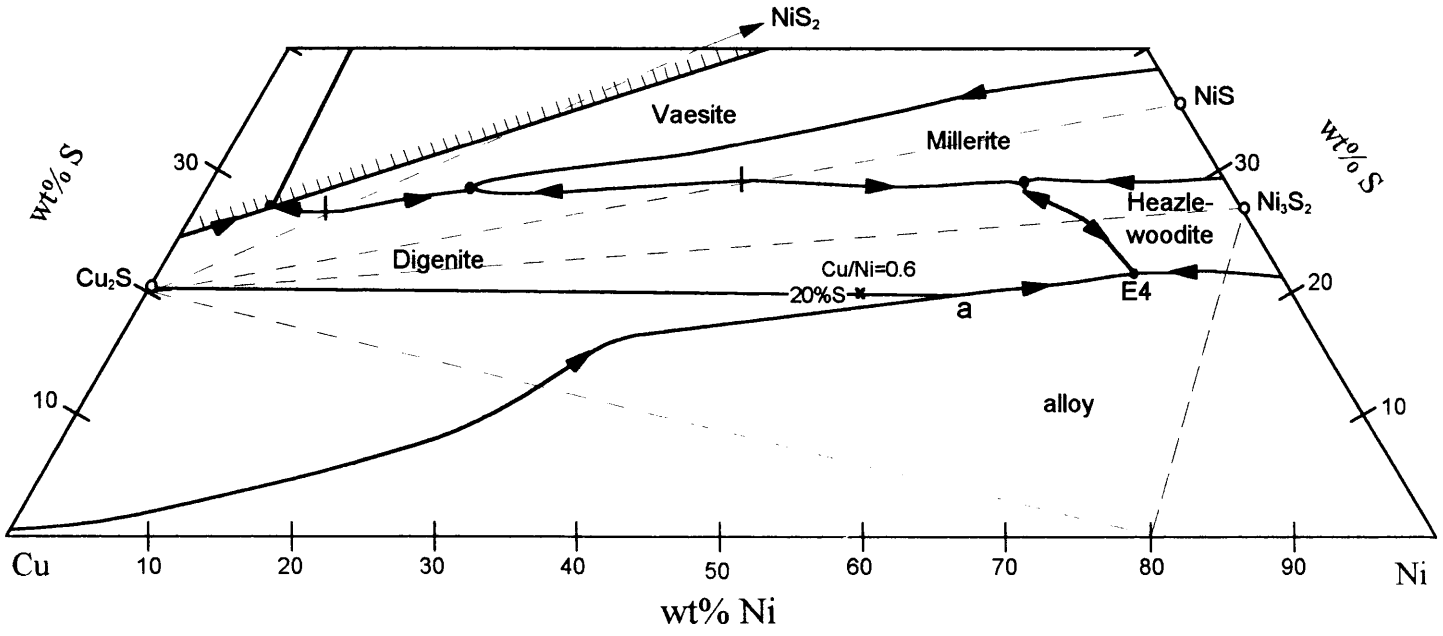

Figure 62. The crystallisation path of a sample with 20 wt% S and a Cu/Ni ratio of 0.6 (marked with x). Cu_2S crystallises first, causing the liquid to fractionate from x to point a, where Cu_2S and alloy crystallise simultaneously (a-E4), until the eutectic point E4 is reached, where Cu_2S, alloy, and Ni_3S_2 crystallise until the sample is solidified. Point E4 is from Sproule et al. *(1960).*

iii) Path C

As shown in Figure 60 the critical sulphur content is 21 wt % (Cu/Ni ratio of 0.8) or 21.3 wt% (Cu/Ni ratios of 0.4). With such compositions the matte will follow the crystallisation path as shown in Figure 63, using a sulphur content of 21.2 wt% and a Cu/Ni ratio of 0.6. The matte will crystallise Cu_2S first and the liquid composition will change directly to the eutectic point E4, where Ni_3S_2 and alloy will also start to crystallise. At the eutectic point Cu_2S + Ni_3S_2 + alloy will crystallise until the matte is solidified.

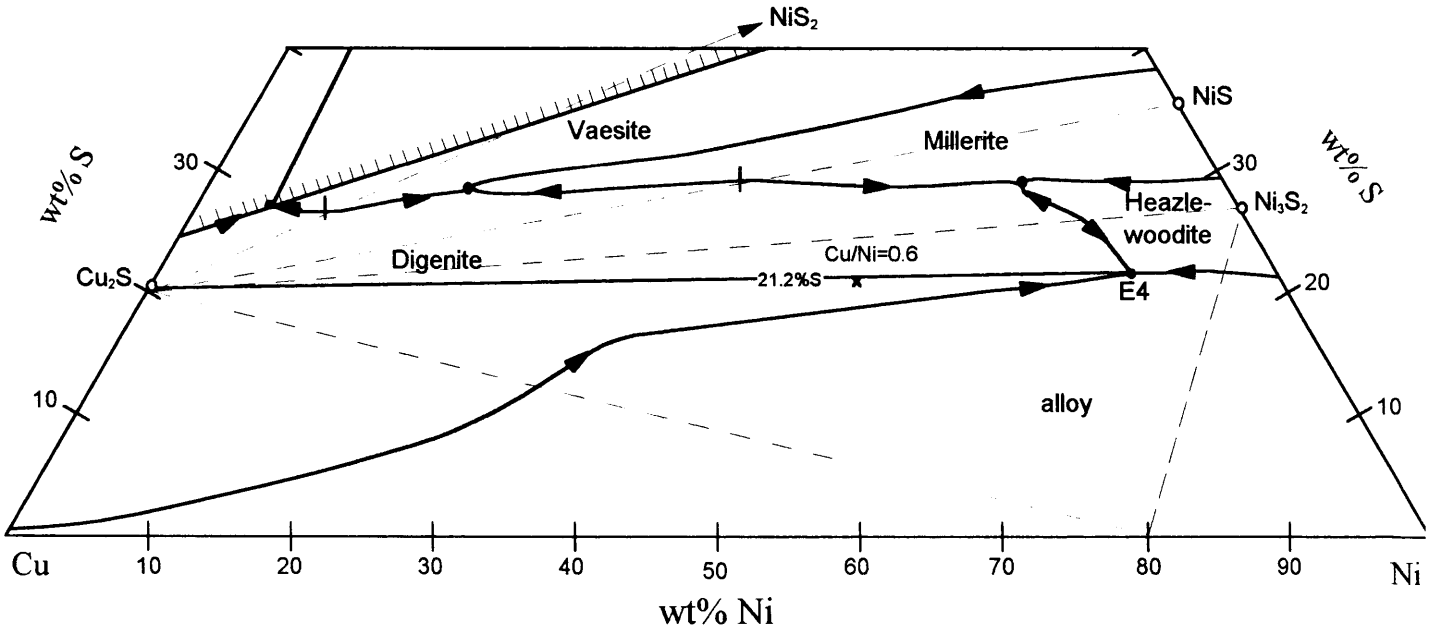

Figure 63. The crystallisation path of a sample with 21.2 wt% S and a Cu/Ni ratio of 0.6 (marked with x). Cu_2S crystallises first, causing the liquid to fractionate from x to the eutectic point E4, where Cu_2S, alloy, and Ni_3S_2 crystallise until the sample is solidified. Point E4 is from Sproule et al. *(1960).*

iv) Path D

With sulphur contents >21 wt % (Cu/Ni ratio of 0.8) or >21.3 wt% (Cu/Ni ratios of 0.4) Cu_2S will crystallise first followed by Ni_3S_2 (Figure 60). An example of the crystallisation path that such mattes will follow is shown in Figure 64, using a sulphur content of 22 wt% and a Cu/Ni ratio of 0.6. Cu_2S will crystallise first and the liquid composition will follow a straight line from the matte composition (x, Figure 64), directly away from the Cu_2S phase, until the Cu_2S - Ni_3S_2 eutectic line is reached at point h. At point h, Ni_3S_2 will start to crystallise and from this point onwards liquid + Cu_2S + Ni_3S_2 will co-exist until the eutectic point (E4) is reached, where alloy will start to form. Cu_2S + Ni_3S_2 + alloy will crystallise at the eutectic temperature until the matte is solidified.

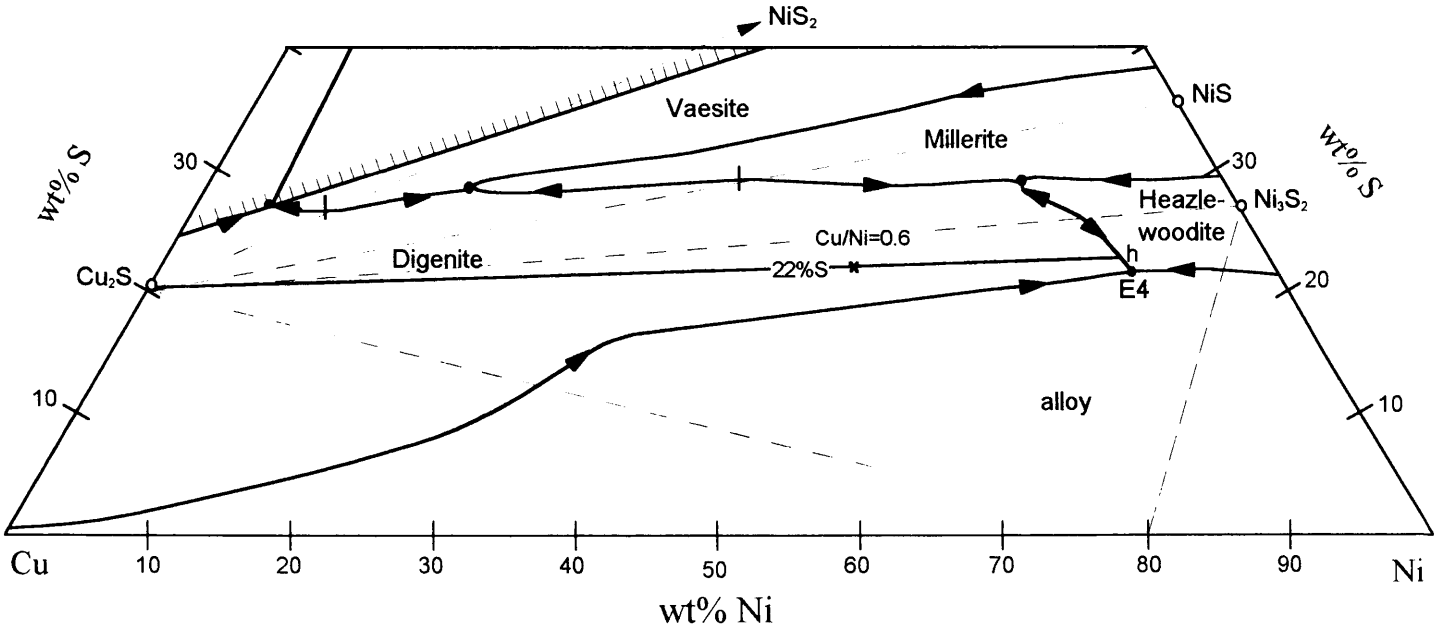

Figure 64. The crystallisation path of a sample with 22 wt% S and a Cu/Ni ratio of 0.5 (marked with x). Cu_2S crystallises first, causing the liquid to fractionate from point x to h, where Cu_2S and Ni_3S_2 crystallise simultaneously (h-E4), until the eutectic point E4 is reached, where Cu_2S, alloy, and Ni_3S_2 crystallise until the sample is solidified. Point E4 is from Sproule et al. *(1960).*

6.2 PHASE SEGREGATION THROUGH AN INGOT:

The typical phase segregation found in slow-cooled matte is Cu_2S enrichment at the top of the ingot, and Ni_3S_2 and alloy at the bottom of the ingot, and this was widely accepted to be due to gravity separation during cooling (Sproule *et al.*, 1960). In this study, however, Cu_2S crystals were not observed to 'float' when equilibrated in the presence of a liquid, but rather for liquid to form a sphere in the centre of the sample, surrounded by Cu_2S. In contrast, gravity segregation of alloy in equilibrium with a sulphide melt was observed frequently in this investigation. The theory of gravity separation in the system Cu-Ni-S can thus not be excluded completely, but it was not observed for any phase association other than liquid + alloy.

Hayward (1915) reported the specific gravity of Cu_2S and Ni_3S_2 to be very similar, (Cu_2S = 5.76 and Ni_3S_2 = 5.84), while the specific gravity of the metallic alloy phase is much higher ($Cu_{20}Ni_{80}$ = 8.82). Although sulphide melt has a low viscosity which could facilitate gravity segregation in a largely molten ingot, the gravity segregation model does not explain why Ni_3S_2 and Cu_2S with such similar relative densities are not found at the same level in the ingot, while Ni_3S_2 and alloy with very different densities are found together. Furthermore, it must be kept in mind that gravity segregation can only occur if there is only a small amount of solid phases present in the melt, in order to facilitate movement. It is quite possible that certain phases can float or sink in an association of a solid phase + liquid, but the segregation of all the phases in an ingot due to gravitation is unlikely.

The cooling paths shown in Figures 62, 63, and 64 indicate that for normal matte compositions high temperature Cu_2S crystallises early in the crystallisation sequence. This phase forms predominantly in the top region of the ingot (Sproule *et al.*, 1960). With continued crystallisation of Cu_2S the molten matte becomes depleted in the Cu_2S component and the composition of the liquid fractionates towards relative enrichment in alloy and Ni_3S_2, which have the lowest formation temperatures. The alloy and Ni_3S_2 is found in the bottom of the ingot (Sproule *et al.*, 1960). It seems therefore that the segregation found in slow-cooled ingots is rather due to fractional crystallisation caused by disparate phase formation temperatures than gravity segregation.

6.3 AMOUNT OF ALLOY

For economic reasons the amount of alloy formed during slow-cooling must not exceed 15 to 20 volume % of the total ingot (Sproule et al, 1960). Changes in the matte composition are related to the proportions of phases that will form. If the composition of the matte is plotted onto the Cu-Ni-S phase diagram, the lever rule can be used to give an indication of the amount of alloy that will form.

The wt % of alloy that forms when the sulphur content and the Cu/Ni ratio is changed is shown in Figure 65. With the higher S content at 22 wt % and the lower S content at 18 wt% the amount of alloy that will form, varies from 8 to 23 wt % respectively for a Cu/Ni ratio of 0.8. The relative change in sulphur content from 22 wt% to 18 wt% leads to a change from 12 to 27 wt % alloy at a Cu/Ni ratio of 0.4. If one were to compare two samples with a similar sulphur content but different Cu/Ni ratios, it can be seen in Figure 65 that more alloy will form at lower Cu/Ni ratios.

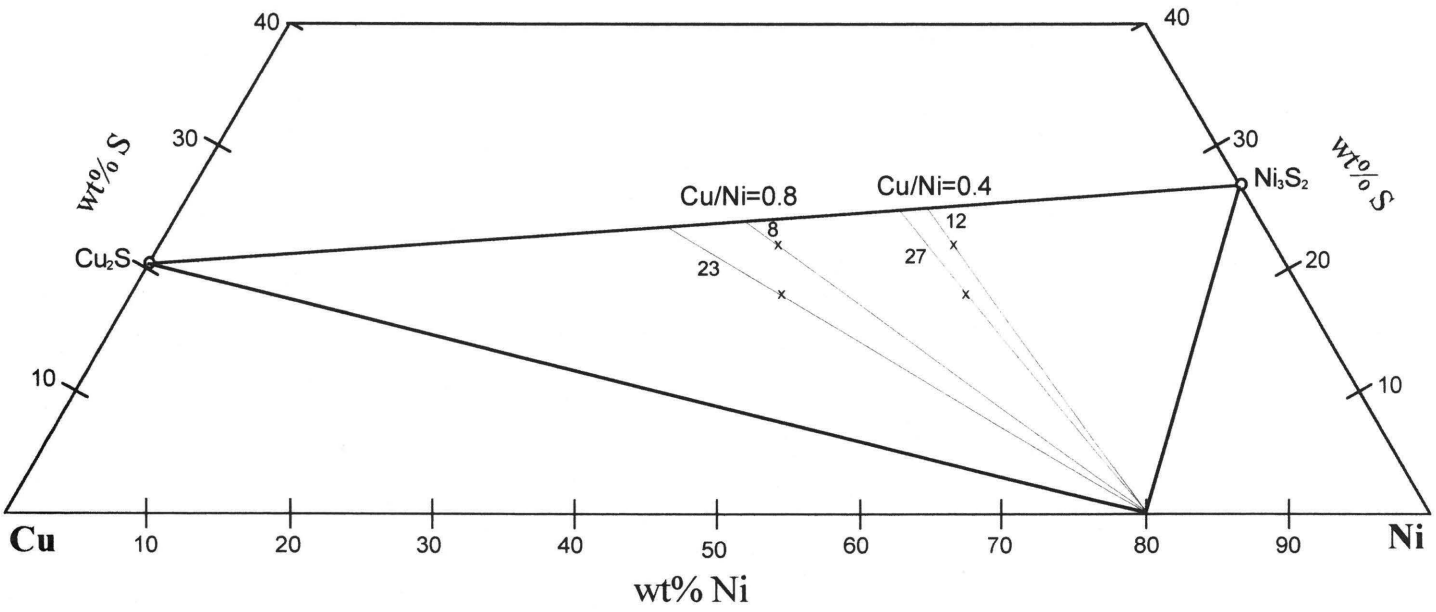

Figure 65. The wt % of phases that the solidified sample will contain can be determined by plotting the sample composition (x) on the phase diagram. The examples shown here plot in the Cu_2S-Ni_3S_2-alloy stability triangle. A line through the sample composition and the eutectic alloy composition $Cu_{20}Ni_{80}$ (Sproule et al., *1960) can be used for alloy wt % determinations by means of the lever rule. Samples being compared are those with similar Cu/Ni ratios (0.8) and sulphur contents of respectively 22 and 18 wt% S, as well as samples with a Cu/Ni ratio of 0.4 and 22 and 18 wt% S. The wt % of alloy that will form increases when the sulphur content decreases (with constant Cu/Ni ratios). The amount of alloy also increases with decreasing Cu/Ni ratio (at a constant sulphur content).*

6.4 THE EFFECT OF Fe ON THE PHASE RELATIONS

The major components of converter matte are Cu, Ni, and S, with small amounts of Fe, PGEs, Co and trace amounts of other elements. These elements may cause differences in the phase diagram of the Cu-Ni-S system. The effect of various PGEs on the phase relations in the Cu-Ni-S system have not yet been systematically investigated (Nell, 1987), and their effect in combination with that of the other mentioned elements in a matte is not known. The largest effect of a single element on the system Cu-Ni-S will probably be that of Fe, because approximately 3 wt% Fe (Mostert and Roberts, 1973) is usually present in converter matte that undergoes slow cooling. It was therefore necessary to estimate what the effect of small amounts of Fe would be on the phase relations of the Cu-Ni-S system.

As can be seen on the schematic Cu-Ni-Fe-S diagrams (Figures 66 and 67) by Craig and Kullerud (1969), the Fe-containing system is very complex and it is vastly different from the Cu-Ni-S system. This is mainly due to the presence of the monosulphide solid solution field which dominates the phase relations at high temperatures. Converter mattes typical for slow-cooling, however, contain only approximately 3 wt% Fe (Mostert and Roberts, 1973) and it should not contain enough sulphur for the formation of a monosulphide phase. Pentlandite can occur (Lindsay and Sellshop, 1988), but it probably becomes significant only when the Fe content of the matte is higher than usual. The presence of pentlandite is detrimental as PGMs have a high affinity for the (Fe or Ni) monosulphide phase (Distler *et al.*, 1977). The small amounts of Fe that is typical for converter matte (<3 wt%) is thus expected to have minor influences on the phase relations of the system.

In slow-cooled matte Fe occurs mainly in the form of Cu-Ni-Fe alloy, with some Fe present in the $Cu_{2-x}S$-Cu_5FeS_4 (chalcocite-bornite) solid solution (Lindsay and Sellshop, 1988) as well as in the $(Fe,Ni)_{3\pm x}S_2$ phase (as observed in experiments by Craig and Kullerud, 1969).

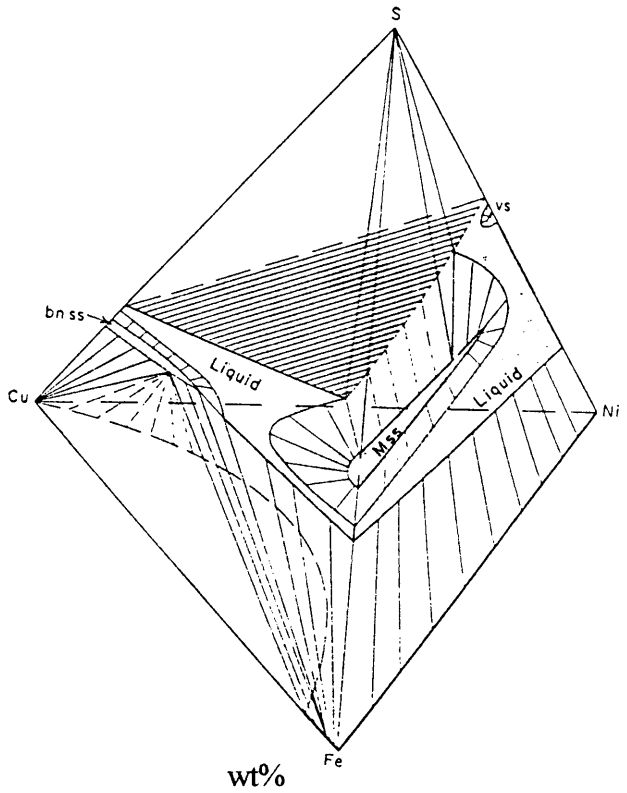

Figure 66. Schematic Cu-Ni-Fe-S diagram at 1000°C by Craig and Kullerud (1969).(Mss - monosulphide solid solution; vs - vaesite; bn ss - bornite solid solution).

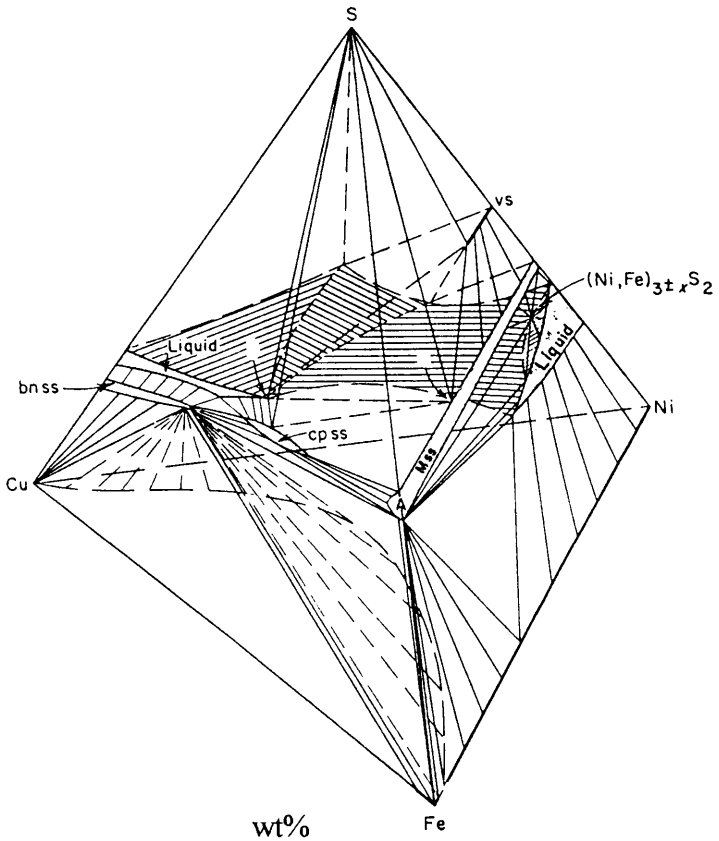

Figure 67. Schematic Cu-Ni-Fe-S diagram at 850°C by Craig and Kullerud (1969). Mss - monosulphide solid solution; vs - vaesite; bn ss - bornite solid solution; cp ss - chalcopyrite solid solution.

i) The effect of Fe on Cu-Ni alloy

Cu-Ni alloys are ferromagnetic if the Ni content is above ~35 wt% (Köster and Mulfinger, 1940). The magnetism of Cu-Ni-S samples was also observed when positioning the samples with a pair of metallic tweezers for mounting in a polished section. Small amounts of Fe in the alloy will probably increase the ferromagnetism of the alloy and facilitate better magnetic separation of slow-cooled matte. It is known that PGEs have very high partition coefficients for Fe-containing metallic phases (Fleet and Stone, 1991). Investigations by Merkle and van den Berg (1996) showed that Pt will be concentrated in a Cu-Ni alloy containing virtually no Fe. The importance of Fe in the alloy is still unclear and it is being investigated further (R. Merkle pers. comm.).

It must be kept in mind that the concentration of Fe in the alloy phase is not only dependent on the amount of Fe in the matte, but also on the amount of alloy that forms. With small amounts of alloy the Fe concentration in the alloy will be higher than with large amounts of alloy.

ii) The effect of Fe on the $Cu_{2-x}S$ - type phase

The presence of Fe in the $Cu_{2-x}S$ - Cu_5FeS_4 solid solution will cause the sulphide phase to have a higher sulphur content than stoichiometric Cu_2S. This can be seen from the extent of the $Cu_{2-x}S$-Cu_5FeS_4 phase field in the Cu-Fe-S system (Figure 68, Chang *et al.*, 1979). If the bulk composition of the matte is such that $Cu_{2-x}S$-Cu_5FeS_4 is the first phase to crystallise then the higher sulphur content of the phase will influence the crystallisation paths that the matte will follow. The high sulphur content has a leverage effect on the composition of the fractionating liquid and the liquid will become more metal rich as the $Cu_{2-x}S$-Cu_5FeS_4 phase crystallises, causing earlier crystallisation of alloy.

iii) The effect of Fe on the Ni_3S_2-type phase

It is not certain what the effect of Fe in the $(Fe,Ni)_{3\pm x}S_2$ phase (Craig and Kullerud, 1969) would be on the phase formation temperatures.

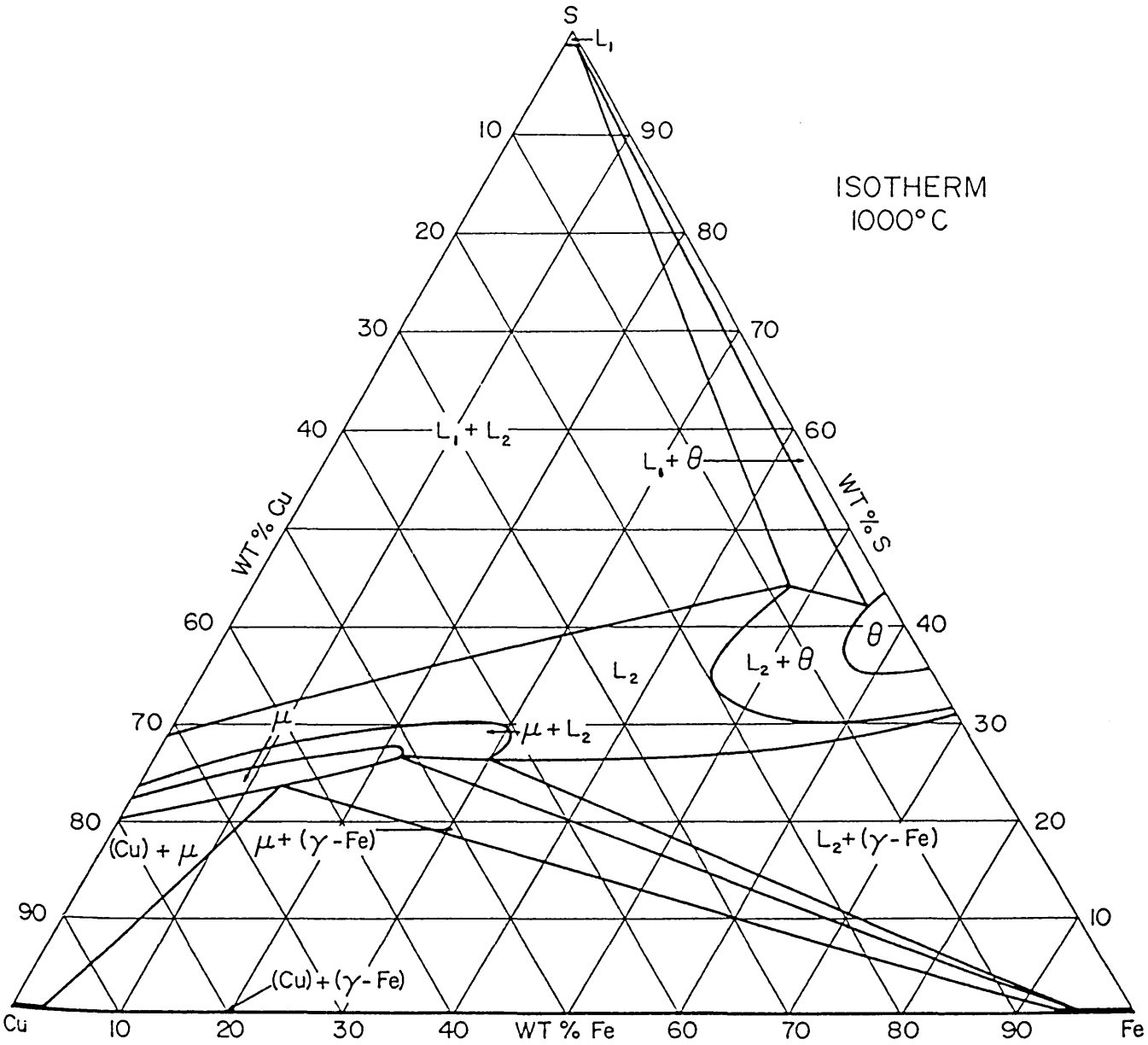

Figure 68. Phase boundaries and tie-lines in the system Cu-Fe-S at 1000°C (Chang et al., *1979), showing that the Cu_2S-Cu_5FeS_4 solid solution contains more sulphur than the iron-free Cu_2S phase.*

6.5 PARTITIONING BEHAVIOUR OF PGEs:

If it is assumed that all platinum group elements (PGEs) occur in a dissolved state in molten converter matte, then the partitioning behaviour of the PGEs will depend on the crystallisation sequence of the phases. It was shown earlier that the sequence of phase formation depends on the composition of the matte. During the slow-cooling of the matte, the PGEs will either partition into a specific solid phase (i.e. Cu-Ni alloy or a sulphide phase) or stay dissolved in the melt until it solidifies. It is, however, important for recovery that the PGEs are accommodated in the magnetic Cu-Ni alloy.

Studies by Distler *et al.* (1977) on the distribution of Pd, Rh and Ru in the Fe-Ni-S system showed that Pd preferentially partitioned into the liquid (of a composition close to M_3S_2), while Ru and Rh preferentially partitioned into the early crystalline phase, namely monosulphide solid solution (Fe or Ni mss). The experimental charges contained high S values with S = 33.3 - 33.8%; Fe = 41%; Ni = 24.7% and Pd = 1%, Rh = 1% and Pd = 0.5%. After cooling and solidification, the solid sulphide phase was enriched in Rh and Ru, while Pd resided in the solidified residual melt. The distribution coefficients from the sulphide melt to the solid sulphides was 1.18 for Rh and 1.22 for Ru. Furthermore it was found that there was virtually no Rh in the sulphide phase that formed in the final stages of crystallisation. All the remaining Rh in the liquid partitioned into the solidifying metallic phase, and this small amount of alloy contained up to 8% Rh. This confirms that even though the partition coefficients of PGEs from a sulphide melt are much higher for the metallic phases (with the exception of Pd, Fleet and Stone, 1991), in the absence of metallic phases some of the PGEs can partition into early forming sulphide minerals.

By analogy it can be assumed that PGEs in the Cu-Ni-S system may react in the same manner. If one would consider the equilibrium cooling path of converter matte using the Cu-Ni-S system as an approximation (Figures 61 to 64), it is evident that the crystallisation sequence and the partitioning behaviour of PGEs into these crystallising phases in the presence of liquid, are very important. There is, however, no information available for the behaviour of PGEs in the presence of only liquid + Cu_2S, or liquid + Ni_3S_2, or liquid + Cu_2S + Ni_3S_2. Even though the partition coefficients for PGEs into sulphide minerals are quite small in comparison to those for alloy, it

must be kept in mind that in the case where only liquid + a sulphide mineral is present in a matte, some PGEs can favour the solid sulphide phase instead of the sulphide melt. It is therefore possible that some of the PGEs will partition into a sulphide phase during the slow-cooling of matte. The presence of Pd in Ni_3S_2 (Merkle and van den Berg, 1996) is evidence for this.

The early formed sulphide phases can contain large amounts of other elements, as can be seen by the large amount of Ni_3S_2 exsolutions in Cu_2S and the large amount of Cu_2S exsolutions in Ni_3S_2 of the quenched minerals. On cooling, these elements will gradually exsolve from the sulphide phases and occur at the grain boundaries if given sufficient time, or form small exsolution phases if cooled too rapidly. It is evident that the presence of these early formed, non-magnetic sulphide phases and their ability to accommodate PGEs at an early stage of cooling will have a negative influence on the beneficiation process.

If alterations to the slow-cooling process are to be made, it is recommended that the matte composition be adjusted so that alloy forms early in the phase formation sequence. Since Pt has a very high affinity for the metallic phase all the Pt will concentrated in the first formed alloy. In addition, alloy will crystallise from a higher temperature which will ensure longer crystallisation times. This can lead to larger alloy grain sizes for easy liberation and magnetic separation.

If alloy is the first phase to form, and there is indeed the tendency for alloy crystals co-existing with a liquid to sink due to density differences (as observed in this investigation), the PGE-containing alloy could be collected in an easily separable form at the bottom of the ingot. Settling alloy will press the remaining liquid out of the lower portion of the ingot, similar to filter pressing due to gravity settling in magma chambers. This may possibly lead to the elimination of the need to separate the matte magnetically, which would solve the associated problems, such as grain sizes, correct crushing and milling and magnetic properties of the alloy.

CHAPTER 7

CONCLUSION

The overall results and implications for the study are summarised. Possible future investigations are briefly discussed.

7. CONCLUSION

7.1 EXPERIMENTAL AND ANALYTICAL TECHNIQUES

Phase relations in the ternary system Cu-Ni-S were investigated in six isothermal sections using 275 charges in evacuated quartz-glass tubes. The samples were investigated microscopically for verification of equilibrium conditions. It was decided that micro-beam techniques are more suitable for analysing quenched sulphide phases than separating the phases for chemical analyses. The micro-beam techniques that were investigated were SEM analyses of areas, EMP analyses of large number of spots in a grid, and defocused beam EMP spots. The technique using averages of defocused beam EMP spots (similar to the technique employed by Fleet and Pan, 1994), were found to give too low totals, possibly due to scattering of the beam.

A comparative statistical evaluation was made between analysed areas (0.12 mm^2) with a SEM and spot analyses with the EMP in a grid pattern. Analyses of areas were found to give more reproducible and statistically meaningful results. It was also found to be the better method for revealing anomalies in heterogeneous phases, like quenched sulphide liquid. Averaged SEM analyses of as many areas as possible of phases in equilibrium phase assemblages were used for construction of the 1200°C, 1100°C, 1000°C, 900°C, 800°C and 700°C isothermal sections.

Microscopic investigation of the phases obtained in the immiscible liquid field at 1200°C, showed that techniques which require that the two immiscible liquids (L_2 + L_3) are quenched while in contact can lead to the physical mixing of the phases before quenching. Other methods, were the liquids are sampled individually at the working temperature (e.g. Lee *et al.*, 1980; Schlitt *et al.*, 1973), are less prone to such errors.

7.2 RESULTS

The 1200°C, 1100°C, 1000°C, 900°C, 800°C and 700°C isothermal sections were determined in this investigation. At 1200°C the largest portion of the phase diagram is liquid ($L_{(2,3)}$), and on the Cu-side of the diagram there is a two liquid immiscible field ($L_2 + L_3$). On cooling, the immiscible liquid fields retracts from the Cu-S binary and $Cu_{2-x}S$ is solid. There are fields surrounding $Cu_{2-x}S$ at 1100°C where $L_{(2,3)}$+ $Cu_{2-x}S$ and $L_3 + Cu_{2-x}S$ exist. The position of the $L_2 + L_3 + Cu_{2-x}S$ field could be deduced using the monotectic reaction temperatures of Schlitt et al. (1973). Below 1067°C (Massalski, 1986) the liquid field retracts from the Cu-S binary and $Cu_{2-x}S$ coexists with Cu-rich alloy. The three-phase field of co-existing $L_{(2,3)} + Cu_{2-x}S$ + alloy, as well as a two phase field of $Cu_{2-x}S$ + alloy, extends to the metal-side of the $Cu_{2-x}S$ field at 1000°C, 900°C, 800°C, and 700°C. These phase fields expand with cooling to the Ni-rich side of the diagram and at 700°C they cover the largest part of the metal-rich side of the diagram. Between the 900°C and 800°C isothermal sections the liquid field ($L_{2,3}$) splits into two different liquid fields. L_4 and $L_{2,3}$ were observed separately at 800°C. The separation of the liquid field is in general accordance with the schematic 780°C isothermal section of Kullerud *et al.* (1969).

From the combined results of the isothermal sections, the liquidus phase diagram could be determined. This diagram, together with the liquid compositions of invariant phase equilibria from the isothermal sections, were used to determine the crystallisation paths of the Cu-Ni-S system.

7.3 IMPLICATIONS

Converter matte that is slow-cooled in the beneficiation process of Cu, Ni, and PGE usually contains elements other than Cu, Ni, and S in small amounts, but it is reasonable to assume that the Cu-Ni-S phase diagrams represents converter matte composition sufficiently well. The phase diagrams of the Cu-Ni-S system could be used to describe the crystallisation path of slow-cooled matte. From these phase diagrams it could be deduced that the previously thought explanation for phase segregation in the ingot is probably not gravity separation (Sproule *et al.*, 1960). Instead, it could be concluded that the segregation is due to the crystallisation of early formed

high temperature Cu_2S in the top portion of the ingot and the subsequent fractionation of the liquid towards relatively more Ni_3S_2 and alloy rich in the central and bottom portion of the ingot.

It was found from results obtained in this study and a combination of previous investigations (Sproule *et al.* 1960; Köster and Mulfinger, 1940), that matte composition has an impact on the crystallisation of slow cooled matte. The S-content of the matte is crucial for determining not only the liquidus temperature, but also the sequence of phase crystallisation and the amount of alloy in the matte. Slight changes of ~1wt% in the region from 18 to 22 wt % S can lead to a variety of crystallisation sequences. There is a critical sulphur-content of ~21 wt% (depending on the Cu/Ni ratio) at which both Ni_3S_2 and alloy will start to crystallise only at the eutectic point. If the sulphur content is higher, Cu_2S forms first followed by Ni_3S_2 and alloy is the last phase to crystallise at the eutectic point. With lower sulphur contents alloy crystallises first, followed by Cu_2S, while Ni_3S_2 crystallises only at the eutectic point.

The crystallisation temperature of the phases and the sequence of crystallisation can possibly influence the partitioning behaviour of PGEs. Pt has a high affinity for alloy, but in some cases the matte composition is such that for a large temperature interval during solidification there will be no solid alloy present in the ingot. Because the affinity of some PGEs for solid sulphide phases is higher than for the sulphide melt in the absence of alloy (i.e. Distler *et al.*, 1977), it is possible that some of the PGEs will preferentially partition into the sulphide phases. These elements can later exsolve from the sulphide minerals (Merkle and van den Berg, 1996) at lower temperatures and form late generation phases.

By crystallising alloy at an early stage, there will be rapid diffusion and sufficient time for most of the PGEs (with the possible exception of Pd; Fleet and Stone, 1991) to partition into the metal phase. Furthermore, alloy will form at higher temperatures and longer crystallisation times will probably lead to larger alloy sizes, facilitating easy liberation and magnetic separation. The sulphur content of the matte will determine the phase formation sequence, and it will have an influence on the texture of alloy crystals and the amount of alloy that forms at the eutectic point.

7.4 RECOMMENDATIONS FOR FURTHER INVESTIGATIONS

i) Related quaternary systems

The Cu-Ni-S phase diagrams can be used as a basis for investigations of related quaternary phase diagrams such as the Cu-Fe-Ni-S system. A detailed experimental investigation of the Cu-Fe-Ni-S system would be extremely valuable not only for explanations of ore formation processes in a wide variety of geological settings, but also for explanations of pyro-metallurgical extraction processes.

Small amounts of other elements, such as PGEs, Co, etc. can also be added to the system to determine their effect on the phase relations of the ternary system. This could be directed towards a better understanding of the of slow cooling process of PGE beneficiation.

ii) Slow-cooling

Experiments with different matte compositions, and various cooling procedures can be conducted to determine their effect on the textures (size) of the forming phases, and on the partitioning behaviour of PGEs.

iii) Partitioning behaviour of PGEs in matte

In order to determine the optimum phase crystallisation sequence, the partitioning behaviour of PGEs in the Cu-Ni-S system (in the presence, and absence of small amounts of Fe) will have to be determined systematically. The partitioning of PGEs in certain phase assemblages will have to be determined. These phase assemblages will have to include the most likely phase assemblages that can coexist during cooling, such as: liquid + Cu_2S, liquid + Cu_2S + Ni_3S_2, and liquid + Cu_2S + alloy.

iv) Surface and intersurface tensions

The intersurface tension in matte-slag systems have been investigated (Ip and Toguri, 1993) and can be used for understanding immiscibility between matte and slag in furnace and converter situations. The effect of surface tensions on phases associations in matte will yield a better understanding of the mechanism of separation of certain phases. Associations such as liquid + Cu_2S, liquid + alloy, liquid + Ni_3S_2, or liquid + Cu_2S + alloy could be studied.

v) Gravity settling

In this investigation it was found that gravity segregation can occur in certain phase assemblages, such as liquid + alloy. The possibility of gravity segregation can be investigated in detail to determine the temperature and time dependency of the process. Experiments on the tendency of layering in matte conducted by Hayward (1915) were inconclusive due to the experimental set-up that was used. Solids of the sulphide minerals were heated and it was found that the liquid phase always collected at the bottom of the crucible. Hayward (1915) concluded that the liquid collected at the bottom of the crucible because of the porous texture of the sulphide minerals which allowed the liquid to settle through. To prevent this, the sample should be heated to a higher temperature, where it is certain to be molten, then the temperature should be lowered. This way, the possibility of gravity settling in certain phase assemblages can be investigated.

vi) Fractionation through a slow-cooled ingot

The fractionation through a slow cooled ingot, and especially the non-equilibrium path that the matte follows can be investigated in more detail.

vii) Temperature-composition diagram

The three-dimensional temperature-composition model of the Cu-Ni-S system can also be investigated. This would require a suitable plotting program.

viii) DTA experiments

DTA can be a useful tool for determining the exact temperatures of the various eutectic points of the Cu-Ni-S system. The experimental set-up and the aim of the present investigation did not include this aspect, but it proved to be useful for narrowing down the areas that need to be investigated using DTA.

REFERENCES

8. REFERENCES:

Arnold R.G. (1971) Evidence of liquid immiscibility in the system FeS-S, Economic Geology, vol. 66, pp. 1121-1130.

Arnold R.G., and Malik O.P. (1975) The NiS-S system above 980°C - A Revision. Economic Geology, vol. 70, pp. 176-182.

Asano N., and Ichio T. (1962) Distribution between nickel and lead between liquid copper and cuprous sulphide, Suiyokwaishi, vol. 14, pp 467-470. (In Japanese, English Abstract).

Bornemann von K. (1908)‡ Metallurgie, vol. 5, pp. 13-19.

Bornemann von K. (1910)‡ Metallurgie, vol. 7, p. 84.

Cemic L., and Kleppa O.J. (1986) High temperature calorimetry of sulphide systems. I. Thermochemistry of liquid and solid phases of Ni+S. Geochimica et Cosmochimica Acta, vol. 50, pp. 1633-1641.

Chuang Y.Y. and Chang Y.A. (1982) Extension of the associated solution model to ternary metal-sulfur melts: Cu-Ni-S. Metallurgical Transactions B, vol. 13B, pp. 379-385.

Chang Y.A., Neumann J.P., and Choudary U.V. (1979) INCRA Monograph VII, Phase Diagrams and Thermodynamic Properties of Ternary Copper-Sulphur-Metal Systems, The International Copper Research Association, Inc., New York.

Chizhikov D. M., Gulyanitskaya Z.F., Belyanina N.V., and Blokhina L.I. (1975) The effect of Fe on the phase composition of Cu-Ni sulphide alloys. Izvestiya Akademii Nauk SSSR Metally, vol. 4, pp. 103-107.

‡ These references are quoted by Meyer *et al.* (1975), but the original publications and titles could not be traced.

Cook W.R. Jr (1972) Phase changes in Cu_2S as a function of temperature. United States National Bureau of Standards, Special Publication. vol. 364, pp. 703-712.

Cooper W.C. (1984) Recent developments in the extractive metallurgy of copper, nickel and cobalt and their industrial applications. Canadian Metallurgical Quarterly, vol. 23, pp. 365-375.

Craig J.R., and Kullerud G. (1969) Phase relations in the Cu-Fe-Ni-S system and their application to magmatic ore deposits: Symposium on Magmatic Ore Deposition: Economic Geology, Monograph 4, pp. 344-358.

Craig J.R., and Scott S.D. (1974) Sulphide Phase Equilibria, In: Sulphide Mineralogy, (ed. P. H. Ribbe) Mineralogical Society of America, Washington DC, vol. 1, chapter 5, pp. C1-104.

Distler V.V., Malevskiy A.Y., and Laputina I.P. (1977) Distribution of platinoids between pyrrhotite and pentlandite in crystallisation of a sulphide melt. Geochemistry International, vol. 14, pp. 30-40.

Doherty R. D., Feest E.A., and Holm K. (1973) Dendritic solidification of Cu-Ni alloys. Part I: Initial growth of dendrite structure. Metallurgical Transactions, vol. 4, pp. 115-124.

Elliot R.P. (1965) Constitution of Binary Alloys: First supplement., McGraw Hill, New York, 910 pp.

Feest E.A., and Doherty R.D. (1973) Dendritic solidification of Cu-Ni alloys: Part II. The influence of initial dendrite growth temperature on microsegregation. Metallurgical Transactions, vol. 4, pp. 125-136.

Flamini A., Graziani G., and Grubessi O. (1973) A new synthetic phase in the Cu-S system. Periodico di Mineralogia, vol. 42, pp. 257-265.

Fleet M.E., and Pan Y. (1994) Fractional crystallisation of anhydrous sulphide liquid in the system Fe-Ni-Cu-S with application to magmatic sulphide deposits. Geochimica et Cosmochimica Acta, vol. 58, no. 16, pp. 3369-3377.

Fleet M.E., and Stone W.C. (1991) Partitioning of platinum-group elements in the Fe-Ni-S system and their fractionation in nature. Geochimica et Cosmochimica Acta, vol. 55, pp. 245-253.

Friedrich K. (1914) Untersuchungen über Schichten bildende Systeme. Die Systeme Cu_2S-Ni_3S_2 und Cu_2S-Ni_2S. Metall und Erz, vol. 4, pp. 160-167.

Godréche C. (Ed) (1992) Solids Far From Equilibrium. Collection Anglea-Saclay: Monographs and Texts in Statistical Physics 1. Cambridge University Press, 588 pp.

Hansen M., and Anderco K. (1958) Constitution of binary alloys. McGraw Hill, New York, 1305 pp.

Hayward C.R. (1915) The equilibrium diagram of the system Cu_2S-Ni_3S_2, Trans. AIME, vol. 48, pp. 141-152.

Ip S.W., and Toguri J.M. (1993) Surface and interfacial tension of the Ni-Fe-S, Ni-Cu-S and Fayalite Slag systems. Metallurgical Transactions B vol. 24B, pp. 657-668.

Kellogg H.H. (1969) Thermochemistry of nickel-matte converting, Canadian Metallurgical Quarterly, vol. 8, p. 3.

Köster W., and Mulfinger W. (1940) Die Systeme Kupfer-Nickel-Schwefel und Kupfer-Nickel-Arsen. Zeitschrift für Electrochemie, vol. 46, no.3, pp. 135-141.

Kullerud G. (1960) The Cu-S system. Carnegie Institution of Washington Year Book. vol. 59. pp. 110 - 111.

Kullerud G. (1964) Review and evaluation of recent research on geologically significant sulphide-type systems. Fortschritte der Mineralogie, vol. 62, pp. 221 - 270.

Kullerud G. (1971) Experimental techniques in dry sulphide research. In: Research techniques for high pressure and high temperature (ed. Ulmer G. C.), Springer, Berlin Heidelberg, New York, chapter 11, pp. 289-315.

Kullerud G., and Yoder H.S. (1959) Pyrite stability relations in the Fe-S system. Economic Geology, vol. 54, pp. 533-572.

Kullerud G., and Yund R.A. (1962) The Ni-S system and related minerals. Journal of Petrology, vol. 3, pp. 126-175.

Kullerud G., Yund R.A., and Moh G.H. (1969) Phase relations in the Cu-Fe-S Cu-Ni-S and Fe-Ni-S systems. In: Magmatic Ore Deposits, a symposium (Ed.: Wilson H.D.B.) Economic Geology Monograph, vol. 4, pp. 323-343.

Kushima I., and Asano N., (1953) The phase diagram of the system nickel sulfide - copper sulfide -iron sulfide. Part I. Binary systems. Journal of the Mining Institute of Japan. vol. 69, pp. 297-300.

Lee S.L., Larrain J.M., and Kellogg H.H. (1980) Thermodynamic properties of molten sulfides: Part III. The system Cu-Ni-S. Metallurgical Transactions B. vol. IIB. pp. 251-255.

Lin R.Y., Hu D., Chang Y.A. (1978) Thermodynamics and phase relationships of transition metal-sulphur systems: II. The nickel-sulphur system. Metallurgical Transactions B, vol. 9B, pp. 531-538.

Liné G., and Huber M. (1963) Étude radiocristallographique a haute température de la phase non stoechiometrique $Ni_{3\pm x}S_2$. Comptes Rendus, vol. 256, pp. 3118-3120.

Lindsay, N.M., and Sellshop, J.P.F. (1988) Routine SIMS microanalysis: Trace Au and Pt in sulphides. Nuclear Instruments and Methods in Physics Research, vol. B 35, pp. 358-363.

Massalski T.B. (Ed) (1986) Binary Alloy Phase Diagrams Volume 1, American Society for Metals, Ohio.

McKay J.D. (1993) The direct electro-refining of copper matte. Journal of Metals, vol. 45, pp. 44-48.

Merkle R.K.W. (1992) Platinum-group minerals in the middle group of chromite layers at Marikana, western Bushveld Complex: Indications for collection mechanisms and postmagmatic modification. Canadian Journal of Earth Sciences, vol. 29, pp. 209-221.

Merkle R.K.W., and van den Berg W. (1996) Observations on an experimental Cu-Ni-PGE-S matte. ICAM'96 congress.

Merkle R.K.W., and Verryn S.M.C. (1991) Cooperite and Braggite - New data, ICAM'91 congress, paper no. 61.

Metcalf P.A., Fanwick P., Kakol Z., and Honig J.M. (1993) Synthesis and characterization of Ni_3S_2 single crystals. Journal of Solid State Chemistry, vol. 104, pp. 81-87.

Meyer G.A., Warner J.S., Rao Y.K., and Kellogg H.H. (1975) Thermodynamic Properties of Molten sulfides: Part I. The system Ni-S. Metallurgical Transactions B, vol. 6B, pp. 229-235.

Moh G.H., and Kullerud G. (1963) The Cu-Ni-S system. Carnegie Institution of Washington Year Book. vol. 62, pp. 189-192.

Moh G.H., and Kullerud G. (1964) The Cu-Ni-S system. Carnegie Institution of Washington Year Book. vol. 63, pp. 209-211.

Moh G.H., and Kullerud G. (1982) The Cu-Ni-S system and low temperature mineral assemblages. In: Ore Genesis - State of the Art (ed. Amstutz *et al.*) 2nd Ed., Springer Verlag, Berlin, Heidelberg, New York, pp. 677-688.

Morimoto N., and Gyobu A. (1971) The composition and stability of digenite. American Mineralogist vol. 56, pp. 1889-1909.

Mostert J.C., and Roberts P.N. (1973) Electric smelting at Rustenburg Platinum Mines Ltd. of nickel-copper concentrates containing platinum-group metals. Journal of the South African Institute of Mining and Metallurgy, April, pp. 290-299.

Nagamori M., and Ingraham T.R. (1970) Thermodynamic properties of Ni-S melts between 700°C and 1100°C. Metallurgical Transactions, vol. 1, pp. 1821-1825.

Nell J. (1987) Phase relations in the system Nickel-Copper-Sulphur-Ruthenium at 1200°C, Report no M307, MINTEK, Johannesburg, 7 pp.

Rau H. (1976) Homogeneity range of high temperature $Ni_{3\pm x}S_2$. Journal of Physical Chemistry Solids, vol. 37, pp. 929-930.

Reid A.M., Le Roex A.P., and Minter W.E.L. (1988) Composition of gold grains in the Vaal Placer, Klerksdorp, South Africa, Mineralium Deposita, vol. 23, pp. 211-217.

Rosenqvist T.J. (1954) A thermodynamic study of the iron, cobalt, and nickel sulfides. Journal of the Iron and Steel Institute, vol. 176, pp. 37-57.

Schlitt W.J., Craig R.H., and Richards K.J. (1973) The miscibility gap and distribution of nickel in the molten system Cu-Ni-S. Metallurgical Transactions, vol. 4, pp. 1994-1996.

Schlitt W.J., and Richards K.J. (1973) The behaviour of selenium and tellurium in metal-matte systems, Metallurgical Transactions, vol. 4, pp. 819-825.

Sharma R.C., and Chang Y.A. (1980) Thermodynamics and phase relationships of transition metal-sulphur systems: IV. Thermodynamic Properties of the Ni-S liquid phase and the calculation of the Ni-S phase diagram. Metallurgical transactions B, vol. 11B, pp. 139-146.

Sproule K., Harcourt G.A., and Renzoni L.S. (1960) Treatment of Nickel-copper matte. Journal of Metals, March, pp. 214-219.

Stansfield A., and Faith W.V. (1924) The constitution of Nickel-Copper mattes. Transactions of the Royal Society of Canada, vol. 18, p. 325.

Uytenbogaart W., and Burke E.A.J. (1971) Tables For Microscopic Identification Of Ore Minerals, Elsevier Scientific Publishing Company, Amsterdam.

Von Grunewald G., Hatton C.J., Merkle R.K.W., Gain S.B. (1986) Platinum-group elements - chromite associations in the Bushveld Complex. Economic Geology, vol. 81, pp. 1067 - 1079.

ACKNOWLEDGEMENTS

I would like to thank my supervisor, Dr. Roland Merkle for suggesting the project to me, for spending a great deal of his time in discussions, and for his continued guidance and support. My sincere thanks goes to Prof. C.P. Snyman, co-supervisor of this project, for his valuable advice throughout my student years at Pretoria University.

MINTEK was the main sponsor of the two year project, and apart from personal financial support, there were funds for equipment and consumables in the sulphide laboratory (Geology Department, University of Pretoria). I would like to express my sincere thanks to the staff at MINTEK (especially Dr. J.P.R. de Villiers, Dr. J. Nell, Mr. A. McKenzie and Mrs. F. Stander) for references to relevant articles, helpful suggestions, and discussions. Analyses of the samples, which contributed to a very large extent to the success of the project, were carried out on the SEM at MINTEK, and I would like to thank the various departmental heads (Dr. E.J. Oosthuizen, and Dr. J.P.R. de Villiers) for the use of the SEM. A special word of thanks goes to Mr. Pierre Ellis for all the late hours, and dedicated work on the SEM. The use of a tube furnace at MINTEK is highly appreciated, and I wish to thank the MINTEK staff (A. McKenzie, and S. McKullagh) who supported me with the logistics of tempering charges in this furnace.

I wish to thank Dr. J.R. Taylor and Dr J. Nell for their help in the interpretation of parts of the phase diagram and for all the valuable hours spent in discussions.

Contributors to the sulphide laboratory that I would like to thank are:
Genmin; Anglo Alpha for two muffle furnaces; Prof. E. Fortsch for approximately 30 g of Pt; The Institute for Research on the Bushveld Complex; Dr. G. Grantham for glass tubes and rods.

The love and keen interest of my parents, Deléne and Christo Cilliers, for the past 26 years are highly appreciated. I would like to thank the Cilliers, Bruwer, and Schenk families for financial and moral support throughout my student years.

Lastly, I would like to thank my dear husband, Andreas Bruwer for all the hours of proof reading. His devoted love, support and inspiration led me to complete this dissertation.

9. APPENDIX A: EXPERIMENTAL CHARGES

Tables 20 to 25 contain information about the composition, pre-reaction, tempering and quenching of charges made for the investigation of the 1200°C, 1100°C, 1000°C, 900°C, 800°C and 700°C isothermal sections.

All charges were sealed in quartz glass tubes with 6 mm outer diameter and 4 mm inner diameter unless the tube size is specified in the 'Remarks' column. The starting materials of all charges were similar as given in the experimental procedure.

'Cu wire' of 99.98% purity, and Cu and Ni wire and S powder of unknown purity ('impure starting materials') were also used in a few cases as indicated in the Tables.

Other abbreviations used in the Tables:

med. = quenching medium
W = water
WI = water and ice
WIS = water, ice and NaCl
N / N2 = liquid nitrogen
Dupl. = duplicate charge
f.c. = furnace cooled*
Q = quenched (in water unless specified)
min = minutes
vis = visible macroscopically
eq = equilibrium

* unless the cooling is specified as furnace cooled, quenched, or some quenching medium is given, the ampoules were cooled in air.

Table 20. A-1 Composition of charges, and their pre-reaction, tempering and quenching histories for investigation of the 1200°C isothermal section.

Nr	Weight measured (g)			Total	Weight %			Pre-reaction				Tempered	Quench		Remarks
	Cu	Ni	S	(g)	Cu	Ni	S	°C	days	°C	days	days	med.	Date	
1	0.1540	0.0245	0.0221	0.2006	76.77	12.21	11.02	300	5	400	8	4	WIS	12/04/94	
2	0.1624	0.0316	0.0042	0.1982	81.94	15.94	2.12	300	5	400	8	4	WIS	12/04/94	
3	0.0981	0.0817	0.0189	0.1987	49.37	41.12	9.51	300	5	400	8	-		-	damaged
4	0.1078	0.0842	0.0093	0.2013	53.55	41.83	4.62	400	8	-	-	4	WIS	12/04/94	
5	0.0503	0.1257	0.0239	0.1999	25.16	62.88	11.96	300	5	400	8	4	WIS	12/04/94	
6	0.0566	0.1324	0.0146	0.2036	27.80	65.03	7.17	400	8	-	-	4	WIS	12/04/94	
7	0.0865	0.0544	0.1080	0.2489	34.75	21.86	43.39	300	5	400	8	-		-	8/4 mm Failed
11	0.0769	0.0477	0.0195	0.1441	53.37	33.10	13.53	400	12	-	-	9	WIS	29/04/94	impure starting materials
46	0.1460	0.0278	0.0256	0.1994	73.22	13.94	12.84	600	90	-	-	4	N2	26/8/94	MINTEK
49	0.1550	0.0078	0.0401	0.2029	76.39	3.84	19.76	600	90	-	-	4	N2	26/8/94	MINTEK
69	0.0212	0.2568	0.0229	0.3009	7.05	85.34	7.61	800	27	-	-	14	WIS	19/09/94	
70	0.0452	0.2337	0.0210	0.2999	15.07	77.93	7.00	800	27	-	-	14	WIS	19/09/94	
71	0.0755	0.2097	0.0158	0.3010	25.08	69.67	5.25	800	27	-	-	14	WIS	19/09/94	
72	0.1139	0.1738	0.0121	0.2998	37.99	57.97	4.04	800	26	-	-	14	WIS	19/09/94	Dupl 101,102
73	0.1408	0.1527	0.0084	0.3019	46.64	50.58	2.78	800	27	-	-	14	WIS	19/09/94	
101	0.1143	0.1742	0.0126	0.3011	37.96	57.85	4.18	800	26	-	-	14	WIS	19/09/94	Dupl 72,102
102	0.1521	0.2322	0.0158	0.4001	38.02	58.04	3.95	800	26	-	-	14	WIS	19/09/94	Dupl 72,101
103	0.2628	0.1328	0.0058	0.4014	65.47	33.08	1.44	800	26	-	-	14	WIS	19/09/94	

Table 21. A-2 The compositions, pre-reaction and tempering histories of charges for investigation of the 1100°C isothermal section.

Nr	Weight measured (g) Cu	Ni	S	Total (g)	Weight % Cu	Ni	S	Pre-reaction °C	days	°C	cooled	days	Temper days	Quench med	Date	Remarks
8	0.0107	0.1580	0.0367	0.2054	5.21	76.92	17.87	400	29	1200	f.c.		16		16/05/94	
9	0.0374	0.1360	0.0193	0.1927	19.41	70.58	10.02	400	29	1200	f.c.		16		16/05/94	
10	0.0813	0.1034	0.0181	0.2028	40.09	50.99	8.93	400	29	1200	f.c.		16		16/05/94	break on quenching
12	0.1635	0.0074	0.0416	0.2125	76.94	3.48	19.58	400	29	1200	f.c.		16		16/05/94	
13	0.1628	0.0255	0.0156	0.2039	79.84	12.51	7.65	400	29	1200	f.c.		16		16/05/94	
14	0.1624	0.0075	0.0325	0.2024	80.24	3.71	16.06	400	29	1200	f.c.		16		16/05/94	
15	0.1386	0.0078	0.0604	0.2068	67.02	3.77	29.21	400	21	1200	f.c.		16		16/05/94	8/4 mm visible S2
16	0.0773	0.0388	0.0825	0.1986	38.92	19.54	41.54	400	21	1200	f.c.		-		-	8/4 mm failed on melting
17	0.0665	0.0716	0.0594	0.1975	33.67	36.25	30.08	400	21	1200	f.c.		16		16/05/94	impure , failed on melting
19	0.0109	0.0985	0.1016	0.2110	5.17	46.68	48.15	400	21	750		2	-		-	8/4 mm, failed
20	0.2073	0.0227	0.0609	0.2909	71.26	7.80	20.94	400	21	1200	f.c.		16		16/05/94	impure starting materials
21	0.2350	0.0491	0.0141	0.2982	78.81	16.47	4.73	400	21	1200	f.c.		16		16/05/94	impure starting materials
22	0.1552	0.0412	0.0053	0.2017	76.95	20.43	2.63	400	21	1200	f.c.		16		16/05/94	
23	0.1140	0.0709	0.0125	0.1974	57.75	35.92	6.33	400	21	-		-	16		16/05/94	
47	0.1955	0.0276	0.0274	0.2505	78.04	11.02	10.94	600	8	-		-	10	N	22/8/94	MINTEK
129	0.0083	0.2286	0.0383	0.2752	3.02	83.07	13.92	800	2				13	W	22/12/94	Separated into drops
130	0.0239	0.2139	0.0357	0.2735	8.74	78.21	13.05	800	2				13	W	22/12/94	
131	0.0364	0.1645	0.0253	0.2262	16.09	72.72	11.18	800	2				13	W	22/12/94	
132	0.0653	0.1393	0.0202	0.2248	29.05	61.97	8.99	800	2				13	W	22/12/94	
133	0.0836	0.1233	0.0176	0.2245	37.24	54.92	7.84	800	2				13	W	22/12/94	
134	0.1005	0.1098	0.0131	0.2234	44.99	49.15	5.86	800	2				13	W	22/12/94	Break on Q non equilibrium
135	0.1164	0.0931	0.0145	0.2240	51.96	41.56	6.47	800	2				13	W	22/12/94	
136	0.1414	0.0752	0.0087	0.2253	62.76	33.38	3.86	800	2				13	W	22/12/94	Break on Q
137	0.1937	0.0715	0.0101	0.2753	70.36	25.97	3.67	800	2				13	W	08/02/95	
138	0.2225	0.0455	0.0068	0.2748	80.97	16.56	2.47	800	2				13	W	08/02/95	separated non equilibrium
139	0.2394	0.0319	0.0040	0.2753	86.96	11.59	1.45	800	7				13	W	08/02/95	
140	0.2589	0.1510	0.0013	0.4112	62.96	36.72	0.32	800	7				13	W	08/02/95	Polished out
141	0.2361	0.0055	0.0333	0.2749	85.89	2.00	12.11	800	7				13	W	08/02/95	Polished out
142	0.2310	0.0117	0.0333	0.2760	83.70	4.24	12.07	800	7				13	W	08/02/95	
143	0.2232	0.0160	0.0360	0.2752	81.10	5.81	13.08	800	7				13	W	08/02/95	Separate non equilibrium
144	0.2141	0.0217	0.0388	0.2746	77.97	7.90	14.13	800	7				13	W	08/02/95	Dupl. 151
145	0.2060	0.0244	0.0440	0.2744	75.07	8.89	16.03	800	7				13	W	08/02/95	Separate non equilibrium
146	0.1978	0.0306	0.0462	0.2746	72.03	11.14	16.82	800	7				13	W	08/02/95	Dupl. 222
147	0.1930	0.0299	0.0520	0.2749	70.21	10.88	18.92	800	7				13	W	08/02/95	
148	0.1987	0.0220	0.0522	0.2729	72.81	8.06	19.13	800	7				13	W	08/02/95	Oxidized
149	0.2129	0.0030	0.0591	0.2750	77.42	1.09	21.49	800	7				13	W	08/02/95	Oxidized
150	0.2099	0.0072	0.0596	0.2767	75.86	2.60	21.54	800	7				13	W	08/02/95	Oxidized
151	0.2143	0.0218	0.0386	0.2747	78.01	7.94	14.05	800	7				13	W	08/02/95	Oxidized ,Dupl. 144, C/N wire
222	0.1978	0.0300	0.0464	0.2742	72.14	10.94	16.92	750	8				4	W	10/07/95	Dupl 146
223	0.1832	0.0349	0.0516	0.2697	67.93	12.94	19.13	750	8				4	W	10/07/95	Dupl. 224
224	0.1836	0.0349	0.0517	0.2702	67.95	12.92	19.13	750	8				4	W	10/07/95	Dupl. 223
225	0.2063	0.0246	0.0438	0.2747	75.10	8.96	15.94	750	8				4	W	10/07/95	Dupl. 145
226	0.1013	0.1104	0.0131	0.2248	45.06	49.11	5.83	750	8	1100		4	4	W	27/09/95	Dupl. 134. poss. crack, new tube
227	0.1172	0.0948	0.0132	0.2252	52.04	42.10	5.86	750	8				4	W	10/07/95	Dupl. 135
238	0.1806	0.0537	0.0357	0.2700	66.89	19.89	13.22	750	3				4	W	19/09/95	MINTEK
239	0.1672	0.0656	0.0376	0.2704	61.83	24.26	13.91	750	3				4	W	27/09/95	
240	0.1565	0.0729	0.0408	0.2702	57.92	26.98	15.10	750	3				4	W	27/09/95	possible crack, new tube
241	0.1511	0.0697	0.0481	0.2689	56.19	25.92	17.89	750	3				4	W	19/09/95	MINTEK
242	0.2396	0.0061	0.0040	0.2497	95.96	2.44	1.60	750	3				4	W	27/09/95	
271	0.1806	0.0542	0.0350	0.2698	66.94	20.09	12.97	750	2				5	W	11-10-95	Dupl. 238
272	0.1673	0.0640	0.0379	0.2692	62.15	23.77	14.08	750	2				5	W	11-10-95	Dupl. 239
273	0.1560	0.0737	0.0409	0.2706	57.65	27.24	15.11	750	2				5	W	11-10-95	Dupl. 240
274	0.1517	0.0702	0.0487	0.2706	56.06	25.94	18.00	750	2				5	W	11-10-95	Dupl. 241
276	0.2402	0.0068	0.0043	0.2513	95.58	2.71	1.71	750	2				5	W	11-10-95	Dupl. 242 Dropped
277	0.2361	0.0054	0.0327	0.2742	86.11	1.97	11.93	750	2				5	W	11-10-95	Dupl. 243

Table 22. A-3 The compositions, pre-reaction, and tempering of charges for investigation of the 1000°C isothermal section.

Nr	Weight measured (g) Cu	Ni	S	Total (g)	Weight % Cu	Ni	S	Pre-reaction °C	days	°C	days	°C	days	Melt Temp C	cooled	days	Temper days	Quench med.	Date	Remarks
18	0.0375	0.0716	0.0922	0.2013	18.63	35.57	45.80	400	21	750	2	600	60	-			18		19/07/94	8/4 mm S2 after Q; possible non eq.
34	0.0760	0.0610	0.0545	0.1915	39.69	31.85	28.46	600	59	1000	18	-	-	-			45	WIS	02/09/94	Visible S
35	0.1038	0.0297	0.0637	0.1972	52.64	15.06	32.30	600	24	1000	22	-	-	-			28	N2	26/09/94	MINTEK
37	0.0092	0.1448	0.0477	0.2017	4.56	71.79	23.65	400	8	600	29	-	-	-			22	WIS	01/07/94	
38	0.0481	0.1092	0.0496	0.2069	23.25	52.78	23.97	400	8	600	29	-	-	-			22	WIS	01/07/94	
39	0.0656	0.1074	0.0257	0.1987	33.01	54.05	12.93	400	8	600	29	-	-	-			22	WIS	01/07/94	Dupl 110,111
40	0.1159	0.0731	0.0135	0.2025	57.23	36.10	6.67	400	8	600	29	-	-	-			22	WIS	01/07/94	
41	0.1293	0.0435	0.0285	0.2013	64.23	21.61	14.16	400	8	600	29	-	-	-			22	WI	01/07/94	
42	0.1505	0.0424	0.0080	0.2009	74.91	21.11	3.98	400	8	600	29	1000	22	-			18	WIS	19/07/94	
43	0.1821	0.0185	0.0021	0.2027	89.84	9.13	1.04	400	8	600	29	1000	22	-			45	WIS	02/09/94	
44	0.0859	0.0755	0.0392	0.2006	42.82	37.64	19.54	600	62	-	-	-	-	-			28	N2	26/10/94	MINTEK
45	0.1765	0.0107	0.0142	0.2014	87.64	5.31	7.05	600	37	1000	18	-	-	-			28	N2	26/09/94	MINTEK
48	0.1515	0.0044	0.0452	0.2011	75.34	2.19	22.48	600	37	1000	18	-	-	-			18	WIS	19/07/94	S2 after Q
52	0.0747	0.0500	0.0757	0.2004	37.28	24.95	37.77	800	63	-	-			1100		-	-	-	-	Dupl 104,105 8/4mm. Failed
55	0.0080	0.1223	0.0703	0.2006	3.99	60.97	35.04	600	63	-	-			-			45	WIS	02/09/94	visible S2
56	0.0043	0.1150	0.0824	0.2017	2.13	57.02	40.85	600	63	-	-	-	-	-			28	N2	26/10/94	MINTEK separated
57	0.0050	0.1174	0.0780	0.2004	2.50	58.58	38.92	600	63								45	WIS	02/09/94	Visible S2 separated
58	0.0065	0.1228	0.0740	0.2033	3.20	60.40	36.40	600	37	1000	18			1200	f.c.	8	28	WI	25/10/94	Glass re-crystallized
59	0.0039	0.1267	0.0707	0.2013	1.94	62.94	35.12	600	37	-	-	-	-	-			18	WIS	19/07/94	S2 after Q
60	0.0045	0.1316	0.0672	0.2033	2.21	64.73	33.05	600	37	-	-	-	-	-			18	WIS	19/07/94	
61	0.0128	0.1385	0.0537	0.2050	6.24	67.56	26.20	600	37	-	-	-	-	-			18	WIS	19/07/94	Dupl 106/107
62	0.0295	0.1288	0.0442	0.2025	14.57	63.60	21.83	600	37	-	-	-	-	-			18	WIS	19/07/94	
63	0.0144	0.1572	0.0330	0.2046	7.04	76.83	16.13	600	37	-	-	-	-	-			18	WIS	19/07/94	
64	0.0076	0.1638	0.0303	0.2017	3.77	81.21	15.02	600	23	-	-	-	-	-			18	WIS	19/07/94	
65	0.0168	0.1725	0.0125	0.2018	8.33	85.48	6.19	600	23	1000	18			-			28	N2	26/09/94	MINTEK
66	0.0528	0.1387	0.0103	0.2018	26.16	68.73	5.10	600	23	1000	18			-			28	N2	26/09/94	MINTEK
67	0.1353	0.0158	0.0482	0.1993	67.89	7.93	24.18	600	48	-	-	-	-	-			28	N2	26/10/94	MINTEK
68	0.1333	0.0255	0.0400	0.1988	67.05	12.83	20.12	600	48	-	-	-	-	-			28	N2	26/10/94	MINTEK Dupl 108, 109
100	0.1230	0.1486	0.0266	0.2982	41.25	8.92	49.83	600	31	1000	22	1000	45	1200	f.c.	1	28	WI	25/10/94	Impure starting materials
106	0.0132	0.1385	0.0539	0.2056	6.42	67.36	26.22	800	22	-	-	-	-	-			18	WIS	19/07/94	Dupl 61,107
107	0.0253	0.2769	0.1071	0.4093	6.18	67.65	26.17	600	23	-	-	-	-	-			18	WIS	19/07/94	Dupl 61,106
108	0.1331	0.0260	0.0400	0.1991	66.85	13.06	20.09	800	23	1000	22	-	-	1200	f.c.	8	28	WI	25/10/94	Dupl 109,68
109	0.2670	0.0508	0.0800	0.3978	67.12	12.77	20.11	600	23	-	-	-	-	-			18	WIS	19/07/94	Dupl 108
110	0.0654	0.1081	0.0261	0.1996	32.77	54.16	13.08	800	27	-	-	-	-	1100	f.c.	1	29	W	20/01/95	Homogenized
111	0.1311	0.2148	0.0508	0.3967	33.05	54.15	12.81	600	7	1000	22	-	-	-			28	N2	26/09/94	Dupl 39, 110 MINTEK separated
152	0.2127	0.0032	0.0320	0.2479	85.80	1.29	12.91	800	18					-			28	N2	26/09/94	Oxidized
153	0.2108	0.0085	0.0314	0.2507	84.08	3.39	12.52	800	18								45	N2	21/04/95	MINTEK
154	0.2065	0.0164	0.0271	0.2500	82.60	6.56	10.84	800	18								45	N2	21/04/95	MINTEK
155	0.1993	0.0238	0.0273	0.2504	79.59	9.50	10.90	800	18								45	N2	21/04/95	MINTEK
156	0.1908	0.0282	0.0312	0.2502	76.26	11.27	12.47	800	18								45	N2	21/04/95	MINTEK
157	0.1742	0.0402	0.0347	0.2491	69.93	16.14	13.93	800	18					-			-	-	-	Oxidized
158	0.1526	0.0675	0.0298	0.2499	61.06	27.01	11.92	800	36					-			-	-	-	Oxidized
159	0.1271	0.0974	0.0247	0.2492	51.00	39.09	9.91	800	36					1100	f.c.	1	29	w	03/04/95	cracked
160	0.1153	0.1103	0.0258	0.2514	45.86	43.87	10.26	800	18					1100	f.c.	1	29	W	03/04/95	
161	0.1053	0.1202	0.0240	0.2495	42.20	48.18	9.62	800	18					1100	f.c.	1	29	W	03/04/95	see 159
162	0.0922	0.1333	0.0258	0.2513	36.69	53.04	10.27	800	18					1100	f.c.	1	29	W	03/04/95	
163	0.0784	0.1460	0.0250	0.2494	31.44	58.54	10.02	800	18					1100	f.c.	1	29	W	03/04/95	
164	0.0700	0.1551	0.0244	0.2495	28.06	62.16	9.78	800	18					1100	f.c.	1	29	W	03/04/95	
165	0.0519	0.1721	0.0241	0.2481	20.92	69.37	9.71	800	18					1100	f.c.	1	29	W	03/04/95	
166	0.0397	0.1847	0.0243	0.2487	15.96	74.27	9.77	800	18					1100	f.c.	1	29	W	03/04/95	
167	0.0275	0.1965	0.0245	0.2485	11.07	79.07	9.86	800	18					1100	f.c.	1	29	W	03/04/95	
168	0.2055	0.0083	0.0567	0.2705	75.97	3.07	20.96	800	3	-	-						29	W	03/04/95	Separated
169	0.2048	0.0180	0.0572	0.2800	73.14	6.43	20.43	800	3	-	-						20	N2	15/05/95	MINTEK
170	0.0076	0.1302	0.1122	0.2500	3.04	52.08	44.88	750	14					1100		-	20	N2	15/05/95	MINTEK
171	0.1447	0.0752	0.0299	0.2498	57.93	30.10	11.97	800	3	-	-	-	-				-	-	-	Failed
173	0.0029	0.1483	0.1287	0.2799	1.04	52.98	45.98	750	14	750	12						10	N2	15/05/95	MINTEK
174	0.1828	0.0441	0.0532	0.2801	65.26	15.74	18.99	800	3	-	-						-	-	-	Failed
175	0.0020	0.1722	0.1062	0.2804	0.71	61.41	37.87	800	3	-	-						20	N2	15/05/95	MINTEK separated
220	0.1625	0.0513	0.0564	0.2702	60.14	18.99	20.87	750	14	1000	12						20	N2	15/05/95	MINTEK, homogenize new tube.
221	0.1484	0.0727	0.0486	0.2697	55.02	26.96	18.02	750	14	-	-	-	-	1100		-	14	w	26/07/95	
234	0.1482	0.0728	0.0483	0.2693	55.03	27.03	17.94	750	12	1000	12						-	-	-	Failed
																	14	w	26/07/95	Dupl 221

Table 23. A-4 Compositions, pre-reaction and tempering of charges for investigation of the 900°C isothermal section.

Nr	Weight measured (g)			Total	Weight %			Pre-reaction						Melt			Temper		Quench	Remarks
	Cu	Ni	S	(g)	Cu	Ni	S	°C	days	°C	days	°C	days	Temp.	duration	cooled	days	med.	Date	
74	0.0190	0.1555	0.0265	0.2010	9.45	77.36	13.18	800	2					1100	3 d	f.c.	49	w	9/12/94	
75	0.0337	0.1377	0.0279	0.1993	16.91	69.09	14.00	800	2					1100	3 d	f.c.	49	w	9/12/94	
76	0.0510	0.1210	0.0279	0.1999	25.51	60.53	13.96	800	2					1100	3 d	f.c.	49	w	9/12/94	
77	0.0717	0.0993	0.0296	0.2006	35.74	49.50	14.76	800	2					1100	3 d	f.c.	49	w	9/12/94	
78	0.0935	0.0981	0.0243	0.2159	43.31	45.44	11.26	800	2					1100	3 d	f.c.	49	w	9/12/94	
79	0.1242	0.0538	0.0200	0.1980	62.73	27.17	10.10	800	2					1100	3 d	f.c.	49	w	9/12/94	
80	0.1464	0.0312	0.0233	0.2009	72.87	15.53	11.60	800	2					1100	3 d	f.c.	49	w	9/12/94	
81	0.1581	0.0138	0.0280	0.1999	79.09	6.90	14.01	800	2					1100	3 d	f.c.	49	w	9/12/94	
82	0.1473	0.0060	0.0472	0.2005	73.47	2.99	23.54	750	8					-	-	-	42	N2	13/12/94	MINTEK
83	0.1270	0.0300	0.0455	0.2025	62.72	14.81	22.47	750	8					-	-	-	42	N2	13/12/94	MINTEK separated
84	0.1222	0.0243	0.0515	0.1980	61.72	12.27	26.01	750	8					-	-	-	42	N2	13/12/94	MINTEK
85	0.1153	0.0247	0.0591	0.1991	57.91	12.41	29.68	750	8	1000	9	1000		1100	15 min	Q	9	W	28/09/95	
86	0.0874	0.0499	0.0624	0.1997	43.77	24.99	31.25	750	8					-	-	-	42	N2	13/12/94	Non equilibrium MINTEK
87	0.0918	0.0542	0.0535	0.1995	46.02	27.17	26.82	750	8					-	-	-	42	N2	13/12/94	MINTEK
88	0.0590	0.0810	0.0571	0.1971	29.93	41.10	28.97	750	8					-	-	-	-	-	-	Cracked pre-reaction 1050C
89	0.0201	0.0964	0.0828	0.1993	10.09	48.37	41.55	750	8					-	-	-	58	N2	03/03/95	MINTEK vis S2 separated
90	0.0086	0.1279	0.0664	0.2029	4.24	63.04	32.73	750	8					-	-	-	58	N2	03/03/95	MINTEK
91	0.0183	0.1207	0.0656	0.2046	8.94	58.99	32.06	750	8					-	-	-	-	-	-	Cracked pre-reaction 1050C
92	0.0216	0.1202	0.0590	0.2008	10.76	59.86	29.38	800	17					-	-	-	58	N2	03/03/95	MINTEK
93	0.0192	0.1120	0.0683	0.1995	9.62	56.14	34.24	800	17					-	-	-	58	N2	03/03/95	MINTEK separated
94	0.0967	0.0580	0.0480	0.2027	47.71	28.61	23.68	800	17					-	-	-	58	N2	03/03/95	MINTEK separated
95	0.0351	0.1402	0.0945	0.2698	13.01	51.96	35.03	750	1					1100	20 min	Q	-	-	-	Dropped broke
97	0.0592	0.1134	0.0969	0.2695	21.97	42.08	35.96	750	2	1000	1	900	7	1100	15 min	Q	9	W	28/09/95	
98	0.1783	0.0269	0.0646	0.2698	66.09	9.97	23.94	750	2					<1000	1	f.c.	7	W	15/09/95	MINTEK
99	0.1463	0.0566	0.0675	0.2704	54.11	20.93	24.96	750	2					<1000	1	f.c.	7	W	15/09/95	MINTEK
188	0.0536	0.1187	0.0975	0.2698	19.87	44.00	36.14	750	35					1100	15 min	Q	9	W	28/09/95	
228	0.1192	0.1105	0.0405	0.2702	44.12	40.90	14.99	750	1	*							7	W	28/10/95	
235	0.1231	0.0700	0.0773	0.2704	45.53	25.89	28.59	750	1	*							7	W	28/10/95	
236	0.1146	0.0725	0.0822	0.2693	42.55	26.92	30.52	750	2	1000	1	900	7	1100	15 min	Q	9	W	28/09/95	
237	0.1184	0.0949	0.0566	0.2699	43.87	35.16	20.97	750	2					<1000	1	f.c.	7	W	15/09/95	MINTEK
243	0.1026	0.0726	0.0944	0.2696	38.06	26.93	35.01	750	1					1100	20 min	Q				Cracked
244	0.0834	0.0944	0.0918	0.2696	30.93	35.01	34.05	750	1					1100	20 min	Q	7	W	05/10/95	MINTEK, vis S2
248	0.1296	0.0673	0.0729	0.2698	48.04	24.94	27.02	750	1	*							7	W	28/10/95	

* nrs. 228, 235, 248 : 750°C 1d; 1100°C 20 min; 900°C 7d; 1050°C 20 min; 800°C 1d;

Table 24. A-5 The compositions, pre-reaction and tempering histories of charges for investigation of the 800°C isothermal section.

Nr	Weight measured (g) Cu	Ni	S	Total (g)	Weight % Cu	Ni	S	Pre-reaction °C	days	°C	days	°C	days	cooled	°C	days	cooled	Melt °C	days	cooled	Temper days	Quench med	Date	Remarks
121	0.2695	0.0129	0.0186	0.3010	89.53	4.29	6.18	800	4									1100	2	f.c.	110	w	03/04/95	
122	0.2562	0.0234	0.0247	0.3043	84.19	7.69	8.12	800	4									1100	2	f.c.	110	w	03/04/95	
123	0.2415	0.0423	0.0193	0.3031	79.68	13.96	6.37	800	4									1100	2	f.c.	110	w	03/04/95	
124	0.2288	0.0453	0.0277	0.3018	75.81	15.01	9.18	800	4									1100	2	f.c.	63	w	08/02/95	
125	0.1502	0.099	0.0511	0.3003	50.02	32.97	17.02	800	4									1100	2	f.c.	110	w	03/04/95	
126	0.1471	0.1294	0.0249	0.3014	48.81	42.93	8.26	800	4									1100	2	f.c.	110	w	03/04/95	
127	0.1168	0.1515	0.0326	0.3009	38.82	50.35	10.83	800	4									1100	2	f.c.	110	w	03/04/95	Cracked, Oxidized
128	0.0816	0.176	0.0431	0.3007	27.14	58.53	14.33	800	4									-	-	-	24	w	10/07/95	MINTEK
176	0.0702	0.151	0.03	0.2512	27.95	60.11	11.94	750	11									-	-	-	24	w	10/07/95	MINTEK
177	0.0559	0.1628	0.0311	0.2498	22.38	65.17	12.45	750	11												30	w	10/08/95	
178	0.0456	0.1751	0.0306	0.2513	18.15	69.68	12.18	750	11								f.c.	1000	4	f.c	14	w	04/09/95	Non eq. dupl. 199
179	0.0377	0.1797	0.0326	0.2500	15.08	71.88	13.04	750	11	800	30	1100	2					1000	7	f.c.	2	w	14/09/95	melted several times
180	0.0251	0.1951	0.0302	0.2504	10.02	77.92	12.06	750	11	800	24	1000	9		*			-	-	-	24	w	10/07/95	MINTEK
181	0.0153	0.2429	0.0422	0.3004	5.09	80.86	14.05	750	11									-	-	-	26	w	09/06/95	
182	0.0081	0.2037	0.0882	0.3000	2.70	67.90	29.40	<800	22									-	-	-	26	w	09/06/95	Separated
183	0.0078	0.1987	0.0928	0.2993	2.61	66.39	31.01	<800	22									-	-	-	26	w	09/06/95	Separated
184	0.0092	0.1943	0.0955	0.2990	3.08	64.98	31.94	<800	22									-	-	-	26	w	09/06/95	Separated
185	0.0228	0.1832	0.094	0.3000	7.60	61.07	31.33	<800	22									-	-	-	26	w	09/06/95	Separated
186	0.0283	0.1375	0.0855	0.2513	11.26	54.72	34.02	<800	22									-	-	-	26	w	09/06/95	Separated Non equilibrium
187	0.0212	0.1379	0.1112	0.2703	7.84	51.02	41.14	<800	22									-	-	-	26	w	09/06/95	Non-equilibrium
189	0.0457	0.1061	0.1193	0.2711	16.86	39.14	44.01	<800	22									-	-	-	26	w	09/06/95	Visible S_2
190	0.0688	0.0963	0.1347	0.2998	22.95	32.12	44.93	<800	22									-	-	-	26	w	09/06/95	
191	0.1298	0.0648	0.0557	0.2503	51.86	25.89	22.25	<800	22									-	-	-	26	w	09/06/95	
192	0.1328	0.0612	0.0598	0.2538	52.32	24.11	23.56	<800	22									-	-	-	26	w	09/06/95	dupl. 198
193	0.131	0.0548	0.0658	0.2516	52.07	21.78	26.15	<800	22															
194	0.1301	0.0502	0.0701	0.2504	51.96	20.05	28.00	750	11	800	24	1000	9		1100	2		1000	4	f.c	14	w	04/09/95	
196	0.1299	0.04	0.0801	0.2500	51.96	16.00	32.04	750	7	800	30							1000	4	f.c	14	w	04/09/95	
197	0.1329	0.0441	0.0994	0.2764	48.08	15.96	35.96											-	-	-	-	-	-	Failed
198	0.1432	0.0602	0.0715	0.2749	52.09	21.90	26.01	750	7	1000	9	800	30		1100	2		1000	4	f.c.	14	w	04/09/95	dupl. 193
199	0.0453	0.2157	0.0393	0.3003	15.08	71.83	13.09	750	11	1000	9							1100	1	f.c.	8	W	20/10/95	dupl. 179
213	0.1065	0.1053	0.1181	0.3299	32.28	31.92	35.80	<800	22									-	-	-	26	w	09/06/95	Non-equilibrium
231	0.059	0.1295	0.0807	0.2692	21.92	48.11	29.98	750	12?												30	w	10/08/95	
233	0.0864	0.089	0.0945	0.2699	32.01	32.98	35.01	750	12?	800	30							1000	4	f.c.	14	w	04/09/95	
245	0.0228	0.1827	0.0939	0.2994	7.62	61.02	31.36	750	1									1100	1	f.c.	8	W	20/10/95	Dupl. 185
275	0.1932	0.0142	0.0632	0.2706	71.40	5.25	23.36	750	1									1100	1	f.c.	8	W	20/10/95	

* 1100 2d; 1000 4d; 800 14d;

Table 25. A-6 The compositions, pre-reaction and tempering histories of charges for investigation of the 700°C isothermal section.

Nr	Weight measured (g) Cu	Ni	S	Total (g)	Weight % Cu	Ni	S	Pre-reaction °C	days	°C	days	°C	days	°C	days	°C	days	Melt °C	days	cooled	Temper days	Quench med	Date	Remarks
172	0.2163	0.0028	0.0607	0.2798	77.31	1.00	21.69	800	3	-	-					1100	15 min	1050	1	f.c.	6	W	05/10/95	
195	0.1299	0.0450	0.0753	0.2502	51.92	17.99	30.10	750	7	800	30	1000	4 f.c.	800	14	1100	15 min	1050	1	f.c.	6	W	05/10/95	
219	0.0024	0.1807	0.0981	0.2812	0.85	64.26	34.89	750	7			1000	30			1100	15 min	1050	1	f.c.	6	W	05/10/95	
230	0.0214	0.1727	0.0751	0.2692	7.95	64.15	27.90	750	12	800	30					1100	15 min	1050	1	f.c.	6	W	05/10/95	
232	0.0806	0.0970	0.0915	0.2691	29.95	36.05	34.00	750	12	800	30	1000	4	800	21	1100	15 min	1050	1	f.c.	6	W	05/10/95	
250	0.2216	0.0216	0.0271	0.2703	81.98	7.99	10.03														51	W	31/08/95	MINTEK
251	0.2001	0.0430	0.0267	0.2698	74.17	15.94	9.90														51	W	31/08/95	MINTEK
252	0.1803	0.0630	0.0270	0.2703	66.70	23.31	9.99														51	W	31/08/95	MINTEK
253	0.1563	0.0863	0.0269	0.2695	58.00	32.02	9.98														51	W	31/08/95	MINTEK
254	0.0977	0.1372	0.0356	0.2705	36.12	50.72	13.16	750	51									1000			-	-	-	cracked on melt
255	0.0648	0.1590	0.0459	0.2697	24.03	58.95	17.02	750	12							1100	15 min	1050	1	f.c.	6	W	05/10/95	
256	0.0544	0.1756	0.0406	0.2706	20.10	64.89	15.00	750	12							1100	15 min	1050	1	f.c.	6	W	05/10/95	
257	0.0410	0.1884	0.0400	0.2694	15.22	69.93	14.85	750	12							1100	15 min	1050	1	f.c.	6	W	05/10/95	
258	0.0227	0.2074	0.0401	0.2702	8.40	76.76	14.84	750	1							1100	15 min	1050	1	f.c.	6	W	05/10/95	
259	0.0109	0.2190	0.0405	0.2704	4.03	80.99	14.98	750	12							1100	15 min	1050	1	f.c.	6	W	05/10/95	
260	0.0436	0.1649	0.0621	0.2706	16.11	60.94	22.95	750	12							1100	15 min	1050	1	f.c.	6	W	05/10/95	
261	0.0183	0.1892	0.0635	0.2710	6.75	69.82	23.43	750	1							1100	15 min	1050	1	f.c.	6	W	05/10/95	
262	0.0256	0.1818	0.0632	0.2706	9.46	67.18	23.36	750	12							1100	15 min	1050	1	f.c.	6	W	05/10/95	
265	0.0706	0.1422	0.0583	0.2711	26.04	52.45	21.50	750	12							1100	15 min	1050	1	f.c.	6	W	05/10/95	
266	0.0780	0.1241	0.0673	0.2694	28.95	46.07	24.98	750	1							1100	15 min	1050	1	f.c.	6	W	05/10/95	
267	0.0673	0.1218	0.0809	0.2700	24.93	45.11	29.96	750	1							1100	15 min	1050	1	f.c.	6	W	05/10/95	
268	0.0672	0.1163	0.0866	0.2701	24.88	43.06	32.06	750	1							1100	15 min	1050	1	f.c.	6	W	05/10/95	
270	0.0684	0.1388	0.0622	0.2694	25.39	51.52	23.09	750	12							1100	15 min	1050	1	f.c.	6	W	05/10/95	

10. APPENDIX B: SULPHUR PARTIAL PRESSURE

There are different reasons suggested for the failure of the evacuated quartz glass tubes:
i) Sulphur liquid expands thermally to up to 50% of its original volume when heated from 100°C to 1100°C (Arnold, 1971).
ii) Sulphur can reach partial pressures far in excess of 12 MPa at 1200°C (Kullerud and Yoder, 1959).

10.1 Thermal expansion of sulphur liquid

During an investigation of the FeS-S system Arnold (1971) reported the failure of tubes which contained virtually no open spaces. In these experiments only S were used, and it was found that S liquid expands by 50% when heated from 100°C to 1100°C. It was concluded that the failure of the tubes were due to the thermal expansion of S liquid.

During this investigation it was found that as soon as the starting material reacted during pre-reaction it occupied much less space than the loose powder that was weighed in. There were always voids in the tubes before tempering and the thermal expansion of sulphur-rich liquid could not have had a large influence on the walls of the tubes, since there was enough space for expansion.

10.2 High partial pressure of sulphur

S_2 reaches very high partial pressures at high temperatures (Figure 69), and the extremely high partial pressures of sulphur gas are more likely to be the cause of the failure of tubes. Free S_2 can be present in the charges under various conditions. Firstly the composition of the sample lies above the Cu_2S-NiS_2 line and is oversaturated in sulphur. Unreacted sulphur can also be present when the reaction between the metals and sulphur to form sulphide minerals is not completed.

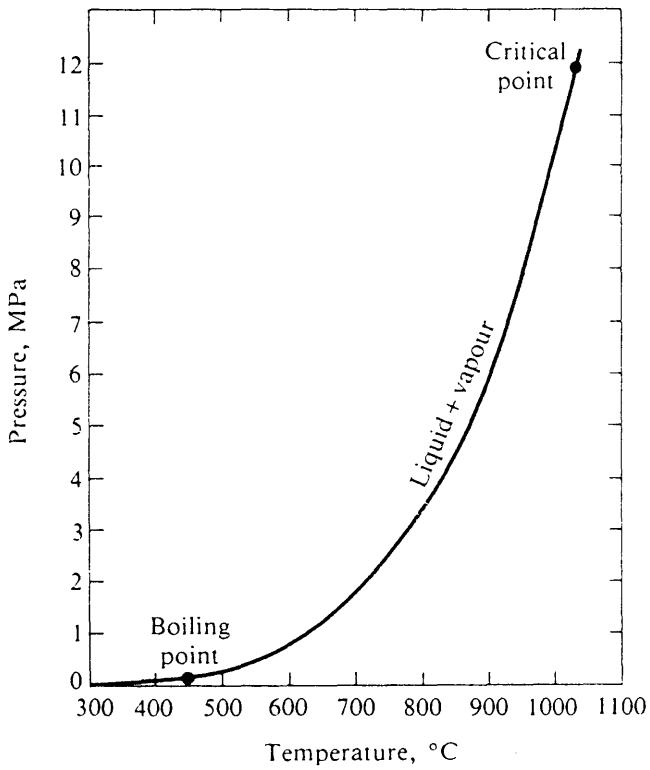

Figure 69. The temperature-pressure curve for liquid and vapour sulphur (Kullerud and Yoder, 1959).

APPENDIX B-1 :The internal pressure that a quartz glass tube can withstand, from Merck.

Merk- und Arbeitsblätter

Betriebsdrücke für runde Glas-Hohlzylinder

Arbeitsblatt:
0 2 5

GIT 7 (1963) Heft 1 (Januar)

Das Diagramm gilt für spannungsfreie Rohre und zylindrische Hohlkörper mit kreisrundem Querschnitt, gleichmäßiger Wanddicke und freien Enden, wenn nicht gleichzeitig ungünstige thermische Belastung vorliegt. Der 1-Minuten-Berstdruck (Kaltwasser-Prüfdruck)-Mittelwert liegt beim 5-fachen, der Dauer-Berstdruck-Mittelwert beim 2,5-fachen Druck. Streuen die Berstdruckwerte mit 15% so ist die Bruchwahrscheinlichkeit bei Dauerbeanspruchung etwa $1:10^8$. Wird durch ungünstigen Spannungsgehalt oder Unrundheit die maximale Wandspannung verdoppelt, so nimmt die Bruchwahrscheinlichkeit bei Dauerdruck auf etwa 1:200 zu.

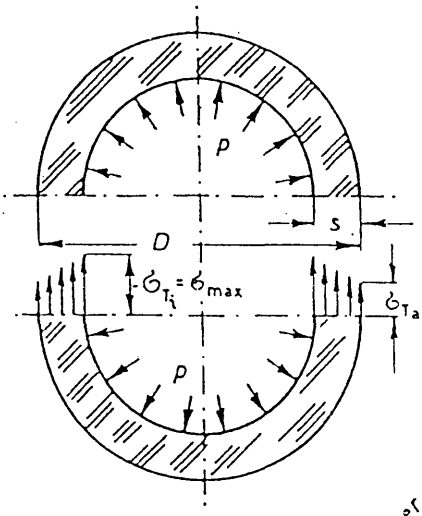

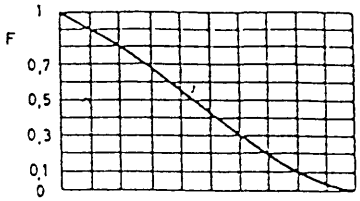

$\sigma_{T_i} = \sigma_{max}$

σ_{T_a} = F mal σ_{T_i}

Maximale Glasanstrengung durch tangentiale Zugspannung an der Innenwand.

Lastannahme:
$\sigma_{T_i} = 0{,}8\ kP/mm^2$

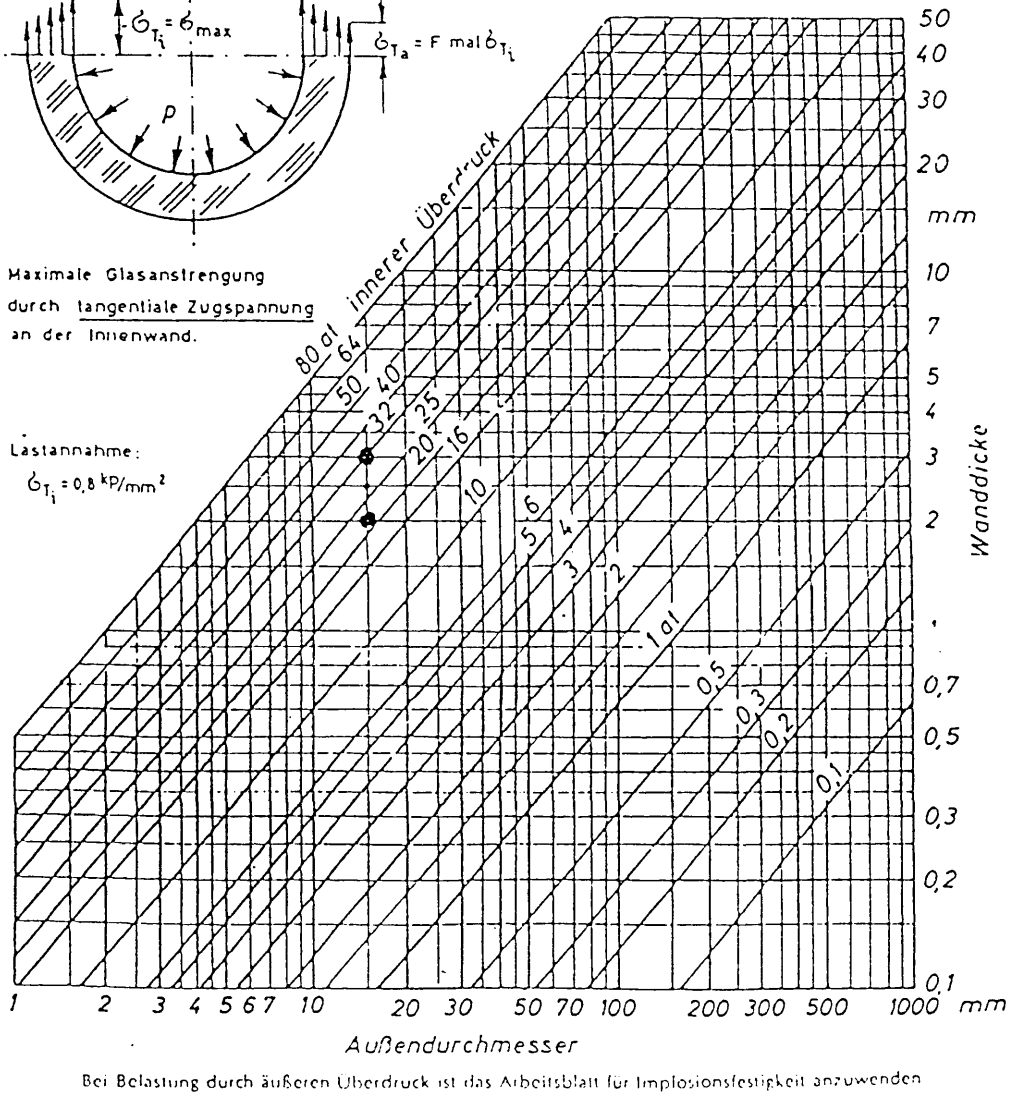

Bei Belastung durch äußeren Überdruck ist das Arbeitsblatt für Implosionsfestigkeit anzuwenden

11. APPENDIX C: SELECTED FURNACE TEMPERATURE PROFILES

See Figure 23 for the positions of the tubes.

Furnace set at 1250°C

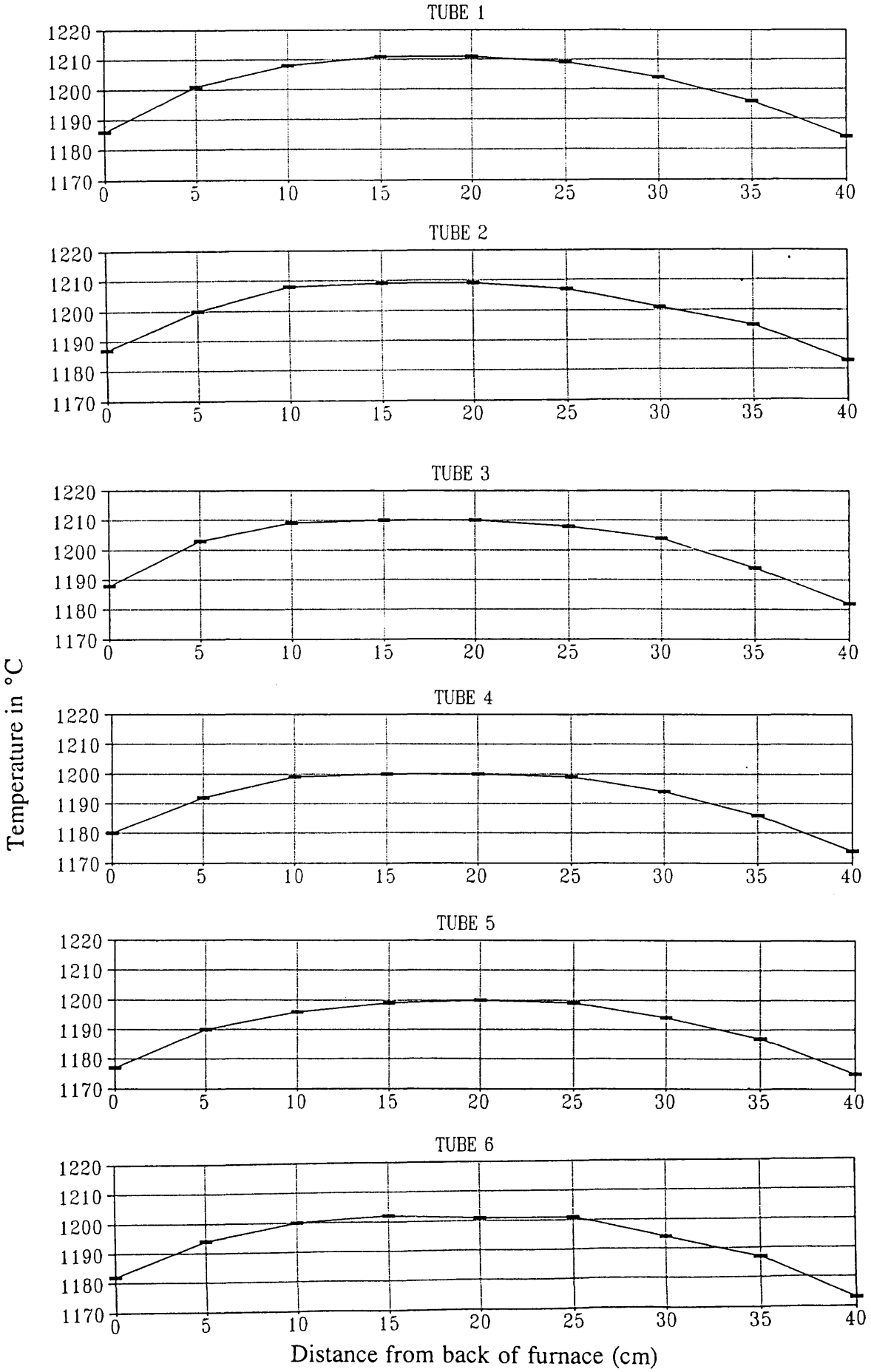

Furnace set at 1000°C

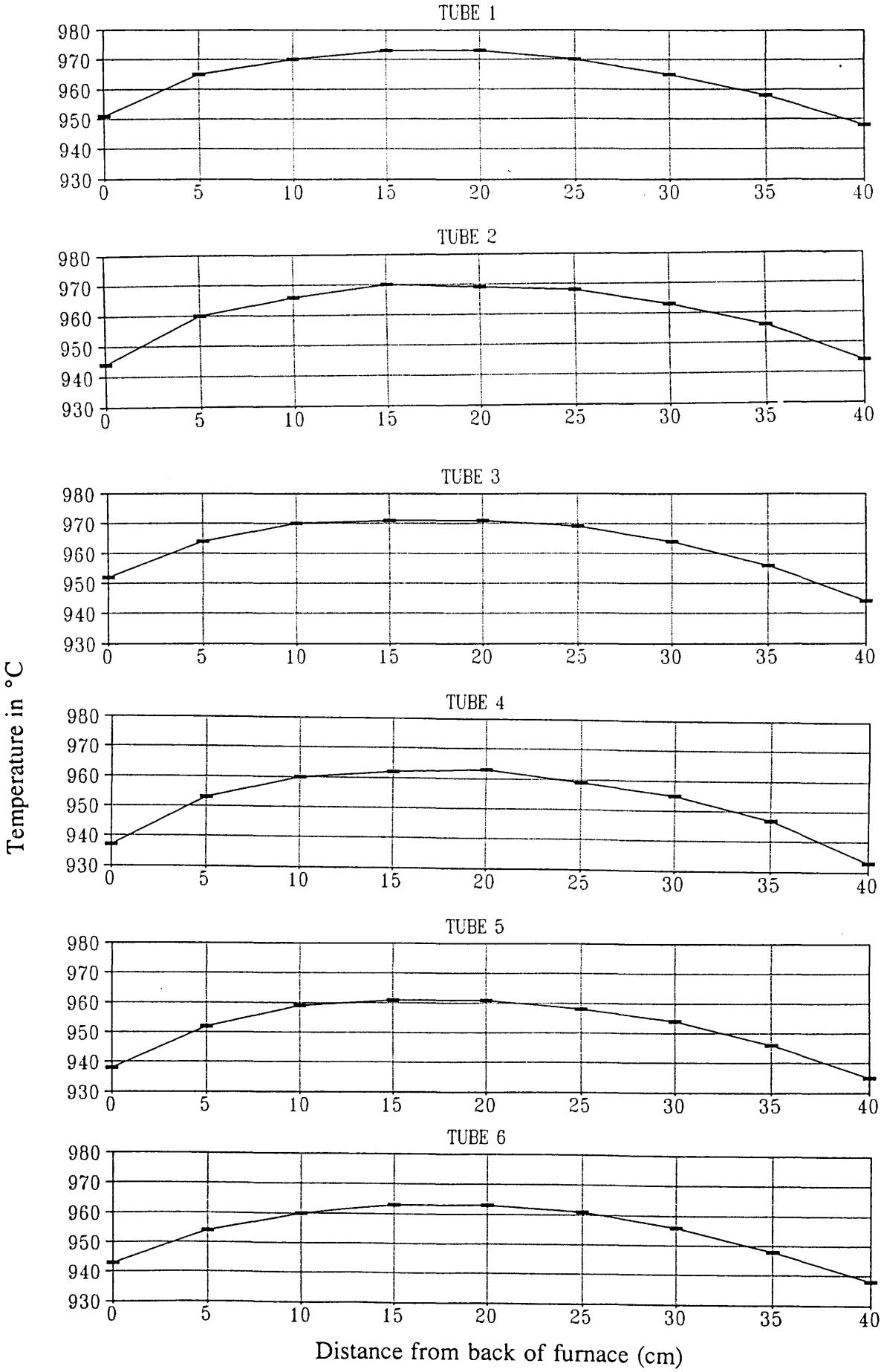

156

Furnace set at 1140°C